RE-ANALYSING THE PHYLOGENY, MORPHOLOGY AND ECOLOGY OF PHYTOSAURIA AND ITS EVOLUTIONARY CONVERGENCE WITH CROCODYLOMORPHA

by

ANDREW STEPHEN JONES

A thesis submitted to the University of Birmingham for the degree of DOCTOR OF PHILOSOPHY

School of Geography, Earth and Environmental Sciences

College of Life and Environmental Sciences

University of Birmingham

September 2018

Abstract

Phytosauria is a clade of large, semi-aquatic archosauromorphs which reached its peak diversity and an almost global distribution in the late Triassic (c. 230–201 Mya). Their characteristic morphological convergence with crocodylomorphs has led to the acceptance of ecological equivalence, but comparisons between the groups have been entirely qualitative. Here, I present the first attempt to quantify ecological convergence between phytosaurs and crocodylomorphs. Previous phylogenetic analyses of Phytosauria have been limited in taxonomic scope; therefore, to provide an evolutionary context for subsequent analyses I produced the first comprehensive phytosaur phylogeny, aided by recently developed analytical techniques. The resulting trees presented two partially conflicting topologies, but were generally consistent with previous phylogenetic hypotheses. The discrete character tree was incorporated into geometric morphometric analyses to quantify phytosaur cranial convergence with extant and extinct crocodylomorphs, and to investigate morphological evolutionary trends. Phytosaurs were found to be morphologically distinct from all crocodylomorphs except thalattosuchians. Similarities were observed between phytosaurs and some crocodylids, including repeated morphological divergences and potential similarities in cranial modularity. Convergence of dietary ecology was investigated using dental microwear, with phytosaurs projected into crocodylian dietary space. Phytosaurs were recovered as generalists, with no partitioning of food material properties observed between dental positions or cranial ecomorphs.

Acknowledgements

I wish to express a deep gratitude to my supervisor Richard Butler, for being a source of endless support, patience and generosity both with his time and experience, and being an all-around exemplary supervisor throughout my PhD. Richard has provided insightful comments and suggestions throughout this project, and has offered numerous opportunities to develop skills and partake in unforgettable experiences that would have never otherwise been possible. Suffice to say that Richard's input has greatly enhanced this project in many ways.

I also extend thanks to my secondary supervisor Ivan Sansom, who provided valuable insight in the latter part of my PhD, was a positive presence throughout, and allowed me the opportunity to gain fantastic teaching experience.

I thank CENTA (Central England NERC Training Alliance) for providing funding to support my project, and the SYNTHESYS Access scheme, which provided additional funding for particular data collection trips.

Thanks also to my internal and external examiners (Jason Hilton and Paul Barrett) for insightful comments that improved the content of the thesis.

Many thanks to Pablo Goloboff for TNT script suggestions and bug fixes, which allowed me to analyse my phylogenetic data in all the ways, and with all the rigour that I desired. Thanks also to Caroline Parins-Fukuchi, William Parker & Axel Hungerbühler for constructive comments and discussion pertaining to my phylogenetic work. I also extend enormous thanks to Octavio Mateus and Marco Marzola for useful discussions regarding phylogenetic characters and for offering me multiple extraordinary opportunities to visit field

locations and collaborate on exciting material that greatly enhanced my understanding of both phytosaurs and many aspects of palaeontology.

Many thanks also to Pedro Godoy for the use of his crocodylomorph photos, to build a comparative geometric morphometric dataset with phytosaurs. Also for useful discussions about geometric morphometrics and assistance and advice regarding crocodylomorph phylogeny. Thanks also to Emma Dunne for fielding numerous questions in the use of R, which greatly assisted analysis of my geometric morphometric dataset.

I am greatly indebted to Jordan Bestwick and Mark Purnell for invaluable training in data collection and analysis techniques pertaining to dental microwear, and for generous access to equipment and resources at the University of Leicester. I am particularly grateful to Jordan for allowing me the use of his reptile microwear dataset as a comparative tool against which to analyse my phytosaur data. Many thanks also to Lin Marvin-Dorland and Thomas Clements for short-notice assistance with the preparation and delivery of solvent cleaning gel, which allowed me to greatly increase the size of my microwear dataset.

I thank the following people for access to, and assistance with, specimens in their care: Carl Mehling (AMNH), Oliver Rauhut (BSPG), William Simpson (FMNH), Philipe Havlik and Davit Vasilyan (GPIT), Daniela Schwarz and Thomas Schossleitner (MB), Ronan Allain (MNHN), Casey Holliday and James Schiffbauer (MU), Lorna Steel (NHMUK), Ursula Göhlich (NHMW), Eckhard Mönnig (NMC), Amanda Cantrell (NMMNHS), William Parker and Matthew Smith (PEFO), Rainer Schoch and Erin Maxwell (SMNS), Kenneth Bader and Matthew Brown (TMM), Bill Mueller (TTU-P), Patricia Holroyd (UCMP), Michael Brett-Surman (USNM), Daniel Brinkman (YPM), and Robert Bronowicz and Tomasz Sulej (ZPAL). Special thanks are extended to Erin Maxwell and Bill Mueller for accommodating

my needs regarding tooth cleaning and casting, and to Eckhard Mönnig for showing me the type locality of *Coburgosuchus* and making me feel very welcome in Coburg.

I am tremendously grateful for the support of my friends at the University of Birmingham and farther afield, in particular Dan Cashmore, Emma Dunne, Pedro Godoy and Juan Benito Moreno, whose shared love of creative mischief and warped humour allowed me to retain my insanity.

I owe an immense debt of gratitude to my family, David, Elaine, Mark, Milly and Dennis. Their unwavering support, patience, kindness and love has, and continues to be, one of the most important parts of my life; constantly encouraging me in all that I do. I therefore thank them, not only for their support over the past four years, but for instilling in me from an early age the importance, not necessarily of succeeding, but of trying my best. It is because of this that I have reached this point.

Finally, I thank my best friend and partner Zoë Wood; a constant source of love, support and inspiration, and the best companion I could ever hope for, keeping me going every step of the way. Thank you, Friend; I couldn't have done it without you.

Table of Contents

List of Figures

List of Tables

Chapter 1: Introduction

Phytosauria represents one of the most successful groups of large-bodied reptiles within late Triassic ecosystems, displaying an almost global distribution in fluvial, lacustrine and marine deposits across Europe (Meyer, 1861, 1865; Kuhn 1936; Renesto & Paganoni, 1998; Dzik, 2001; Hungerbühler & Hunt, 2000; Hungerbühler, 2002; Butler *et al.*, in review), North America (Cope, 1881; Huene, 1913; Camp, 1930; Long & Murry, 1995; Stocker, 2010, 2012, 2013; Hungerbühler *et al*., 2013), South America (Kischlat & Lucas, 2003), Asia (Chatterjee, 1978; Buffetaut & Ingavat, 1982; Stocker *et al.*, 2017) and Africa (Dutuit, 1977a, b, 1978) comprising at least 30 currently recognised species (Stocker & Butler, 2013).

Time-calibrated phylogenies indicate that phytosaurs originated in the early Triassic, soon after the Permo-Triassic mass extinction, although only one confirmed phytosaur taxon is known prior to the late Triassic (Stocker *et al*., 2017). In recent phylogenetic analyses, Phytosauria has been consistently placed close to the base of Archosauria, a group that dominated Mesozoic ecosystems, with its two major lineages today represented by birds (Avemetatarsalia) and crocodylians (Pseudosuchia). Most recently Ezcurra (2016) recovered phytosaurs as the most basal clade within the pseudosuchian archosaur lineage, and prior to this Nesbitt (2011) found phytosaurs as the sister group to Archosauria itself. Phytosaurs have long been regarded as functionally and ecologically equivalent to extant and extinct crocodylomorphs due to their striking morphological similarity and are generally interpreted as filling the same role in ecosystems, i.e. large carnivorous and piscivorous apex predators (Figure 1.1) occupying aquatic and semi-aquatic habitats (Fraas, 1896; McGregor, 1906; Camp, 1930; Colbert, 1947; Eaton, 1965; Hunt, 1989; Hungerbühler, 2000; Stocker & Butler,

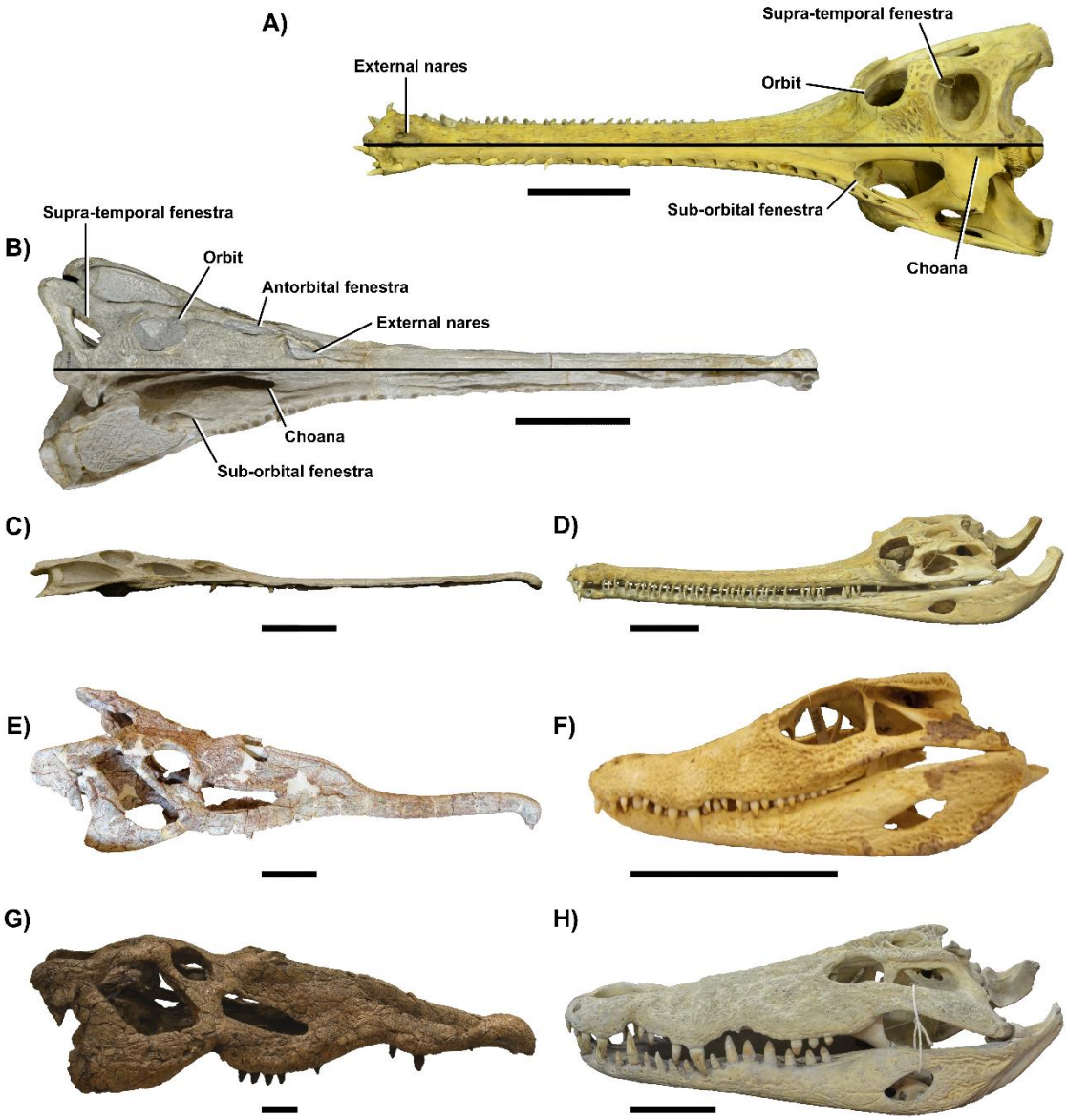

Figure 1.1: Similarities and differences in the convergent morphology of phytosaurs and crocodylomorphs: A, D) *Gavialis gangeticus* and B, C) *Ebrachosuchus neukami*; the upper and lower halves of A and B display dorsal and ventral morphologies respectively. Note the positions of the external nares, sub-orbital fenestrae and choanae in each group. C–H represent previously hypothesised ecological analogues between phytosaurs (C, E, G) and extant crocodylomorphs (D, F, H) (Hunt, 1989): piscivores (C, D) *Ebrachosuchus neukami* (BSPG 1931 X 501) and *Gavialis gangeticus* (BMNH 1935.6.4.1); generalists (E, F) *Leptosuchus crosbiensis*. (TMM 31173-120) and *Paleosuchus palpebrosus* (AMNH R-58136); carnivores (G, H) *Smilosuchus gregorii* (AMNH FR-3060) and *Crocodylus niloticus* (BMNH 1959.1.8.55). Scale bars = 100mm.

(2013). In some cases this morphological similarity led to phytosaurs being classified within Crocodylia (Huxley, 1875; Lucas, 1898). The phylogenetic position of phytosaurs, however, indicates that no close evolutionary link exists between the morphologies of phytosaurs and crocodylomorphs, with similar adaptations arising convergently, presumably in response to shared ecology (Figure 1.2).

Until recently few studies explicitly explored the biology of phytosaurs as living organisms (Camp, 1930; Anderson, 1936; Hunt, 1989). However, recent advances in analytical techniques and a shift in research interests towards biological aspects of fossil organisms have led to the study of phytosaurs as an important component of late Triassic ecosystems, focussing on aspects of phytosaur palaeobiology such as ontogeny (Irmis, 2007) and neurosensory adaptions (Holloway *et al.*, 2013; Lautenschlager & Butler, 2016), as well as biogeography (e.g. Buffetaut, 1993; Brusatte *et al.*, 2013; Stocker & Butler, 2013).

For much of the history of study of the group, the primary focus of phytosaur research has been on systematics (Huene, 1922; Camp, 1930; Gregory, 1962a, b; Ballew, 1989; Long & Murry, 1995; Hungerbühler, 1998a, 2002; Parker & Irmis, 2006; Stocker, 2010, 2012, 2013; Hungerbühler *et al.*, 2013; Butler *et al.*, 2014; Kammerer *et al.*, 2015), with the resulting taxonomic and phylogenetic hypotheses informing biostratigraphy. The identification of easily recognisable and temporally distinct phytosaur subclades, combined with the abundance and cosmopolitanism of the group, led to the use of phytosaurs as key stratigraphic index taxa (Long & Ballew, 1985; Parrish & Carpenter, 1986; Hunt & Lucas, 1991; Lucas & Hunt, 1993; Hunt, 1994a; Lucas, 2010; Martz & Parker, 2017). Despite the importance of phytosaur systematics in biostratigraphy and the recent increased interest in broader evolutionary studies within the group, no taxonomically comprehensive phylogenetic analysis has yet been conducted. The first section of this thesis (Chapter 2) presents the most

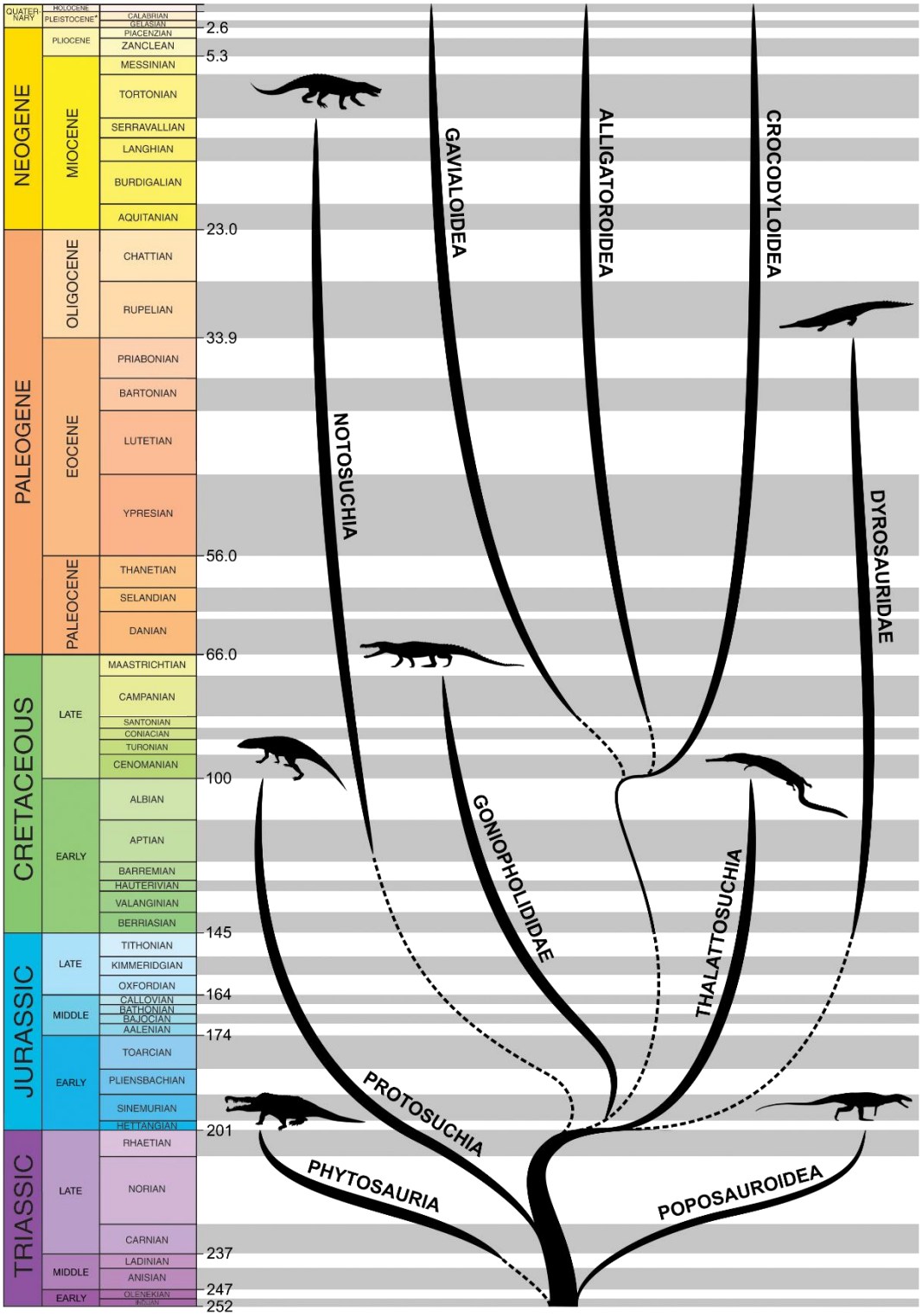

Figure 1.2: Stylised time-calibrated phylogeny showing the relationships within Pseudosuchia, including extant crocodilians, their stem-lineage and phytosaurs (Ezcurra, 2016). This phylogeny is based on data from Nesbitt (2011), Bronzati *et al*. (2012), Brochu (2012), and Ezcurra (2016). Stratigraphic ranges are primarily from the Paleobiology Database (www.paleobiodb.org).

comprehensive phylogenetic analysis of Phytosauria yet undertaken, with an almost two-fold increase in both the number of phylogenetic characters and operational taxonomic units (OTUs) over previous studies. Recently developed character scoring techniques, including continuous and geometric morphometric coding (Goloboff *et al.*, 2006, 2008b; Catalano *et al.*, 2010; Goloboff & Catalano, 2011, 2016), are implemented to aid precision in scoring the group's conservative morphology, and extended implied character weighting (Goloboff & Catalano, 2016) is used to limit the effects of homoplasy.

The resulting phylogeny forms the basis for comparative evolutionary analyses in Chapter 3, which aim to quantify the cranial morphological convergence between phytosaurs and extant and extinct crocodylomorphs. Although a broad similarity between phytosaurs and crocodylomorphs is widely accepted, few studies have attempted to explore these similarities at the species-level (Hunt, 1989; Kimmig & Spielmann, 2011) (Figure 1.1) and none have considered the wide morphological variation present in the crocodylomorph fossil record. By investigating a wide range of potential phytosaur analogues in a phylogenetic context, common morphological evolutionary trends may be recognised, such as iterative divergence into particular areas of morphospace and co-evolving morphologies.

Chapter 4 directly tests previous hypotheses of phytosaur ecology relating to diet (Figure 1.1) using comparative 3D dental microwear analysis with a range of extant crocodylomorphs to reconstruct phytosaur diet. A recognised, but unusual, feature of phytosaur systematics is the simultaneous presence of a robust and a gracile species within most genera (Abel, 1922; Hungerbühler, 2002; Kimmig & Spielmann, 2011; Stocker & Butler, 2013). This has been interpreted in some studies as evidence of sexual dimorphism (Colbert, 1947; Zeigler *et al.*, 2002a, 2003a; Hunt *et al.*, 2006); another view, though not entirely mutually exclusive, is the possibility of dietary niche partitioning (Irmis, 2005),

potentially explaining how multiple phytosaur species were supported in a single ecosystem, as suggested by autochthonous (in-situ) and/or allochthonous (transported) thanatocoenoses. A further feature of phytosaurs is the presence of heterodonty, with three distinct cranial dental morphologies (Hungerbühler, 2000) (Figure 1.3). The function of this heterodonty has never been tested; one hypothesis is the differential use of each dental morphology for separate aspects of food processing (Hungerbühler, 2000), though they alternatively could have been used specifically for the capture/processing of different prey types. In Chapter 4 the association between cranial/dental morphology and diet are investigated, as are the ecological hypotheses of Hunt (1989) (Figure 1.1) which relate phytosaurs to extant crocodylomorph taxa.

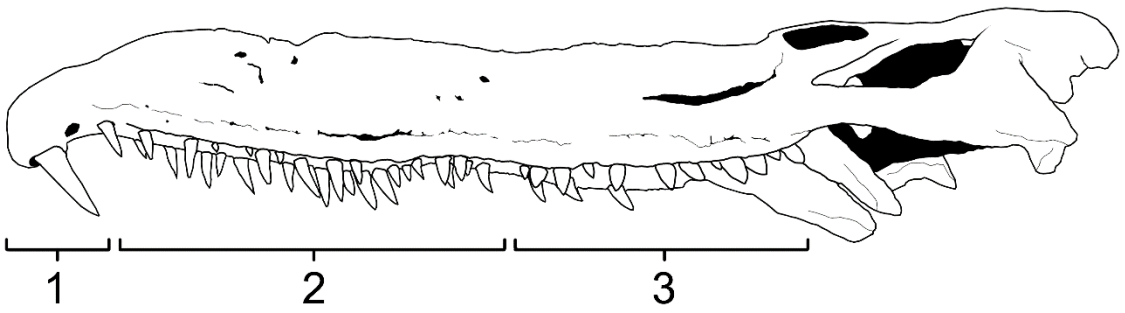

Figure 1.3: Distinct regions of cranial heterodonty in phytosaurs. 1) Large, robust anterior four teeth; 2) slender, recurved conical teeth; 3) robust, slightly recurved phylloform teeth. Image based on SMNS 5727.

The combination of these chapters reveals a great quantity of new information regarding phytosaurs and their morphological and hypothesised ecological convergence with crocodylomorphs. Long held hypotheses of phytosaur relationships, convergence and dietary ecology are also tested in an explicit and quantitative framework, and provide a robust basis from which further studies of phytosaur and archosaur macroevolution can build.

Chapter 2 Publication Statement:

Prior to the submission of this thesis, Chapter 2 was accepted for publication (and is now published) in the academic peer-reviewed journal PeerJ, as "Jones & Butler (2018) *A new phylogenetic analysis of Phytosauria (Archosauria: Pseudosuchia) with the application of continuous and geometric morphometric character coding*".

Chapter 2: A new phylogenetic analysis of Phytosauria

2.1. *Introduction*

By far the most intensively investigated aspect of Phytosauria is their systematics, and due to their abundance, rich fossil record and cosmopolitan distribution phytosaurs have featured heavily in biostratigraphical hypotheses for the late Triassic terrestrial record (Long & Ballew, 1985; Parrish & Carpenter, 1986; Lucas & Hunt, 1993; Lucas, 2010; Martz & Parker, 2017). An important factor for these analyses and others is a robust understanding of evolutionary relationships within Phytosauria. Phytosaur taxonomy has a long, problematic and convoluted history, adding considerable complication to later attempts at understanding phytosaur evolutionary history (Hungerbühler, 2002; Stocker & Butler, 2013). However, with the advent and continued improvement of cladistic techniques, a more cohesive picture has begun to form.

Most previous phylogenetic analyses of the ingroup relationships of Phytosauria have primarily focused on elucidating the relationships of individual or specific sets of taxa (Table 2.1). To achieve this, many analyses opted to reduce their taxonomic scope, and as such have greatly enhanced current knowledge of many areas in phytosaur systematics. However, there is currently no taxonomically comprehensive cladistic dataset which can be used to investigate relationships across all known phytosaur species and clades. The development of such a dataset is an essential prerequisite for carrying out broader evolutionary analyses. To address this gap, this paper has three primary aims:

1) To present the most taxonomically comprehensive phylogeny of Phytosauria to date, including nearly all currently recognized species;

2) To use this phylogeny to investigate the phylogenetic relationships of a number of species and higher-level taxa that have previously been recognized as problematic;

3) To assess the utility of continuous and geometric morphometric character coding techniques, as tools that can potentially expand the information available to assess phytosaur interrelationships.

Table 2.1: Details of all previous cladistic studies of the ingroup relationships of Phytosauria.

	Phyto. OTUs	Characters	Notes on Matrix	Purpose of Analysis
Ballew (1989)	11	64 (39 autapomorphic, five for missing clade)	Novel matrix	First attempt to resolve the ingroup taxonomic relationships of Phytosauria using cladistic methods.
Hungerbühler (1998a)	22	49	Novel matrix. Characters and scorings based on first-hand study only of European taxa; others based on literature.	Tests the proposed monophyly of '*Paleorhinus*' and clarifies the position of *Mystriosuchus*.
Hungerbühler (2002)	10	47	Heavily revised matrix of Hungerbühler (1998a). All scorings based on first-hand study.	Assesses the taxonomic position of *Mystriosuchus* generally, and specifically the newly named species *M. westphali*.
Parker & Irmis (2006)	11	47	Matrix of Hungerbühler (2002), plus *Machaeroprosopus jablonskiae*.	Establishes the taxonomic position of the newly described species *M. jablonskiae*.
Stocker (2010)	19	43	Novel matrix.	Clarifies the interrelationships of *Leptosuchus* and previously associated taxa, and finds the position of the newly described *Pravusuchus hortus*.
Stocker (2012)	19	43	Matrix of Stocker (2010).	Describes and taxonomically places *Protome batalaria*.
Stocker (2013)	19	43	Matrix of Stocker (2010).	Identifies and descries *Wannia scurriensis* as the most basal phytosaur, and discusses the paraphyly of '*Paleorhinus*'.
Hungerbühler *et al*. (2013)	12	41	Novel matrix.	Assesses the interrelationships of *Machaeroprosopus* and '*Redondasaurus*', and provides a description and taxonomic placement for *M. lottorum*.
Butler *et al*. (2014)	22	46	Matrix of Stocker (2010) plus *Ebrachosuchus neukami*, *Parasuchus angustifrons* & *Machaeroprosopus jablonskiae*, and three additional characters.	Redescribes *Ebrachosuchus neukami* and '*Francosuchus*' *angustifrons*; tests and establishes a new monophyletic definition of '*Paleorhinus*'.
Kammerer *et al*. (2015)	24	48	Matrix of Butler *et al*. (2014) plus *Parasuchus hislopi*, *Leptosuchus imperfecta*, and two additional characters.	Redescribes *Parasuchus hislopi*, demonstrates the seniority of the latter genus over '*Paleorhinus*', and overhauls the names of phytosaur sub-family groups.

2.1.1. *Previous cladistic analyses*.

The first cladistic analysis of the ingroup relationships of Phytosauria was performed by Ballew (1989). Her analysis included 11 operational taxonomic units (OTUs) and 64 characters with the aim of establishing character polarity and revising the diagnoses and species assignments of the genera *Rutiodon* and '*Pseudopalatus*'. The analysis generated a tree topology which, in its general structure, has changed relatively little in subsequent analyses. '*Paleorhinus*' and *Angistorhinus* were recovered at the base of Phytosauria, and a polytomy of taxa which Ballew synonymized into *Rutiodon* was recovered as the sister taxon to a clade consisting of *Nicrosaurus*, '*Pseudopalatus*' and *Mystriosuchus* (Figure 2.1a).

Ballew's phylogeny (Figure 2.1a) was used as a basis for Long & Murry (1995) to present a comprehensive taxonomic review of Phytosauria, including the erection of three new genera ('*Arganarhinus*', *Smilosuchus*, '*Arribasuchus*') and the identification of numerous new anatomical characters with potential taxonomic or phylogenetic significance. No numerical phylogenetic analysis or phylogenetic tree was presented, but based on the identification of novel characters a taxonomy was constructed, differing from the phylogeny of Ballew (1989) most importantly in the separation of the taxa included in *Rutiodon* by Ballew into *Leptosuchus* Case, 1922 and the new genus *Smilosuchus*, and in the basal position of *Mystriosuchus* as the sister taxon to '*Paleorhinus*' (previously suggested by Gregory [1962a] and Hunt & Lucas [1989]).

Hungerbühler (1998a) increased taxonomic sampling, including 22 species-level OTUs, and presented a largely novel matrix of 49 characters, of which 12 were based on or reused from previous studies (Ballew, 1989; Long & Murry, 1995). The aims were twofold: to test the idea of a monophyletic '*Paleorhinus*' (Ballew, 1989; Hunt & Lucas, 1991; Long & Murry, 1995), and to more thoroughly assess the phylogenetic position of *Mystriosuchus*.

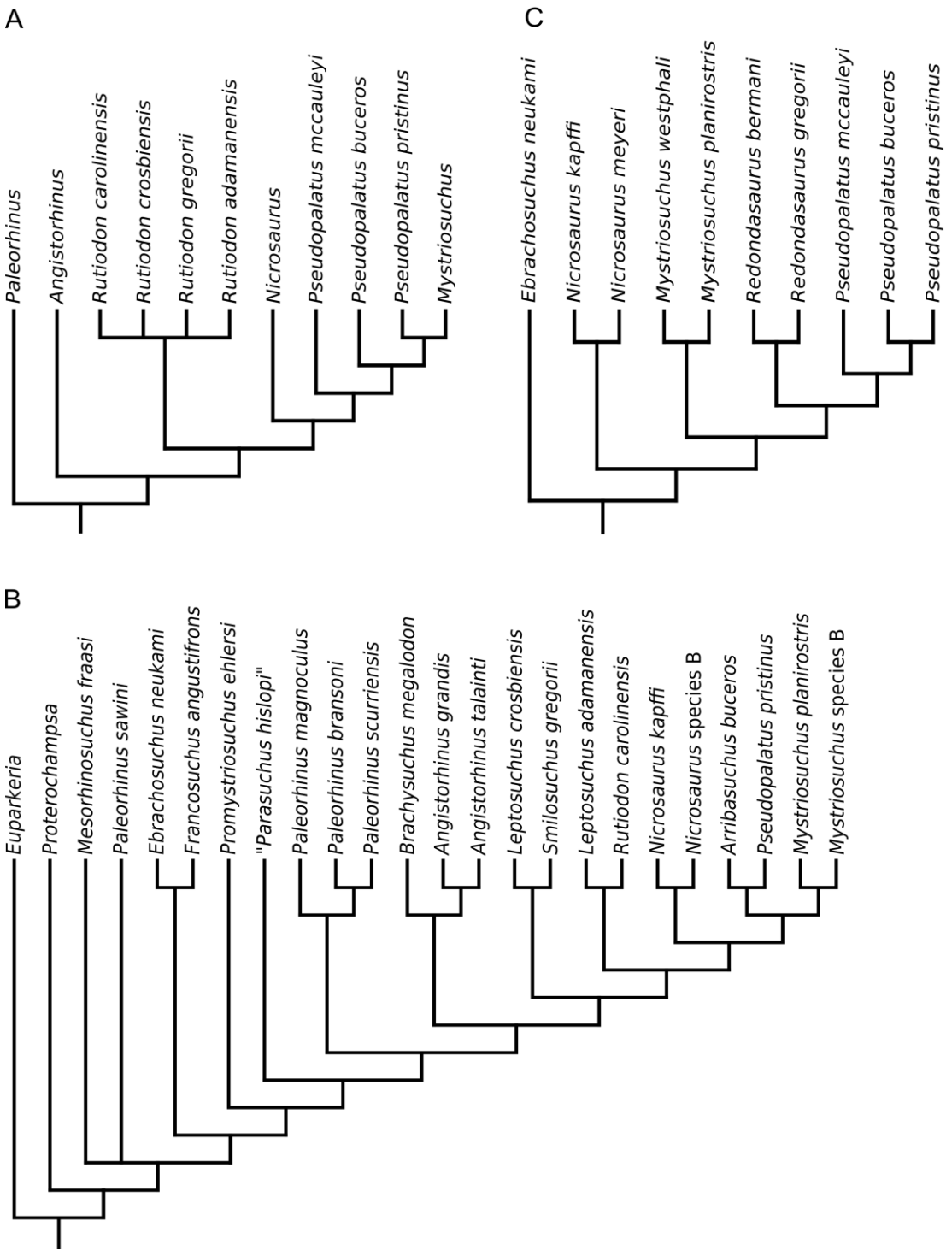

Figure 2.1: Phylogenetic trees from the analyses of (A) Ballew (1989); (B) Hungerbühler (1998a); (C) Hungerbühler (2002).

'*Paleorhinus*' was found to be paraphyletic, with the species previously assigned to the genus recovered as a grade of iteratively more derived taxa at the base of Phytosauria. In agreement with Ballew (1989; Figure 2.1a), *Mystriosuchus* was found in a more derived position than '*Paleorhinus*', but nested as the sister taxon to '*Pseudopalatus*' rather than within this genus (Figure 2.1b).

A substantially revised version of Hungerbühler's (1998) matrix was used by Hungerbühler (2002) to further investigate the relationships of *Mystriosuchus* and assess the phylogenetic position of the newly described species *Mystriosuchus westphali*. Sampling was reduced to 11 taxa and 47 characters (16 taken from the previous study), to focus the analysis on the clade formed of *Nicrosaurus*, *Mystriosuchus* and '*Pseudopalatus*', named 'Pseudopalatinae' by Long & Murry (1995). *Mystriosuchus* was again recovered as the sister taxon to '*Pseudopalatus*'; additionally, the genus '*Redondasaurus*' was found to be monophyletic and outside of '*Pseudopalatus*', contra Hungerbühler *et al.* (2003), but closer to the latter taxon than to *Mystriosuchus*. *Nicrosaurus* was recovered as the sister-taxon of the *Mystriosuchus* + ('*Redondasaurus*' + '*Pseudopalatus*') clade (Figure 2.1c).

The matrix of Hungerbühler (2002) was subsequently used to test the phylogenetic position of '*Pseudopalatus*' *jablonskiae* by Parker & Irmis (2006). This taxon was the only addition to the matrix and was found to occupy the most basal position in the genus '*Pseudopalatus*', with no other changes in tree topology (Figure 2.2a).

In order to better resolve the relationships of the stratigraphically important genus *Leptosuchus* (Camp, 1930; Hunt & Lucas, 1991; Lucas, 2010) and other associated taxa (including those that were synonymized into *Rutiodon* by Ballew, 1989), Stocker (2010) produced a largely novel matrix, incorporating three characters from the matrix of Sereno (1991), and 18 either taken or modified from Hungerbühler (2002). The full matrix consisted

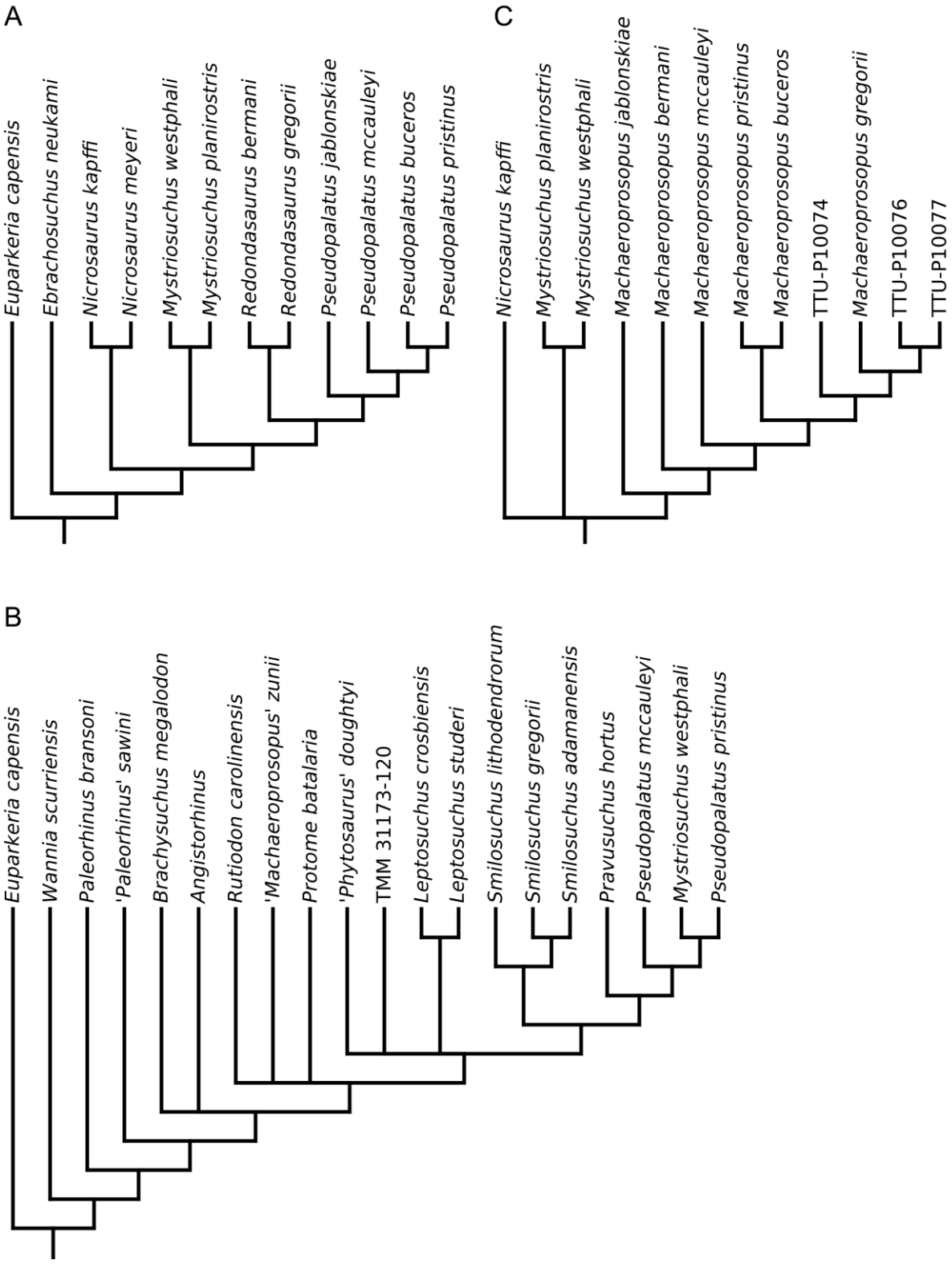

Figure 2.2: Phylogenetic trees from the analyses of (A) Parker & Irmis (2006); (B) Stocker (2013) (topology identical to Stocker, 2010 and 2012); (C) Hungerbühler *et al*. (2013).

of 43 characters scored for 24 OTUs and found *Leptosuchus* to be polyphyletic, with '*Leptosuchus' adamanensis* forming a monophyletic group with *Smilosuchus gregorii* and '*Machaeroprosopus*' *lithodendrorum* (Figure 2.2b). As a result, '*Leptosuchus' adamanensis* and '*Machaeroprosopus*' *lithodendrorum* were reassigned to the genus *Smilosuchus*. *Rutiodon* was not found to be synonymous with *Angistorhinus*, *Brachysuchus* or *Leptosuchus*, contra Ballew (1989), Long & Murry (1995) and Hungerbühler & Sues (2001). The new genus and species *Pravusuchus hortus* was recovered as the sister taxon to 'Pseudopalatinae', and '*Paleorhinus*' *scurriensis* Langston, 1949 was found to occupy the most basal position within Phytosauria (Figure 2.2b).

Following this, Stocker (2012, 2013) presented two further studies in which she first described the new taxon *Protome batalaria* and then redescribed '*Paleorhinus*' *scurriensis*, assigning the latter to the new genus *Wannia*. Phylogenetic aspects of both studies were based on the dataset of Stocker (2010) with no changes or additions. In the latter study, Stocker (2013) provided further discussion questioning the existence of a monophyletic '*Paleorhinus*', supporting the findings of Hungerbühler (1998a; Figure 2.1b).

Although not a phylogenetic study, an important taxonomic alteration was made by Parker *et al.* (2012). The genus name *Machaeroprosopus* was previously considered invalid because the sole specimen of its presumed type species (*Machaeroprosopus validus*, UW 3807) has been lost (Gregory, 1962a); however, Parker *et al.* (2012) established that the holotype specimen of the species *Machaeroprosopus buceros* actually takes priority. The species *Machaeroprosopus buceros* was initially assigned to the genus '*Belodon*', but subsequently made the type species of the genus *Metarhinus* (Jaekel, 1910); however, when this genus was found to be preoccupied, a replacement genus, *Machaeroprosopus*, was erected by Mehl (1915). Inexplicably, the species *Machaeroprosopus validus* was long used

as the genotype of *Machaeroprosopus* despite *Machaeroprosopus buceros* having priority. As the holotype specimen of *Machaeroprosopus buceros* is readily available to study, the genus *Machaeroprosopus* was considered valid by Parker *et al.* (2012), with the type species being *Machaeroprosopus buceros*. Furthermore, *Machaeroprosopus buceros* has been recovered frequently as the sister taxon to '*Pseudopalatus*' *pristinus*, the type species of '*Pseudopalatus*', and has taxonomic priority over that species. As a result, all of the species previously assigned to '*Pseudopalatus*' were reassigned to *Machaeroprosopus* by Parker *et al.* (2012). The clade 'Pseudopalatinae' was, however, retained, as its usage lies outside of the remit of the ICZN, although it has subsequently been replaced by Mystriosuchini (see below, but see Martz & Parker, 2017).

The monophyly of the newly diagnosed *Machaeroprosopus* with respect to '*Redondasaurus*' was tested by Hungerbühler *et al.* (2013); the two species of '*Redondasaurus*' were previously found to nest paraphyletically within *Machaeroprosopus* (Hungerbühler *et al.*, 2003). The primary purpose of the analysis was, however, to test the phylogenetic position of the newly described species *Machaeroprosopus lottorum*. Taxonomic sampling was restricted to 12 OTUs, focussing on the group 'Pseudopalatinae', and 41 characters of which 21 were to some extent based on characters from previous studies (Hungerbühler, 1998a; 2002; Stocker, 2010). '*Redondasaurus*' was found to be paraphyletic and nest within *Machaeroprosopus* (Figure 2.2c), contra Hungerbühler (2002; Figure 2.1c) and Parker & Irmis (2006; Figure 2.2a). *Machaeroprosopus lottorum* was also found to nest within *Machaeroprosopus*, bridging the gap between the more derived species and specimens previously referred to '*Redondasaurus*' and the specimens traditionally belonging to *Machaeroprosopus.*

Finally, two further studies were carried out based on the matrix of Stocker (2010, 2012, 2013), both with the aim of redescribing basal phytosaur taxa previously assigned to '*Paleorhinus*' and elucidating the relationships of basal phytosaurs. Butler *et al.* (2014) redescribed the taxa '*Paleorhinus*' *angustifrons* (Kuhn, 1936) (formerly '*Francosuchus*') and *Ebrachosuchus neukami* Kuhn, 1936, and established a robust set of synapomorphies (which were incorporated into the phylogenetic data matrix) to diagnose a revised, restricted definition of '*Paleorhinus*' that included the species '*Paleorhinus*' *bransoni* and '*Paleorhinus*' *angustifrons* (Figure 2.3a).

Kammerer *et al.* (2015) produced a redescription of *Parasuchus hislopi* Lydekker, 1885 and found it to be the sister taxon to '*Paleorhinus*' *angustifrons*, supported by two unambiguous synapomorphies. Given the designation by the ICZN of a neotype for *Parasuchus* (Chatterjee, 2001; ICZN, 2003), this genus takes priority over '*Paleorhinus*' as the senior synonym. As a result, all species in the monophyletic '*Paleorhinus*' group were reassigned to the genus *Parasuchus* (Figure 2.3b). Kammerer *et al.* (2015) also presented an update to phytosaur family-level and subfamily groups, including the following groups, from most inclusive to most exclusive: Parasuchidae Lydekker, 1885, Mystriosuchinae von Huene, 1915 (formerly Phytosauridae Jaeger, 1828), Leptosuchomorpha Stocker, 2010, and Mystriosuchini von Huene, 1915 (formerly 'Pseudopalatinae' Long & Murry, 1995 [sensu Parker & Irmis, 2006]). For consistency, the nomenclature used by Kammerer *et al.* (2015) is used henceforth throughout this study, with some minor modification to phylogenetic definitions (Table 2.2; see below).

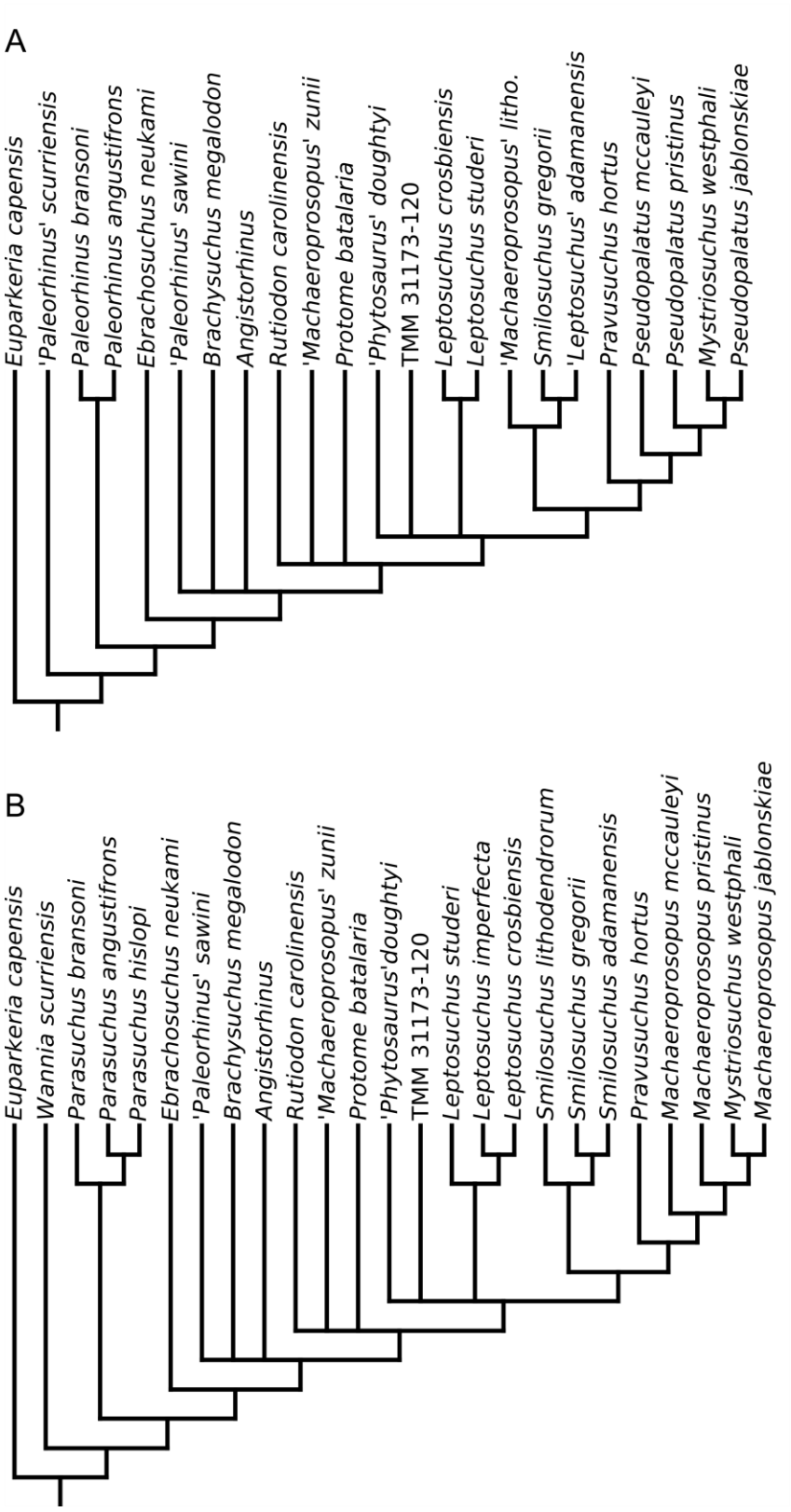

Figure 2.3: Phylogenetic trees from the analyses of (A) Butler *et al*. (2014); (B) Kammerer *et al*. (2015).

2.1.2. *Current consensus*.

Following the revision conducted by Kammerer *et al*. (2015), phytosaurs are currently considered to fall into five successively less inclusive groups: Phytosauria, Parasuchidae, Mystriosuchinae, Leptosuchomorpha and Mystriosuchini (Table 2.2).

Phytosauria Jaeger, 1828, is a stem-based clade which encompasses all phytosaurs. Previously the membership of the groups Phytosauria and Parasuchidae overlapped completely (Kammerer *et al.*, 2015); however, since the re-evaluation of *Diandongosuchus* (Stocker *et al.*, 2017) this taxon has been included within Phytosauria, but excluded from Parasuchidae. However, this placement remains untested in any analysis of ingroup phylogeny to date.

Parasuchidae Lydekker, 1885 (Chatterjee, 1978; Kammerer *et al*., 2015) contains the basal genera *Parasuchus*, *Ebrachosuchus* and *Wannia*, plus all phytosaurs belonging to Mystriosuchinae, Leptosuchomorpha and Mystriosuchini. Following the work of Stocker (2013), *Wannia* has consistently been recovered as the most basal phytosaur within Parasuchidae (Figure 2.2b), being distinct from the more derived *Parasuchus* clade defined by Butler *et al*. (2014) and Kammerer *et al*. (2015). The latter two studies also recovered *Ebrachosuchus* in a more derived position than *Parasuchus* (Figure 2.3a, b).

Mystriosuchinae von Huene, 1915 excludes basal phytosaurs, being defined as 'the last common ancestor of *Mystriosuchus planirostris* (Meyer, 1863) and *Angistorhinus grandis* Mehl, 1913 and all of its descendants' (Kammerer *et al*., 2015), and is largely equivalent to Phytosauridae of previous analyses. In addition to Leptosuchomorpha and Mystriosuchini, this group may also contain taxa previously synonymized with '*Paleorhinus*', such as '*Paleorhinus*' *sawini*, and other genera, including *Rutiodon, Angistorhinus, Brachysuchus,* and *Protome*. The relationships between *Angistorhinus*, *Brachysuchus* and '*Paleorhinus*' *sawini* are unresolved, but all of these taxa have been recovered as more derived than

Parasuchus and basal to *Rutiodon* and *Protome*, with the latter two taxa being placed in a polytomy together with Leptosuchomorpha (Figures 2.2b, 2.3a, b).

Leptosuchomorpha Stocker, 2010, was previously defined as the most recent common ancestor of *Leptosuchus studeri* and *Machaeroprosopus pristinus* and all descendants thereof. I introduce a slight modification to this definition here (Table 2.2) in response to my phylogenetic results, and include *'Smilosuchus' lithodendrorum* as an additional internal specifier to ensure that minor topological rearrangements between taxa that have consistently been considered as leptosuchomorphs do not jeopardize the stability of the clade. Therefore, in addition to members of Mystriosuchini, Leptosuchomorpha contains all species of *Leptosuchus* and *Smilosuchus*, as well as probably the taxa '*Phytosaurus*' *doughty* and *Pravusuchus hortus*. *Leptosuchus* has been supported as monophyletic by recent analyses, though its possible relationship with '*Phytosaurus*' *doughty* is unresolved. *Smilosuchus* has also been supported as monophyletic, and recovered as the sister taxon to *Pravusuchus* + Mystriosuchini.

Mystriosuchini von Huene, 1915, excludes all but the most derived phytosaurs, and was defined by Kammerer *et al*. (2015) as 'the last common ancestor of *Mystriosuchus planirostris* (Meyer, 1863), *Nicrosaurus kapffi* (Meyer, 1860) and *Machaeroprosopus buceros* (Cope, 1881) and all of its descendants'. I modify this definition here by excluding *Nicrosaurus kapfii* from the list of internal specifiers and introducing *Machaeroprosopus jablonskiae* as a replacement to maximize the taxonomic stability of Mystriosuchini among the trees recovered here (Table 2.2; see below). Mystriosuchini is largely synonymous with 'Pseudopalatinae' Long & Murry (1995), defined phylogenetically by Parker & Irmis (2006), with the exception of the inclusion of *Mystriosuchus* and the possible exclusion of *Nicrosaurus*. Although a basal position of *Mystriosuchus* within Phytosauria, such as

Table 2.2: Higher-level taxonomic changes to family and sub-family group definitions. Included are the two most recent revisions of Phytosauria (Stocker & Butler, 2013; Kammerer *et al*., 2015) and the present study.

Stocker & Butler (2013)	Kammerer *et al.* (2015)	Present study
Phytosauria Jaeger, 1828 (stem): *Rutiodon carolinensis* and all taxa more closely related to it than *Aetosaurus ferratus*, *Rauisuchus tiradentes*, *Prestosuchus chiniquensis*, *Ornithosuchus woodwardi* or *Crocodylus niloticus*	Phytosauria Jaeger, 1828 (stem): unchanged	Phytosauria Jaeger, 1828 (stem): unchanged
(Unnamed node)	Parasuchidae Lydekker, 1885 (node): *Wannia scurriensis*, *Parasuchus hislopi*, *Mystriosuchus planirostris* and all descendants of their most recent common ancestor	Parasuchidae Lydekker, 1885 (node): unchanged
Phytosauridae Jaeger, 1828 (node): *Angistorhinus*, *Leptosuchus studeri*, *Mystriosuchus westphali* and all descendents of their most recent common ancestor	Mystriosuchinae von Huene, 1915 (node): *Mystriosuchus planirostris*, *Angistorhinus grandis* and all descendants of their most recent common ancestor	Mystriosuchinae von Huene, 1915 (node): unchanged
Leptosuchomorpha Stocker, 2010 (node): *Leptosuchus studeri*, *Machaeroprosopus pristinus* and all descendants of their most recent common ancestor	Leptosuchomorpha Stocker, 2010 (node): unchanged	Leptosuchomorpha Stocker, 2010 (node): *Smilosuchus lithodendrorum*, *Leptosuchus studeri*, *Machaeroprosopus pristinus* and all descendents of their most recent common ancestor
Pseudopalatinae Long and Murry, 1995 (node): *Nicrosaurus kapffi*, *Mystriosuchus westphali*, *Machaeroprosopus pristinus*, *Redondasaurus gregorii* and all descendants of their most recent common ancestor	Mystriosuchini von Huene, 1915 (node): *Nicrosaurus kapffi*, *Mystriosuchus planirostris*, *Machaeroprosopus buceros* and all descendants of their most recent common ancestor	Mystriosuchini von Huene, 1915 (node): *Mystriosuchus planirostris*, *Machaeroprosopus jablonskiae*, *Machaeroprosopus buceros* and all descendents of their most recent common ancestor

positioned as the sister taxon to '*Paleorhinus*', has been suggested in multiple studies (Gregory 1962a; Hunt & Lucas, 1989; Long & Murry, 1995), this hypothesis has not been supported by quantitative cladistic analyses. A derived position for *Mystriosuchus* within Mystriosuchini has been found in all cladistic analyses thus far (Ballew, 1989; Hungerbühler, 1998a; 2002; Parker & Irmis, 2006; Stocker, 2010; 2012; 2013; Hungerbühler *et al.*, 2013; Butler *et al.*, 2014; Kammerer *et al.*, 2015), and therefore seems relatively uncontroversial. The position of *Mystriosuchus* with respect to other taxa in Mystriosuchini is less well resolved, as discussed below. The European genus *Nicrosaurus* has been included within Mystriosuchini (Long & Murry, 1995; Parker & Irmis, 2006; Kammerer *et al.*, 2015); however, the validity of this is also discussed below. The remainder of Mystriosuchini consists of species referred to *Machaeroprosopus* and '*Redondasaurus*', the relationships of which also differ between studies.

2.1.3. *Current uncertainties*.

Although *Rutiodon* has been consistently found close to, but in a more derived position than, *Angistorhinus*, this relationship has been tested in only three relatively independent matrices (Ballew, 1989; Hungerbühler, 1998a; Stocker, 2010), of which the two earliest contain potential problems, including the use of parsimony uninformative characters, and the outgroup taxon representing homoplastic, rather than ancestral morphology. It has previously been suggested that *Angistorhinus* and *Rutiodon* may be synonymous (Hungerbühler & Sues, 2001), although this has never been explicitly tested or fully published.

Aside from the study of Hungerbühler (1998a), *Angistorhinus* has only been used as a generic-level OTU, or represented by a single species (Kammerer *et al.*, 2015). Kammerer *et al*. (2015) used *Angistorhinus grandis* to score the genus; however, no further discussion of

relationships within the genus was presented. The systematics of the genus *Angistorhinus* are another important area which is currently poorly understood within phytosaurs.

Nicrosaurus kapffi is generally accepted as the most basal member of Mystriosuchini, and was used as a reference taxon in the previous phylogenetic definition of the group (Kammerer *et al*., 2015; Table 2.2); however, only the early studies of Ballew (1989) and Hungerbühler (1998a) have tested this position. *Nicrosaurus* has been included in two other relatively independent analyses (Hungerbühler, 2002; Hungerbühler *et al*., 2013); however, the aims of these studies did not necessitate the inclusion of taxa from outside of Mystriosuchini, and therefore the position of the genus within global phytosaur phylogeny was not tested. Therefore, although the position of *Nicrosaurus* has not been contested, it is also not especially well supported by available data.

The position of *Mystriosuchus* within Mystriosuchini remains unclear, having been placed as either sister to the clade of *Machaeroprosopus* + '*Redondasaurus*' (Hungerbühler, 1998a; 2002; Parker & Irmis, 2006; Hungerbühler *et al*., 2013) or nested within *Machaeroprosopus* (Ballew, 1989; Stocker, 2010; Butler *et al*., 2014; Kammerer *et al*., 2015). As the genus name *Mystriosuchus* Fraas, 1896 has priority over *Machaeroprosopus* Mehl, 1915, this later relationship may have extensive taxonomic implications.

In multiple studies '*Redondasaurus*' has been found to nest within *Machaeroprosopus* (Ballew, 1989; Hungerbühler *et al*., 2003; Stocker, 2010; Hungerbühler *et al*., 2013; Butler *et al*., 2014; Kammerer *et al*., 2015), whereas in others '*Redondasaurus*' is monophyletic to the exclusion of *Machaeroprosopus* (Hungerbühler, 1998a; 2002; Parker & Irmis, 2006). In the most recent phylogeny of derived phytosaurs (Hungerbühler *et al*., 2013), '*Redondasaurus*' was found to nest within *Machaeroprosopus* and the two were tentatively synonymized, but this hypothesis requires further testing.

2.2. *Materials & Methods*

2.2.1. *Institutional abbreviations*

AMNH: American Museum of Natural History, New York, USA; **GPIT**: Institut für Geologie und Paläontologie Tübingen, Tübingen, Germany; **KU**: University of Kansas, Lawrence, USA; **MB**: Museum für Naturkunde, Berlin, Germany; **MNHN**: Muséum National d'Histoire Naturelle, Paris, France; **MU**: University of Missouri, Columbia, Missouri, USA; **NHMW**: Naturhistorisches Museum Wien, Vienna, Austria; **NMMNHS**: New Mexico Museum of Natural History and Science, Albuquerque, USA; **OMNH**: Oklahoma Museum of Natural History, Norman, USA; **PEFO**: Petrified Forest National Park, Arizona, USA; **SMNS**: Staatliches Museum für Naturkunde Stuttgart, Stuttgart, Germany; **TMM**: Texas Memorial Museum, Austin, USA; **TTU-P**: Museum of the University of Texas Tech, Lubbock, USA; **UCMP**: University of California Museum of Paleontology, Berkeley, USA; **UMMP**: University of Michigan Museum of Paleontology, Ann Arbor, USA; **USNM**: National Museum of Natural History, Washington D.C., USA; **UW**: University of Wisconsin Geological Museum, Madison, USA; **YPM**: Yale Peabody Museum, New Haven, USA.

2.2.2. *Material*

The analysis presented here uses species as OTUs to facilitate comparison with previous phylogenetic analyses. There has been recent interest in specimen-level phylogenetic analyses in vertebrate palaeontology (e.g. Upchurch *et al.*, 2004; Tschopp *et al.*, 2015), but the validity of this approach and its results remain largely unexplored. I did not use a specimen-level phylogeny here as it would be hampered by the range of intraspecific variation found in most

taxa, and would be further compounded by poor preservation in many specimens resulting in high quantities of missing data and widespread polytomies due to unstable terminals.

The OTUs included in this analysis consist of 34 species across 18 genera which are fully detailed in Appendix section S1.1. An additional nine specimen level OTUs were also included to test their affinities. I attempted to sample all phytosaur species currently regarded as taxonomically valid or potentially taxonomically valid, with the exception of a number of problematic species that were excluded for reasons discussed below. *Euparkeria capensis* was used to root the analysis as it displays a generalized archosauriform cranial morphology (Sookias, 2016) which has been used in previous studies for character polarization (Hungerbühler, 2002; Parker & Irmis, 2006; Stocker, 2010; 2012; 2013; Butler *et al.*, 2014; Kammerer *et al.*, 2015). *Diandongosuchus fuyuanensis*, a taxon from the Middle Triassic of China initially identified as a basal poposauroid (Li *et al*., 2012), was recently re-interpreted as the basal-most phytosaur currently known (Stocker *et al.*, 2017) and is therefore included in this analysis to verify its basal position within Phytosauria.

Of the 43 OTUs included in this analysis, 39 were scored based on first-hand study of at least one of the referred specimens. Photographs and published descriptions and figures were also used where available. The remaining four terminals (*Leptosuchus studeri*, *Diandongosuchus fuyuanensis*, *Euparkeria capensis* and *Parasuchus hislopi*) were not studied first hand for the purposes of this study, and were scored from photographs and/or published descriptions and figures.

2.2.3. *Excluded taxa*

Although this analysis was designed to be the most comprehensive cladistic dataset for phytosaurs to date, a small number of taxa were excluded for various reasons.

Angistorhinus gracilis Mehl, 1915, from the Popo Agie Formation in Wyoming, was only very briefly described in the original paper, and a holotype was not formally designated, despite apparently consisting of a large skull and much of the postcrania of a single phytosaur. When ASJ visited the University of Missouri this material could not be found; however, it may be located in one of many footlockers containing the 'Mehl collection' in the basement of the department (James Schiffbauer, pers. comm. to ASJ, 2016). At present this material is considered lost with no images available other than a line drawing of the antorbital region and two photographs of an anterior thoracic vertebra (Mehl, 1915); because the proportion of missing data would likely hinder any analysis more than its inclusion would contribute, I excluded this taxon.

Angistorhinus maximus Mehl, 1928 is known from the orbital and postorbital portions of a single skull (MU 531) from the top of the Popo Agie Formation in Wyoming. Long & Murry (1995) noted apparent similarities between this species and *Angistorhinus talainti* from Morocco, but also suggested this material may represent a more derived taxon, not referable to *Angistorhinus*. They noted that determining the taxonomic affinities would require detailed study and the type material 'may be lost' (Long & Murry, 1995:42). This material is also suspected to reside in the 'Mehl collection' of the University of Missouri. As this material is considered lost and no images exist aside from the five line drawings in Mehl (1928), it was excluded from analysis.

Angistorhinus alticephalus Stovall and Wharton, 1936 is represented by an incomplete skull, nine vertebrae, rib fragments and osteoderms (OMNH 733) from the Dockum Group of Texas. This species is differentiated from other *Angistorhinus* species primarily by the more laterally directed orbits, the shape of the squamosal and the straight mediolateral frontal-parietal suture (Stovall and Wharton, 1936). It has been suggested that the direction of the

orbits should be used cautiously due to taphonomic distortion (Gregory, 1962a; Hungerbühler, 1998a) and is 'severely restricted' in practical use due to the difficulty in taking measurements and previous scoring subjectivity (Hungerbühler, 1998a: 130); therefore, a more detailed taxonomic analysis of this specimen is required to verify its distinctness, which is beyond the scope of this study. Given the incomplete nature of the type material, the range of better *Angistorhinus* material available to study and the taxonomic uncertainty regarding its validity, *A. alticephalus* was excluded from this study.

Angistorhinus aeolamnis Eaton, 1965 is known from a single skull, lacking approximately its dorsal 50–80 millimetres (KU 11659) from the Dockum Group of Texas. As far as can be seen from its original description, the skull does not preserve any of the features indicative of the genus *Angistorhinus*, such as posterior parietal extensions or the parietal-squamosal bars forming a posterolateral curve when viewed dorsally (Long & Murry, 1995). The loss of the dorsal part of the skull also greatly reduces the number of characters for which this specimen could be scored, making it likely to be problematic in phylogenetic analysis; this combined with its unclear taxonomic affinities leads me to exclude this taxon.

Brachysuchus megalodon Case, 1929 is a very robust taxon, represented by the largely complete, but dorsoventrally crushed holotype skull (UMMP 10336), a likely associated mandible (UMMP 10336a) and a second, well preserved, also largely complete skull (UMMP 14366), from the Dockum Group of Texas. *B. megalodon* has historically been a difficult taxon to interpret, being synonymized with '*Phytosaurus*' (Gregory, 1962a) and *Angistorhinus* (Long and Murry, 1995) before being provisionally resurrected by Stocker (2010) pending a full reanalysis of the taxon. *B. megalodon* is excluded here because the material was unavailable for study due to the redevelopment of the UMMP museum. Although the original description by Case is very detailed and contains many line drawings, it

was deemed unfeasible to score such a taxonomically problematic specimen that has been subjected to severe taphonomic distortion from images alone, especially as the less distorted referred specimen has only ever been figured in palatal view (Case & White, 1934).

'*Machaeroprosopus validus*' Mehl, 1916 was erected on the basis of an incomplete skull (UW 3807) from the Chinle Formation of Arizona. This specimen, which has been lost (Westphal, 1979), was long considered to be the holotype specimen for the genus *Machaeroprosopus* (Case, 1920; Camp, 1930; Colbert, 1947; Ballew, 1989; Hungerbühler, 1998a). However, the holotype of *Machaeroprosopus buceros* was recently found to take priority (Parker *et al.*, 2012). Considering the loss of the only specimen and its now decreased taxonomic significance and uncertain taxonomic position this taxon is here excluded.

Mesorhinosuchus fraasi (Jaekel, 1910) was named based on a single partial skull, reportedly from the Middle Buntsandstein of Saxony-Anhalt, Germany. The supposed type locality is dated as Olenekian in age, making this potentially the stratigraphically oldest phytosaur, and predating even *Diandongosuchus* by approximately 10 million years. The specimen, which was housed at the University of Göttingen, was destroyed in WWII and only one photograph exists in the original description by Jaekel (1910); moreover, its stratigraphic provenance has frequently been questioned (Gregory, 1962a; 1969; Hunt and Lucas, 1991). In any case this species is excluded due to the loss of the type specimen.

'*Paleorhinus magnoculus*' Dutuit, 1977a is represented by a single, very small (275 mm anteroposterior length) juvenile skull (MNHN ALM 1) from the Argana Formation of Morocco. It was originally described as a unique species of '*Paleorhinus*' due to (among other features) its proportionately enormous orbits and small antorbital fenestrae; however, these putative autapomorphies were later reinterpreted as a reflection of the early ontogenetic stage of the type specimen (Fara and Hungerbühler, 2000) and the species was reclassified as

an indeterminate specimen of *Parasuchus*, a view that is shared in this study (but see Kammerer *et al*., 2015). This taxon is therefore excluded from this study because the inclusion of ontogenetically variable features could affect its phylogenetic placement, as has been extensively reported in dinosaurs (Rozhdestvensky, 1965; Dodson, 1975; Sampson *et al.*, 1997; Scanella & Horner, 2010; Tsuihiji *et al*., 2011).

Promystriosuchus ehlersi (Case, 1922) is known from a poorly preserved partial skull from the Dockum Group in Texas (UMMP 7487). The specimen displays extensive dorso-ventral crushing with many elements not retaining their original associations; as such, it is a difficult specimen to interpret. It has previously been referred to '*Paleorhinus*' (=*Parasuchus*) (Gregory, 1962a; Hunt and Lucas, 1991; Long and Murry, 1995), but more recently its taxonomic position has been seen as uncertain (Kammerer *et al*., 2015). As with *B. megalodon* the sole specimen of this taxon was unavailable for study, and it represents a taxonomically uncertain specimen with challenging morphology and few images available in the literature; for these reasons *Promystriosuchus ehlersi* is not included in this study.

2.2.4. *Continuous data in cladistics*

The use of continuous characters in cladistics has historically been controversial, with many researchers questioning their validity and appropriateness to cladistic methods (Crisp & Weston, 1987; Pimentel & Riggins, 1987; Cranston & Humphries, 1988; Felsenstein, 1988; Stevens, 1991). The majority of concerns raised have been around the discretization of frequently overlapping taxonomic ranges of continuous measurements into distinct character states using methods often criticized as arbitrary (Poe & Wiens, 2000).

Indeed, techniques such as gap-coding (Mickevich & Johnson, 1976) and segment-coding (Thorpe, 1984; Chappill, 1989) do suffer from elements of arbitrariness: in gap-coding

the size of the fundamental gap, and in segment-coding the number of segments, must be specified by the researchers (Rae, 1998). These metrics may be based on various statistical concepts, such as 95% confidence intervals or standard deviations about the mean, and data may be treated on a linear or logarithmic scale; however, as shown by Gift & Stevens (1997) the choice of which metric to use can have a profound effect on the final character states.

Despite the general rejection of continuous data by many authors, continuous ranges of overlapping data have remained common in cladistic matrices, scored via character states with arbitrary 'discrete' cutoffs, which are generally not explained or justified, e.g. 'ratio of femoral length to width: <6 [0], ≥6 [1]', or 'shape of orbit: circular [0], oval [1]' (Stevens, 1991; Poe & Wiens, 2000; Wiens, 2001). These arbitrary character states have been shown to convey little phylogenetic information compared to identical data ranges coded using gap-weighting (Garcia-Cruz & Sosa, 2006). Despite this, these types of characters are frequently found in modern cladistic datasets, including recent analyses of phytosaur phylogeny (Hungerbühler, 2002; Hungerbühler *et al.*, 2013; Parker & Irmis, 2006; Stocker, 2010; 2012; 2013; Butler *et al.*, 2014; Kammerer *et al.*, 2015). This study aims to incorporate continuous morphological data, including that of 'shape', characterized in a non-arbitrary manner to increase the quantity of phylogenetically useful information available to studies of phytosaur systematics, with the goal of increasing their accuracy and resolution.

As expressed above, the main problem with many continuous coding techniques is the arbitrary splitting of range data into discrete character states. The software package TNT overcomes this problem by employing a similar technique to gap-weighting (Thiele, 1993) and step-matrix gap-weighting (Wiens, 2001). Gap-weighting splits the range of species mean values into as many character states as allowed by the software (32 in PAUP*), thus increasing coding resolution and (as the characters are ordered) ensuring large changes must

pass through many steps in comparison to small changes, thus increasing their weight. This technique is, however, hampered by the limits imposed by the software. Step-matrix gap-weighting follows a similar initial procedure, but circumvents the limit on character weighting by using the sizes of the gaps between unique character states, rescaled along a range from zero to the maximum steps allowed by the software (1000 in PAUP*), to create step-matrix values to weight character state changes. Although gap-weighting provides a higher resolution of states into which measured variation can be categorized, the categorization method is still fundamentally arbitrary and, due to this, taxon ranges that are significantly different may be grouped together and those that are statistically identical may be split up (Farris, 1990).

The techniques developed in TNT (Goloboff *et al.*, 2006; Goloboff *et al.*, 2008b), and used in this study, remove arbitrary discretization by analysing the taxon range values as they are, i.e. without being grouped into character states. This is possible through the use of Farris' (1970) down-pass and Goloboff's (1993) up-pass algorithms which are designed to use numerical differences between the states being optimized; therefore, the actual intervals between taxon data ranges, being numerical, are treated in the same way as ordered character states (Goloboff *et al.*, 2006). As mentioned in Goloboff *et al.* (2006), step-matrix gap-weighting would produce the same outcome as the TNT technique; however, this approach becomes difficult with a large number of taxa and is not capable of handling ranges of variation. As the scale of the step changes, and therefore weights, are directly proportional to the measured data, the magnitude on which the original measurements were made could have a large (and often unwarranted) influence on character weighting. Goloboff *et al.* (2006) suggested that implied weighting (re-weighting of characters based on their level of homoplasy) can reduce this issue, however, this was found to be only a partial solution and a

combination of implied weighting and re-scaling trait measurement values to unity produced far more satisfactory results (Koch *et al.*, 2015).

2.2.5. *Geometric morphometric data*

Geometric morphometric (GM) characters are a relatively new development in cladistics (Catalano *et al.*, 2010; Goloboff & Catalano, 2011, 2016). In relation to phylogenetics, the use of geometric morphometrics tends to be equated with phenetic studies and the use of techniques such as principal components analysis to reduce overall morphology to a small number of axes of covariation. The method presented by Catalano *et al.* (2010) avoids this: x, y and z landmark coordinates are used, without transformation, to generate ancestral state reconstructions using a spatial optimization technique which minimizes displacement between individual, or configurations of, landmarks from two descendants. A thorough discussion of the applicability of geometric morphometrics in phylogeny is given by Catalano *et al.* (2010) in which previous arguments against its use are also addressed. When integrated into a phylogenetic analysis of Vespinae (Perrard *et al.*, 2015), landmark characters were generally found to improve tree resolution when combined with a morphological character matrix. Landmark characters still exerted a noticeable effect with the addition of molecular data, though only four of the ten relationships generated by landmark data were supported in the morphological + landmark + molecular data trees (Perrard *et al.*, 2015). In these trees the landmark data mostly affected poorly supported nodes - allowing greater resolution, though possibly only due to over-resolution due to the analysis techniques. It was also found that the landmark data alone were insufficient to reliably resolve relationships, likely due to homoplasy arising from the functional unit in which the landmark characters were placed (Perrard *et al.*, 2015). Although the quantity of information may be increased by using

landmark characters, not all information is included, which could lead to important features being excluded.

2.2.6. *Character coding*

The character list (Appendix section S1.2) was constructed by combining those used in previous analyses (Ballew, 1989; Hungerbühler, 2002; Stocker, 2010; Butler *et al*., 2014; Kammerer *et al.*, 2015) as well as by identifying new characters based on first-hand study of specimens and published literature. In order to compare the effects of different character types on phylogenetic results, all characters (including continuous and GM) were scored and inputted into one matrix, each character type as a different data block. The resulting matrix contained three blocks of data: discrete scores, continuous ranges and GM coordinates. Many of the continuous and GM characters were based on discrete characters from previous analyses, for which the categorization of character states seemed inappropriate, e.g. for relative linear measurements of morphological features, or complex morphologies. Therefore, some characters in the discrete data block are discrete versions of continuous or GM characters. Some continuous and GM characters incorporated here were novel; therefore, discrete versions of these were also created in the discrete data block to ensure that where phylogenies were analysed using different data types, any differences in results would not be affected simply by differences in the exact morphological information included. The different combinations of character types were incorporated into different analyses by setting either the continuous, GM, or both character blocks to ‘active’ or ‘inactive’ in the phylogenetic software TNT (see below).

The number of characters and proportion of missing data in each data block are summarized in Tables S1.1 & S1.2. No characters were excluded based on quantity of

missing data in scored taxa as including more characters, even if this increases the proportion of missing data, has been shown to increase accuracy in phylogenetic analysis (Wiens, 1998). This technique increases the possibility of long branch attraction (Swofford *et al.*, 1996), but is less likely in a dataset where missing data is distributed randomly among all taxa (Poe & Wiens, 2000); in my dataset missing data seem more likely to occur in certain taxa and certain characters, therefore the possibility of long branch attraction should be kept in mind when interpreting the results.

A consistent discrete matrix was used as a base for each analysis, into which continuous or GM characters were swapped with their discrete counterparts. The discrete data block consisted of 94 characters, the continuous block 10 characters and the GM block five characters. These were combined in four analyses (Table 2.3): 1) discrete characters only (D coding treatment) (94 characters, 21 of which are ordered), 2) discrete + continuous characters (DC coding treatment) (94 characters, 21 ordered), 3) discrete + GM (DM coding treatment) (90 characters, as some GM characters encompass variation described by more than one character in the discrete dataset; 19 ordered), 4) discrete + continuous + GM (DCM coding treatment) (90 characters, 19 ordered). A full list of all characters, ordering and the correspondences of continuous and GM to discrete characters is available in Appendix section S1.2. The coding procedures used here for continuous and GM characters are described below, as are the methods of character state distinction for their discretized counterparts.

It is important to note here that when incorporating continuous and geometric morphometric character scorings for analysis, the format of the TNT data file requires these characters to be presented first in the file. This differs from how the characters are ordered in my character list (Appendix section S1.2). My character list presents characters in the order in which they occur for the base discrete data block; where a character possesses a continuous or

GM variant this is flagged next to that character. It should also be noted that characters in a TNT file begin at zero, whereas I shift my characters such that the list begins at one.

Table 2.3: Summary of the character composition for all four datasets (D, DC, DM & DCM) analysed in this study.

	No. of characters	Description	Characters encoded using continuous or GM methods
D	94	Discretely encoded characters only	None
DC	94	Discretely & continuously encoded characters (no characters scored using GM)	8, 11, 25, 38, 43, 54, 60, 87, 89, 94
DM	90	Discretely & GM encoded characters (no characters scored continuously) *[Reduced character count, as GM characters often correspond to multiple discrete characters]*	39, 40, 46, 50, 54, 55, 81, 89, 91
DCM	90	Discretely, continuously & GM encoded characters (all scoring methods used) *[Reduced character count, as above]*	8, 11, 25, 38, 39, 40, 43, 46, 50, 54, 55, 60, 81, 87, 89, 91, 94

2.2.6.1. *Continuous characters*

Measurements were taken from all referred specimens with the appropriate morphology preserved, either directly, using digital callipers, or from photographs, using the software ImageJ. Standard error was calculated about the mean score of each species, this was then used to calculate min-max species ranges with statistically meaningful differences (Goloboff *et al.*, 2006). Min-max species range values were rescaled in each character using the formula: $z_i = x_i - min(x) / max(x) - min(x)$ where z_i is the rescaled value, x_i is the original value and min/max(x) are respectively the minimum and maximum original values in the range of

variation across all taxa for that character. This rescales values onto a 0–1 scale, ensuring that magnitudes of interspecific differences within characters are maintained, whilst between-character weighting is standardized. The rescaled range values (and where only one specimen is known, the single values) were input into the data matrix file and treated as ordered.

2.2.6.2. *GM characters*

Many features of phytosaur skulls that are appropriate for shape analysis contain few discrete landmark positions, making traditional landmark analysis difficult, and the resolution of the morphology influencing the results would be poor. For example, only two sutures regularly form connections on the border of the antorbital fenestra that could be landmarked in all phytosaurs, and due to the variable shape of the fenestra there are no consistent 'corners' or other morphological features that can be traditionally landmarked on the border, aside from the most anterior and posterior extremities. Conversely, these problems can be resolved by using sliding semi-landmarks to approximate outline shape; this is the technique used here. In techniques such as principal components analysis, semi-landmarks require special treatment, on account of their reduced dimensionality and therefore degrees of freedom (Bookstein, 1996; Zelditch *et al.*, 2012); however, as TNT does not use such analyses and providing the user employs appropriate Procrustes alignment techniques, nothing precludes their use. Semi-landmarks were digitized from photographs using the 'Draw background curves' tool in the software tpsDig2 (Rohlf, 2015) to capture a detailed outline of the structure; this was then resampled to contain a consistent number of equally spaced points which were used for alignment. See Figure S1.1 for configurations of landmarks in GM characters. Semi-landmarks were subjected to sliding and Procrustes superimposition to minimize distances between configurations using the R package Geomorph (Adams & Otarola-Castillo, 2013). In

TNT, landmark configurations were scaled to unity using the command '*lmark rescale =*;*'. Whole configurations of landmarks were used for optimization and to calculate support values, rather than a pairwise approach with each individual landmark, as semi-landmarks define curves and not homologous points.

2.2.6.3. *Discrete characters*

Characters consisting of continuous measurements such as ratios were discretized into character states using primarily quantitative, but also qualitative approaches; all measurements from all referred specimens were sorted numerically and character state divisions were introduced where gaps occurred in their sequence. Where no substantial gaps occurred character states were introduced at points between substantial transitions in the data. For example: in a hypothetical dataset of four taxa, A–D, each represented by four specimens which all occupy a 0–10 continuous scale for one of their characters, if all or a substantial majority of specimens from taxa A and B sit between zero and five, whereas those of taxa C and D sit between five and ten, the continuous character range would be divided into two character states at number five. This therefore splits the continuous range into discrete states in the absence of gaps.

This treatment was designed to mimic the presumably qualitative techniques for dividing continuous data into discrete states used in previous analyses (although the delimitation technique has never been described in any previous phytosaur phylogeny), and represents a similar treatment to the 'arbitrary' method of Garcia-Cruz and Sosa (2006). Discrete characters used as counterparts to implicitly ordered continuous characters were also treated as ordered. This means that different topologies resulting from different combinations

of character types reflect changes in character coding approach rather than differences in the approach to character ordering.

2.2.6.4. *Implied weighting*

Implied weighting (Goloboff, 1993) is a method of character weighting in which the number of step changes a character undergoes in its current tree topology is compared to the minimum possible for that character, as a metric for homoplasy. Each character in a tree topology is then weighted in inverse proportion to its level of homoplasy, with a concavity constant (k) ascribing the severity of weighting. These weighted scores of 'character fit' are then summed to provide an estimate of character fit for the whole tree; each tree topology in the analysis undergoes the same procedure, with the 'best' overall tree(s) having the best character fit score. I primarily use implied weights here for its apparent advantages in the analysis of matrices high in homoplasy (Goloboff *et al.*, 2008a); a problem well-recognized in Phytosauria (Hungerbühler, 1998a, 2002). Although implied weighting has been criticized recently (Congreve & Lamsdell, 2016) it does also have advantages when using continuous and GM character scorings. Continuous characters may be measured on different scales, and this difference in scaling is transferred to a character's step-matrix (arbitrarily increasing the impact of 'large-scale' characters); accordingly, homoplasy in characters measured on large scales tends to be greater and these characters are thus down-weighted in proportion with this (Goloboff *et al.*, 2006). In this study I further address issues of scaling by standardizing continuous character ranges into a 0–1 range, as described above. Implied weighting also provides a method for weighting landmark-based characters and can be performed either for each individual landmark within a configuration or for whole configurations using the average homoplasy. The latter method is particularly useful in this study as I use semilandmarks; as

such the individual landmarks do not necessarily represent homologous points, rather it is the overall structure that is important - it is therefore the whole configuration of landmarks that should be treated as a single character for weighting.

2.2.7. *Analyses*

All analyses were performed in the software TNT version 1.5 (Goloboff & Catalano, 2016), under extended implied weighting with the concavity constant 'k' set to vary for each character depending on the quantity of missing entries (using '*xpiwe (*' commands).

Implied weighting requires the minimum possible length for each character coding in order to calculate homoplasy; however, this is problematic in landmark data (Goloboff & Catalano, 2016). Therefore, TNT provides an option to find minimum values for each landmark using heuristic searches; this search function was applied before analysing any dataset incorporating GM characters, then the minima were added to the file for use during tree searching. Furthermore, GM characters were each weighted separately according to the average homoplasy of their landmark configuration (using '*xpiwe [*' commands); therefore, weighting was based on entire configurations rather than the sum of component landmarks, which as stated above, may not be individually homologous.

2.2.7.1. *Analysis parameters*

Tree searches were performed using the new technology algorithms in TNT: 10,000 random addition sequences, analysed using TBR swapping with 10 iterations of drift and ratchet, followed by a sectorial search and finally three rounds of tree fusing. The search was performed until the minimum tree length was hit five times. The duration of tree searches dramatically increased with the addition of GM characters; therefore, only 200 random

addition sequences were used and minimum length was found only once. Furthermore, because landmark data is relatively unstructured the perturbation phases of ratchet and drifting can produce trees that are 'too suboptimal' and therefore greatly increase the search time (Goloboff & Catalano, 2016). I therefore followed the suggestion of Goloboff & Catalano (2016) and increased the drift 'xfactor' to 5, decreased the percentage of swapping to be completed to 90%, decreased the number of substitutions to 45, and for ratchet, lowered the probability of reweighting (both up and down) to 3 and decreased the number of substitutions to 30.

Bremer supports were calculated using 10,000 (D and DC) or 1000 (DM and DCM) trees suboptimal by a fit of 10; branch swapping using TBR was performed and absolute supports were calculated based on the results. Robusticity analysis was carried out using symmetric frequencies, with TBR swapping beginning from 10 Wagner trees and 10,000 (D, DC) or 100 (DM, DCM) replicates. As the matrices including GM data were exceptionally computationally heavy and time consuming, parameters were altered such that trees were accepted without consideration of error margin during landmark searches and that swapping distance for branch swapping was reduced (commands respectively: '*lmark errmarg 0*' and '*bbreak : limit 5*').

2.2.7.2. *Output processing and comparisons*

Where more than one tree of best character fit resulted from an analysis, a strict consensus was generated. With implied weighting in effect, ties in tree length (resulting in multiple best fitting trees) become very uncommon due to the use of floating-point character-fit calculations. Additionally, continuous data are analysed as actual numerical differences, rather than categorical steps, also reducing the chance of exact ties. To avoid over-resolution

due to the acceptance of a single or few trees showing only an extremely small difference in character fit compared to other topologies, an arbitrary Bremer support cut-off value of 0.08 was implemented, below which nodes were judged to be poorly supported and were collapsed. In addition a second cut-off value was used (0.11) which was equal to the average step-length of a single character following weighting. This particular number was used in an attempt to emulate the procedure common in phylogenetics, to collapse nodes with a Bremer support of less than one step. These cut-offs were maintained throughout the four treatments, allowing the effects on tree resolution to be compared.

Best character fit trees resulting from each of the four analyses using different combinations of character data types (see above) were compared using several techniques. CI and RI were compared to assess the homoplasy present in the trees resulting from each analysis. Maximum agreement subtrees were constructed for each comparison to compare the number of congruent relationships between the trees; this was supplemented with a strict consensus of the two trees in case lower level congruence was masked in the agreement subtree by higher level polytomies (Goloboff *et al.*, 2006). Subtree pruning and regrafting (SPR) distances were calculated to find the minimum number of changes under the SPR search algorithm required to convert one tree topology into the other - essentially a numerical description of tree similarity. The rooted Robinson-Foulds (RF) distance, which measures the differential presence/absence of phylogenetic relationships between trees, was also used to measure tree-similarity.

The effect of each coding technique was assessed and compared to its alternative counterparts in several ways. Trees were initially compared using mean and summed frequency and Bremer supports across each collapsed tree, alongside the number of nodes retained after collapsing each tree to get a broad view of any major differences. For a more

detailed view of the effects of data type on the nodal support each non-collapsed best fit tree was split into five tree-regions; 1) the most basal portion of the tree, including all non-Mystriosuchinae members of Phytosauria; 2) the clade formed by *Rutiodon* and *Angistorhinus*; 3) *Leptosuchus*-grade taxa, here composed of all *Leptosuchus, Smilosuchus* and *Nicrosaurus* species, plus PEFO 34852, '*Phytosaurus*' *doughtyi, Pravusuchus hortus* and *Coburgosuchus goeckeli*; 4) all members of *Machaeroprosopus* and '*Redondasaurus*', plus USNM V 17098, NMMNHS-P 4256, NMMNHS-P 31094 and *Protome batalaria*; 5) the clade composed of named species of *Mystriosuchus* plus NHMW 1986 0024 0001 and MB.R. 2747. The mean frequency and Bremer supports were calculated within each region to investigate the effects of different character coding techniques at a greater resolution.

The support for monophyly of groups/taxa of interest was investigated by placing them in alternative positions in a constraint tree, then re-running the analysis whilst imposing those constraints and observing the effect on character fit in the resulting trees.

The accuracy of trees, as denoted by the various nodal support metrics and comparisons described above, is a measure of internal consistency; regardless of a tree's accuracy it may still be spurious. Stratigraphic congruence was used here as an independent estimate of tree-validity; four metrics were employed which measure stratigraphic congruence differently. (1) The stratigraphic consistency index (SCI) (Huelsenbeck, 1994) measures the proportion of nodes within which the first appearance datum is of the same age or younger than the sister node; these nodes are considered stratigraphically consistent. (2) The relative completeness index (RCI) (Benton & Storrs, 1994) reports the ratio between the sum of ranges for taxa in the tree and the sum of ghost-range length within the tree. (3) The Manhattan stratigraphic measure (MSM*) (Siddall, 1998; Pol & Norell, 2001) optimizes the difference in age between the first appearances of taxa (Manhattan distance) as a Sankoff

character on the proposed tree. The MSM is the ratio between the minimum possible tree length based on taxon ranges (topology determined by the Manhattan distance character), and the tree length when Manhattan distance is optimized to the original topology. The MSM is basically the consistency index of the distance character (Pol & Norell, 2006). Pol & Norell (2001) introduced a correction to prevent reversals in the Manhattan distance character 'states', presenting the updated metric, MSM*. (4) The gap excess ratio (GER) (Wills, 1999) finds the proportion of ghost range in a tree, relative to the minimum and maximum possible sum of ghost ranges for the corresponding dataset. It also optimizes age range differences on the tree in the same manner as the MSM*, but is calculated as the retention index for the distance character (Pol & Norell, 2006). More recently two modifications were introduced to the GER: GER* and GERt (Wills *et al.*, 2008); certain aspects of these modifications were included in my analyses, such as the retention of tree-shape while only swapping OTUs (discussed below), but these methods were not explicitly used. This decision is based on the necessity for a large number of replicates to achieve accurate results (50,000 in Wills *et al.*, 2008), which would prohibitively increase the computational requirements for this empirical dataset, especially if also extended to the other methods used. Furthermore, in 'strap' the P-values are calculated differently for GER* and GERt, in comparison to other methods, and may therefore cause confusion if presented together.

The 'strap' package (Bell & Lloyd, 2014) for the software R version 3.2.5 (R Core Team, 2016) implements all the above metrics, and was used for all analyses of stratigraphic congruence in this study. The strap package also implements a test of statistical significance for each metric, based on random permutations. In calculating significance values I made use of two additional options offered by strap: the first is to generate random trees by swapping OTUs, whilst maintaining tree shape; the second is to fix the outgroup OTU such that it is not

randomized. These additions respectively resolve issues of random trees being more symmetrical than commonly found in fossil groups (Wills *et al.*, 2008), and the deliberate assignment of the outgroup prior to analysis, removing the need for its position to be tested (Bell & Lloyd, 2014). The random trees therefore provide a closer estimate of the original tree topology and a more robust test of significance (Bell & Lloyd, 2014). Primarily the P-values from the significance tests are used here for comparisons of stratigraphic congruence, rather than the raw metrics, as the latter are strongly influenced by tree balance, the arrangement of taxon stratigraphic ranges and tree size (Siddall, 1996; Willis, 1999). The results of randomization tests are free from these influences and should therefore be more directly comparable (Wills, 1999; Benton *et al.*, 1999).

In this study significance tests were carried out with 1000 random permutations. The strict consensus trees resulting from the four data treatments were analysed, as were the three most recent alternative phylogenetic hypotheses of phytosaur relationships (Parker & Irmis, 2006; Hungerbühler *et al.*, 2013; Kammerer *et al.*, 2015). Where a previous analysis included specimen-level OTUs or taxa not present in this study, these terminals were removed; three terminals were removed from the tree of Kammerer *et al.* (2015) and two from Hungerbühler *et al.* (2013). Three alternate hypotheses of topology were presented by Hungerbühler *et al.* (2013), though with the two terminals missing from this analysis removed, two of the trees become synonymous; therefore, only two hypotheses are tested here from Hungerbühler *et al.* (2013).

2.2.8. *Model-based cladistic methods*

In palaeontology, parsimony-based methods of phylogenetic analysis have historically dominated the field and continue to be the preferred analysis method for morphological data.

Although model-based approaches to phylogenetics, such as maximum likelihood and Bayesian methods, are relatively common in analyses including molecular data, their application to palaeontological datasets has only recently become more widespread (Lee & Worthy, 2012). It seems likely that the tardiness with which palaeontologists have taken up probabilistic methods is linked to the ongoing debate over the relative performance of parsimony and probabilistic methods (Huelsenbeck, 1995; Lee & Worthy, 2012; Wright & Hillis, 2014; O'Reilly *et al.*, 2016, 2017; Goloboff *et al.*, 2017, 2018; Sansom *et al.*, 2018), especially regarding morphological characters which constitute the vast majority of palaeontological datasets. However, theoretical criticisms have also been made against both model-based (Kolaczkowski & Thornton, 2004; Goloboff & Pol, 2005; Livesey & Zusi, 2007; Wagner, 2012) and parsimony approaches (Felsenstein, 1978; Kuhner & Felsenstein, 1994; Lewis, 2001).

Advances in the probabilistic approach to phylogeny, stemming from the Mk model of discrete trait evolution (Lewis, 2001), have led to a more robust framework with which to analyse morphological datasets (Ronquist & Huelsenbeck, 2003; Wagner, 2012; Wright *et al.*, 2015). Similarly to parsimony methods, recent advances have seen the development of procedures to incorporate both continuous (Parins-Fukuchi, 2017) and geometric morphometric data (Parins-Fukuchi, 2018) into probabilistic analyses of phylogeny. Both methods utilise alternative models of evolution to the Mk model: Brownian motion (Felsenstein, 1973, 1985; Gingerich, 1993) and Ornstein–Uhlenbeck (Hansen, 1997; Butler & King, 2004; Beaulieu *et al.*, 2012) models simulate random, normally distributed phenotypic evolution, and stabilising evolution respectively in the analysis of continuous data, while a Brownian motion model is used again, with branch lengths representing morphological variation, to analyse morphometric data (Parins-Fukuchi, 2017, 2018).

Probabilistic methods of phylogenetic analysis are not explored further in this study, largely for practical reasons. I note that the use of continuous and morphometric data in probabilistic methods is very new and as such lacks intuitive implementation in software packages, resulting in a requirement for careful documentation and testing of methodological properties, especially for an empirical dataset. Further analyses of this dataset under probabilistic methods could be very illuminating, and a potentially fruitful avenue of future research, but will be explored elsewhere.

2.3. *Results*

A total of eight best fit trees were found across all four coding variants; in each of the D and DC treatments three equally 'fitting' trees were found, whereas DM and DCM each returned only one best fit tree. My results are presented as the strict consensus trees of the best fit trees or single best fit trees resulting from each of the four different variants of character coding (D, DC, DM and DCM) with absolute and relative symmetric resampling frequencies above nodes, and Bremer supports below (Figures 2.4–2.7). I also present the strict consensus and maximum agreement subtree of these four trees, to summarize the most consistent relationships across all coding treatments (Figure 2.8).

The tree lengths resulting from the four coding treatments are summarized in Table 2.4, as are the consistency and retention indices (CI and RI). Tree lengths are not directly comparable between treatments including or excluding GM coding; this arises because the morphology encoded in some GM characters encompasses more than one discretely coded character. Therefore, analyses incorporating GM data contain fewer characters than the other scoring types and will likely show lower tree lengths as a result.

Conversely, providing that continuous characters replace their corresponding discrete characters with one-to-one equivalence (which they do here), their alternative coding method alone should not affect tree length. Continuous characters are here scored as ratios and are transformed to occupy a 0–1 scale; the standard treatment of continuous characters by TNT uses the numerical differences between scores to create the step-matrix. As these values are constantly below 1 it may be expected that the greater proportion of continuous characters in a dataset would result in lower tree length. However, due to my use of implied weighting this should not present a problem, as tree length is the sum of homoplasy-adjusted character weight. Homoplasy is, in the simplest sense, calculated as a proportion of the minimum length of a character in topology X, and the minimum possible length of a character in any topology. Character weight is then calculated from this proportion (homoplasy) and is then summed across all characters to generate tree length. As character weight is based on a character-specific proportion, the actual size of changes in the character step-matrix should not affect the final tree length. Simply put, if equivalent discrete and continuous characters share a consistent proportion of homoplasy, their effect on tree-length under implied weighting will be identical regardless of how they are scored.

Table 2.4: Consistency index (CI), retention index (RI) and 'tree-lengths' of the four phylogenetic trees corresponding to the four data treatments.

	Consistency Index (CI)	Retention Index (RI)	Tree Length
Discrete only (D)	0.383	0.689	31.90
Discrete + Continuous (DC)	0.409	0.684	27.46
Discrete + GM (DM)	0.391	0.691	30.52
Discrete + Continuous + GM (DCM)	0.420	0.689	25.44

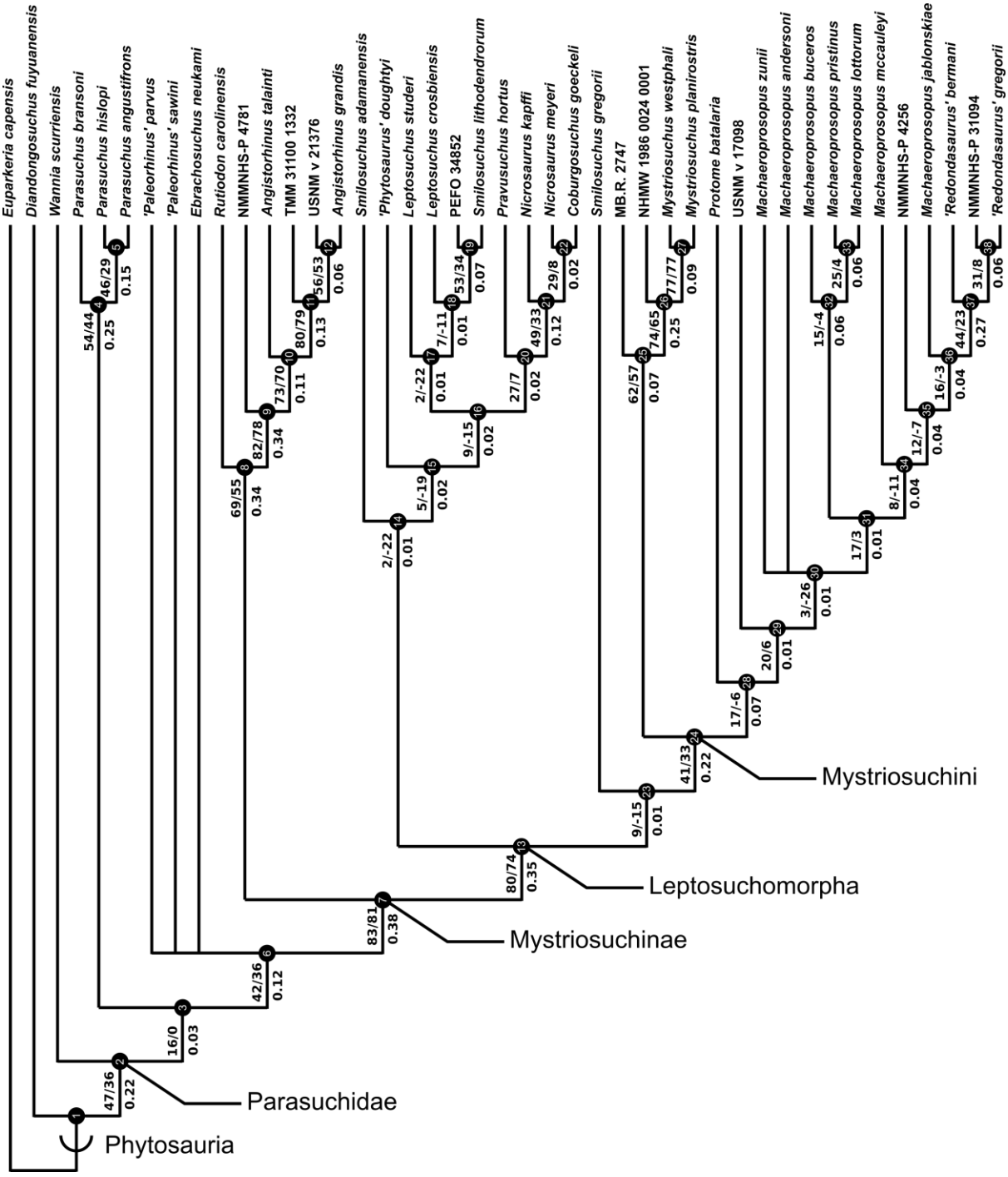

Figure 2.4: Strict consensus of the three trees resulting from the analysis treatment incorporating discrete characters only (D). Node numbers are labelled within black circles. Absolute frequencies/frequency differences are presented to the left of the node's stem; Bremer support values are reported to the right of the node's stem.

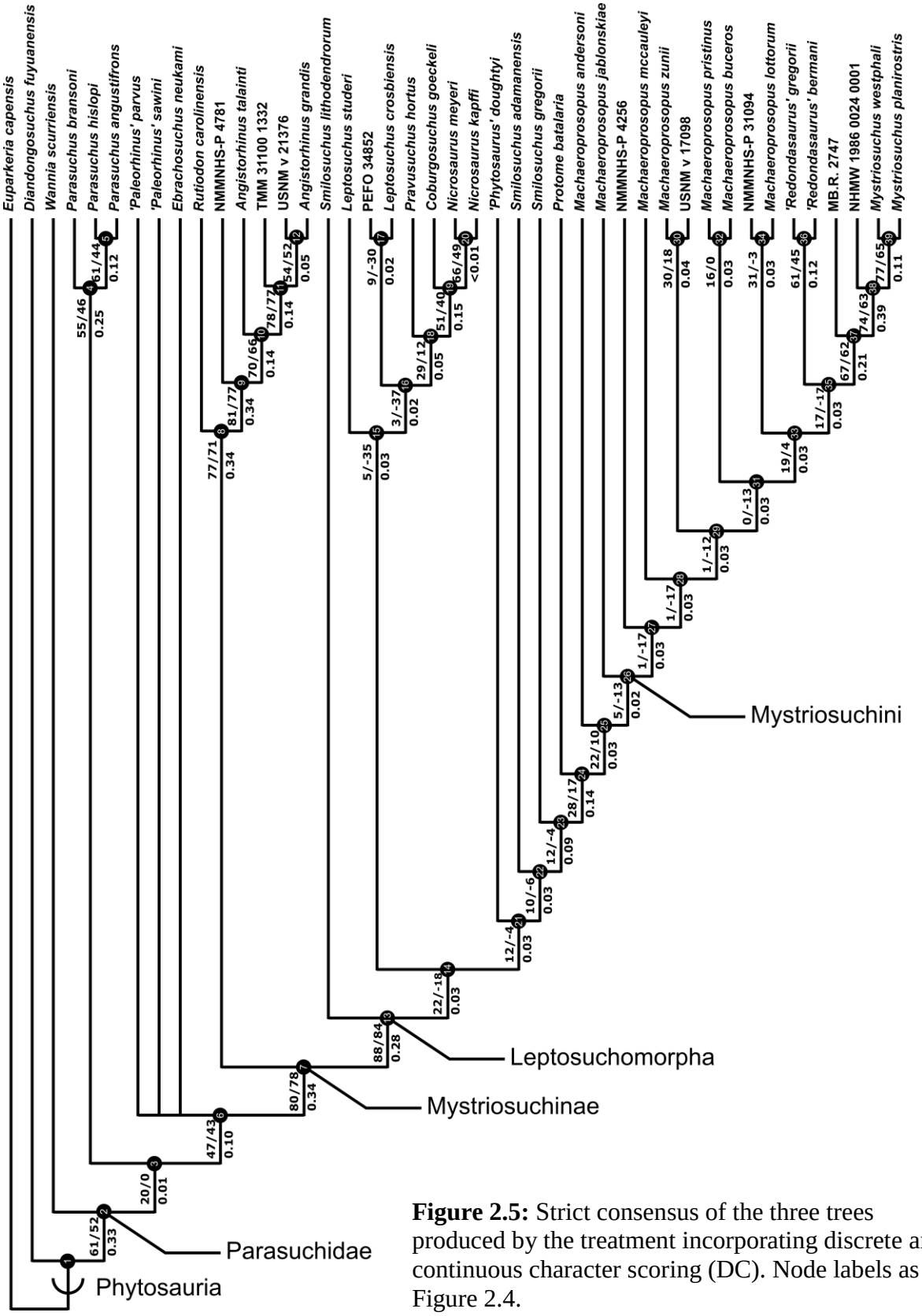

Figure 2.5: Strict consensus of the three trees produced by the treatment incorporating discrete and continuous character scoring (DC). Node labels as in Figure 2.4.

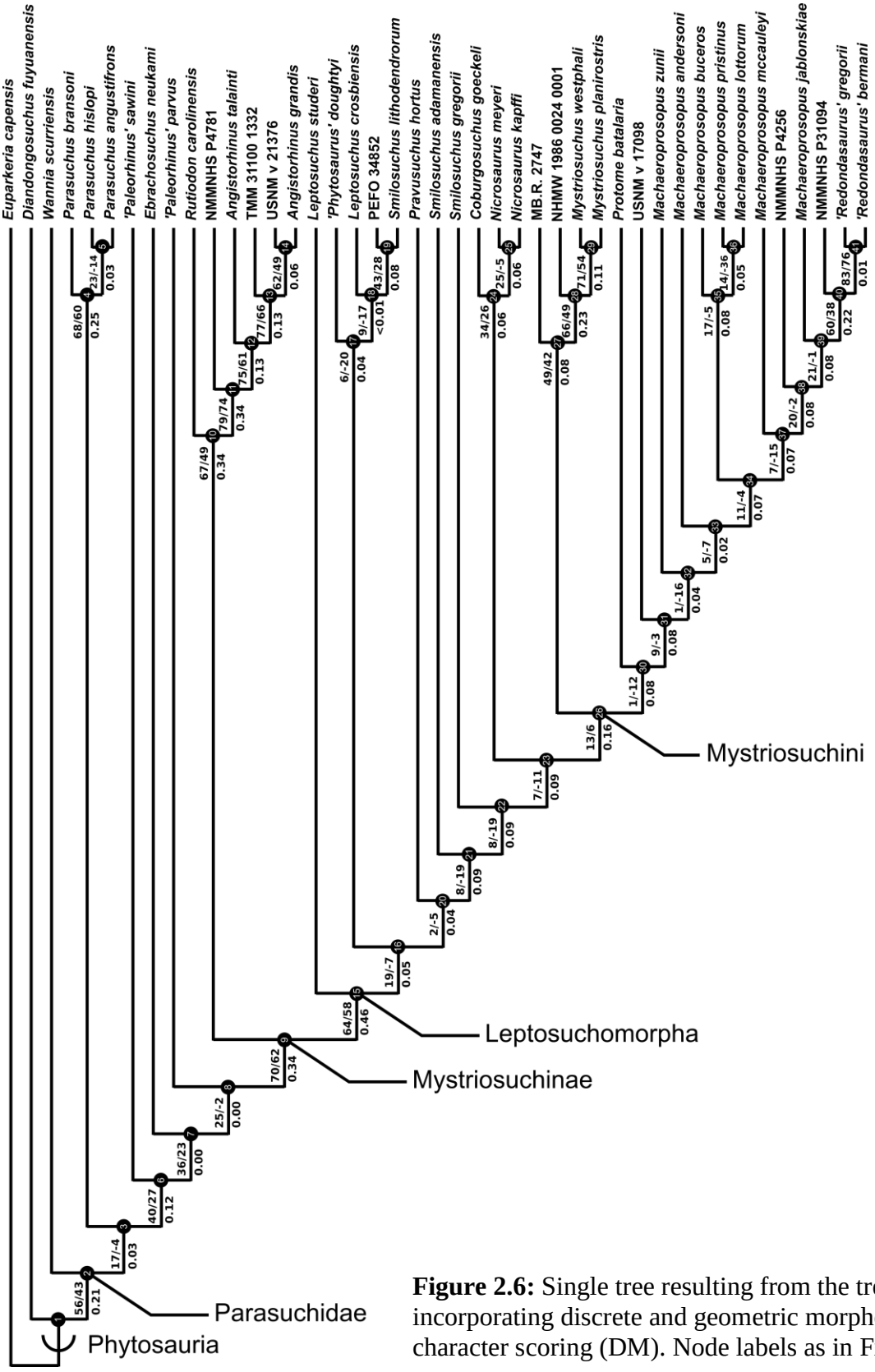

Figure 2.6: Single tree resulting from the treatment incorporating discrete and geometric morphometric character scoring (DM). Node labels as in Figure 2.4.

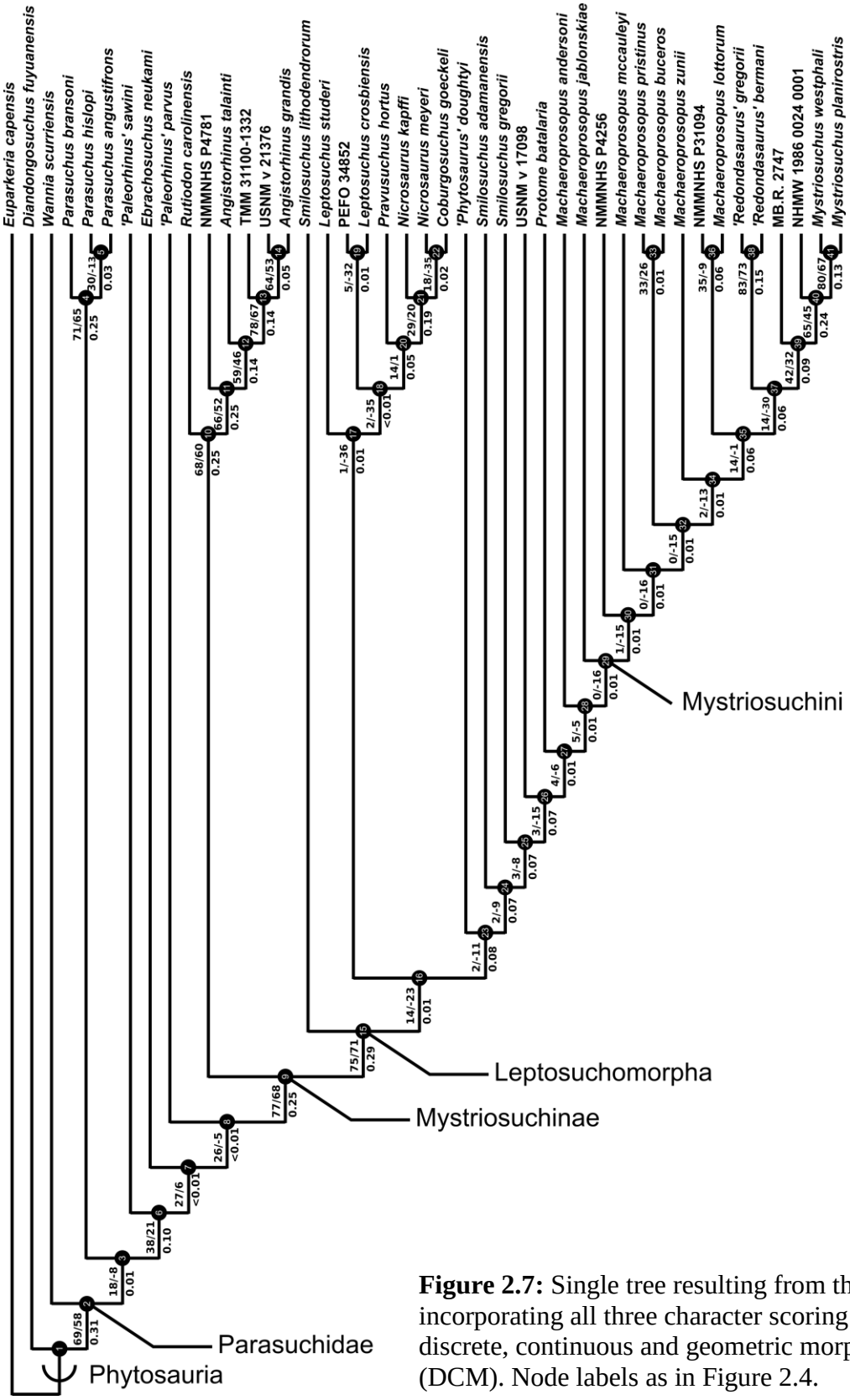

Figure 2.7: Single tree resulting from the treatment incorporating all three character scoring methods; discrete, continuous and geometric morphometric (DCM). Node labels as in Figure 2.4.

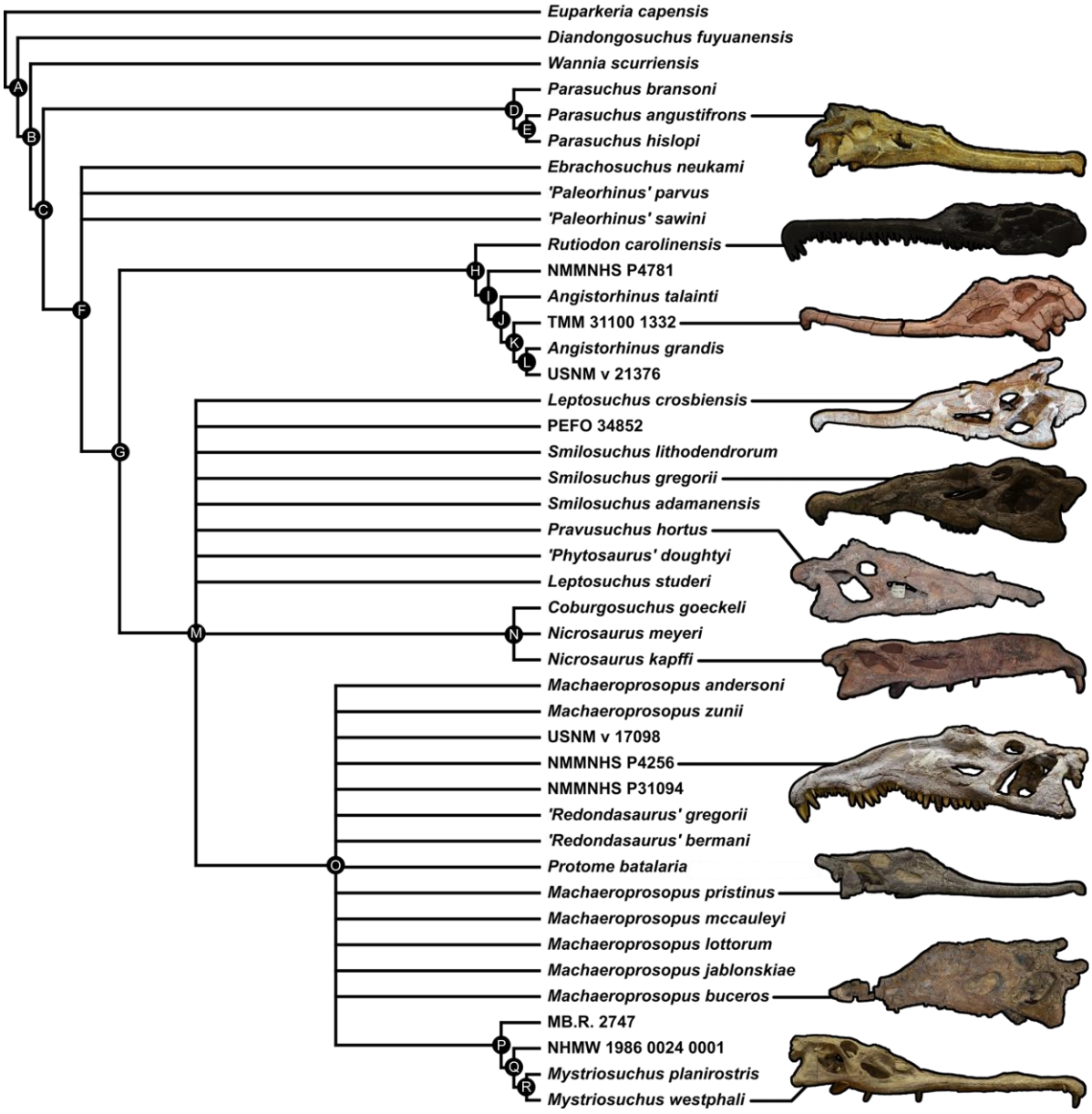

Figure 2.8: Strict consensus tree constructed with the four trees presented in Figs. 2.4, 2.5, 2.6 & 2.7 (D, DC, DM & DCM).

2.3.1. *Comparisons of similarity*

Comparisons of trees are presented in Tables 2.5 and 2.6, using the number of taxa retained by maximum agreement subtrees, the SPR distance and the RF distance as metrics of similarity. Maximum agreement subtrees essentially produce fully resolved consensus trees by pruning taxa in conflict between the input trees; the number of taxa retained in a maximum agreement subtree can be used as a measure of topological similarity between two or more trees.

All four trees were found to be significantly similar to each other. For all pairwise comparisons between different coding treatments the number of taxa retained in the maximum agreement subtrees was statistically much greater than expected by chance. Statistical significance was established using 5,000 agreement subtrees constructed with randomized tree topologies. None of these subtrees retained more than 14 OTUs and subtrees retaining the highest number of OTUs (14) comprised only 0.96% of the data. All pairwise comparisons yielded multiple maximum agreement subtrees of the same length showing alternative prunings (Table 2.5).

The two coding treatments that utilized continuous data (DC and DCM: Figures 2.5, 2.7) were consistently found to be the most similar tree topologies using all similarity metrics. The trees generated from discrete and discrete + GM coding treatments (D and DM: Figures 2.4, 2.6) also showed a high degree of similarity to each other. However, there is greatly reduced similarity when the DC/DCM trees are compared with the D/DM trees. Broadly speaking, this suggests there are two partially conflicting phylogenetic hypotheses, one represented by the DC and DCM trees and one by the D and DM trees. However, the agreement subtrees suggest that the amount of overlap between these hypotheses is still greater than would be expected to occur by chance.

Table 2.5: Similarity of the trees from each coding treatment. Trees are compared using number of taxa retained in their maximum agreement subtree (green), and the number of moves under SPR swapping to move from one tree to the other (blue). The pair of most similar trees are highlighted and emboldened in both comparison techniques. Multiple maximum agreement subtrees are frequently produced where several OTUs are in conflict with each other and when any combination of their pruning results in the same final subtree; the number of trees produced is also included in the table.

	Discrete only (D)	Discrete + Continuous (DC)	Discrete + GM (DM)	Discrete + Continuous + GM (DCM)	Maximum Agreement Subtrees
Discrete only (D)		27 taxa (62.8%) 39 trees	33 taxa (76.7%) 18 trees	26 taxa (60.5%) 27 trees	
Discrete + Continuous (DC)	13 moves (Similarity: 0.675)		24 taxa (55.8%) 36 trees	**38 taxa (88.4%) 9 trees**	
Discrete + GM (DM)	6 moves (Similarity: 0.850)	11 moves (Similarity: 0.725)		26 taxa (60.5%) 6 trees	
Discrete + Continuous + GM (DCM)	12 moves (Similarity: 0.700)	**3 moves (Similarity: 0.925)**	12 moves (Similarity: 0.700)		
	SPR Distances				

Table 2.6: Similarity of tree topologies as measured using Robinson-Foulds distance. The most similar combination of topologies, indicated by the shortest distance between input trees, is highlighted and emboldened.

	Discrete only (D)	Discrete + Continuous (DC)	Discrete + GM (DM)
Discrete + Continuous (DC)	0.45122		
Discrete + GM (DM)	0.23171	0.48780	
Discrete + Continuous + GM (DCM)	0.45122	**0.21951**	0.48780
	Robinson-Foulds Distance		

2.3.2. *Consistent relationships*

A list of nodal synapomorphies for each tree is presented in Appendix section S1.3. The following relationships were found to be consistent in the trees of all four scoring treatments, and match the topology of the strict consensus tree (Figure 2.8).

Diandongosuchus is recovered as the most basal phytosaur in every tree. Its position outside of all other phytosaurs is supported well by frequency and Bremer supports, and two consistent synapomorphies supporting Parasuchidae (Figure 2.8, node B) to the exclusion of *D. fuyuanensis* in every tree [13: 0→1; 22: 0→1].

Wannia scurriensis is consistently found as the most basal member of Parasuchidae, outside the clade that includes *Parasuchus* and Mystriosuchinae. The latter clade (Figure 2.8, node C) is, however, poorly supported, with only two synapomorphies supporting *Parasuchus* + Mystriosuchinae to the exclusion of *Wannia* in all four trees [36: 0→1; 69: 0→1].

Parasuchus (Figure 2.8, node D) is consistently found to include the species *Parasuchus bransoni*, *Parasuchus hislopi*, and *Parasuchus angustifrons*, and is well supported by frequency and Bremer scores, with three synapomorphies common to all trees [23: 0→1; 26: 0→1; 50: 0→1].

'*Paleorhinus*' *parvus*, '*Paleorhinus*' *sawini* and *Ebrachosuchus neukami* are closer to Mystriosuchinae than to *Parasuchus* in all trees; however, the interrelationships of these species and their exact relationships to Mystriosuchinae are variable in the different coding treatments. Mystriosuchinae itself (Figure 2.8, node G) is supported by three synapomorphies common to all trees [9: 0→1; 14: 1→2; 80: 0→1].

Rutiodon carolinensis and *Angistorhinus* form a clade at the base of Mystriosuchinae that is consistently well supported by frequency and Bremer supports (Figure 2.8, node H) and is united by two synapomorphies in all trees [22: 2→1; 92: 0→1]. Within this clade, *Rutiodon* is consistently the sister taxon to *Angistorhinus*; the clade composed of *Angistorhinus* and *Angistorhinus*-like specimens, to the exclusion of *Rutiodon carolinensis* (Figure 2.8, node I), is supported by two synapomorphies [56: 0→1; 58: 0→1]. The relationships of the species and specimen-level OTUs within *Angistorhinus* are consistent in all coding treatments: *A. talainti* is the most basal of the two named species and *A. grandis* is more derived, with the specimen-level OTUs representing either potential additional species within the genus, or morphologically diverse representatives of existing *Angistorhinus* species.

Leptosuchomorpha (Figure 2.8, node M) possesses two synapomorphies common to all tree topologies that separate it from the more basal taxa [16: 1→0; 25: 0→1]. Within Leptosuchomorpha the four phylogenies are more variable (Figure 2.8, node M). Among the leptosuchomorph OTUs not included in Mystriosuchini there is only one clade common to all

tree topologies: the clade which unites *Nicrosaurus kapffi* and *Nicrosaurus meyeri* with *Coburgosuchus goeckeli*, although the relationships between these three species are variable in the different coding treatments (Figure 2.8, node N). This clade is supported by a single synapomorphy [57: 1→2].

Although there are conflicting relationships, the majority of the leptosuchomorph taxa that have been excluded from Mystriosuchini by previous analyses (e.g. Kammerer *et al*., 2015) are also consistently excluded from Mystriosuchini as defined in the current analysis (with *Mystriosuchus planirostris*, *Machaeroprosopus jablonskiae* and *Machaeroprosopus buceros* as exemplars of the clade; see Table 2.2). Non-Mystriosuchini leptosuchomorphs in this analysis include all members of *Smilosuchus*, *Leptosuchus* and *Nicrosaurus* plus '*Phytosaurus*' *doughty*, *Pravusuchus hortus*, *Coburgosuchus goeckeli* and PEFO 34852, as well as *Protome* in some of the coding treatments (see below).

There is only one synapomorphy of Mystriosuchini common to all trees (Figure 2.8, node O) [43: 2→0]. Much like the non-Mystriosuchini leptosuchomorphs, interrelationships within Mystriosuchini are generally inconsistent across the different coding treatments; however, as in previous analyses, the clade includes all named species of *Machaeroprosopus*, '*Redondasaurus*' and *Mystriosuchus*, as well as USNM v 17098, NMMNHS P4256, NMMNHS P31094, MB.R. 2747 and NHMW 1986 0024 0001. *Protome batalaria* has been placed close to *Rutiodon* by previous studies (Stocker, 2012; Butler *et al*., 2014; Kammerer *et al*., 2015). In this study it is consistently found to be either nested just inside Mystriosuchini (Figures 2.4, 2.6) or as the sister taxon to this clade (Figures 2.5, 2.7). In both trees in which *Protome* is recovered within Mystriosuchini (D & DM trees) the node is supported by the presence of 'parietal prongs' [65: 0→1]; additionally, in the DM tree the node is supported by the presence of a small elongate depression on the postorbital bar just posterodorsal to the

orbit [29: 0→1], as well as all GM characters. Parietal prongs are exclusive only to *Protome* and members of *Machaeroprosopus* and '*Redondasaurus*', whereas the groove on the descending process of the postorbital is common to many taxa throughout Parasuchidae.

Within Mystriosuchini, *Mystriosuchus* (Figure 2.8, node P) is the only consistently supported clade. Within this clade MB. R. 2747 and NHMW 1986 0024 0001 form successive sister taxa to *Mystriosuchus planirostris* and *Mystriosuchus westphali*; it is likely that these two specimen-level OTUs also represent unnamed species of *Mystriosuchus*. *Mystriosuchus* and its internal nodes are statistically well supported. The basal node of the clade and the internal nodes are each supported by single synapomorphies common to all trees (Figure 2.8, node P) [85: 1→0], (Figure 2.8, node Q) [2: 1→2], (Figure 2.8, node R) [88: 0→1].

2.3.3. *Conflicting relationships*

As discussed above, relationships among the non-Mystriosuchinae taxa are almost entirely consistent across all four trees with the exception of '*Paleorhinus*' *parvus*, '*Paleorhinus*' *sawini* and *Ebrachosuchus neukami* (Figure 2.8). The relationships between these taxa are poorly supported statistically and variable, and the three form a polytomy together with Mystriosuchinae in the strict consensus trees of the D and DC analyses (Figures 2.4, 2.5). In the DM and DCM analyses (Figures 2.6, 2.7) the relationships are consistent, if not well supported. '*Paleorhinus*' *parvus* is the sister taxon of Mystriosuchinae, with *Ebrachosuchus neukami* and '*Paleorhinus*' *sawini* forming successively more distant sister groups.

Those non-Mystriosuchini members of Leptosuchomorpha in this analysis comprise species assigned to the genera *Smilosuchus, Leptosuchus*, '*Phytosaurus*', *Pravusuchus, Nicrosaurus* and *Coburgosuchus*. Relationships between these taxa are entirely consistent in

the DC and DCM trees (Figures 2.5, 2.7). However, the D and DM trees each show different topologies (Figures 2.4, 2.6). In the DC and DCM trees, *'Smilosuchus' lithodendrorum* is the most basal taxon in Leptosuchomorpha. Within Leptosuchomorpha there are two clades: one containing all species of *Leptosuchus* and *Nicrosaurus*, in addition to *Pravusuchus hortus*, *Coburgosuchus goeckeli* and PEFO 34852; and one containing '*Phytosaurus*' *doughtyi*, *Smilosuchus adamanensis*, *Smilosuchus gregorii*, *Protome* and Mystriosuchini.

In the D tree, all the aforementioned taxa with the exception of *Smilosuchus gregorii* form an unnamed clade (Figure 2.4, node 14), which forms a sister relationship within Leptosuchomorpha with *Smilosuchus gregorii* + Mystriosuchini. The basalmost taxon within this unnamed clade is *Smilosuchus adamanensis*, which in the other three trees presented here is recovered as a branch just basal to *S. gregorii*; the next taxon in the clade, '*Phytosaurus*' *doughtyi*, also falls closer to *S. gregorii* than *Leptosuchus* in the DC, DM and DCM trees. Above '*Phytosaurus*' *doughtyi*, two distinct clades are present as sister taxa. One of these (Figure 2.4, node 17) contains *Leptosuchus* spp., plus *'Smilosuchus' lithodendrorum* and PEFO 34852; the second (Figure 2.4, node 20) contains *Pravusuchus hortus*, *Nicrosaurus* spp. and *Coburgosuchus goeckeli*. Relationships in both clades have weak Bremer support, with the exception of the node uniting *Nicrosaurus kapffi*, *N. meyeri* and *C. goeckeli* (Figure 2.4, node 21), in which frequency supports are generally better.

The topology for this region of the DM tree is very different from that of the D tree (to which it is very similar in most other respects). The taxa that form a distinct clade in the D tree (Figure 2.4, node 14) instead form a largely pectinate series of outgroups to Mystriosuchini in the DM tree (Figure 2.6, nodes 15–25). The most basally branching taxon is *Leptosuchus studeri*, which falls outside of Leptosuchomorpha in this tree. At the base of Leptosuchomorpha is a relatively poorly supported (according to frequency supports) clade

including '*Phytosaurus*' *doughtyi*, *Leptosuchus crosbiensis*, and a sister taxon relationship between *'Smilosuchus' lithodendrorum* and PEFO 34852 (Figure 2.6, node 17). *Pravusuchus hortus*, *Smilosuchus adamanensis* and *Smilosuchus gregorii* form a series of outgroups to a clade consisting of Mystriosuchini and the *Nicrosaurus* + *Coburgosuchus* clade. In the DM tree the *Nicrosaurus* species are sister taxa (Figure 2.6, node 25). In this topology, *Nicrosaurus* occupies a position consistent with that recovered in previous analyses of Mystriosuchini (Hungerbühler, 2002; Hungerbühler *et al*., 2013) and with the group's previous definition (Kammerer *et al.*, 2015).

The main inconsistency within Mystriosuchini is the fluctuating position of the *Mystriosuchus* clade (*Mystriosuchus* spp. plus NHMW 1986 0024 0001 and MB. R. 2747). In both trees incorporating continuously scored data (DC, DCM) this group is recovered as highly derived within Mystriosuchini (Figures 2.5, 2.7), as has previously been found by Stocker (2010, 2012, 2013), Butler *et al.* (2014) and Kammerer *et al.* (2015) (Figures 2.2b; 2.3a, b). In the D and DM coding treatments, however, the *Mystriosuchus* clade forms the sister group to *Protome batalaria* + *Machaeroprosopus* (Figures 2.4, 2.6), as has been found by Hungerbühler (2002), Parker and Irmis (2006) and Hungerbühler *et al.* (2013) (Figures 2.1a; 2.2a, c).

Relationships among other species within Mystriosuchini are highly variable, though the general pattern is of a highly laddered series of sequentially more derived terminals. Although the order of OTUs varies considerably, there are some similarities across different coding treatments; taxa in the less derived positions are generally *Protome batalaria* and *Machaeroprosopus andersoni*, which are then followed by *Machaeroprosopus pristinus*, *Machaeroprosopus buceros* and *Machaeroprosopus lottorum* and then a clade containing both species of '*Redondasaurus*' (Figure S1.2).

As previously mentioned, the two conflicting hypotheses regarding the position of *Mystriosuchus* (basal or derived within Mystiosuchini) split the results of the four coding methods into two alternative topological hypotheses. The positions of *Machaeroprosopus mccauleyi* and *Machaeroprosopus jablonskiae* also consistently differ between these topologies. In the trees in which *Mystriosuchus* occupies a derived position within Mystriosuchini (DC, DCM), *Machaeroprosopus mccauleyi* and *Machaeroprosopus jablonskiae* form successive sister taxa, basal to the clade comprising *Machaeroprosopus pristinus*, *Machaeroprosopus buceros* and *Mystriosuchus*. In topologies where *Mystriosuchus* is recovered basal to *Machaeroprosopus* (D, DM), *Machaeroprosopus mccauleyi* and *Machaeroprosopus jablonskiae* are more derived than the clade composed of *Machaeroprosopus pristinus*, *Machaeroprosopus buceros* and *Machaeroprosopus lottorum*, forming successive sister taxa to '*Redondasaurus*'.

The position of *Machaeroprosopus zunii* is more consistent; in three trees (D, DC and DM) it is recovered basal to the clade composed of *Machaeroprosopus pristinus*, *Machaeroprosopus buceros*, and all more derived taxa. In the DCM results *Machaeroprosopus zunii* is placed more derived than than *Machaeroprosopus pristinus* and *Machaeroprosopus buceros*, but less derived than *Machaeroprosopus lottorum*.

Machaeroprosopus lottorum is another taxon which varies consistently between the two broad topological hypotheses presented. In the trees incorporating continuously scored data, in which *Mystriosuchus* is highly derived (DC, DCM), *Machaeroprosopus lottorum* forms a clade with NMMNHS-P 31094 (Figures 2.5, 2.7), closely related to '*Redondasaurus*' and *Mystriosuchus*, as was found by Hungerbühler *et al.* (2013). In the alternative topologies (D, DM) *Machaeroprosopus lottorum* nests with *Machaeroprosopus pristinus*, to the exclusion of *Machaeroprosopus buceros* (Figures 2.4, 2.6). Both positions are similarly

poorly supported by Bremer analyses, but possess relatively good frequency scores. In this topology NMMNHS-P 31094 is consistently found within '*Redondasaurus*', as the sister taxon of '*Redondasaurus*' *gregorii*, to the exclusion of '*Redondasaurus*' *bermani*.

2.3.4. *Accuracy and validity*

2.3.4.1. *Bremer supports*

With poorly supported nodes collapsed below Bremer values of 0.08, the DM condition produced greatest tree resolution, retaining 23 nodes; however, its mean Bremer score is one of the lowest among the four trees, suggesting that the additional nodes supported in this tree only exceed the cut-off by a small amount (Table 2.7). When using the mean step length of a single character (0.11) as a cut-off for node-collapsing, the DM and DCM conditions were found to perform more poorly than the D and DC conditions in terms of nodes retained and total Bremer support. Mean Bremer values for the retained nodes remained almost consistent across all trees (Table 2.7).

When broken down into regions, it appears that the extra support in the DM tree is added in regions three and four, which are almost consistently the worst supported in all trees. Despite this extra support, relationships within these regions are still relatively poorly supported in the DM condition, and the support for region one also becomes among the poorest in both GM trees (DM and DCM) (Table 2.8).

The best condition for overall Bremer support was the DC tree (Figure 2.5), achieving the highest, or equal highest support in all regions except three and four, with a sum of mean support equalling 0.75. Conversely, despite maximizing support in the poorest regions of the tree, the DM condition scored second worst for overall support, with a sum total of 0.60; this was followed by the DCM condition with a score of 0.58 (Table 2.8).

Table 2.7: Bremer (above) and frequency (below) supports resulting from each of the four data conditions. Values below which nodes were collapsed, were set as 0.08 and [0.11] for Bremer, and 10 for frequency supports. Largest values in each category are shown in bold.

	Discrete (D)	Discrete + Cont. (DC)	Discrete + Morph. (DM)	Discrete + Cont. + Morph. (DCM)	
No. of nodes retained	15 [14]	17 **[15]**	**23** [13]	15 [12]	<0.08 [<0.11] Bremer collapsed
Total Bremer support	3.34 [3.25]	3.59 **[3.40]**	**3.86** [3.04]	2.86 [2.59]	
Mean Bremer support	**0.22 [0.23]**	0.21 **[0.23]**	0.17 **[0.23]**	0.19 [0.22]	
No. of Nodes retained	29	**30**	29	26	<10 Frequency collapsed
Total freq. support	1337	**1416**	1305	1207	
Mean freq. support	46.10	**47.20**	45.00	46.42	

2.3.4.2. *Frequency supports*

With a cut-off for node collapsing of <10, symmetric frequency support produced broadly similar results for all the trees, with the DC condition producing a marginally higher resolution and mean support value. Conversely to the results from Bremer supports, the DM condition was the poorest supported topology based on symmetric resampling, although the difference between 'best' and 'worst' is minor (Table 2.7).

Split into regions, the overall sum of mean supports follows the same trend as that of the Bremer supports; DC is best, with a sum of 240.56, then D (229.47), DM (213.16) and finally DCM (199.11). The DC tree holds the highest mean support compared to the other

trees in regions one, three and five. The DM tree only holds the highest support value in region four; however, this is one of the two poorest supported regions (three and four), and is therefore important in achieving the best possible resolution in all parts of the tree (Table 2.9).

Table 2.8: Mean Bremer supports calculated in five tree-regions within each of the four data conditions. Largest values in each region are shown in bold. The data condition with the highest summed mean Bremer support is highlighted with a green border.

	Discrete (D)	Discrete + Cont. (DC)	Discrete + Morph. (DM)	Discrete + Cont. + Morph. (DCM)
Region 1 Bremer mean	0.15	**0.16**	0.09	0.11
Region 2 Bremer mean	**0.23**	**0.23**	0.20	0.17
Region 3 Bremer mean	0.06	0.07	**0.10**	0.09
Region 4 Bremer mean	0.06	0.05	**0.07**	0.05
Region 5 Bremer mean	0.14	**0.24**	0.14	0.16
Total	0.64	**0.75**	0.60	0.58

2.3.4.3. *Stratigraphic congruence*

All tree topologies recovered under the four data conditions tested in this analysis were found to be significantly better correlated with stratigraphy than would be expected of random data. Among the raw results from each correlation metric, there is no consistent trend indicating one or more of the four topologies are optimal. The SCI metric suggests the D and DM topologies (in which *Mystriosuchus* is basal to *Machaeroprosopus*) to be better

stratigraphically correlated than the DC and DCM topologies (in which *Mystriosuchus* is the most derived member of Mystriosuchini); however, this finding is not borne out by any other metric. Among the other three metrics the only consistent trend is the slightly worse performance of the two datasets incorporating GM characters (DM and DCM); however, the difference in fit is almost negligible (Table 2.10).

Table 2.9: Mean frequency supports calculated in five tree-regions within each of the four data conditions. Largest values in each region are shown in bold. The data condition with the highest summed mean frequency support is highlighted with a green border.

	Discrete (D)	Discrete + Cont. (DC)	Discrete + Morph. (DM)	Discrete + Cont. + Morph. (DCM)
Region 1 freq. mean	41.00	**48.80**	37.86	39.86
Region 2 freq. mean	**73.83**	73.33	72.00	67.00
Region 3 freq. mean	24.73	**27.91**	20.55	15.00
Region 4 freq. mean	18.91	17.85	**20.75**	14.92
Region 5 freq. mean	71.00	**72.67**	62.00	62.33
Total	229.47	**240.56**	213.16	199.11

The previous phylogenetic analyses of Parker & Irmis (2006) and Kammerer *et al.* (2015) (based respectively on the original matrices of Hungerbühler [2002] and Stocker [2010]), also correlate well with the stratigraphic data used in this study, generally achieving significance values equal to those of the current study. The topologies of Hungerbühler *et al.* (2013) were found to correlate poorly with stratigraphy and were not statistically differentiable from random data; however, the analysis of Hungerbühler *et al.* (2013) focuses only on one area of the tree, roughly corresponding to 'region four' in this study. This region

is poorly supported in terms of accuracy and robusticity. The poor stratigraphic correlation of the analysis of Hungerbühler *et al.* (2013) may indicate that this region has poor stratigraphic support, but this is masked in the stratigraphic correlations of other studies by good correlation overall in other areas of the tree.

Table 2.10: Stratigraphic consistency metrics for each of the four tree topologies, compared with those of three previous phylogenetic analyses of ingroup phytosaur relationships. Raw analysis output values are displayed on the left and significance values generated via random permutations are presented on the right.

	SCI	RCI	GER	MSM*	P. Sig. SCI	P. Sig. RCI	P. Sig. GER	P. Sig. MSM*
D	0.737	-9.272	0.777	0.150	<0.0001	<0.0001	<0.0001	<0.0001
DC	0.615	-9.369	0.777	0.150	<0.0001	<0.0001	<0.0001	<0.0001
DM	0.732	-10.343	0.775	0.149	<0.0001	<0.0001	<0.0001	<0.0001
DCM	0.634	-11.032	0.773	0.148	<0.0001	<0.0001	<0.0001	<0.0001
Kammerer *et al.*	0.750	-16.042	0.805	0.291	<0.0001	-	0.0002	<0.0001
Hungerbühler *et al.* #1	0.400	19.878	0.163	0.258	0.20	-	0.96	0.77
Hungerbühler *et al.* #2	0.429	25.841	0.247	0.278	0.08	-	0.81	0.58
Parker & Irmis	0.700	-57.830	0.797	0.389	<0.0001	-	<0.0001	<0.0001

2.3.4.4. *Tree choice*

In order to carry out further investigations into the effects of alternative, or previously reported topologies, it was decided to select only two of the four topologies presented above to avoid unnecessarily long comparisons of fit between multiple alternative taxonomic relationships within multiple tree topologies. As there is a general dichotomy within the four trees, it would be arbitrary to favour one topology over the other, so a representative of each was chosen.

The DC condition exhibits an almost identical topology to the DCM condition, but consistently outperforms the latter in the various robusticity analyses described above. Comparisons of topological similarity do not assist in selecting one of these topologies over the other as they are shown to be almost identical, with neither being more representative of all topologies.

The D and DM conditions are less similar to each other than are the DC and DCM conditions, though they show largely the same topology. Between the Bremer and frequency analyses the D and DM conditions outperform each other in various aspects; when the trees are regionalized the DM condition generally provides slightly better support in the worst-supported areas of the tree, but is poorly supported in most other areas. The sum of Robinson-Foulds distances for the D tree in comparison to all others suggests that it is the most representative topology of the four trees recovered in this study; this was never found to be the case with the DM topology.

Ultimately the D and DC trees (Figures 2.4, 2.5) were selected for further analysis based partially on the above metrics, but partially due to the relative difficulty of undertaking multiple further GM analyses. Continuous and discrete characters boast substantial advantages in analysis duration, and the comparative simplicity of data acquisition and

processing, over GM characters. Because of these reasons continuous and discrete data are far more accessible and provide a better basis on which future studies can build.

2.3.5. *Alternative taxonomic relationships*

The consistent recovery of a sister-relationship between *Rutiodon carolinensis* and the genus *Angistorhinus* makes the decision of whether or not to synonymize these taxa entirely arbitrary (see below); therefore, to test for their synonymy would also be meaningless and as such these taxa were excluded from these analyses.

Nicrosaurus was previously found as the basal-most member of Mystriosuchini (Hungerbühler, 2002; Hungerbühler *et al*., 2013) and was therefore used as an internal specifier for the most recent phylogenetic definitions of the clade, preceding this study (Parker & Irmis, 2006; Kammerer *et al*., 2015); however, as described in the introduction little data has been provided to support this. Here I find *Nicrosaurus* to group closer to *Leptosuchus* than to *Mystriosuchus* or *Machaeroprosopus*, and thus outside of Mystriosuchini according to my redefinition of the clade (Table 2.2). I tested the previously proposed position of *Nicrosaurus*, i.e. as the most basal group within Mystriosuchini (Kammerer *et al*., 2015). To achieve this, the clade of *Nicrosaurus* and *Coburgosuchus* was constrained to its previous position in relation to Mystriosuchini, such that all members of *Machaeroprosopus* and *Mystriosuchus* fell in more derived positions. Additionally, *Pravusuchus hortus* was constrained as the basal sister taxon to *Nicrosaurus*, *Coburgosuchus* and Mystriosuchini, to replicate the previous hypothesis that *Pravusuchus* is the immediate sister taxon to Mystriosuchini (Stocker, 2010). Under these topological constraints tree character fit worsened by 0.693 in the D condition, and 1.013 in the DC condition.

The tree topology resulting from the D condition places *Mystriosuchus* as the sister clade to *Machaeroprosopus*; for this analysis I constrained *Mystriosuchus* to nest within *Machaeroprosopus* as found by Stocker (2010), although its exact position within the clade was left flexible. Under this condition the tree-fit worsens by 0.584. In contrast, in the DC condition *Mystriosuchus* was found to occupy a position within the *Machaeroprosopus* clade; therefore, I constrained it as sister to this clade, leading to a decline in tree fit by 0.714.

Unlike the findings of Hungerbühler *et al*. (2013), in my phylogenies the two species of '*Redondasaurus*' do appear to form a sister taxon relationship; however, in accordance with their findings and those of other studies (Ballew, 1989; Hungerbühler *et al.*, 2003; Stocker, 2010; Butler *et al*., 2014; Kammerer *et al*., 2015) '*Redondasaurus*' remains nested within *Machaeroprosopus*. When the two genera are forced into a sister group relationship the tree fit deteriorated considerably by a score of 0.857 under the D condition, and 1.004 in the DC condition.

2.4. *Discussion*

2.4.1. *Higher-level taxonomy*

The recently revived family-level name Parasuchidae Lydekker, 1885 (Kammerer *et al.*, 2015) was suggested by Stocker *et al*. (2017) to exclude the proposed basal phytosaur *Diandongosuchus fuyuanensis*. My analysis corroborates the hypothesis of Stocker *et al*. (2017) that *Diandongosuchus* is the most basal phytosaur, and the only taxon to fall outside of Parasuchidae but within Phytosauria using current definitions.

The taxonomic content of Mystriosuchinae von Huene, 1915, defined as the last common ancestor of *Angistorhinus grandis* and *Mystriosuchus planirostris* and all its

descendants by Kammerer *et al*. (2015), is largely compatible between the phylogenetic hypotheses presented here and that presented by Kammerer *et al.* (2015). However, in the phylogeny of Kammerer *et al.* (2015) '*Paleorhinus*' *sawini* falls within Mystriosuchinae whereas here it is excluded from this clade.

Stocker (2010) erected the clade Leptosuchomorpha, defined as the most recent common ancestor of *Leptosuchus studeri* and *Machaeroprosopus pristinus*, and all descendants thereof. In the D and DM trees presented here this definition is perfectly compatible with previous definitions of the clade; however, in the DC and DCM conditions *'Smilosuchus' lithodendrorum* is recovered in a more basal position than all other previous members of Leptosuchomorpha, and would thus be excluded from the group based on the definition of Stocker (2010), despite exhibiting numerous similarities with other members. I therefore redefine Leptosuchomorpha such that it includes the latest common ancestor of *'Smilosuchus' lithodendrorum*, *Leptosuchus studeri* and *Machaeroprosopus pristinus*, and all of its descendants (Table 2.2). In addition, *Protome batalaria* and '*Machaeroprosopus*' *zunii* are consistently recovered within Leptosuchomorpha in the analyses presented here, whereas they were previously excluded (Stocker, 2010; Butler *et al.*, 2014; Kammerer *et al.*, 2015).

The definition of Mystriosuchini von Huene, 1915 proposed by Kammerer *et al.* (2015) is problematic with regard to the results presented here, due to my general result that *Nicrosaurus* is deeply nested with taxa such as *Leptosuchus* and *Smilosuchus* that are traditionally excluded from Mystriosuchini. This problem is especially pronounced in the D tree (Figure 2.4), in which the previous definition of Mystriosuchini renders the group entirely synonymous with Leptosuchomorpha; the DC and DCM trees produce a very similar result, though excluding *'Smilosuchus' lithodendrorum* from Mystriosuchini (Figures 2.5, 2.7). In the DM tree (Figure 2.6) the taxonomic content of Mystriosuchini using the previous

phylogenetic definition is essentially the same as in previous studies, with the inclusion of a few additional taxa such as *Protome batalaria*.

To resolve this taxonomic issue, I propose that *Nicrosaurus kapffi* is removed from the definition of Mystriosuchini due to its conflicting phylogenetic position, and is replaced with *Machaeroprosopus jablonskiae* to stabilize the taxonomic content of the clade (see above; Table 2.2). Without the addition of *Machaeroprosopus jablonskiae* as a specifier, *Machaeroprosopus mccauleyi* and *Machaeroprosopus jablonskiae* would be variably excluded from Mystriosuchini, despite consistent previous findings of their inclusion in the clade. A number of other taxa would also be variably included in Mystriosuchini, leading to increased instability of the clade.

Machaeroprosopus jablonskiae is recovered in a similar position to that found by previous phylogenetic analyses (Parker & Irmis, 2006; Hungerbühler *et al.*, 2013; Butler *et al.*, 2014; Kammerer *et al*., 2015) in all of my trees. In the DC and DCM trees *Machaeroprosopus jablonskiae* is recovered as one of the most basal taxa within *Machaeroprosopus* (Figures 2.5, 2.7), as in the studies of Parker & Irmis (2006) and Hungerbühler *et al.* (2013) (Figure 2.2a, c). In the D and DM trees *Machaeroprosopus jablonskiae* is placed in a more derived position in the *Machaeroprosopus* clade (Figures 2.4, 2.6), similar to the findings of Butler *et al.* (2014) and Kammerer *et al*. (2015) (Figure 2.3a, b); however, as this coincides with the migration of *Mystriosuchus* to a more basal position with respect to *Machaeroprosopus*, the taxa retained in Mystriosuchini remain largely identical among my four trees. Crucially, *Machaeroprosopus jablonskiae* consistently nests within Mystriosuchini in previous studies (Parker & Irmis, 2006; Hungerbühler *et al.*, 2013; Butler *et al.*, 2014; Kammerer *et al*., 2015), and in this sense my proposed definition errs on the side of caution in ensuring the definition of Mystriosuchini used here is as compatible as

possible with the phylogenetic topologies of previous studies. This being the first investigation of this dataset, it seems likely that future analyses of this data could disagree with my findings, in which case a definition that maximizes compatibility between recent studies may be the most useful. I therefore tentatively suggest Mystriosuchini should henceforth be defined as the most recent common ancestor of *Mystriosuchus planirostris*, *Machaeroprosopus jablonskiae* and *Machaeroprosopus buceros*, and all its common ancestors (Table 2.2).

2.4.2. *Lower-level taxonomy*

2.4.2.1. *Synonymy of* Rutiodon *and* Angistorhinus

The results of this analysis depart from both previously proposed hypotheses of the relative phylogenetic positions of these taxa: that *Rutiodon* occupies a derived position within the monophyletic clade of *Angistorhinus* (Hungerbühler and Sues, 2001), or that *Rutiodon* sits in a more derived position than *Angistorhinus*, closer to *Leptosuchus* (Hungerbühler, 1998a; Stocker, 2010). Supporting character data were not provided for the proposal of synonymy made by Hungerbühler & Sues (2001), which was published in an abstract only. In my results the two taxa form a monophyletic group, supported by two synapomorphies common to all four best-fit trees [22: 2→1; 92: 0→1]. However, the fact that *Rutiodon* consistently forms the sister group to *Angistorhinus* makes the decision of whether or not to synonymize the genera entirely arbitrary. Unfortunately, I was unable to study any material of *Brachysuchus megalodon*, which has been suggested to be synonymous with *Angistorhinus* (Long & Murry, 1995), but which was also found to be distinct by Stocker (2010).

2.4.2.2. *Angistorhinus*

In her discussion of the relationships of *Angistorhinus*, Stocker (2010) advocated the necessity for future in-depth analysis of *Angistorhinus* and its affinities. I do not present a detailed analysis or redescription of any species within *Angistorhinus*; however, my analysis is only the second to include more than one species (Hungerbühler, 1998a), and the first to incorporate further specimens that have been identified previously as *Angistorhinus*. My results provide a stable and consistently well-supported phylogenetic position for *Angistorhinus* that future descriptive and taxonomic work can build on. Furthermore, I provide additional synapomorphies for both the *Angistorhinus* clade, and relationships within it.

The *Angistorhinus* clade (Figures 2.4, 2.5, node 9; Figures 2.6, 2.7, node 11) is distinguished by two unambiguous synapomorphies common to all trees, pertaining to the parietal/squamosal bars being medially convex, and at least as wide as the postorbital/squamosal bars [56: 0→1; 58: 0→1]. Both of these characters have previously been suggested to be diagnostic features of *Angistorhinus* Mehl, 1913 (Mehl, 1915; Gregory, 1962a; Stocker, 2010) or 'Angistorhininae' Camp, 1930 (Long & Murry, 1995).

The next most inclusive clade contains *Angistorhinus talainti*, *A. grandis*, TMM 31100-1332 and USNM V 21376. This group is distinguished by the presence of a sulcus running longitudinally along the postorbital/squamosal bar [42: 0→1], and the partial or total squaring of the medial rim of the postorbital/squamosal bar and posterior process [51: 0→1].

The next most inclusive clade excludes *A. talainti*, leaving only *A. grandis*, TMM 31100-1332 and USNM V 21376. This clade is well supported by four unambiguous synapomorphies, though within the clade the basal-most member (TMM 31100-1332) shows no autapomorphies and the sister grouping of *A. grandis* with USNM V 21376 is supported by

only one synapomorphy [69: 2→1] and displays poor support values. Given the strong support for the wider clade, but the relatively poor differentiation of the OTUs within it, there may be a case for referring both TMM 31100-1332 and USNM V 21376 to *A. grandis*. The synapomorphies of this clade are: the division of the narial openings into an anterior 'anteriorly opening' section and a posterior 'dorsally opening' section [12: 0→1]; the raising of the external nares above the level of the skull roof [17: 0→1]; the posttemporal fenestra being moderately wide and dorsoventrally compressed [66: 0→1]; and the presence of an anteroposteriorly oriented ridge on the midline of the basioccipital between the basitubera [70: 0→1].

Based on these results I suggest *A. grandis* to be one of the most derived members of *Angistorhinus*, and *A. talainti* to be less derived. At face value, there does not appear to be any clear relationship between palaeogeography and phylogeny; *A. talainti*, from Morocco, nests amongst the specimens known from the west and south central USA. This finding should be expected as these locations were placed at broadly similar palaeolatitudes and were closely connected in the late Triassic.

2.4.2.3. *Monophyly of* Leptosuchus

Stocker (2010) found a strongly supported monophyletic relationship between *Leptosuchus crosbiensis* and *Leptosuchus studeri*; here, I found almost all nodes relating to *Leptosuchus*-grade taxa were extremely poorly supported in each tree. Only in the D tree did I find an arrangement approaching a monophyletic *Leptosuchus* (Figure 2.4, node 17), though with the addition of *'Smilosuchus' lithodendrorum* and PEFO 34852 as a sister clade to *L. crosbiensis*. In the DC and DCM trees *Leptosuchus studeri* forms the sister group to a clade containing *Leptosuchus crosbiensis*, but also *Pravusuchus*, *Coburgosuchus* and *Nicrosaurus* (Figure 2.5,

node 15; Figure 2.7, node 17). Support values are generally poor. In the DM tree *Leptosuchus*-grade taxa occur as a paraphyletic grade of sequentially more derived branches (Figure 2.6).

Stocker (2010) found one synapomorphy to support the monophyly of *Leptosuchus* and one further potential apomorphy under DELTRAN optimization.

Distal end of paroccipital process of opisthotic rounded, distal edge is curved rather than straight (36: 1→2). This character was excluded from analysis here as the associated morphology appears to be highly variable both inter- and intraspecifically, is often subject to damage, and scoring may change depending on small differences in viewing angle.

Jugal contributing to antorbital fenestra (4: 0→1) (potential apomorphy under DELTRAN). In my analysis this character state is optimized as basal to the entire tree, and is found in the vast majority of taxa. In this position the character does not provide unambiguous support for the monophyly of *Leptosuchus.*

2.4.2.4. *Monophyly of* Smilosuchus

The previously proposed taxonomic content of *Smilosuchus* is not monophletic in any of my best-fit trees. In the D tree (Figure 2.4) all three species are found in different locations: *S. adamanensis* forms the basal-most taxon in a clade containing all leptosuchomorph taxa excluded from Mystriosuchini except *S. gregorii* (Figure 2.4, node 14); *'S'. lithodendrorum* is deeply nested within this group, forming a close relationship with *Leptosuchus crosbiensis* (Figure 2.4, node 18); *S. gregorii* forms its own distinct branch forming a sister relationship with Mystriosuchini (Figure 2.4, node 23).

In none of the trees presented here does *'Smilosuchus' lithodendrorum* form a close relationship with any other member of *Smilosuchus*. Instead, its relationships are divergent,

being recovered in two trees as the most basal member of the newly defined Leptosuchomorpha (DC & DCM; Figures 2.5, 2.7) and in the other two nesting closely with *Leptosuchus crosbiensis* (D & DM; Figures 2.4, 2.6). The similarity to *Leptosuchus crosbiensis* has previously been noticed, leading Long & Murry (1995) to regard *'S'. lithodendrorum* as a junior synonym of the former taxon, though without a written justification (see Appendix section S1.1 for more details). I do not here revise the taxonomy of *'S'. lithodendrorum*, as the instability of its position does not allow any consistent hypothesis of its relationships to be reached. Instead, I consider the phylogenetic position of this taxon as uncertain pending a more detailed investigation into its similarity to *L. crosbiensis*.

In Stocker's (2010) analysis, the monophyly of *Smilosuchus* was supported on the basis of two synapomorphies and a further possible apomorphy under ACCTRAN optimization.

Ventral margin of squamosal gently sloping anteroventrally from posterior edge of posterior process to opisthotic process (28: 1→0). In contrast to the scorings of Stocker (2010), I found no specimen of *'S'. lithodendrorum* with a gently sloping posteroventral squamosal margin. This state was, however, found to be present in both *S. adamanensis* and *S. gregorii*. The latter taxon displays polymorphism for this character as AMNH D. VP. 3060 displays a morphology that is neither a gentle slope, nor a sharp shelf, but sits somewhere between.

In the D and DM trees (Figures 2.4, 2.6) *S. adamanensis* and *S. gregorii* apparently gain this character state (0) independently, though because the latter taxon is polymorphic for this character, the ancestral state (1) is partially retained. In the DC and DCM trees (Figures 2.5, 2.7) the ancestral state is polymorphic; therefore, depending on the tree in question this

character is either partially consistent or inconsistent with the hypothesis of monophyly between *S. adamanensis* and *S. gregorii*.

Interestingly, if *S. gregorii* is scored as '0' rather than as polymorphic, both taxa consistently form a monophyly in the D tree, whereas they were previously relatively distant phylogenetically from each other. This was also tested in the DC tree (which shares the same relative phylogenetic positions of *S. adamanensis* and *S. gregorii* as in the DM and DCM trees). However, the phylogenetic positions of these two taxa were not modified, and state '0' was also reconstructed as ancestral to the clade including *Protome batalaria* and Mystriosuchini.

Squamosal fossa extends to posterior edge of squamosal (30: 1→0). The scores for this character in the current analysis are inconsistent with those of Stocker (2010); I observed a polymorphic state in both *'S'. lithodendrorum* (TMM 31173-121: 0; UCMP 26688: 1) and *S. gregorii* (UCMP 27200: 0; AMNH 3060: 1). My character optimization is inconsistent with the hypothesis of a monophyletic *Smilosuchus*, given that character state '0' is ancestral to the majority of taxa (excluding many basal taxa for which the character is inapplicable and most species of *Machaeroprosopus*) in all four of my trees.

Lateral border of posttemporal fenestra formed by the contact of the parietal process of the squamosal and the paroccipital process of the opisthotic (37: 1→0) (potential apomorphy under ACCTRAN). My scoring for this character differs from that of Stocker (2010); I concur that *'S'. lithodendrorum* displays state '0', whereas both *S. adamanensis* and *S. gregorii* are scored as possessing a thin lamina of squamosal that slightly undercuts the border of the fenestra ventrolaterally (character state '2'). The latter condition is ancestral to both species of *S. adamanensis* and *S. gregorii*, all species of *Machaeroprosopus* and closely related taxa in all four trees (though in the D tree the ancestral state is polymorphic '0, 2'). In

trees D, DC and DCM character state ‘2’ independently characterizes the clade formed by *Nicrosaurus* and *Coburgosuchus*. Character state ‘0’ is the ancestral condition for *‘Smilosuchus’ lithodendrorum* in all four trees presented here. None of the optimizations of this character presented here support the monophyly of *Smilosuchus*.

2.4.2.5. *Position of* Pravusuchus hortus

Pravusuchus hortus has previously been indirectly implied to potentially form a close relationship with *Nicrosaurus*: *Pravusuchus* was found to form the immediate outgroup to Mystriosuchini by Stocker (2010), while *Nicrosaurus* has long been hypothesized to form a close relationship with *Mystriosuchus* and *Machaeroprosopus* (Ballew, 1989) as the most basal taxon within Mystriosuchini (Long & Murry, 1995; Hungerbühler, 2002; Parker & Irmis, 2006; Hungerbühler *et al.*, 2013). Thus my a priori assumption was that these taxa would be closely related. My results corroborate this view, with *Pravusuchus* forming the outgroup to a clade containing *Nicrosaurus* and *Coburgosuchus* in three of the four analyses (D, DC, DCM); however, these taxa are found here to nest deeply within a clade of non-Mystriosuchini leptosuchomorph taxa in all but the DM analysis.

The analysis of Stocker (2010) identified a single synapomorphy in support of a clade containing *Pravusuchus*, *Machaeroprosopus mccauleyi*, *Machaeroprosopus pristinus* and *Mystriosuchus westphali*. In the three trees in which *Pravusuchus* is the immediate outgroup of *Nicrosaurus* I found two consistent synapomorphies supporting the clade of *Pravusuchus, Nicrosaurus* and *Coburgosuchus*: presence of an infranasal recess, and absence of a furrow or ridge on the lateral surface of the squamosal/post-orbital bar [21: 0→1; 29: 1→0]. The synapomorphy identified by Stocker (2010) is discussed below.

Subsidiary opisthotic process of the squamosal present (29: 0→1). My scores for this character are partially inconsistent with those of Stocker (2010); I found *Pravusuchus* to be polymorphic for this character (PEFO 31218: 0 [although this absence may be attributable to poor preservation]; AMNH FR. 30646:1), as was the case in *Machaeroprosopus mccauleyi* (UCMP 126999: 0; PEFO 31219: 1), *Machaeroprosopus pristinus* (PEFO 382: 0; MU 525: 1; AMNH FR. 7222: 1; NMMNHS P50040: 1), and *Mystriosuchus westphali* (AMNH FR. 10644: 0; GPIT 261/001: 1).

In all four trees presented here, the most exclusive clade that contains *Pravusuchus* is not supported by the synapomorphy of Stocker (2010); instead, character optimization finds the absence of the subsidiary opisthotic process [47: 0] to be symplesiomorphic for this clade. Here I find that the presence of a subsidiary opisthotic process of the squamosal [47: 1] primarily optimizes in two alternative positions depending on tree topology. In the D and DM trees (in which *Mystriosuchus* is basal within Mystriosuchini), the presence of this character is a synapomorphy of the clade formed by USNM v 17098 and all more derived taxa. This clade includes *Machaeroprosopus mccauleyi* and *Machaeroprosopus pristinus*, but excludes *Mystriosuchus westphali* and *Pravusuchus hortus*. Therefore in these topologies, this synapomorphy is partially consistent with the aforementioned clade of Stocker (2010), though fundamentally excludes *Pravusuchus* and therefore does not provide support for its position in my trees. In the DC and DCM trees (in which *Mystriosuchus westphali* occupies a more derived position within the *Machaeroprosopus* clade), the presence of a subsidiary opisthotic process is optimized as polymorphic for the clade that includes *Machaeroprosopus mccauleyi* and all more derived taxa (including *Machaeroprosopus pristinus* and *Mystriosuchus westphali*, but excluding *Pravusuchus*). At the node one step more derived, (thus excluding *Machaeroprosopus mccauleyi*) the character is optimized as ‘present’ (1) however cannot be

regarded as a synapomorphy due to the uncertain optimization of the previous node. This is also partially consistent with the optimization of this character by Stocker (2010); however, the clade supported by this character state excludes *Pravusuchus*, and is inconsistent with Stocker's phylogenetic hypothesis.

2.4.2.6. *Position of* Nicrosaurus

The most recent novel cladistic analysis to investigate the position of *Nicrosaurus* was that of Hungerbühler (2002). The analysis found *Nicrosaurus* as the sister taxon to a clade formed by *Mystriosuchus*, '*Redondasaurus*' and *Machaeroprosopus* - congruent with the later definition of Mystriosuchini by Kammerer *et al*. (2015); however, no synapomorphies were reported in support of this clade.

In three of the four trees identified in this study (D, DC, DCM) *Nicrosaurus* groups more closely with a number of non-Mystriosuchini leptosuchomorph taxa than with Mystriosuchini. *Nicrosaurus* differs from Mystriosuchini in all trees due to the possession of a relatively long free-section of the postorbital/squamosal bar, rather than a short bar as is synapomorphic for the latter clade [43: 2→0] (although *Nicrosaurus meyeri* independently acquires a short postorbital/squamosal bar). Character optimization suggests that the relatively long 'free-section' is plesiomorphic to almost all phytosaurs. This character therefore provides no support for the hypothesized position of *Nicrosaurus* suggested by Hungerbühler (2002).

2.4.2.7. *Position of* Mystriosuchus

The dichotomy of topologies regarding the position of *Mystriosuchus*, as presented in the results section, reflects the dichotomy seen in the literature. The two most recent hypotheses

of the position of *Mystriosuchus*, based on independent datasets, are those of Hungerbühler (2002) and Stocker (2010), which respectively place *Mystriosuchus* in the less and more derived positions found in this analysis.

Less derived position. In the analysis of Hungerbühler (2002), the clade in which *Mystriosuchus* is the basal member is diagnosed with three synapomorphies.

Presence of a pre-infratemporal shelf (18: 1). I find this character in three trees (D, DC, DCM) to be a synapomorphy of the clade containing *Mystriosuchus*, '*Redondasaurus*' and many members of *Machaeroprosopus* - generally matching the clade membership of Mystriosuchini as it was previously defined in both Hungerbühler (2002) and Stocker (2010). This character is therefore largely unaffected by the placement of *Mystriosuchus*, and thus supports both hypotheses.

Presence of the pre-infratemporal shelf is restricted in my analysis almost exclusively to the clade discussed above, however this character state independently arises as a polymorphic state in *Nicrosaurus* and *Pravusuchus*, and also in *Parasuchus hislopi*.

Presence of a parietal ledge (21: 2). This character was not included in this analysis as the morphology described is dependent on the morphology of the depressed squamosal processes of the parietal, which is scored elsewhere (character 75). The morphology of this area of the skull is partially considered in character 74, which scores the ratio of width to length of the parietals between the supratemporal fenestrae. Regardless, this morphology appears to be present in all leptosuchomorph phytosaurs, and would thus be unlikely to support the clade detailed above.

Parieto/squamosal bar is strongly depressed (23: 2). I find this character to be synapomorphic for a more inclusive group than that of Hungerbühler (2002), consisting of

Smilosuchus gregorii, *Mystriosuchus planirostris*, their common ancestor and all its descendants [49: 1→2]. In three of the trees presented here (D, DC and DCM) this transformation independently occurs in *Nicrosaurus* and *Coburgosuchus*, whereas in the DM tree *Nicrosaurus* and *Coburgosuchus* are included in the clade described above. This character distribution therefore is not found here to support the clade described by Hungerbühler (2002).

No synapomorphies were listed by Hungerbühler (2002) for the clade from which *Mystriosuchus* was immediately excluded; therefore, I am unable to comment of the consistency of my synapomorphies with those of Hungerbühler (2002), for a clade containing *Machaeroprosopus* and '*Redondasaurus*' but excluding *Mystriosuchus.* The characters supporting this phylogenetic arrangement in my study are detailed in the results section.

More derived position. Stocker (2010) identified eight synapomorphies (and two potential synapomorphies under ACCTRAN) supporting a clade consisting of *Machaeroprosopus mccauleyi*, *Machaeroprosopus pristinus* and *Mystriosuchus westphali*, which, in her analysis, represented Mystriosuchini.

Interpremaxillary fossa present - narrow slit (8: 1→2). Here this character state is restricted only to *Mystriosuchus* and NHMW 1986 0024 0001, which consistently sits within the same clade as *Mystriosuchus* (and probably represents an unnamed species within this this genus), and is a synapomorphy of the node uniting these taxa in all four trees [2: 1→2]. It therefore does not provide support in my analysis for the topology hypothesized by Stocker.

Alveolar ridges not visible in lateral view (9: 0→1). I find this character to optimize as a synapomorphy in multiple locations across my four trees; however, these are mostly inconsistent with Stocker's hypothesis of this character's optimization.

In both trees which present the same topological hypothesis of the relationships of *Mystriosuchus* as Stocker (2010) (DC, DCM), this character is found as a synapomorphy of a clade containing *Machaeroprosopus pristinus*, *Machaeroprosopus buceros*, *Machaeroprosopus lottorum*, both species of '*Redondasaurus*', and *Mystriosuchus* [3: 0→1]. This synapomorphy, however, describes a morphological reversal, i.e. state 1→0, rather than 0→1 as suggested by Stocker. In the two trees in which *Mystriosuchus* occupies a more basal position (D, DM), this character is optimized as a 0→1 synapomorphy, as suggested by Stocker (2010), of a clade similar to that described above, though differing by containing all members of *Machaeroprosopus* and excluding *Mystriosuchus.* In summary, I find this character to contradict the hypothesized optimization of Stocker (2010), in that a 0→1 change is only found when *Mystriosuchus* is one of the sister taxa to *Machaeroprosopus*, rather than nesting within the clade.

Postorbital squamosal articulation approximately transverse (22: 1→2). The distribution of character state (2) is here restricted to members of *Machaeroprosopus*, *Mystriosuchus* and '*Redondasaurus*', though it twice arises independently in the *Leptosuchus*-grade OTUs PEFO 34852 and *Coburgosuchus.* Despite its restricted occurrence, this trait change [33: 1→2] is not optimized as a synapomorphy here, though the change from 0→1 is optimized in two trees (DC, DCM) as a synapomorphy of the node linking *Smilosuchus adamanensis* with all more derived members of Leptosuchomorpha. In the DM tree a 0→1 change is a defining feature of the most recent node linking the clade of *Nicrosaurus* and *Coburgosuchus* with all more derived members of Leptosuchomorpha.

Although not optimized as a synapomorphy, the distribution of this character state is broadly supportive of not only the hypothesis of Stocker (2010), but also that of Hungerbühler

(2002), as in both topologies, character state (2) is optimized as being plesiomorphic to the clade containing *Machaeroprosopus* and *Mystriosuchus.*

Lateral ridge from postorbital/squamosal bar continues strongly on lateral surface of squamosal as two raised ridges (23: 1→2). This character state was removed from the analysis as it could not be reliably identified in any species of phytosaur. A similar character state was added by Butler *et al*. (2014), referring specifically to the bifurcation of the lateral ridge in species of *Parasuchus*, though this state has not been observed in any other phytosaurs. Here I find the presence of a ridge to occur sporadically throughout the tree, though with a greater frequency in more derived members of *Machaeroprosopus.* In *Mystriosuchus* a ridge is only found as a polymorphism within *Mystriosuchus westphali*, and it is otherwise entirely absent within the genus. In topologies in which *Mystriosuchus* is a sister group of *Machaeroprosopus* the absence state is plesiomorphic to the group. When *Mystriosuchus* is found within *Machaeroprosopus*, the clade containing *Machaeroprosopus mccauleyi*, *Machaeroprosopus pristinus* and *Mystriosuchus westphali* is plesiomorphically polymorphic for this character. Furthermore, the presence of any form of ridge is only found as a synapomorphy of derived members of *Machaeroprosopus* in the D tree; in this topology *Mystriosuchus* is in any case excluded from the *Machaeroprosopus* clade.

Posterior process of squamosal dorsoventrally expanded in lateral view (25: 2→1). This character was altered to use the terminology of Ballew (1989) and Hungerbühler (2002) for the ‘knob-like’ posterior process found in *Machaeroprosopus pristinus*, *Machaeroprosopus buceros* and some specimens of *Machaeroprosopus mccauleyi*; this was done to reduce ambiguity in character scoring.

This character is not optimized as a synapomorphy of any node close to either the base of *Mystriosuchus* or *Machaeroprosopus* in any of the trees presented here. State (1) (which

here refers to the same morphology as Stocker's character) is here found to be more frequent in derived members of *Machaeroprosopus*, (excluding *Machaeroprosopus pristinus* and *Machaeroprosopus buceros* which are characterized by a state change of 1→2) and is plesiomorphic for the clade. Although the general character distribution generally supports Stocker's (2010) topological hypothesis for all other members of Stocker's '*Pseudopalatus*' clade, this character does not convey any information regarding the position of *Mystriosuchus* as the taxon lacks a posterior process and optimization of this character at the base of *Mystriosuchus* relies entirely on its position in the phylogeny. This character therefore provides no support for the inclusion of *Mystriosuchus* within *Machaeroprosopus*.

Supratemporal fenestrae fully depressed, posterior process of parietal and entire parietal/squamosal bar below level of skull roof (32: 1→2). Rather than forming a synapomorphy of only the Mystriosuchini clade used by Stocker (2010), I find this character to be synapomorphic for the node uniting *Smilosuchus gregorii* with all more derived taxa (D, DC: node 23; DM: node 22; DCM: node 25) [49: 1→2]. *Mystriosuchus* is included within this clade regardless of its position with respect to *Machaeroprosopus*, thus this character does not provide any support for the inclusion of *Mystriosuchus* within *Machaeroprosopus.*

Border of posttemporal fenestra formed laterally and slightly ventrally by process of squamosal that extends onto paroccipital process (37: 1→2). Mystriosuchus is scored here as polymorphic for this character. In the trees in which it occupies a more derived position *Mystriosuchus* forms a sister group to '*Redondasaurus*', which consistently displays character state (0); the plesiomorphic state is, in this situation, also polymorphic - providing only limited support for the hypothesis of a derived placement for *Mystriosuchus*. This character is more consistent here with the hypothesis that *Mystriosuchus* is sister to *Machaeroprosopus*, as character state (2) alone is plesiomorphic for *Mystriosuchus* in this position, and forms a

synapomorphy in three of my trees (DC, DM and DCM) for the clade formed by all descendants of the common ancestor of *Smilosuchus adamanensis* and *Mystriosuchus planirostris* [67: 0→2].

Skull shape boxy in posterior view, width across squamosals approximately equal to width across ventral edge of quadrates (38: 1→0). This character was excluded in this analysis as it is extremely sensitive to taphonomic distortion, and is highly subjective. The most basal taxon in Mystriosuchini identified by Stocker (2010) is *Machaeroprosopus mccauleyi*, which contrary to Stocker's scoring would here be considered to possess a trapezoidal skull shape, as would *Machaeroprosopus buceros* and all taxa in '*Redondasaurus*', none of which were included in Stocker's analysis. Despite the exclusion of this character, the inclusion of multiple additional taxa in this analysis may have affected the optimization of synapomorphies in the clade.

Rostral crest present, continuous and sloping steeply anteroventrally from nares to terminal rosette (19: 0→1) (Possibly additional apomorphy under ACCTRAN). The above character was altered slightly in this analysis (Appendix section S1.2); however, character state (1) of Stocker (2010) is still represented by character state (2) here. I find a wide range of synapomorphy optimizations of this character in my trees, none of which are consistent with the results of Stocker (2010).

In the DCM tree a clade containing *Mystriosuchus*, '*Redondasaurus*' and more derived members of *Machaeroprosopus* are partially defined by this character as a synapomorphy; however, *Machaeroprosopus mccauleyi* is excluded from the group and the state transformation is from the presence of a steep, continuous slope posteriorly from the terminal rosette, to the presence of a narial crest - the relatively abrupt rise from a thin, tubular

snout to the nares [7: 2→1]. Within this clade, '*Redondasaurus*' undergoes a state reversal back to the morphology of a steep, continuous crest [7: 1→2].

The D and DM trees both optimize this character as a synapomorphy of a clade including all species of *Machaeroprosopus* and '*Redondasaurus*'; in these trees, the state transformation is from the presence of a narial crest, to the presence of a partial rostral crest [7: 1→4]. A more exclusive clade within the former, containing *Machaeroprosopus mccauleyi*, *Machaeroprosopus jablonskiae* and '*Redondasaurus*' again features this character as a synapomorphy, with a state change from a partial rostral crest, to presence of a continuous steep slope [7: 4→2]; however, this feature is not preserved in *Machaeroprosopus jablonskiae* – its presence is inferred by the analysis based on the morphology present in *Machaeroprosopus mccauleyi* and '*Redondasaurus*'. *Mystriosuchus*, however, occurs in none of these clades in the two trees and this character is not found to support any relatively exclusive clade containing *Mystriosuchus*.

In the DC tree this character is not found to define any clade in which *Mystriosuchus* is placed; within close proximity to *Mystriosuchus* the only clade featuring this as a synapomorphy is '*Redondasaurus*', displaying a change from a narial crest to a continuous, steep rostral crest [7: 1→2].

Supratemporal fenestrae mostly covered/completely closed dorsally, at most only anteromedial corners of supratemporal fenestrae visible in dorsal view (33: 1→2) (Possible additional apomorphy under ACCTRAN). In the trees in which *Mystriosuchus* is recovered in a derived position this character was only found as a synapomorphy of the clade of *Mystriosuchus* + NHMW 1986 0024 0001 + MB.R. 2747; specifically, the synapomorphy denotes a character transformation from state (2) to state (1) [57: 2→1]. This does not provide support for the hypothesis of relationships within Mystriosuchini proposed by Stocker (2010);

however, the majority of nodal optimizations and scorings for this character in the other members of Mystriosuchini (and for all those included in Stocker's analysis), display character state (2). The state change observed by Stocker (2010) is likely not found here due to a polymorphic optimization of states (1) and (2) at the base of the *Machaeroprosopus* clade (*Machaeroprosopus andersoni* and all more derived taxa); at the node one step more derived (*Machaeroprosopus jablonskiae* and all more derived taxa) the character is optimized as state (2), as are the majority of following nodes. It is therefore likely that a state change of (1) to (2) [57: 1→2] is synapomorphic at the base of *Machaeroprosopus* which, in the DC and DCM topologies, is consistent with the phylogenetic hypothesis of Stocker's 'Mystriosuchini' clade.

In the D and DM trees (i.e. where *Mystriosuchus* occupies a less derived position), this character is only optimized as a synapomorphy of '*Redondasaurus*' + NMMNHS P31094, as a state change from the supratemporal fenestrae being mostly covered (state 2), to being fully covered (state 3). However, the synapomorphy suggested by Stocker (2010) is probably again suppressed due to two nodes optimized as polymorphisms bracketing the base of *Machaeroprosopus*. Using the D tree as an example: the two nodes directly basal to *Machaeroprosopus* (Figure 2.4, nodes 28, 29) are optimized as state (1) and (1 or 2) respectively; in the following node (the most basal in *Machaeroprosopus* [node 30]), this character is again optimized as (1 or 2). In the next node (node 31) the character is optimized as state (2), as are the majority of other nodes within the clade. Therefore, I suggest that the topology in the D and DM trees is also mostly consistent with the reduction in supratemporal fenestra visibility identified by Stocker (2010), except that *Mystriosuchus* is excluded from the supported clade in the D and DM trees.

Relatively few of the synapomorphies identified in previous analyses to support particular clades containing *Mystriosuchus* are corroborated here, despite the dichotomy of tree topologies presented in this analysis being broadly consistent with each of the previous studies discussed above.

2.4.2.8. *Implications from the position of* Protome

A common component of previous phylogenetic and biostratigraphic work relating to phytosaurs was the distinction between taxa (in particular *Leptosuchus* and *Machaeroprosopus*) on the basis of isolated squamosals (Ballew, 1989; Long & Murry, 1995; Parker & Irmis, 2006). This was possible because all non-Mystriosuchini members of Leptosuchomorpha possessed generally '*Leptosuchus*-like' squamosals and all members of Mystriosuchini possessed more '*Machaeroprosopus*-like' squamosals (with the exception of *Mystriosuchus* which possesses a distinctive squamosal morphology of its own), providing a clear distinction between two 'grades' of phytosaur with no overlap.

The implication of *Protome batalaria* being recovered in my study within Mystriosuchini (D and DM trees) (Figures 2.4, 2.6), and possessing a '*Leptosuchus*-like' squamosal, is to preclude the use of isolated squamosals to distinguish between Mystriosuchini and non-Mystriosuchini leptosuchomorphs. Conversely, in the DC and DCM trees *Protome* remains outside of Mystriosuchini (Figures 2.5, 2.7) and is thus consistent with the distinction of Mystriosuchini from non-Mystriosuchini taxa using only squamosal morphology.

Regardless of which tree topology is chosen, the usefulness of isolated squamosals for phylogenetic or biostratigraphic purposes is far from lost; *Protome* was never recovered within the *Machaeroprosopus* or *Mystriosuchus* clades in any of my trees, and as such has no

bearing on the identification of members of *Machaeroprosopus* or *Mystriosuchus* based on isolated squamosals. Likewise, the presence of a *Machaeroprosopus*-like or *Mystriosuchus*-like squamosal is still consistent only with members of Mystriosuchini. The placement of *Protome* in all trees in this analysis (i.e. excluded from the main *Leptosuchus* clade, and distinct from *Smilosuchus*) does, however, suggest that isolated '*Leptosuchus*-like' squamosals should no longer be automatically assigned to *Leptosuchus* or *Smilosuchus*, and depending on which phylogeny is used, they should not be used as unequivocal evidence of non-Mystriosuchini taxa. In essence, this means that *Machaeroprosopus*- and *Mystriosuchus*-like squamosals remain indicative of Mystriosuchini, whereas *Leptosuchus*-like squamosals may not be indicative of non-Mystriosuchini Leptosuchomorpha, and further details should be investigated, such as presence/absence of parietal prongs, which are exclusive to *Protome*, *Machaeroprosopus* and '*Redondasaurus*'.

2.4.2.9. *Relationship of* Machaeroprosopus pristinus *and* Machaeroprosopus buceros

Machaeroprosopus pristinus and *Machaeroprosopus buceros* have previously been suggested to be conspecific, representing sexual dimorphs (Zeigler *et al.*, 2002a); a good summary of the current state of this debate is given in Hungerbühler *et al.* (2013). This hypothesis was supported by the phylogenies of Hungerbühler (2002), Parker & Irmis (2006) and Hungerbühler *et al.* (2013) in that they recovered the two taxa as monophyletic, although the hypothesis is inconsistent with the analysis of Ballew (1989). Once again, I find a divergence in my results, with the DC and DCM trees (Figures 2.5, 2.7) supporting the hypothesis of conspecificity by resolving the taxa as sister taxa within the largely pectinate clade of *Machaeroprosopus.* The D and DM trees (Figures 2.4, 2.6) do not support this grouping –

each finding a clade within *Machaeroprosopus* consisting of *Machaeroprosopus buceros* as the sister taxon to a clade of *Machaeroprosopus pristinus* and *Machaeroprosopus lottorum.*

The monophyly of the two taxa is supported at node 32 in the DC tree by two synapomorphies: [39: 1→2] the posterior process of the squamosal is modified into a 'terminal knob', and [90: 0→1] the presence of an additional ridge on the lateral surface of the posterior process of the squamosal, ventral to the ridge or rugosity from the po/sq bar. The relationship in the DCM tree was also supported by character 90, but character 39 was incorporated into the GM character defining the lateral shape of the squamosal; this landmark character does support the node, though all other landmark characters also support the node, and almost every other node in the tree. The node was also supported in the DCM tree by a continuously measured synapomorphy: [38: 0.442-0.457→0.077-0.319] representing an elongation of the posterior process of the squamosal.

No synapomorphies were given in support of the sister relationship between *Machaeroprosopus pristinus* and *Machaeroprosopus buceros* in any of the three studies that found this relationship; however, it was proposed by Zeigler *et al.* (2002a) that the two taxa (or sexual variants) differed only in the lengths and robustness of the premaxillae and septomaxillae. My scoring generally agrees with this assertion. In fact, of the 94 characters included in my analysis, *Machaeroprosopus pristinus* and *Machaeroprosopus buceros* were found to differ in only five characters – four of which are directly related to snout shape, robustness or length (7: rostral crest; 8: relative transverse width of rostrum; 11: ratio of rostral to narial + postnarial length; 79: dorsal surface of snout – cross-sectional shape). The remaining character (89) scores the diagonal aspect ratio of the infratemporal fenestra, with *Machaeroprosopus pristinus* possessing an infratemporal fenestra with a higher aspect ratio, i.e. the fenestra is more compressed/acute.

In the D and DM trees, the relationship between *Machaeroprosopus pristinus* and *Machaeroprosopus lottorum* to the exclusion of *Machaeroprosopus buceros* is supported consistently by three characters: [7: 4→1] presence of a narial crest; [8: 2→1] relative transverse width of the rostrum - moderate; and [89: 0→1] infratemporal fenestra has a high aspect ratio (although this is represented as a GM character in the DM tree). As is the case for almost all nodes of the trees containing GM data, all landmark-based characters also support this node. It would appear to be a justifiable hypothesis to suggest that in these trees *Machaeroprosopus buceros* and *Machaeroprosopus pristinus* are only separated due to rostral morphology, as suggested by Zeigler *et al.* (2002a). It would seem likely that if rostral robusticity was assumed to be a sexually dimorphic character, and excluded from analysis, that *Machaeroprosopus buceros* and *Machaeroprosopus pristinus* would be recovered together in all tree topologies, thus providing support to the hypothesis of conspecificity.

2.4.2.10. *Monophyly of* ‘Redondasaurus’

‘*Redondasaurus*’ was originally diagnosed by Hunt & Lucas (1993) solely on the basis of the lack of visibility of the supratemporal fenestrae in dorsal view. The genus was re-diagnosed by Spielmann & Lucas (2012) with a broader complement of characters: 1) supratemporal fenestrae concealed in dorsal view; 2) reduced antorbital fenestrae; 3) a prominent pre-infratemporal shelf at the anteroventral margin of the lateral temporal fenestra; 4) septomaxillae wrap around the outer margin of the external narial opening; 5) thickened orbital margin; 6) inflated posterior nasal behind the external narial opening; 7) thickened dorsal osteoderms.

Hungerbühler *et al.* (2013) were unable to recover ‘*Redondasaurus*’ *gregorii* and ‘*Redondasaurus*’ *bermani* as a monophyletic group in any of their trees; however, I find a

monophyletic '*Redondasaurus*' (albeit nested within *Machaeroprosopus*) in all of my trees. A possible contributory factor in this difference is that species in the analysis of Hungerbühler *et al.* (2013) were scored only with reference to holotype specimens – resulting in an increased proportion of missing data in some taxa. Total proportions of missing character data in Hungerbühler *et al.* (2013) are unavailable, and therefore cannot be compared with those of taxa surrounding '*Redondasaurus*' in the present study; a further difference between these studies, however, that may be discussed is the inclusion of different characters. Many of the characters proposed by Spielmann & Lucas (2012) were not implemented in the analysis of Hungerbühler *et al.* (2013); however, in this analysis I included some of these characters that were used in previous phylogenetic studies and independently identified others which overlap to a considerable extent with those proposed synapomorphies of '*Redondasaurus*'. The consistency of the characters included in my analysis with the hypothesis of a monophyletic '*Redondasaurus*' are discussed below.

Supratemporal fenestrae concealed in dorsal view. As was briefly mentioned above, this character is found as a synapomorphy of the '*Redondasaurus*' clade in all trees presented in this study [57: 2→3], and is therefore entirely consistent with the hypothesis of Hunt & Lucas (1993). This character state occurs in no other taxon, though is found in NMMNHS P31094 (referred to '*Redondasaurus*' *gregorii* by Spielmann & Lucas 2012), which in the D and DM trees is included within the '*Redondasaurus*' clade, but in the other trees is recovered as the sister taxon of *Machaeroprosopus lottorum*, the character state having arisen independently of '*Redondasaurus*'.

Anteriormost border of pre-infratemporal shelf terminates anterior of the posteriormost corner of the antorbital fenestra. The presence of this character state is restricted almost entirely to '*Redondasaurus*' and *Mystriosuchus*; unsurprisingly, where these

two groups form a clade this character is consistently optimized as a synapomorphy. However, in the D and DM trees, where *Mystriosuchus* is placed basally, distant from '*Redondasaurus*', the character only constitutes a synapomorphy for *Mystriosuchus* rather than '*Redondasaurus*'; this may be due to the polymorphic condition of '*Redondasaurus*' *gregorii* for this character. Despite this inconsistency between trees the distribution of this character still broadly supports a monophyletic '*Redondasaurus*'.

The diagnostic characters proposed by Spielmann & Lucas (2012) for '*Redondasaurus*' but not included in my analysis are discussed briefly below. I agree that several of these support a sister taxon relationship between '*Redondasaurus*' *gregorii* and '*Redondasaurus*' *bermani*, and are therefore consistent with my results.

Reduced antorbital fenestrae. Whether or not the antorbital fenestrae are substantially reduced may be subjective; in more robust specimens of '*Redondasaurus*' (NMMNHS P-4256) the antorbital fenestra does appear smaller than in closely related taxa. However, in more gracile specimens (YPM 3294) the fenestra appears similar in proportions to those of other phytosaurs such as *Mystriosuchus.* The antorbital fenestrae do appear to exhibit a unique shape in most specimens of '*Redondasaurus*'; the general shape is roughly triangular, as is common in *Mystriosuchus* and *Machaeroprosopus*, but the anterior- and posterior-most corners of the fenestra are sharp angles, rather than smooth curves.

Septomaxillae wrap around the outer margin of the external narial opening. No taxon studied was observed to possess 'septomaxillae' that extend onto the lateral surface of the external nares. Stocker (2010) noted the presence of this character state in '*Redondasaurus*' and suggested it may also occur in *Pravusuchus hortus*; however, upon inspection of the holotype and referred specimens of *Pravusuchus hortus* it seems equally likely that the morphology described by Stocker pertains to cracks on the holotype, with the true sutures

covered by iron oxide. Rather than a lateral extension of the 'septomaxillae' the feature identified in '*Redondasaurus*' and *Pravusuchus* may represent the paranasals, identified in *Machaeroprosopus lottorum* by Hungerbühler *et al.* (2013).

Thickened orbital margin. I here concur with Spielmann & Lucas (2012); in all specimens of '*Redondasaurus*' I examined, the descending process of the postorbital appears to be greatly thickened to an extent not seen in any other group. For this particular character Spielmann & Lucas (2012) suggested it is also shared with *Coburgosuchus*; however, I see no observable expansion of the postorbital in the latter taxon to distinguish it from the condition present in most other phytosaurs. The descending process of the postorbital in *Coburgosuchus* has a roughly rectangular cross-section, with the external face relatively thin, but facing anterolaterally. If Spielmann and Lucas (2010) measured this feature in *Coburgosuchus* diagonally between the anterolateral and posteromedial corners (i.e. the full width observable in direct lateral view), this could account for the increased width, especially given the oblique angle of the process in direct lateral view. An alternative possibility is that the character is intended to describe a general thickening of the circumorbital bones, resulting in a more blunt appearance and the elevation of the orbital rim; the orbital rim in *Coburgosuchus* is dorsally elevated, but shows no other evidence of thickening (Axel Hungerbühler, pers. comm. to ASJ, 2018). This interpretation would put this character partially in conflict with character 31, 'Medial margins of orbits', and given that this morphology is measured in all other taxa based on only the flat lateral-most face of the descending process, this procedure was also applied here to preserve homology within the character.

Inflated posterior nasal behind the external narial opening. Although this entire area of skull is missing in the type specimen of '*Redondasaurus*' *gregorii* (YPM 3294), it is common to a variable extent in many other specimens referred to the genus by Spielmann &

Lucas (2012). This feature is not, however, restricted to '*Redondasaurus*', as the morphology of specimens from other taxa frequently overlap with the range of variation observed in '*Redondasaurus*'. Examples include: *Nicrosaurus kapffi* (SMNS 4379), *Machaeroprosopus mccauleyi* (PEFO 31219) and *Machaeroprosopus lottorum* (TTU-P 10076). It may be valid to say that '*Redondasaurus*' is the only taxon in which this character state consistently occurs; however, its variability makes the taxonomic utility of this feature unclear. Given the variable presence of this character in more than one species of *Machaeroprosopus*, this character is likely to support the hypothesis that '*Redondasaurus*' is nested within *Machaeroprosopus*, though verification would require the inclusion of this character in phylogenetic analyses.

Thickened dorsal osteoderms. The osteoderms of some large phytosaur taxa are also strongly thickened, e.g. *Smilosuchus gregorii* (AMNH 3060); however, I have not carried out any sufficiently detailed study of osteoderms to fully assess this proposed synapomorphy. Until more detailed work emerges on phytosaur osteoderm variation I tentatively accept this character, though emphasize that potential size correlation should be borne in mind.

2.4.2.11. *Synonymy with* Machaeroprosopus

Hungerbühler *et al*. (2013) presented three lines of reasoning in support of the synonymization of '*Redondasaurus*' into *Machaeroprosopus*. First, they argued that *Machaeroprosopus lottorum* 'bridges the morphological gap' between other members of *Machaeroprosopus* and '*Redondasaurus*' *gregorii* and '*Redondasaurus*' *bermani* in a number of features, and possesses a combination of characters formerly considered exclusive to one or other group. Second, in all trees recovered by Hungerbühler *et al*. (2013), both species of '*Redondasaurus*' were found within the clade of *Machaeroprosopus*; in analyses that were constrained to recover '*Redondasaurus*' as a monophyletic sister group to

Machaeroprosopus, tree fit lengthened by five extra steps. Third, they did not find '*Redondasaurus*' *gregorii* and '*Redondasaurus*' *bermani* to form a clade to the exclusion of species of *Machaeroprosopus* in any of their trees; instead, the two taxa were interspersed with members of *Machaeroprosopus*, with '*Redondasaurus*' *gregorii* being recovered in a substantially more derived position than '*Redondasaurus*' *bermani* in every tree.

The first two points are consistent with my results; however, with regard to their third point I find the exact opposite - that these taxa are always monophyletic to the exclusion of species of *Machaeroprosopus*. In all trees this clade is supported by two to four synapomorphies, with one (supratemporal fenestra completely obscured in dorsal view) consistently present in all trees. One exception is NMMNHS P-31094, which was previously referred to '*Redondasaurus*' (Heckert *et al.*, 2001), yet in half of my trees is found to form a monophyly with *Machaeroprosopus lottorum.* This observation corresponds well with the findings of Hungerbühler *et al*. (2013). On this basis, and due to '*Redondasaurus*' consistently being resolved within *Machaeroprosopus*, I agree with the suggestions of Long & Murry (1995) and Hungerbühler *et al*. (2013) that '*Redondasaurus*' should be synonymized with *Machaeroprosopus*. It is clear, however, from my phylogenies, differences in cranial morphology and the general difference in stratigraphic age, that the species attributed to '*Redondasaurus*' represent some of the most derived taxa within *Machaeroprosopus.*

2.4.2.12. *Specimen-level OTUs*

A number of specimens were included as individual OTUs in my analyses in order to test their affinities. Here I report on those of particular importance and those which occupy an interesting phylogenetic position.

NMMNHS P-4781. This specimen was originally assigned to *Angistorhinus* by Hunt *et al.* (1993) (see Appendix section S1.1); my analyses corroborate that view, recovering the specimen as the most basal member of the *Angistorhinus* clade in all analyses, with the node supported by some of the highest Bremer and frequency support scores in the entire tree. The node is additionally supported by a number of synspomorphies: two synapomorphies were consistent between the D, DC and DM trees [56: 0→1] parietal-squamosal bars curved medially before attaching to squamosal; [58: 0→1] parietal-squamosal bars wide – approximately the same width as the po/sq bar. One further synapomorphy was only present in the DC and DCM trees, being scored continuously [87: 0.106-0.110 (0.106-0.132 in DCM tree)→0.103] relatively robust jugal – becoming slightly more robust. Despite being less derived than all other members of the *Angistorhinus* clade, this specimen is potentially younger than the others – being from the early Norian (225–218 Mya), rather than the Carnian to early Norian (232–225 Mya).

PEFO 34852. This specimen has previously been identified as '*Smilosuchus*' *adamanensis* (Griffin *et al.*, 2017); however, I disagree with their diagnosis (see Appendix 1), suggesting the specimen shares more similarities with *Leptosuchus crosbiensis*. My analysis in part supports my hypothesis, as PEFO 34852 forms a monophyletic group with *L. crosbiensis* in half of my trees (DC and DCM). In the other half (D and DM), PEFO 34852 forms a relationship with '*Smilosuchus lithodendrorum*'; however, this group's closest sister taxon is *L. crosbiensis* in both trees, and in addition '*S. lithodendrorum*' has previously been suggested to be synonymous with *L. crosbiensis* (Long & Murry, 1995). The specimen's relationship with *L. crosbiensis* in the DC and DCM trees was supported by two consistent synapomorphies: [48: 0→1] squamosal fossa does not reach posterior edge of squamosal; [89: 0.457→0.462] increase in the aspect ratio of the infra-temporal fenestra, however the latter

synapomorphy is represented as a GM character in the DCM tree, and all other landmark-based characters also support the node. Griffin *et al.* (2017) scored character 48 in the opposite way to which I did here and could represent some subjectivity with regards to the delimitation of this character's states. This was one of the characters that was used to identify the specimen as '*S*'. *adamanensis*; however, only very few verifiable specimens of '*S*'. *adamanensis* exist and all other '*Smilosuchus*' taxa were observed to be polymorphic with regards to this character, so this may not be an ideal species identifier.

In the D and DM trees, PEFO 34852 forms a relationship with '*S. lithodendrorum*' to the exclusion of *L. crosbiensis* – this relationship is supported by two consistent synapomorphies: [3: 0→1] alveolar ridges inconsistently visible or entirely hidden in lateral view; [33: 0→2] sutural articulation of postorbital and squamosal in dorsal view – approximately transverse. In the D tree only a further synapomorphy is given: [7: 4→2] a straight, steep slope from the nares to the premaxilla; although the crest does undulate to an extent, I feel that this scoring was most appropriate, given the continuous anterior slope of the rostrum, with no horizontally level portions. In the DM condition all landmark-based characters are also found to support the node.

PEFO 34852 is the first phytosaur specimen that has been recorded as possessing three sacral vertebrae (Griffin *et al.*, 2017); however, in their discussion the authors make it clear that this apparent novel morphology is likely widespread throughout Phytosauria, being present in members of non-leptosuchomorph Mystriosuchinae (*Angistorhinus*), other non-Mystriosuchini leptosuchomorphs (holotype of '*S*'. *adamanensis*) and members of Mystriosuchini ('*Machaeroprosopus*' *zunii*, '*Redondasaurus*'), and was previously misinterpreted in past studies. The morphologies only appeared to differ in the extent to which various sutures had fused, which may be due to ontogenetic factors. Given this feature

is seemingly homogeneous within phytosaurs, the different taxonomic position for this specimen that I propose here should not affect the conclusions drawn by Griffin *et al.* (2017).

MB.R.2747. This specimen represents the only substantial Rhaetian phytosaur material from Europe, and by a considerable margin is also the largest phytosaur currently known from that continent. I consistently recovered this specimen as the basalmost taxon in the *Mystriosuchus* clade in all my trees; given the two conflicting positions in which the *Mystriosuchus* clade has been found in my trees, I also find two independent suites of synapomorphies supporting MB.R.2747 at the base of this clade. Only one character was found consistently in all trees: [85: 1→0] the pre-infratemporal shelf merges dorsally into the lateral face of the jugal, rather than continuing as a ridge to contribute to the descending process of the postorbital. In the D and DM trees in which *Mystriosuchus* occupies a more basal position, there are two additional consistent synapomorphies: [59: 1, 2→3] dorsal edge of the parietal/squamosal bar entirely, or in parts vertical; [84: 0→1] the pre-infratemporal shelf extends anteriorly past the posteriormost corner of the antorbital fenestra. In addition, in the DM condition all GM characters support this node.

In the DC and DCM trees the *Mystriosuchus* clade is also supported by two additional synapomorphies: [57: 2→1] supratemporal fenestrae mostly visible in dorsal view; [61: 2→1] lateral wall of the supraoccipital shelf is low and continuously thin. The node is additionally supported by all landmark-based characters in the DCM tree.

Similarly, to *Angistorhinus* and NMMNHS P-4781, MB.R. 2747 is basal to the *Mystriosuchus* clade, yet is younger in age (Appendix section S1.1), suggesting a ghost range for this taxon extending to the middle–late Norian. This specimen was originally referred to '*Angistorhinopsis ruetimeyeri*'; however, the type specimen of that genus and species contains no diagnostic material and may be chimaeric, and as such has been widely accepted

as a nomen dubium. The placement of this specimen at the base of the *Mystriosuchus* somewhat corroborates the speculative cranial reconstruction of the specimen by Huene (1922), in which the depressed temporal arcade and the posterior processes of the squamosals are modelled after *Mystriosuchus.* Further investigation into this specimen, including a thorough redescription, is currently underway.

USNM v 17098. This specimen was referred to *Leptosuchus* sp. by Long & Murry (1995), yet in my analyses it is constantly recovered in a more derived position than other members of non-Mystriosuchini Leptosuchomorpha; in three of my trees it is recovered within Mystriosuchini. The specimen is labelled as '*Machaeroprosopus zunii*' without any written justification, though in support of this I recover this specimen in a similar position to the holotype of '*Machaeroprosopus zunii*' in three of my trees, in one of which the two OTUs form a clade. The single clade that supports the identification of '*Machaeroprosopus zunii*' (DC tree, Figure 2.5, node 30) has a relatively good frequency support score, and possesses two synapomorphies: [39: 1→0] posterior process of the squamosal greatly dorsoventrally expanded; [53: 1→2] dorsally expressed ridge present around anterior and medial edge of the supratemporal fenestra. Whether or not USNM v 17098 is referable to '*Machaeroprosopus zunii*' does, however, remain problematic due to the erection and decription of the species based on many cranial and mandibular fragments, grouped on the basis of their geographic area of discovery, rather than morphological similarity (Camp, 1930). To produce a comprehensive reanalysis of this taxon would require intensive study of all material referred by Camp (1930); however, this is well beyond the scope of this study.

The consistently derived position of '*Machaeroprosopus zunii*' does suggest that it may not be simply a species of *Leptosuchus* as suggested by Long & Murry (1995). The phylogenetic position of USNM v 17098, and of the holotype of '*Machaeroprosopus zunii*'

(where they occupy a similar placement [Figures 2.4, 2.5, 2.6]) is supported by five consistent synapomorphies in the D and DM trees (Figures 2.4, 2.6): [3: 0→1] alveolar ridges inconsistently visible or entirely hidden in lateral view; [4: 0→1] presence of a ventral alveolar bulge between the premaxilla and maxilla; [7: 1→4] rostral crest extends horizontally from nares for less than half the length of the nares, then becomes tubular; [46: 1→0] (incorporated into landmark character in DM tree) ventral margin of squamosal slopes continuously anteroventrally from the posterior edge of the posterior process to the opisthotic process, without any horizontal edge; [47: 0→1] presence of a subsidiary opisthotic process of the squamosal. In the DC tree the position of the clade of USNM v 17098 and the holotype is supported by two different synapomorphies: [22: 3→2] reduced antorbital fossa in which the lacrimal, maxillary and jugal fossae are not touching; [75: 0→1] presence of a prominent, sharp palatal ridge. The character states scored in USNM v 17098, regarding characters 3, 4 and 46 are almost exclusively restricted to members of '*Smilosuchus*' and robust taxa in *Machaeroprosopus*. The states in characters 47 and 75 are almost exclusively limited to most members of *Machaeroprosopus*, though these states also occur in '*Smilosuchus*' *gregorii* and *Mystriosuchus* (in character 47), and in *Rutiodon*, *Nicrosaurus* and *Mystriosuchus* (in character 75). The character states recorded for characters 7 and 22 occur frequently in many taxa throughout the tree, including many members of *Leptosuchus* and '*Smilosuchus*'. Further study is required to ascertain the taxonomic validity of '*Machaeroprosopus zunii*', but I do find a reasonable quantity of evidence to support it as being distinct from *Leptosuchus*.

NMMNHS P-4256 & P-31094. These specimens have both been previously referred to '*Redondasaurus*' (Hunt, 1994a; Heckert *et al.*, 2001); however, their positions in my trees produce some uncertainty regarding this. NMMNHS P-31094 was found to form a clade with both species of '*Redondasaurus*' in two of my trees (D and DM), whilst in the same trees

NMMNHS P-4256 falls basal to *Machaeroprosopus jablonskiae*, and slightly more derived than *Machaeroprosopus mccauleyi*. The supratemporal arcade of *Machaeroprosopus jablonskiae* is robust, and also possesses some of the features of '*Redondasaurus*', such as broad and proportionately short postorbital/squamosal bars and the lack of a knob-like posterior process of the squamosal; its phylogenetic proximity to '*Redondasaurus*' is therefore unsurprising, furthermore NMMNHS P-4256 has also been referred to *Machaeroprosopus mccauleyi* (Hunt *et al.*, 2006), so the proximity of this specimen to *Machaeroprosopus mccauleyi* is also understandable. Conversely, in the DC and DCM trees NMMNHS P-4256, alongside *Machaeroprosopus mccauleyi* and *Machaeroprosopus jablonskiae* are recovered at the base of the *Machaeroprosopus* clade, suggesting that rather than being closely associated with '*Redondasaurus*', NMMNHS P-4256 appears to be more closely linked to *Machaeroprosopus mccauleyi* and *Machaeroprosopus jablonskiae*. In these tree topologies, NMMNHS P-31094 remains one of the more derived members of the *Machaeroprosopus* clade; however, it forms a clade with *Machaeroprosopus lottorum* exclusive to the slightly more derived clade formed by the two species of '*Redondasaurus*'. The node uniting NMMNHS P-31094 and *Machaeroprosopus lottorum* is supported by five synapomorphies in the DC tree, and three synapomorphies (plus all five landmark-based characters) in the DCM tree, with all synapomorphies at this node in the DC tree overlapping with those in the DCM tree. The synapomorphies are as follows: [25: 0.439-0.514 (DCM: 0.325-0.439)→0.113] antorbital fenestra is relatively short anteroposteriorly; [34: 1→2] anteroventral corner of infra-temporal fenestra in front of anterior rim of the orbit; [53: 1→0] absence of a dorsally expressed ridge around the anterior or medial edges of the supratemporal fenestra; [54: 0.180-0.197→0.039-0.095 (DCM: landmark-based)] relatively wide postorbital/squamosal bar; [89: 0.550-0.620→0.710 (DCM: landmark-based)] relatively

high aspect-ratio of the infra-temporal fenestra. In the D and DM trees the '*Redondasaurus*' clade (if defined to include both conventional species plus NMMNHS P-31094), is consistently supported by only four synapomorphies (and all landmark-based characters in the DM tree): [19: 1→0] interorbital-nasal area is flat in lateral view; [57: 2→3] supratemporal fenestra completely obscured in dorsal view; [59: 2→3] dorsal edge of the parietal/squamosal bar is either entirely or in parts vertical; [63: 1→0] supraoccipital shelf is shallow and its longitudinal axis is predominantly vertical.

Martz & Parker (2017) in part defined the base of the Apachean biozone (207–202 Ma) as the stratigraphically lowest occurrence of '*Redondasaurus*'; NMMNHS P-31094 is dated to the Rhaetian (208.5–201.3 Mya), which largely overlaps the Apachean biozone; however, NMMNHS P-4256 does not, being instead dated to the late Norian (*c.* 218–208 Mya). If the latter specimen was found to be consistently recovered within '*Redondasaurus*' it would extend the age range of this taxon, thus invalidating the definition of the Apachean given by Martz & Parker (2017). Given that NMMNHS P-4256 was never recovered within '*Redondasaurus*' in my analysis, and was separated from '*Redondasaurus*' by *Machaeroprosopus jablonskiae*, I find no reason to doubt the biozones of Martz & Parker (2017).

2.4.3. *Effects of scoring method*

2.4.3.1. *CI and RI*

The consistency indices calculated for the four character coding variables (D, DC, DM and DCM) were broadly similar; though as noted above, those which incorporated continuous data produced slightly better scores than the others. Regardless, all CI values displayed a significantly higher consistency than expected of random data (for a dataset of 43 taxa and

between 90 and 94 characters), based on comparisons with simulated data in Klassen *et al.* (1991). Differences in the retention indices (RI) were marginal between all conditions, indicating that despite the increased homoplasy in GM datasets, the same proportion of synapomorphic information was retained as in datasets excluding GM data. As the RIs of the continuous and non-continuous datasets are almost identical, it is unlikely that the difference in homoplasy indicated by CI between the datasets can be ascribed to a greater proportion of uninformative or autapomorphic characters in the continuous dataset.

2.4.3.2. *Tree length*

When comparing the tree-length (weighted homoplasy) produced by datasets with equal numbers of characters, trees that incorporate continuous data are consistently shorter than those which exclude it. The D tree (94 characters) produced a tree-length of 31.90, whereas the DC tree (94 characters) produced a length of 27.46. Likewise, the DM tree (90 characters) recovered a length of 30.52, while the DCM (90 characters) tree-length was 25.44.

The effects of including GM data cannot be interpreted in the same way as above; the base D dataset contains more characters than the DM dataset, and I would therefore naturally assume that the DM tree would be shorter just by virtue of having fewer characters. It is, however, possible to say that the continuous characters in this study do have a shortening effect on tree-length when compared to the standard discrete data tree (D vs DC tree-length). Furthermore, the incorporation of continuous data into the DM dataset (DM vs DCM tree-length) resulted in a greater reduction in tree length than was produced by the combined effect of incorporating GM data into the D dataset and the associated reduction in the number of characters (D vs DM). This may indicate that the continuous characters in this dataset produced a stronger influence on tree length than the GM characters. Additionally, as

extended implied weighting was in effect the shorter tree lengths equate to reduced homoplasy. Considering the higher consistency index of the continuous datasets, it is unsurprising that the continuous datasets also produce the shortest tree lengths when compared to D and DM, as under implied weighting, the 'length' of each character is partially calculated using the same technique as the consistency index. The overall tree-length is an ensemble score of estimated homoplasy within the dataset - similarly the CI measures ensemble consistency.

2.4.3.3. *Topological similarity*

In analyses of topological similarity (maximum agreement subtrees, SPR distances and Robinson-Foulds distance) the DC tree differed from the base discrete data tree by 37.2%, 32.5% and by 0.45122 in each respective metric, whereas the DM tree only differed from the base tree by 23.3%, 15% and 0.23171 respectively. This suggests that the incorporation of continuous characters into the base dataset altered the topology of the output tree to a greater extent than by incorporating GM characters.

Within my overall dataset, continuous characters appear to exert a stronger influence on tree topology and tree length than GM characters, and the incorporation of continuous rather than GM characters produces a tree that is found to be slightly less homoplastic by consistency index and implied weighting.

It should be noted that the elevated influence of continuous data may be related to variations in my dataset rather than an inherent property of the scoring method. For example, in the DC condition continuous data accounted for 10.64% of the characters used, but in the DM condition GM data only accounted for 5.56% of the total characters; therefore, continuous data may have more influence as it constituted a greater proportion of the data.

Alternatively, it is possible that the characters scored as continuous data may, by chance, have been less homoplastic than those scored using GM techniques. It should also be noted that these two influences are not mutually exclusive.

2.4.3.4. *Support metrics*

A slightly different finding to the above was obtained when investigating Bremer and frequency supports. When collapsing nodes with Bremer scores less than that of the average character step length (0.11), the datasets incorporating GM data (DM and DCM) produced consistently poorer total Bremer support for the collapsed tree, and retained less nodes than the non-GM datasets (D and DC). The mean Bremer support values for nodes exceeding the cut-off were almost entirely consistent between all four data treatments, whereas at the lower cut-off (0.08) these means were more variable. This suggests that the cut-off of 0.11 largely retained the nodes for which the Bremer support values were more resistant to the effects of data treatment.

In contrast to Bremer scores, frequency supports performed more consistently between scoring techniques in terms of number of nodes retained; however, similarly to the results of Bremer supports, the DCM treatment produced the worst results. The pattern of summed frequency values matched the general trend of the Bremer supports, i.e. the GM conditions produced lower total support for the collapsed tree; although, the mean frequency supports across the four collapsed trees were again relatively constant.

When the Bremer and frequency support values were averaged in five tree regions and summed within each tree, in both metrics the DC condition produced the best values and the two GM conditions produced the worst.

2.5. *Conclusions*

My analyses, split between D+DM and DC+DCM trees, broadly support the partially conflicting phylogenetic relationships recovered by previous studies (Hungerbühler & Sues, 2001; Hungerbühler, 2002; Parker & Irmis, 2006; Stocker, 2010, 2012, 2013; Hungerbühler *et al.*, 2013; Butler *et al.*, 2014; Kammerer *et al.*, 2015). In particular, a close relationship between *Rutiodon* and *Angistorhinus*, suggested by Hungerbühler & Sues (2001) was recovered in all of my trees, as was the paraphyly of '*Paleorhinus*' (Wroblewski, 2003; Parker & Irmis, 2006; Butler *et al.*, 2014), the monophyly of *Parasuchus* (Kammerer *et al.*, 2015), the placement of *Wannia* as the basalmost member of Parasuchidae (Stocker, 2013; Kammerer *et al*., 2015), the recovery of *Diandongosuchus* as the most basal member of Phytosauria (Stocker *et al*., 2017), and the synonymy of '*Redondasaurus*' and *Machaeroprosopus* (Hungerbühler *et al.*, 2013). The conflicting positions of *Mystriosuchus* were also recovered in my trees; the D and DM trees found *Mystriosuchus* as a clade basal to *Machaeroprosopus* (Hungerbühler, 2002; Parker & Irmis, 2006; Hungerbühler *et al.*, 2013), whereas the DC and DCM trees placed *Mystriosuchus* as one of the most derived clades within Mystriosuchini, and within the *Machaeroprosopus* clade (Ballew, 1989; Stocker, 2010, 2012, 2013; Butler *et al.*, 2014; Kammerer *et al.*, 2015).

Some relationships observed in my trees are inconsistent with previous analyses, such as my recovery of *Nicrosaurus* nested deeply within non-Mystriosuchini leptosuchomorph taxa, as opposed to being a basal member of Mystriosuchini; this led me to redefine Mystriosuchini, by excluding *Nicrosaurus* as an internal specifier.

Machaeroprosopus pristinus and *Machaeroprosopus buceros* were found to form a monophyly in half of my trees (DC and DM), supporting the hypothesis of conspecificity

(Zeigler *et al.*, 2002a). Furthermore, in the trees in which *Machaeroprosopus pristinus* instead formed a relationship with *Machaeroprosopus lottorum* to the exclusion of *Machaeroprosopus buceros* (D and DM), the relationship was predominantly supported by characters pertaining to rostral morphology, which have previously been proposed as signals of gender rather than species (Abel, 1922; Colbert, 1947; Zeigler *et al.*, 2002a; Hunt *et al.*, 2006; Kimmig, 2009), and if so would be irrelevant to phylogenetic analysis.

Protome was recovered in a far more derived position than before, being consistently found within Leptosuchomorpha, and in two trees within Mystriosuchini. This has the potential to cause wide ranging implications for the use of isolated phytosaur squamosals in biostratigraphy; *Leptosuchus* and leptosuchomorph phytosaurs play a prominent role in the definition of late Triassic 'biochrons' in the western US (e.g. Otischalkian, Adamanian), and phytosaur squamosals are robust, preserve well and are highly taxonomically variable (Parker & Martz, 2011; Martz & Parker, 2017). *Leptosuchus*-type squamosals have previously been restricted to non-Mystriosuchini taxa, however the potential inclusion of *Protome* (which possesses *Leptosuchus*-type squamosals) in Mystriosuchini indicates this distinction between phytosaur 'grades' may not be justified. Currently the phylogenetic placement of *Protome* is not problematic for late Triassic biochrons, as they are defined at the level of the genus (of which none of the voucher genera include *Protome*) rather than sub-family clades (e.g. Leptosuchomorpha, Mystriosuchini), and using the lowest stratigraphic occurrence; therefore even if an isolated squamosal of *Protome* is mistaken for one of the leptosuchomorph voucher genera, A) its stratigraphic position is well within the range of other leptosuchomorph taxa, B) a significantly higher stratigraphic position will not change the boundary of the Adamanian (which is defined by the base of *Machaeroprosopus*) and C) its morphology is distinct from

Machaeroprosopus-type squamosals, so regardless of its stratigraphic position it will not be used to draw down the Adamanian boundary.

I found a great deal of inconsistency in the relationships of leptosuchomorph phytosaurs, especially non-Mystriosuchini leptosuchomorphs. In contrast to the findings of Stocker (2010), I found inconsistent support for a monophyletic *Leptosuchus* (present only in condition D), and no support for the monophyly of *Smilosuchus*. The inconsistency among these phytosaurs is reminiscent of their difficult taxonomic and phylogenetic history, in which these taxa were shuffled between genera including *Rutiodon*, *Leptosuchus*, *Smilosuchus* and *Machaeroprosopus*, in various combinations (Camp, 1930; Colbert, 1947; Gregory, 1962b; Ballew, 1989; Long & Murry, 1995; Stocker, 2010). Although the overall consensus tree (Figure 2.8) suggests most derived phytosaurs could be classified as numerous monospecific genera, it seems more likely that the true phylogenetic relationships are masked by wildcard taxa/specimens and uncertainties in intra/interspecific variation. Further work, investigating the relationships of leptosuchomorph phytosaurs, building on the studies of Stocker (2010) and Hungerbühler *et al.* (2013) and including predominantly well-known, morphologically complete taxa would be very useful.

To broadly summarize my findings regarding character use - for my dataset it appears that continuous characters consistently exert a greater influence over the results than GM characters, and in comparison to datasets excluding continuous characters, they also appear to reduce homoplasy. GM characters in this study produced trees with generally worse nodal support values, and despite the lack of polytomies within the best-fit trees, when collapsing nodes to adjust for over-resolution of the tree the GM datasets retained fewer nodes at a reasonable cut-off value than the continuous and discrete trees.

A potential drawback of using GM data in particular is the relative difficulty, in comparison to discrete characters, of interpreting morphological changes in a way that is useful for producing written diagnoses. For synapomorphic continuous characters it is possible to express the character 'state' of a taxon or group as a numerical range and transformations as shifts from one range to another; however, describing subtle, but apparently phylogenetically relevant changes in shape according to geometric morphometrics necessitates either multiple diagrams of landmark displacements at supported nodes, or long breakdowns of morphology, and an elevation of analytical complexity for relatively little gain (at least in the case of this dataset). An example of the perplexity caused by GM data may be seen in the nodal synapomorphies in the treatments which incorporate GM data (Appendix section S1.3); in both trees (DM and DCM) almost all GM characters are optimized as synapomorphies for almost every node.

A further obstacle to incorporating substantial amounts of GM data into phylogenetic analyses is that in palaeontological datasets, and especially with phytosaurs, it is relatively uncommon to find the pristine, non-deformed morphologies necessary for geometric morphometric comparisons. Furthermore, GM characters may inherently encompass multiple discrete characters; if one aspect of a morphological feature is deformed (thus rendering the feature unusable for GM), all associated morphological features to be scored by the same configuration of landmarks would also have to be excluded from the analysis. In this sense, the addition of GM characters into a dataset may actually increase the quantity of missing data in a dataset where the characters could be alternatively scored with discrete or continuous methods.

Despite their drawbacks, some other studies have found GM landmark characters to improve the results of phylogenies; in a study on Vespinae, including GM characters

pertaining to wing venation, Perrard *et al.* (2016) found that when GM characters were added to a discrete character dataset, the majority of node changes in the resultant phylogeny occurred at previously poorly supported nodes in the discrete phylogeny. In a similar vein, I found that the Bremer values for tree regions 3 & 4 (i.e. the worst supported tree regions, Table 2.8) were highest in the discrete + GM character tree. In a study of 22 species of mustelid, Catalano *et al.* (2015) produced a phylogeny based exclusively on GM landmark characters. Similar to this study, the difference between their optimal phylogeny and a reference molecular phylogeny (using SPR moves) was much less than expected of random data (7 SPR moves). In this study, the difference between the discrete condition phylogeny and the discrete + GM phylogeny was only 6 SPR moves. By this criterion of success, the present study may be 'splitting hairs' in preferring discrete and continuous characters over GM ones, especially as many of the nodes that differ between these trees are poorly supported and could reasonably be collapsed.

One benefit of GM landmark-based characters was raised by Smith & Hendricks (2013) in their phylogenetic analysis of gastropod shells; in many organisms, the structures with the highest preservation potential (e.g. shells, carapaces etc.) lack discrete, scorable morphological features. In these cases, GM characters may be key in allowing greater refinement and definition in phylogenetic studies, which in-turn open the door to an array of interesting evolutionary studies, previously precluded by poor phylogenetic resolution.

Considering the pros and cons of the scoring methods outlined above, I prefer the D and DC trees as they either incorporate continuous data, exclude GM data, or both. These trees are also representative of the two conflicting topologies found in this study and are generally consistent with previous analyses of ingroup Phytosauria. On the basis of statistical comparisons and similar nodal support values I suggest that either tree would be equally valid

for use in further study; however, I find the D tree to be potentially less computationally and systematically problematic. First, the D matrix uses only discrete characters and is therefore more easily implemented into a broad range of phylogenetic software packages, allowing new data to be easily added and analysed in the future, rather than the DC matrix which (in its current form) is restricted to the software TNT. Additionally, whilst neither tree recovers high support values for non-Mystriosuchini Leptosuchomorpha, the D tree does retain a monophyletic *Leptosuchus* clade (with the addition of '*Smilosuchus lithodendrorum*'). The D tree also recovers *Mystriosuchus* as distinct from *Machaeroprosopus*, thus maintaining a valid distinction between genera respectively endemic to Europe or the USA. The genus '*Redondasaurus*' forms a clade within *Machaeroprosopus* in both trees, but in the D tree the specimen NMMNHS P-31094, (diagnosed as '*Redondasaurus*' on the basis of possessing many of the group's synapomorphies) is also a member of the clade, as expected, rather than forming a sister-group with *Machaeroprosopus lottorum* as in the DC tree. The position of *Machaeroprosopus lottorum* in the D tree, in a sister-group with *Machaeroprosopus pristinus*, supports the validity of the latter taxon, suggesting it is not a sexual dimorph of *Machaeroprosopus buceros*. For these reasons, I tentatively suggest the use of the discrete-character tree for further analyses.

Chapter 3 Authorship Statement:

The content of Chapter 3 was created in collaboration with Pedro Godoy; Andrew Jones devised the study, collected all phytosaur data, carried out all analyses, produced all figures and entirely wrote the chapter.

Pedro Godoy provided crocodylomorph data and phylogenetic trees, and provided suggestions and insight into the timescaling of trees for evolutionary rates analysis.

Chapter 3: A two-dimensional geometric morphometric comparison of cranial convergence and evolution in phytosaurs and crocodylomorphs

3.1. *Introduction*

The apparent morphological convergences between phytosaurs and crocodylians have led to the latter group being used as models to generate hypotheses of phytosaur ecology (Colbert, 1947; Hunt, 1989; Kimmig & Arp, 2010). Despite their excellent fossil record, including abundant cranial remains, there have been few studies attempting to quantitatively compare phytosaur and crocodylian morphologies (Colbert, 1947; Hurlburt *et al*., 2003; Irmis, 2007; Kimmig & Spielmann, 2011), and thus these hypotheses of morphological and ecological convergence remain largely untested.

The disparity of morphologies within Phytosauria has also never been explicitly investigated, although numerous hypotheses have been proposed. Most phytosaur genera apparently contain at least one gracile/uncrested and one robust/crested skull morphology (Ballew, 1989; Hunt, 1989), though there is disagreement in whether this represents sexual dimorphism (Zeigler *et al.*, 2002a; 2003a), ontogenetic effects (Colbert, 1947; Gregory, 1962a) or ecological partitioning of distinct taxa (Ballew, 1989; Hunt, 1989; 1994). Hunt (1989) qualitatively suggested the existence of three phytosaur 'morphotypes', based primarily on the disparity of robust to gracile cranial morphologies, and he argued that these morphotypes represent predaceous, generalist and piscivorous ecologies, based upon comparisons to *Crocodylus niloticus, Alligator mississippiensis* and *Gavialis gangeticus* respectively. This hypothesis of distinct ecological morphotypes within Phytosauria appears

plausible; however, the direct mapping of morphotypes between phytosaurs and crocodylians is precluded by distinct morphological differences. For example, modern crocodylians achieve cranial robusticity via medio-lateral rostral expansion and dorso-ventral expansions of areas along the tooth row; robust phytosaurs share the expansion of the alveolar borders with crocodylians (Camp, 1930), but more typically have dorsoventrally expanded rostra.

A quantitative geometric morphometric analysis of phytosaurs and extant crocodylian taxa was briefly presented by Kimmig and Spielmann (2011) and displayed an apparent separation of phytosaurs and crocodylians in morphospace with a small amount of overlap. It is however difficult to draw conclusions from this analysis as no outgroup taxa were included to provide evolutionary context, there is no indication of the shape differences that separate the groups, and the positions of landmarks used for the analysis were not reported.

I here aim to quantify the morphological variation in phytosaur crania noted in previous studies, and identify cranial traits that may covary. In addition, I aim to address a number of questions:

1) What are the primary trajectories of shape variation present within and between phytosaurs and crocodylomorphs: how and to what extent do their morphologies overlap?

2) Are phytosaurs and crocodylomorphs comparable in their breadth of morphological disparity and how does the disparity of crown Crocodylia compare to that of Phytosauria?

3) Can phytosaurs be quantitatively divided into distinct morphotypes in the manner suggested by Hunt (1989)?

4) Are there significant changes in the rates of cranial morphological evolution either within phytosaurs and crocodylomorphs, or between these groups?

3.2. *Materials and Methods*

3.2.1. *Data collection*

Two photographic datasets were compiled, corresponding to dorsal and lateral skull orientations. The dorsal dataset comprised 50 crocodylomorphs, 21 phytosaurs and six outgroup taxa; the lateral dataset consisted of 36 crocodylomorphs, 24 phytosaurs and seven outgroup taxa. Phytosaur and crocodylomorph taxa were sampled as widely as possible, such that the majority of major groups (and theoretically therefore the majority of morphologies) were represented. Special emphasis was put on incorporating taxa from crown Crocodylia, being the most frequent analogy to phytosaurs in the literature. Specimens were selected based on the completeness of the skull and level of deformation to ensure that a full suite of landmarks could be digitised for every taxon. For direct comparison of morphological evolutionary tempo between phytosaurs and crocodylomorphs a single phylogenetic tree was required, containing both groups. To facilitate this a series of outgroup taxa were incorporated into both datasets to a) represent generic carnivorous archosauromorph cranial morphologies, basal to all groups, and b) bridge the evolutionary gap between phytosaurs and crocodylomorphs. Outgroup taxa were chosen to represent the diverse array of morphologies among late Triassic pseudosuchians, and taxa basal to Archosauria and Dinosauria. The majority of phytosaur specimens in the analysis were examined and photographed by A. Jones; the majority of crocodylomorph specimens were examined and photographed by P. Godoy. The images used in landmarking the outgroup taxa and a small number of phytosaurs and crocodylomorphs were obtained from figures published in the literature. The outgroup taxa were all landmarked on the basis of cranial reconstructions previously published in the

literature; all reconstructions were compared against images of the specimen(s) upon which they were based, to ensure they represented realistic hypotheses of shape. It should be noted that the shapes of outgroup taxa in these analyses do not represent their true shape, but a close approximation, therefore conclusions should not be drawn about these taxa specifically; their purpose here is to help define the morphospace with a range of late Triassic morphological diversity and more generic ancestral archosauromorph cranial shapes. A full list of taxa, specimen numbers and references (where images were used from the literature), for both dorsal and lateral conditions, is available in Tables S2.1 & S2.2.

3.2.2. *Choice of landmarks*

Cranial shape was summarised using two-dimensional Cartesian coordinate-based landmarks. A 2D geometric morphometric analysis was prioritised here over a 3D analysis due to the greater and more inclusive sample size afforded by 2D data. Two-dimensional images of phytosaurs, crocodylians and outgroup taxa can commonly be found in the literature, and were made available by my collaborator (P. Godoy) whereas sufficiently non-distorted 3D models are largely absent. This being said, I have collected a photogrammetric dataset incorporating both phytosaurs and extant crocodylomorphs, though this will be analysed elsewhere.

Separate landmarking regimes were used for the dorsal and lateral conditions. Sliding semilandmarks were used alongside Type I and Type II landmarks (Rohlf & Bookstein, 1990) to allow overall shape to be captured. Type I and II landmarks correspond to homologous points on each specimen; however, the use of homologous points when comparing convergently evolved structures (where similar morphologies may have evolved from

different underlying elements) may be problematic. For example, while phytosaurs and extant crocodylomorphs share similar general cranial morphology, the roles and locations of individual bones are in many cases highly divergent. The elongation of the rostrum in phytosaurs is predominantly attributable to the anteroposterior extension of the premaxillae; however, in crocodylomorphs the elongate rostrum is primarily formed by the maxillae. Including one or more type I landmarks for the premaxilla-maxilla suture might therefore lead to strong separation of phytosaur and crocodylomorph rostra in morphospace due to the relative size differences of the premaxillae and maxillae, despite the apparent overall shape similarity. The aims of this study were to investigate the evolutionary convergence of overall morphology, therefore Type I and II landmarks were used sparingly and only for certain structures; precedence was given to sliding semilandmarks to define the majority of skull shape. Landmarking was performed in the software tpsDig2 v.2.19 (Rohlf, 2015). Semilandmark paths were digitised using the 'draw background curves' tool to define shape; landmark points defining the curves were then resampled to a predefined number of points and equally spaced along the length of the path. Two '.tps' files containing landmark data for all specimens in each condition were read into the Geomorph package in R (Adams *et al.*, 2018), in which landmarks to be considered as 'sliding semilandmarks' were defined, as well as the vectors along which they would be permitted to move during Procrustes superimposition.

In dorsal orientation landmarks were placed on only one half of the skull as few specimens preserved pristine morphology on both their left and right sides. During landmarking specimens were mirrored as necessary to ensure landmarks could always be placed on the left side of the specimen. Landmarking both sides was unnecessary as all taxa

included in this study display bilateral symmetry, and would only serve to artificially increase the degrees of freedom.

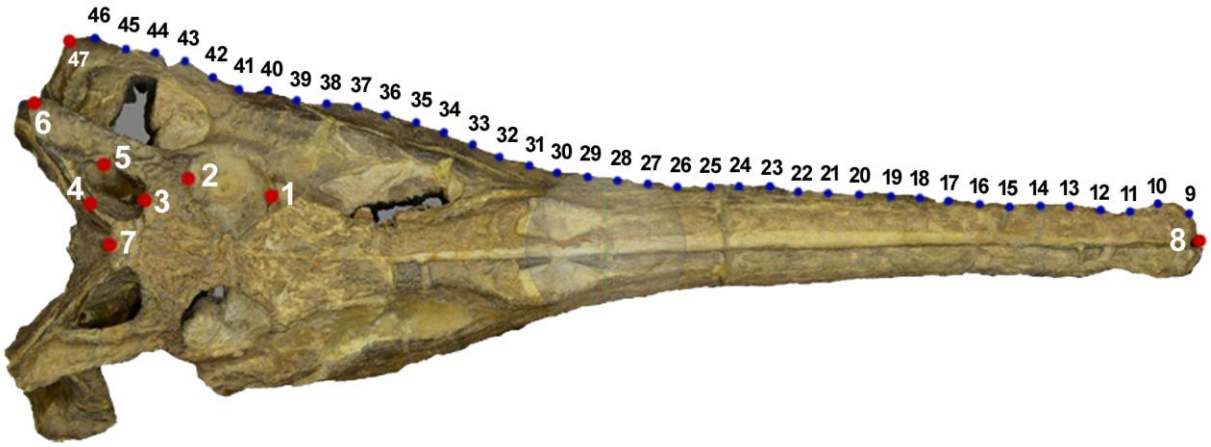

Figure 3.1: Dorsal landmarking regime. Larger red circles, numbered in white indicate type I and II landmarks, smaller blue circles, labelled in black represent sliding semilandmarks. Numbers indicate the order of digitisation.

Landmarks (Figure 3.1) were placed as follows: 1) anterior-most orbital border; 2) posterior-most orbital border; 3) anterior-most border of the supratemporal fenestra; 4) medial border of the supratemporal fenestra at the midpoint between the anterior and posterior fenestral border; 5) lateral border of the supratemporal fenestra at the midpoint between the anterior and posterior fenestral border; 6) posterior-most extent of the squamosal; 7) the posterior-most extent of the parietals on the midline; 8) the anterior-most point of the rostrum on the midline. From landmark 8 a series of 38 sliding semilandmarks extended posteriorly, defining the lateral border of the cranium, delimited posteriorly by landmark 47: the postero-lateral corner of the quadrate.

In lateral orientation specimens were again mirrored to maintain a standard right-side view. Landmarks (Figure 3.2) were placed as follows: 1) postero-ventral corner of the

quadrate; 2) posterior-most border of the orbit; 3) anterior-most border of the orbit; 4) the ventral border of the skull at the posterior extent of the maxilla. From landmark 4, a series of 28 semilandmarks extended along the ventral border of the skull corresponding to the tooth row, delimited anteriorly by landmark 33: the anterior border of the first tooth alveolus (or if not visible at the antero-ventral corner of the rostrum).

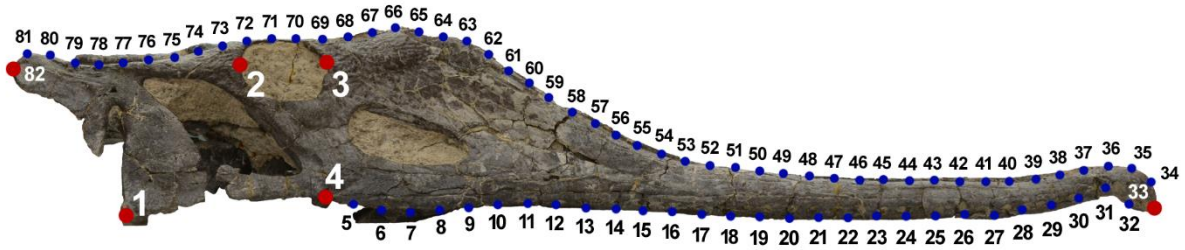

Figure 3.2: Lateral landmarking regime. Circle and numbering styles remain the same as in Figure 3.1. Sliding semilandmarks are split into two separate curves, each defined anteriorly at landmark 33.

From landmark 33, a series of 48 semilandmarks defined the anterior and dorsal borders of the skull, delimited posteriorly by landmark 82: the posterior-most extent of the squamosal.

3.2.3. *Procrustes alignment*

Prior to Procrustes alignment an additional step was performed on dorsal coordinate data to ensure specimens were aligned along the midlines of each specimen, rather than the centroid of all specimens, which in this case would be calculated from landmarks representing only one half of each skull. Not aligning along the midline would result in a proportion of laterally directed shape variation being erroneously attributed to misaligned midlines (Figure 3.3a). To resolve this the local coordinate system of each dorsally orientated specimen was rotated such

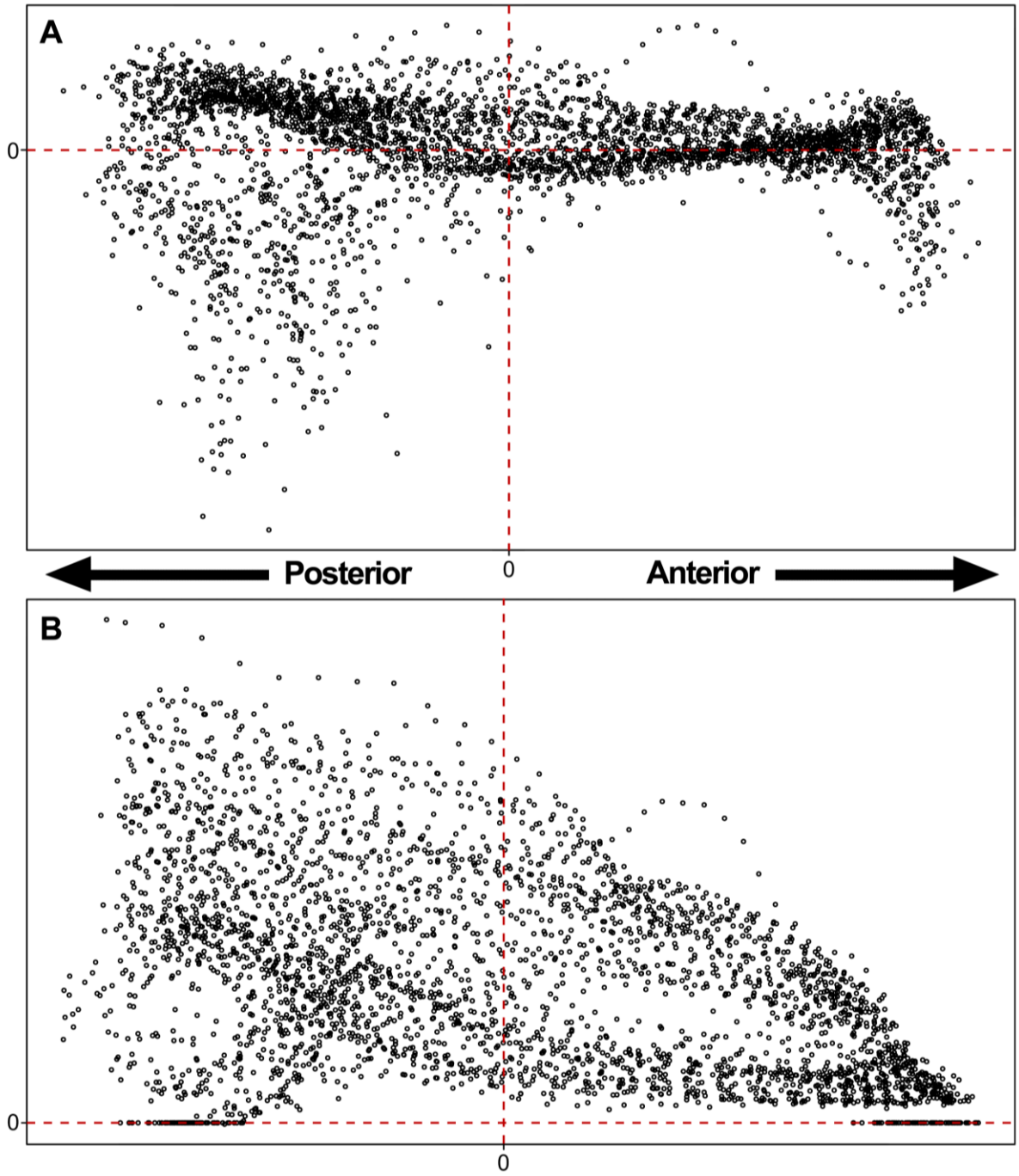

Figure 3.3: Procrustes alignment of landmarks in dorsal view; only one half of the skull is landmarked to avoid an arbitrary doubling of symmetric landmark information. A) Landmark alignment when using standard Procrustes superimposition: specimens are aligned on the Y axis by the centroid, resulting in misaligned midlines and significant variation occurring 'past' the midline. B) Procrustes alignment in which the Y axis is correctly aligned on the midline.

that landmarks 7 and 8 (posterior extremity of parietal and anterior extremity of the rostrum, respectively) were aligned at zero on the Y-axis, then all landmarks (excluding 7 and 8) were mirrored to create a perfectly 'bilateral' set of landmarks. Due to the perfect symmetry of all specimens about the X-axis, Procrustes superimposition aligned all specimens along their line of bilateral symmetry. Following alignment, all duplicate coordinates were removed (Figure 3.3b).

Artificially creating perfect bilateral symmetry also allowed landmarks 1 and 2, which summarise the relative size of the orbit, to be adjusted to account for mediolateral variation in the anterior and posterior extremities of the orbit, caused by differences in orbital shape. Mediolateral paths were defined, along which orbital landmarks could slide during alignment – leaving only variation due to the relative antero-posterior size of the orbit. This procedure was carried out in the software R (R core team, 2016).

The Geomorph package for R was used to perform all Procrustes superimposition (Adams & Otarola-Castillo, 2013); during the procedure semilandmarks were allowed to 'slide' to minimise the bending energy along their curve (Bookstein, 1997). Principal Components Analyses (PCAs) were also performed, and the resulting morphospaces produced in Geomorph.

3.2.4. *Creating phylogenetic trees*

Phylogenetic trees for Phytosauria, corresponding to the taxon sampling of the dorsal and lateral conditions were constructed in the software Mesquite (Maddison & Maddison, 2016), and were based on the topology of the discrete character tree of Chapter 2. Where species were represented by more than one specimen, the relationships between specimens were

portrayed as polytomies. This resulted in a tree for the dorsal condition containing 21 specimens across 16 species (Figure 3.4a) and for the lateral condition 24 specimens across 15 species (Figure 3.4b).

The general relationships between major crocodylomorph clades (i.e. Notosuchia, Thalattosuchia, Tethysuchia and Neosuchia) follow that of the supertree proposed by Bronzati *et al*. (2015) and Godoy *et al*. (2018). The relationships among taxa within Notosuchia follow the general arrangement presented by Pol *et al.* (2014). Within Tethysuchia, relationships follow Meunier & Larsson (2017) and Hastings *et al*. (2015). Relationships among thalattosuchians follow Young (2014) and Herrera *et al*. (2015). For the relationships within the crown-group, I follow Brochu (2012), Brochu *et al*. (2012), Scheyer *et al*. (2013) and Narváez *et al.* (2015). Sampling of crocodylomorph taxa included only one specimen of each taxon, therefore a species-level tree was sufficient rather than specimen-level. For the dorsal condition this tree contained 50 taxa (Figure 3.5a) and in the lateral condition 36 taxa (Figure 3.5b).

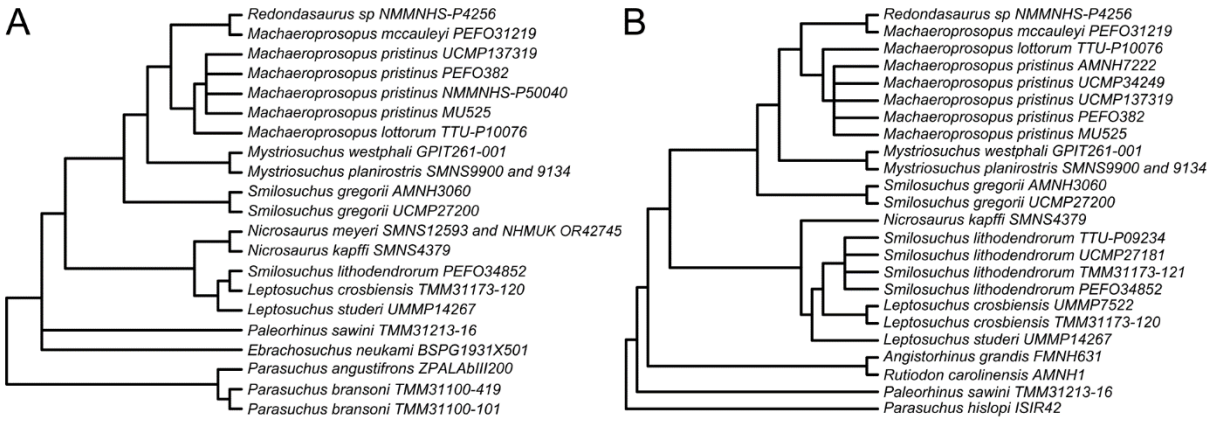

Figure 3.4: A) Phylogeny of Phytosauria used in analyses of the dorsal dataset. B) Phylogeny of Phytosauria used in analyses of the lateral dataset.

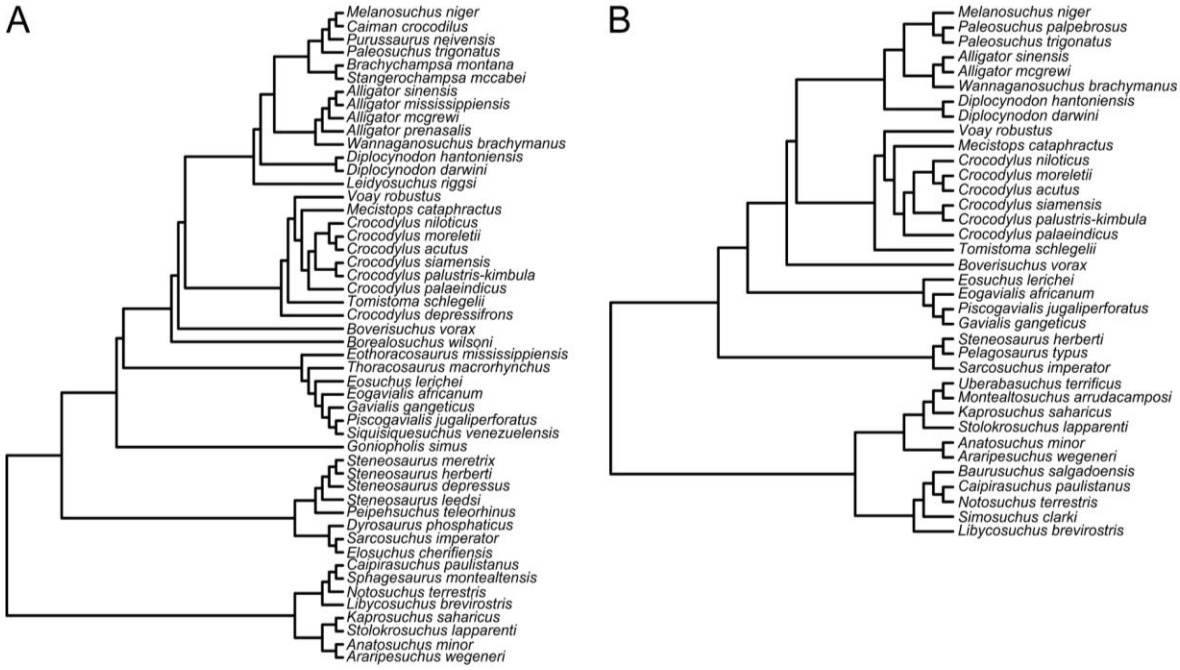

Figure 3.5: A) Phylogeny of Crocodylomorpha used in analyses of the dorsal dataset. B) Phylogeny of Crocodylomorpha used in analyses of the lateral dataset.

Relationships among outgroup taxa were defined based on the phylogenies of Nesbitt (2011) and Ezcurra (2016), with phytosaurs occupying the most basal position within Pseudosuchia, as is consistent with the latter analysis. The full composite trees for the dorsal and lateral conditions are shown in Figure 3.6.

For analysis, phytosaurs and crocodylomorphs were split into a series of smaller clades and taxonomic grades to allow comparison at higher resolution. Phytosauria was split into the grades non-Mystriosuchinae parasuchids (basal Parasuchidae), non-leptosuchomorph Mystriosuchinae (basal Mystriosuchinae), non-Mystriosuchini leptosuchomorphs (basal Leptosuchomorpha), and the clade Mystriosuchini. Crocodylomorpha was split into Notosuchia, Tethysuchia, Thalattosuchia, stem Neosuchia, Gavialoidea, Planocraniidae, Crocodyloidea and Alligatoroidea. Group membership is shown in Figure 3.6.

3.2.5. *Analyses of disparity*

Although inferences of ecology based on morphology can be problematic (Wainwright *et al.*, 2005), it is generally accepted that a major proportion of rostral morphological variation in extant Crocodylia is explained by ecological niche exploitation (Piras *et al.*, 2013). Studies have identified morphological convergence to exist within Crocodylia that can be linked to shared ecological/functional pressures (McHenry *et al.*, 2006; Pierce *et al.*, 2008; Sadleir & Makovicky, 2008); further studies have analysed various aspects of rostral/cranial morphology in relation to feeding and ecology (Bolt, 1974; Thorbjarnarson, 1990; Busbey, 1995; Erickson, 2003, 2005, 2012; McHenry *et al.*, 2006; Walmsley *et al.*, 2013). Although the ecology of phytosaurs is not directly observable, given their general morphological convergence with crocodylomorphs they were likely affected by the same biomechanical constraints, with some quantitative evidence supporting this (Lemanis, 2012). Here, I therefore use morphological disparity as an approximation of ecological variability, to compare phytosaurs with crown Crocodylia – the crocodylomorph group with which they are most often compared. Disparity was calculated using a modified R script from Foth *et al.* (2016), which allowed statistical comparison of groups by comparing the test dataset with 10,000 permutations of the same dataset in which taxa and principal component (PC) scores were randomly shuffled. In both dorsal and lateral orientations, I compared morphological disparity between phytosaurs and crown Crocodylia, as well as its three constituent subclades, Alligatoroidea, Crocodyloidea, and Gavialoidea.

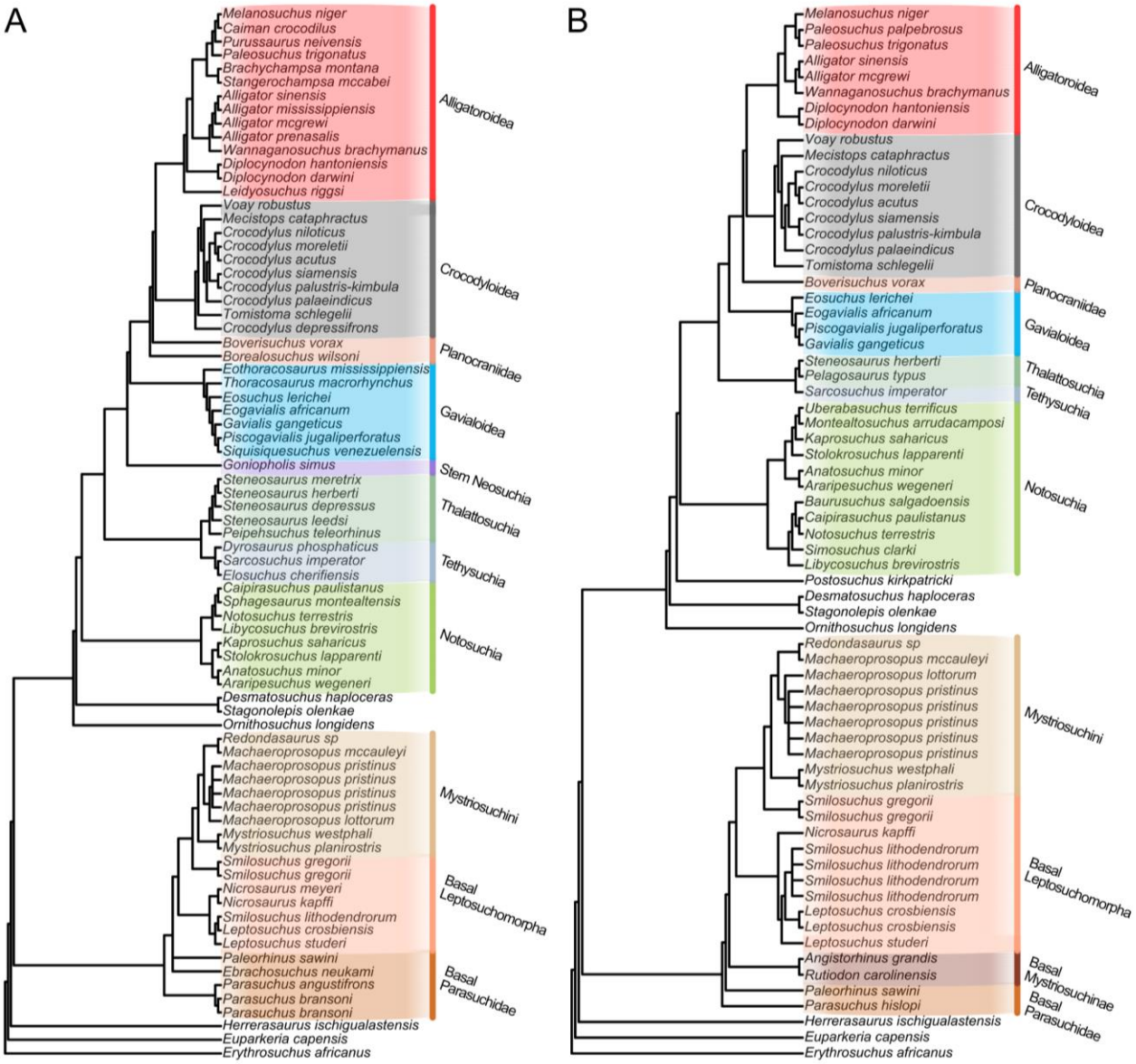

Figure 3.6: Complete phylogenies including Phytosauria, Crocodylomorpha and all outgroup taxa; all phytosaur and crocodylomorph groups investigated in analyses are colour-coded and labelled. A) Dorsal condition phylogeny. B) Lateral condition phylogeny.

3.2.6. *Testing the 'three phytosaur morphotypes' of Hunt (1989)*

In his study, Hunt (1989) identified three exemplar phytosaur taxa for each of his three morphotypes (1. slender snouted with homodont dentition; 2. Moderately slender snouted with heterodont dentition; 3. Massive snouted). However, of the nine examples provided, only

five are represented in this study in either of the dorsal or lateral conditions. Furthermore, three of the examples presented by Hunt (1989) were at genus level ('*Paleorhinus*', *Angistorhinus* and '*Brachysuchus*'). The taxa formerly considered to be part of '*Paleorhinus*' are now split into more than one genus, including *Wannia*, *Parasuchus* and *Ebrachosuchus* (see Chapter 2), and show varying levels of robusticity. *Ebrachosuchus* is extremely gracile, *Parasuchus bransoni*, *P. angustifrons* and *P. hislopi* are intermediate, while '*Paleorhinus*' *sawini* is much more robust. Similar variation also occurs among species within *Angistorhinus*. Given that there is some ambiguity in Hunt's suggestions, the phytosaur taxa included within this study were assigned into the three morphotype groups in a qualitative manner – following the more specific suggestions of Hunt (1989) and taking into account his criteria for each morphotype (Hunt 1989: p. 350):

> "1. A form with a slender, elongate snout with homodont dentition consisting of cylindrical, usually, non-serrated teeth.
>
> 2. A relatively slender snouted form with a more robust rostrum, usually surmounted by a crest, with heterodont dentition including slicing blade teeth.
>
> 3. A massive skulled form with heterodont dentition and a proportionately short snout."

A list of assigned morphotype groups is available in Table 3.1.

Following group assignment, PC scores were obtained from the phytosaur-only PCAs of the dorsal and lateral conditions. These scores were subjected to linear discriminant analysis (LDA) in the software PAST (Hammer *et al.*, 2001) with jackknife cross validation to test the efficacy of group separation according to the above criteria. PC scores were

incorporated into the LDA until their proportion of total variance dropped to below 5%, in order to ensure that only meaningful covariation was incorporated into the analysis.

Table 3.1: Assigned phytosaur morphotypes, based on the criteria of Hunt (1989).

Taxon	Putative Morphotype
Ebrachosuchus neukami	Gracile/Piscivorous
Machaeroprosopus lottorum	Gracile/Piscivorous
Machaeroprosopus pristinus	Gracile/Piscivorous
Mystriosuchus planirostris	Gracile/Piscivorous
Rutiodon carolinensis	Gracile/Piscivorous
Angistorhinus grandis	Moderate/Generalist
Leptosuchus crosbiensis	Moderate/Generalist
Leptosuchus studeri	Moderate/Generalist
Mystriosuchus westphali	Moderate/Generalist
Nicrosaurus meyeri	Moderate/Generalist
Parasuchus angustifrons	Moderate/Generalist
Parasuchus bransoni	Moderate/Generalist
Parasuchus hislopi	Moderate/Generalist
'Redondasaurus' ?bermani	Robust/'Predaceous'
'Smilosuchus lithodendrorum'	Robust/'Predaceous'
Machaeroprosopus mccauleyi	Robust/'Predaceous'
Nicrosaurus kapffi	Robust/'Predaceous'
'*Paleorhinus*' *sawini*	Robust/'Predaceous'
Smilosuchus gregorii	Robust/'Predaceous'

3.2.7. *Time-scaling and rates analyses*

Trees were time-scaled using the function 'timePaleoPhy' within the R package 'Paleotree' (Bapst, 2012). Taxon time-ranges represented stratigraphic uncertainty rather than definite first and last appearance dates. To accommodate this uncertainty, the function offers the option to randomly draw single-point dates for each terminal, from a uniform distribution

bounded by the corresponding terminal's temporal range. For every tree undergoing this procedure, I produced 100 replicate time-calibrated trees with randomly permuted tip-ages. For time-scaling, the method 'minimum branch length' was used (Laurin, 2004), with each branch being greater than or equal to one million years in duration. Phytosaur age range estimates were taken from Appendix section S1.1, and range estimates for crocodylomorphs and outgroup taxa were taken from the Paleobiology Database (https://paleobiodb.org/#/).

Two methods of analysing morphological evolutionary rate were employed in this study; the first uses likelihood methods to simulate rates of evolution, while the second directly calculates evolutionary rates as morphological change over branch duration, as in Lloyd *et al*. (2011), and in part is similar to the 'Branch Randomization' procedure of that study, but modified to accommodate continuous morphological data.

The first method, henceforth referred to as 'SimRates', was conducted in Geomorph, using the function 'compare.evol.rates' which uses a Brownian motion evolutionary model to compare evolutionary rates (Adams, 2014). To allow effective comparison within and between phytosaurs and crocodylomorphs, taxa were split into a series of smaller, phylogenetically meaningful groups, summarised in Tables S2.1 and S2.2. Significance of differences in evolutionary rates between groups was calculated using the 'simulation' method, as in Juarez (2015) and Sherratt *et al*. (2017). The analysis was performed on each of the 100 replicate variants of the time-scaled tree. P values were calculated for each tree to indicate whether any significant differences in rates occurred between any groups; if more than 95% of P values from these trees were found to be significant at $P<0.05$, it was accepted that significant differences in evolutionary rate were present between taxonomic groups.

In the second method (here referred to as "CalcRates"), Procrustes aligned specimen data was first plotted with a corresponding phylogenetic tree as a phylomorphospace (Sidlauskas, 2008) with the Geomorph function 'plotGMPhyloMorphoSpace', in which x, y landmark coordinate data of estimated ancestral morphologies (i.e. the nodes of the phylogeny) were calculated using maximum likelihood by the 'fastAnc' phytools function. These data were combined with those Procrustes aligned landmark coordinates of the original terminal taxa and subjected to PCA; this resulted in the same distribution of terminal taxa in morphospace as in the original phylomorphospace, but allowed plotting of the ancestral phylogenetic nodes. Observation of scree plots from PCAs of the original terminal taxa, suggested that PCs 1 and 2 were sufficient to encompass the most important components of shape variation; therefore, PC scores from the first two principal components were collected. These PC scores were used as coordinates to calculate the Euclidean distances in morphospace between nodes of the phylogeny, thus producing a dataset of phylogenetic branch lengths for all branches in the tree, scaled by morphological change between nodes. Values of morphological change were then divided by the duration of their corresponding branches on the time scaled trees to produce a dataset of observed rates of morphological evolution in 100 variants of time-scaled trees.

This dataset was then analysed to investigate whether any evolutionary rates were faster or slower than expected under a null hypothesis of evolution; this used conceptually similar techniques to the 'Branch Randomization' of Lloyd *et al*. (2011).

A dataset was created to model the null hypothesis by creating 1000 trees with random levels of morphological change mapped along the branches. To achieve this the mean morphological change across the entire tree (multiplied by 1000 due to low morphological change) was multiplied by the number of branches, to give the value 'reps'. Having multiplied

mean morphological change by 1000, values were randomly drawn from a uniform distribution between 0 and 0.002, and were added to the tree at random branches; the procedure was repeated for 'reps' iterations.

This procedure models the null hypothesis that morphological evolution is equally likely to occur at any point on the tree, at any point in time. The sum and mean quantities of morphological change for each resulting tree were approximately equal to that of the original tree, allowing for variation in each 'unit' of random morphological variation added to the tree to simulate stochasticity.

Rates for these trees were calculated in the same way as in the original tree (change/time), again with the rate of each branch calculated 100 times, to take into account variability in taxonomic temporal ranges. This resulted in a null-hypothesis dataset of 1000 trees with randomised rates of evolution, with 100 estimates of evolutionary rate per branch.

Morphological rate differences were investigated among the same groups as used in the SimRates technique (above) by concatenating the rates of all branches within a given group into a single distribution, spanning all evolutionary rates within that group. The method of comparison used by Lloyd *et al.* (2011) for their "branch randomization" analysis essentially comprised a comparison of the overlap between the random and observed distributions. A 'significant' difference was assumed when both distributions overlapped by less than 5%. I use the same approach, but modified to compare groups rather than individual branches, using the R package 'Overlapping 1.5.0' (Pastore, 2017) to estimate overlap between random and observed distributions. This method does not constitute a true statistical test of significant differences as is achieved by, for example, a T-test but was chosen because the dataset does not satisfy the criteria of either parametric or non-parametric tests (normal

distribution of residuals and equality of variances). Whilst I am presently unable to assess statistical differences in this analysis, the method employed here does allow quantitative differences to be identified and discussed in a qualitative way, which should be at-least sufficient to inform future analyses.

3.3. *Results*

3.3.1. *Trends of shape variation within Phytosauria*

Dorsal view: The scree plot derived from PCA of phytosaurs alone suggests that the first three PC axes represent the most significant aspects of cranial morphological variation in this group.

The first principal component accounts for 71.2% of variation, and predominantly represents changes in the robusticity of the lateral margin of the skull, including (at the robust end of the scale) the lateral expansion of the terminal rosette, lateral bulge at the anteriormost contact of the premaxilla and maxilla, lateral convexity of the maxilla, and a general increase in width, resulting in the margin of the skull becoming more laterally positioned with respect to the orbit and supratemporal fenestra (Figure 3.7a).

Principal component 2 represents 11.7% of variation and encapsulates the shrinking of the supratemporal fenestra in dorsal view (as it becomes depressed below the level of the skull roof in more derived phytosaurs) and the anteroposterior elongation of the posterior process of the squamosal with respect to the position of the quadrate condyle.

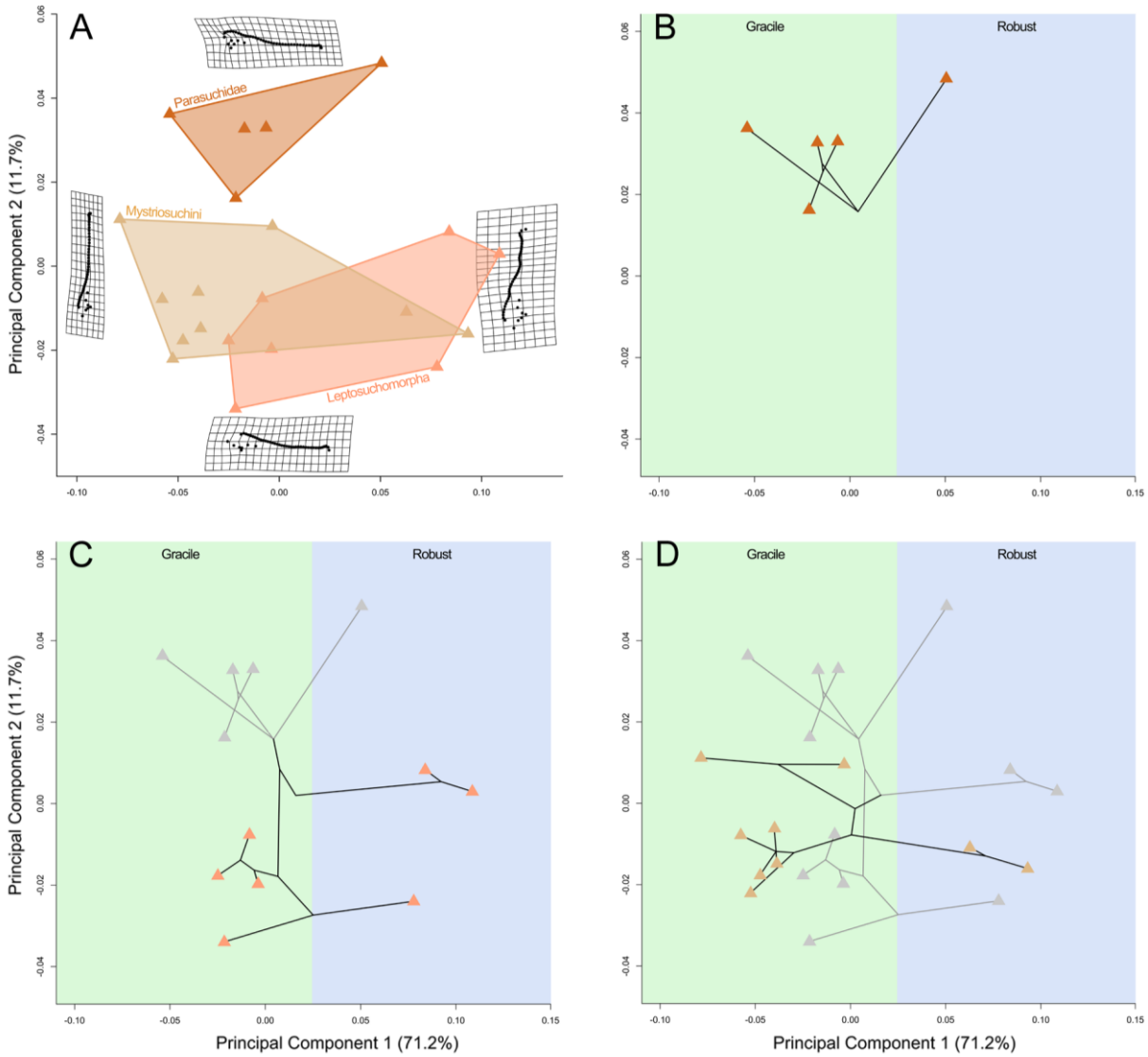

Figure 3.7: Dorsal phytosaurian morphospace and phylomorphospace: PC 1 vs PC 2. A) Areas occupied by basal Parasuchidae, basal Leptosuchomorpha and Mystriosuchini are delimited with convex hulls; morphological reconstructions represent shape deformation at each end of PC 1 and PC 2. B–D) Iterative phylomorphospace beginning with basal Parasuchidae (B), then basal Leptosuchomorpha (C) and Mystriosuchini (D).

Principal component 3, which encompasses 7.8% of variation, represents a very subtle shortening of the supratemporal fenestra in more derived phytosaurs, which is also associated with a slightly more abrupt posterior expansion of the skull and a subtle increase in the lateral

convexity of the maxilla, rather than a very gradual posterior cranial expansion, with the maxilla remaining approximately flat (Figure S2.1).

Of all three principal component axes, only PC 2 provides any statistical separation of the taxonomic groups of Phytosauria included within the analysis (Kruskal-Wallis + Dunn's post-hoc test with Bonferroni correction) (Figure 3.7a). Basal Leptosuchomorpha and Mystriosuchini show extensive overlap ($p=1$), but basal Parasuchidae remains separate from both other groups ($p=0.004$, $p=0.017$ respectively) due to the more plesiomorphic morphology of the supratemporal fenestra. PC 1 allows no differentiation of these taxonomic groups; however, phytosaurs can be separated into two distinct areas of morphospace based on cranial robusticity. Repeated evolution towards more or less robust morphologies occurs within each taxonomic grouping considered (basal Parasuchidae, basal Leptosuchomorpha, Mystriosuchini) (Figure 3.7b–d).

When analysed as a whole, across the first three PC axes none of these groups differ statistically in their positions in morphospace (one way PERMANOVA with Bonferroni corrected pairwise test [performed in the software PAST]; $F=2.4$, $p=0.067$).

Lateral view: In lateral view the first four principal components constitute the most important aspects of variation. PC 1 (constituting 53.4% of variance) describes elongation of the pre-narial rostrum, alongside an abrupt and considerable reduction in its dorsoventral height (Figure 3.8a). One end of this scale represents the most robust phytosaur taxa, with brachyrostral/oreinorostral snouts, whilst the other end represents the more gracile taxa which possess slender dolichorostral snouts. Other covarying features along this axis include the increasing ventral convexity of the posterior premaxillary and maxillary tooth row, and a more heavily pronounced downturn of the terminal rosette in the most robust taxa (Figure

3.8a). PC 2 (14.9% of variation) is associated with changes in anteroposterior length of the squamosal in relation to the quadrate condyle, and a trend of increasing narial height with decreasing rostral height – representing the 'volcano-shaped' naris that is present in some taxa (Figure 3.8a). PC 3 (10.3% of variation) encompasses the anteroposterior shifting of the external naris, and as such it separates non-Mystriosuchinae (basal) members of Parasuchidae from other phytosaur groups. Covarying with this are dorsoventral changes in the size of the terminal rosette and anteroposterior elongation/reduction of the squamosal (Figure S2.2). PC 4 (6.6% of variation) describes a variant of gracile to robust snout/crest morphology, focusing on the dorsoventral expansion of the anterior prenarial rostrum (rather than the posterior end of the rostrum, as in PC 1). One end of the axis represents the unique morphology of *Nicrosaurus kapffi*, where the prenarial crest extends anteriorly in a level plane, before descending just posterior to the terminal rosette. At the other end of the axis is a slightly more gracile snout profile, which gradually expands posteriorly into a 'volcano' type naris and ventrally convex maxilla. With this in mind, PC 4 also describes dorsoventral compression/expansion of the narial and postnarial portions of the skull (Figure S2.2).

Similarly to the dorsal orientation, basal parasuchids (and also here non-leptosuchomorph Mystriosuchinae) are relatively conservative in their morphospace occupation; however in contrast to the dorsal orientation non-Mystriosuchini leptosuchomorph taxa tend to all evolve toward an area of more brevirostrine morphospace in the lateral condition (Figure 3.8c), rather than repeatedly evolving divergent morphologies (Figure 3.7c). The disparate evolutionary trajectories seen in Mystriosuchini in lateral

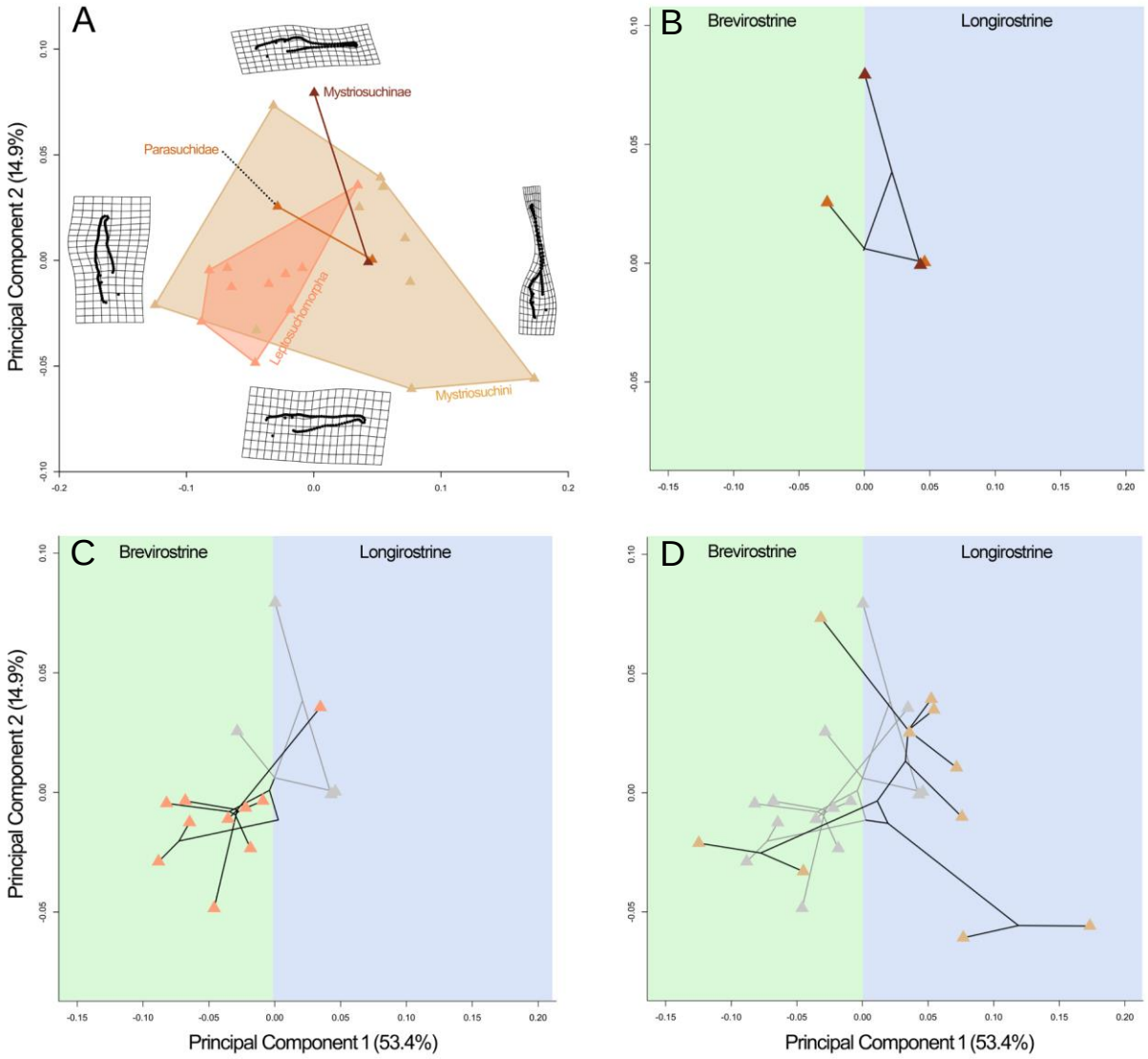

Figure 3.8: Lateral phytosaurian morphospace and phylomorphospace: PC 1 vs PC 2. A) Areas occupied by basal Leptosuchomorpha and Mystriosuchini are delimited with convex hulls, lines represent the morphological distributions of basal Parasuchidae and basal Mystriosuchinae; morphological reconstructions represent shape deformation at each end of PC 1 and PC 2. B–D) Iterative phylomorphospace beginning with basal Parasuchidae and basal Mystriosuchinae (B), then basal Leptosuchomorpha (C) and Mystriosuchini (D).

orientation (Figure 3.8d) are consistent with the disparate evolution of Mystriosuchini in dorsal view (Figure 3.7d). Only basal Leptosuchomorpha displays a disconnect between its range of evolutionary disparity in dorsal and lateral views. One basal leptosuchomorph

specimen (UCMP 27181) does branch out further into the more longirostrine area of morphospace; however this specimen represents a juvenile individual. Although it is an outlier for basal Leptosuchomorpha as a whole, its trajectory may be more revealing of ontogenetic change in the group.

When morphological separation between groups is tested, a statistically significant difference is found under one-way PERMANOVA ($F=2.4$, $p=0.04$). However, when subjected to post-hoc pairwise analysis with Bonferroni correction for type 1 errors, all significant differences disappear, with the most distinct groups being non-Mystriosuchini Leptosuchomorpha and Mystriosuchini ($p=0.088$).

3.3.2. *Trends of shape variation within Crocodylomorpha*

Dorsal view: PCs 1 and 2 represent the major components of variation in this sample. PC 1 (80.1% of variation) predominantly summarises the marked elongation/abbreviation of the skull anterior to the orbit, which separates longirostrine and brevirostrine taxa. Covarying alongside this trend are relative changes in cranial and rostral width between dolichorostral and platyrostral morphologies, and the overall sizes of the orbit and supratemporal fenestra and their relative positions in the skull (Figure 3.9a). PC 2 (8.6% of variation) describes changes to the width of the snout anterior to the orbit, the development of a distinct terminal rosette, the anteroposterior shifting of the orbit and associated anteroposterior lengthening of the supratemporal fenestra (Figure 3.9a).

Notosuchia by far appears to display the most divergent evolutionary trajectories (Figure 3.9b), with the clade formed by Uruguaysuchidae and Peirosauridae (Pol & Leardi, 2015) showing considerable divergence across the more positive values of PC 2, while

Ziphosuchia plus “advanced notosuchians” form a more morphologically conserved clade at the negative end of both PCs 1 and 2. Notosuchia is also one of the few groups which diversified into both brevirostrine and longirostrine morphologies; the only other group in this analysis to exhibit repeated evolution between these two morphologies is Crocodyloidea, although this group is relatively conserved in not deviating far from central morphospace (Figure 3.9e). Both Tethysuchia and Thalattosuchia exhibit considerably divergent evolution across PC 2 (Figure 3.9c), both possessing a hypothetical common ancestor close to the centre of the axis, prior to each diverging in positive and negative directions, largely corresponding to the widening/narrowing of the pre-orbital rostrum. Gavialoidea also displays some divergence in its evolutionary trends; however, it remains relatively constrained in morphology at the positive end of PC 1 and relatively neutral on PC 2 (Figure 3.9d). The evolutionary trajectories within Alligatoroidea are complex, displaying multiple wide divergences of sister taxa in morphospace (Figure 3.9f). The majority of variation within Alligatoroidea occurs along PC 2, delimited by *Paleosuchus trigonatus* (negative values) and *Diplocynodon hantoniensis* (positive values). Of all alligatoroids, only the basal taxon *Leidyosuchus riggsi* is found to evolve a relatively elongate rostrum in dorsal view.

Pairwise PERMANOVA of the first two principal components with Bonferroni correction finds that Thalattosuchia and Gavialoidea occupy a statistically significantly different area of morphospace than that occupied by Crocodyloidea and Alligatoroidea (Thalattosuchia – Crocodyloidea: $p=0.042$; Thalattosuchia – Alligatoroidea: $p=0.003$; Gavialoidea – Crocodyloidea: $p=0.011$; Gavialoidea – Alligatoroidea: $p=0.003$). No other differences between groups are statistically significant, although Notosuchia displays a relatively substantial difference in morphospace from Gavialoidea ($p=0.081$).

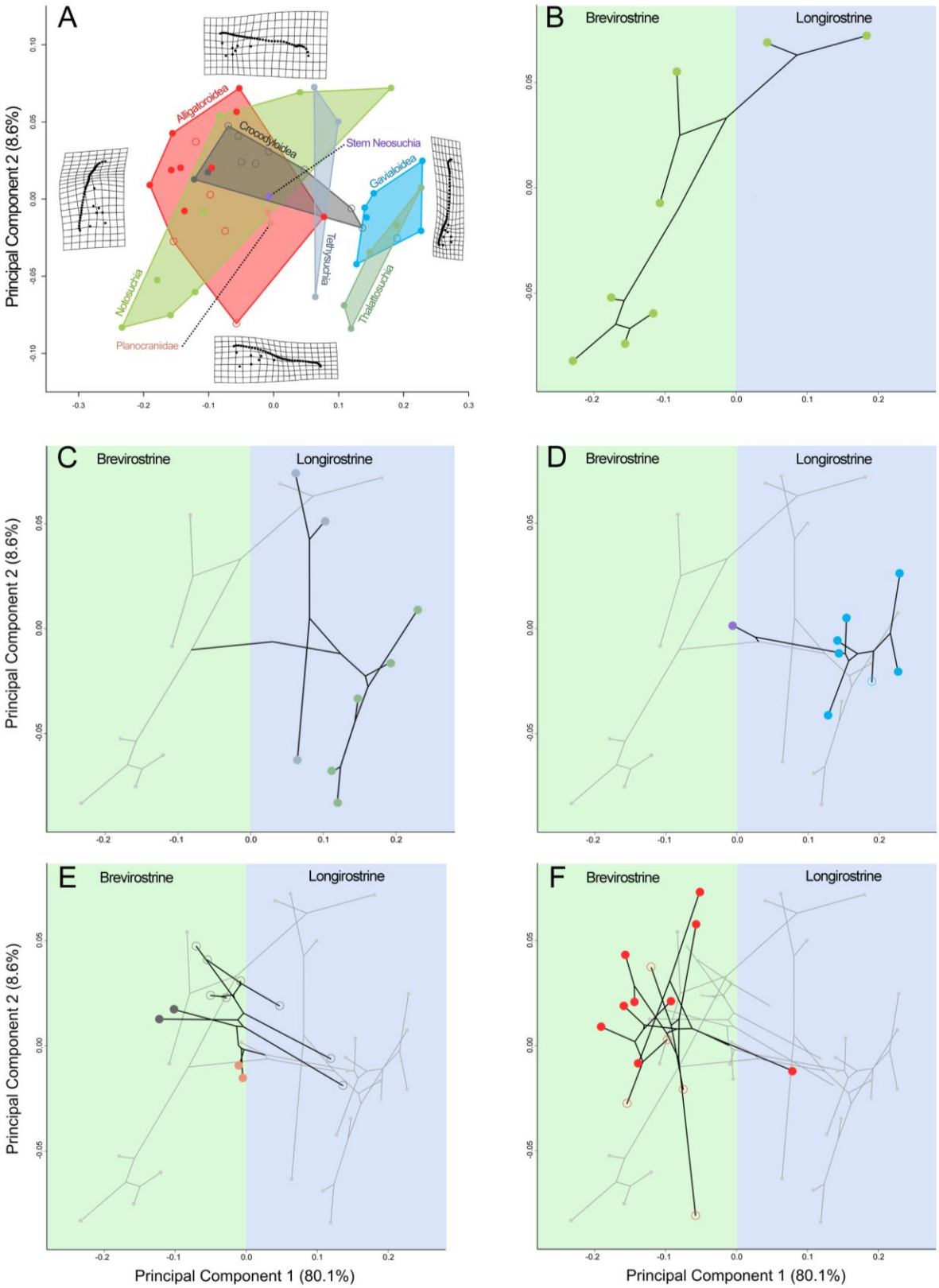

Figure 3.9: Dorsal crocodylomorph morphospace and phylomorphospace: PC 1 vs PC 2. A) Areas occupied by taxonomic groups are delimited with convex hulls; morphological reconstructions represent shape deformation at each end of PC 1 and PC 2. B–F) Iterative phylomorphospace beginning with Notosuchia (B), Tethysuchia and Thalattosuchia (C), Gavialoidea and stem Neosuchia (D), Planocraniidae and Crocodyloidea (E) and Alligatoroidea (F).

Lateral view: In the lateral view dataset the first three principal components constitute the most substantial variation. PC 1 (72% of variation) again reflects the anteroposterior elongation/abbreviation of the preorbital snout between longirostrine and brevirostrine morphologies. PC 1 also describes the dorsoventral height of the skull, particularly the rostrum, being low and gracile in longirostrine morphologies and taller in brevirostrines. Furthermore, this axis also covers the change in relative orbital size and the anterior tilting of the posteriormost portion of the skull, leaving the quadrate condyle projecting posteriorly in longirostrine morphologies (Figure 3.10a). PC 2 (10.6% of variation) describes whether the ventral surface of the premaxilla and maxilla is relatively flat or if it is dorsoventrally irregular, with ventrally projecting convexities and a pronounced, downturned terminal rosette. The relative length of the tooth row also covaries along this axis – at one end extending almost to the posterior extremity of the orbit, and at the other terminating anterior of the orbit. Finally, this axis also summarises the dorsoventral height of the quadrate condyle (Figure 3.10a). PC 3 (5.6% of variation) encompasses variation in the dorsoventral height of the rostrum and posterior extremity of the squamosal, relative to the height of the mid-section of the cranium. The dorsoventral variation of the posterior extremity of the squamosal brings the skull roof into very close proximity to the quadrate at one end of the scale, and also involves the anterior movement of the quadrate condyle in relation to the squamosal. Variation along this axis also covers the irregular/dorsoventrally flat tooth row and the formation of a downturned terminal rosette (Figure S2.3).

Similarly to dorsal view, Notosuchia displays the most divergent array of morphologies, though in this orientation both clades of notosuchians occupy wide areas of morphospace (Figure 3.10b). Again, only Notosuchia and Crocodyloidea feature both brevirostrine and longirostrine morphologies, with crocodyloids mostly occupying a relatively

neutral area of morphopace in comparison to all other groups. Too few members of Tethysuchia and Thalattosuchia are included in this analysis to draw meaningful results from their distributions, though unsurprisingly they inhabit a similar, longirostrine area of morphospace (Figure 3.10c) as in dorsal view. Gavialoidea displays slightly divergent evolutionary trajectories, which closely track those of Thalattosuchia (although here Thalattosuchia comprises only two species) (Figure 3.10d). Crocodyloidea is again characterised by repeated divergences along PC 1; however only one taxon (*Voay robustus*) diverges substantially into the more robust area of morphospace (Figure 3.10e). In lateral view crocodyloids and alligatoroids as whole groups are divergent, each occupying individual areas of morphospace, in contrast to the condition in dorsal view. Crocodyloidea in general appears to be more longirostrine whilst possessing a more rugose and robust ventral tooth-row, while Alligatoroidea is the opposite. Alligatoroidea is again divergent, but sister taxa diverge more along PC 2 than PC 1 (Figure 3.10f). The group is also more conservative in its morphospace occupation in this orientation, being entirely restricted to negative values of PC 1 and mostly to positive values of PC 2.

One-way pairwise PERMANOVA (with Bonferroni correction) finds a number of statistically significant differences between the positions of groups in the first three axes of morphospace: Crocodyloidea – Alligatoroidea ($p=0.013$), Crocodyloidea – Notosuchia ($p=0.029$) and Gavialoidea – Notosuchia ($p=0.023$). Gavialoidea is also found to occupy a substantially different position from Alligatoroidea, but is not supported at the 5% significance level ($p=0.057$).

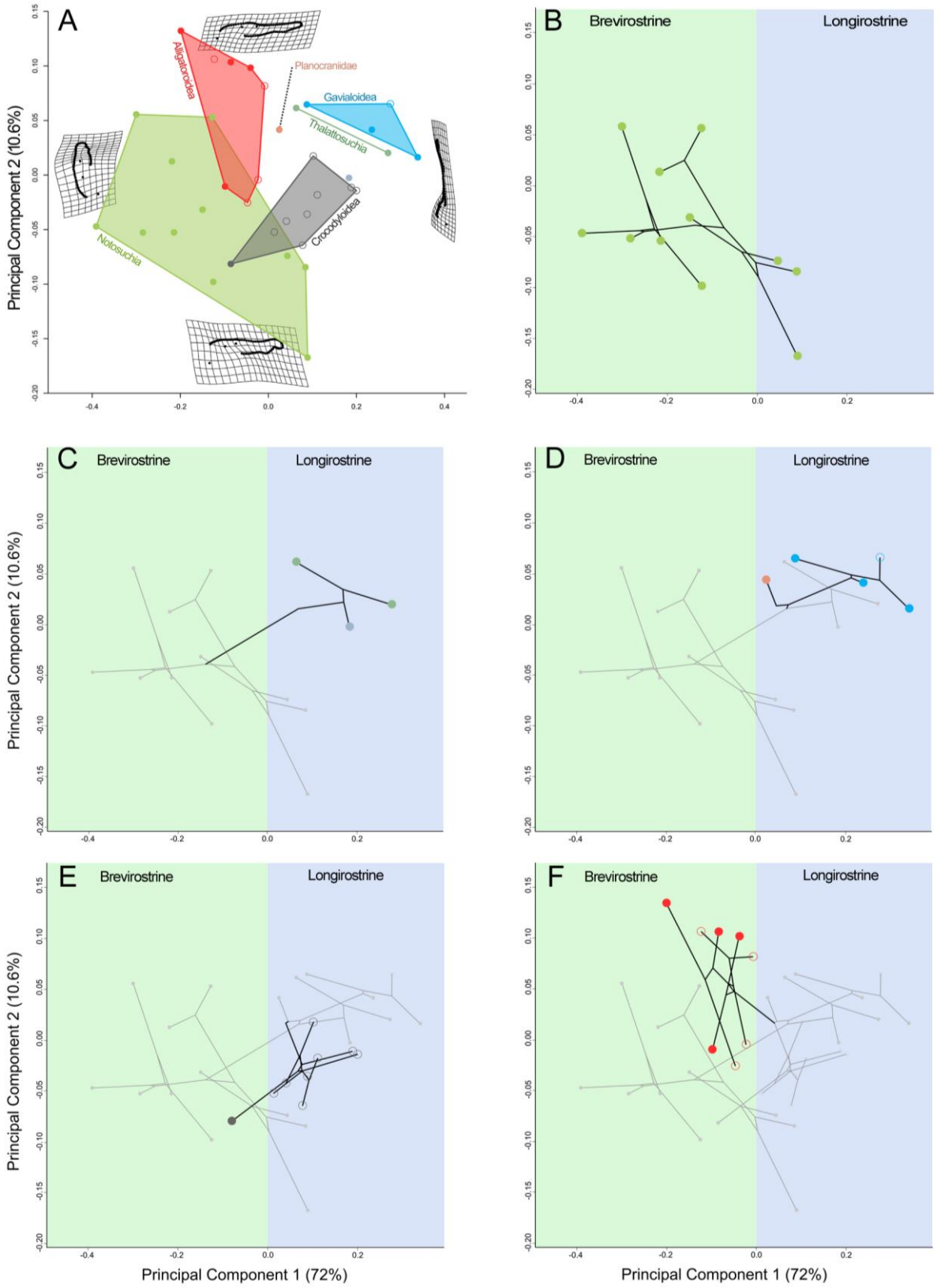

Figure 3.10: Lateral crocodylomorph morphospace and phylomorphospace: PC 1 vs PC 2. A) Areas occupied by taxonomic groups are delimited with convex hulls; morphological reconstructions represent shape deformation at each end of PC 1 and PC 2. B–F) Iterative phylomorphospace beginning with Notosuchia (B), Tethysuchia and Thalattosuchia (C), Gavialoidea and Planocraniidae (D), Crocodyloidea (E) and Alligatoroidea (F).

3.3.3. *Trends of shape variation when comparing Phytosauria and Crocodylomorpha*

Dorsal view: Principal components 1 and 2 constitute the majority of significant variation within this morphospace analysis. PC 1 (83.4% of variation), remains very similar to that for Crocodylomorpha alone, in that it predominantly describes variation in the length of the preorbital region of the skull and the mediolateral expansion/compression of this area, distinguishing between more longirostrine and brevirostrine taxa. Covarying along this axis are also the reduction of the orbit relative to overall cranial length, and variation in the shape of the supratemporal arcade. Regarding the supratemporal arcade, one end of PC 1 represents a relatively standard crocodylomorph morphology wherein the supratemporal fenestra is of a regular shape, well anterior of the posterior cranial border, and there is approximately a straight line formed by linking the posterior midline border of the parietals, the posterior tip of the squamosal, and the posterolateral corner of the quadrate. At the other end of PC 1, the morphology of the arcade is more phytosaurian with the lateral border of the supratemporal fenestra and posterior squamosal tip dramatically elongated posteriorly, producing a mediolaterally thin and elongate fenestra (Figure 3.11). PC 2 (6.7% of variation) represents shape variation in the lateral cranial border – between more ‘robust’ and ‘gracile’ morphologies – and the supratemporal fenestra, and the position of the orbit. At one end of PC 2 the morphology is reminiscent of Thalattosuchia, with the posterior half of the skull relatively wide, but the anterior half becoming abruptly narrow with no terminal rosette. The orbit is positioned at approximately the midpoint of the skull, the supratemporal fenestra is relatively large and regular in shape, and the squamosal tip is slightly anterior of the posterolateral corner of the quadrate. At the other end of PC 2, the general cranial shape is more triangular, with the lateral border forming an almost straight line from the quadrate to the anterior premaxilla but with areas of the tooth row bulging laterally, which contribute to

the ‘robust’ appearance of the skull. The orbit is positioned well into the posterior half of the skull, and the supratemporal fenestra is also pushed posteriorly, has become reduced in size and more irregular in shape, with the lateral border becoming more extended posteriorly, and the posterior tip of the squamosal also migrating posterior to the posterolateral corner of the quadrate (Figure 3.11).

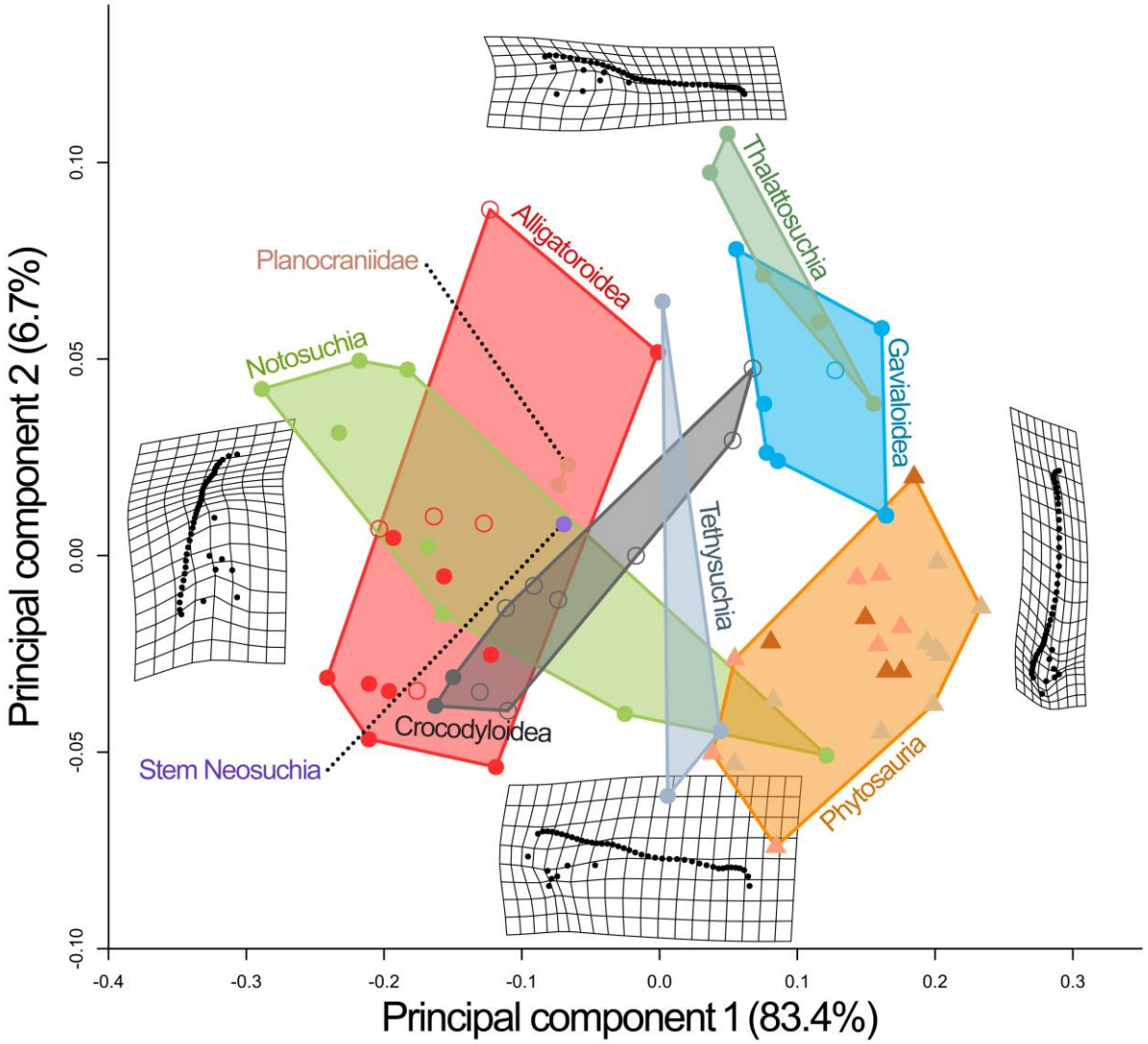

Figure 3.11: Dorsal morphospace incorporating Phytosauria and Crocodylomorpha. Convex hulls delimit the morphospace occupation of Phytosauria as a whole, and each individual crocodylomorph group. Morphological reconstructions represent landmark deformation at the extreme ends of PCs 1 and 2.

Despite showing some minor overlap in morphospace with Notosuchia, Tethysuchia and Thalattosuchia, Phytosauria occupies a significantly different area of morphospace to Alligatoroidea (p=0.004), Crocodyloidea (p=0.004), Gavialoidea (p=0.032), Notosuchia (p=0.004), Tethysuchia (p=0.040) and Thalattosuchia (p=0.004) across the first two principal components (one-way pairwise PERMANOVA with Bonferroni correction). Gavialoidea also occupies a significantly different area to Alligatoroidea (p=0.004), Crocodyloidea (p=0.018) and Notosuchia (p=0.050). Thalattosuchia also differs in morphospace from Alligatoroidea (p=0.004) and Crocodyloidea (p=0.032).

Lateral view: The first three principal components describe the major aspects of variation among phytosaurs and crocodylomorphs in lateral view. PC 1 (65.4% of variation) describes almost exactly the same variation as seen in PC 1 of the crocodylomorph-only morphospace, covering variation in the length, and to a lesser extent the dorsoventral expansion, of the preorbital snout. Also incorporated is the relative size and position of the orbit, and subtle variation in the length of the posterior process of the squamosal (Figure 3.12). PC 2 (11.6% of variation) is substantially different from PC 2 of the crocodylomorph-only morphospace, in that it predominantly summarises variation between a more platyrostral snout morphology and a more brachyrostral/oreinorostral morphology. Alongside this is variation in the relative size of the orbit, being larger in the platyrostral morphology, and variation in the posterior extension of the squamosal tip and the quadrate condyle relative to each other – the squamosal being more posteriorly extended in the brachyrostral morphology. The brachyrostral end of this axis also shows the development of a distinctly downturned terminal rosette and an abrupt dorsal expansion of the rostrum just anterior of the orbit – indicative of the narial placement in many phytosaurs within Mystriosuchinae. In a simplistic sense, this PC axis describes the transition in morphology from a typical platyrostral

crocodylomorph, to a typical brachyrostral/oreinorostral phytosaur (Figure 3.12). PC 3 (7% of variation) is again almost identical to the variation displayed in PC 3 of the crocodylomorph-only morphospace. The axis summarises variation pertaining to the robusticity of the ventral tooth row – being either horizontally flat, or possessing substantial ventral convexities and a large, downturned terminal rosette. At the more robust end of this axis the posterior section of the skull is much more greatly dorsoventrally expanded, whilst it is relatively compressed at the other end of the axis. Finally, the quadrate condyle also varies in its posterior extent – being posterior to the squamosal tip in the more robust morphology, and anterior of the squamosal tip in the less robust morphology (Figure S2.4). It appears that in the morphospace defined by these three axes, cranial robusticity is divided between PC 2 and 3; PC 2 being more representative of variation in robusticity along the dorsal margin of the skull, and PC 3 pertaining more to the ventral cranial border.

One-way pairwise PERMANOVA (Bonferroni corrected) of the first three PC axes finds Phytosauria to occupy a significantly different area of morphospace from Alligatoroidea ($p=0.003$), Crocodyloidea ($p=0.003$), Gavialoidea ($p=0.045$) and Notosuchia ($p=0.003$). Alligatoroidea and Crocodyloidea also differ significantly in morphospace ($p=0.008$), as do Gavialoidea and Notosuchia ($p=0.020$). Notosuchia is also substantially, though not significantly, different from Crocodyloidea ($p=0.0504$), while Gavialoidea and Alligatoroidea also differ to a marked extent ($p=0.053$).

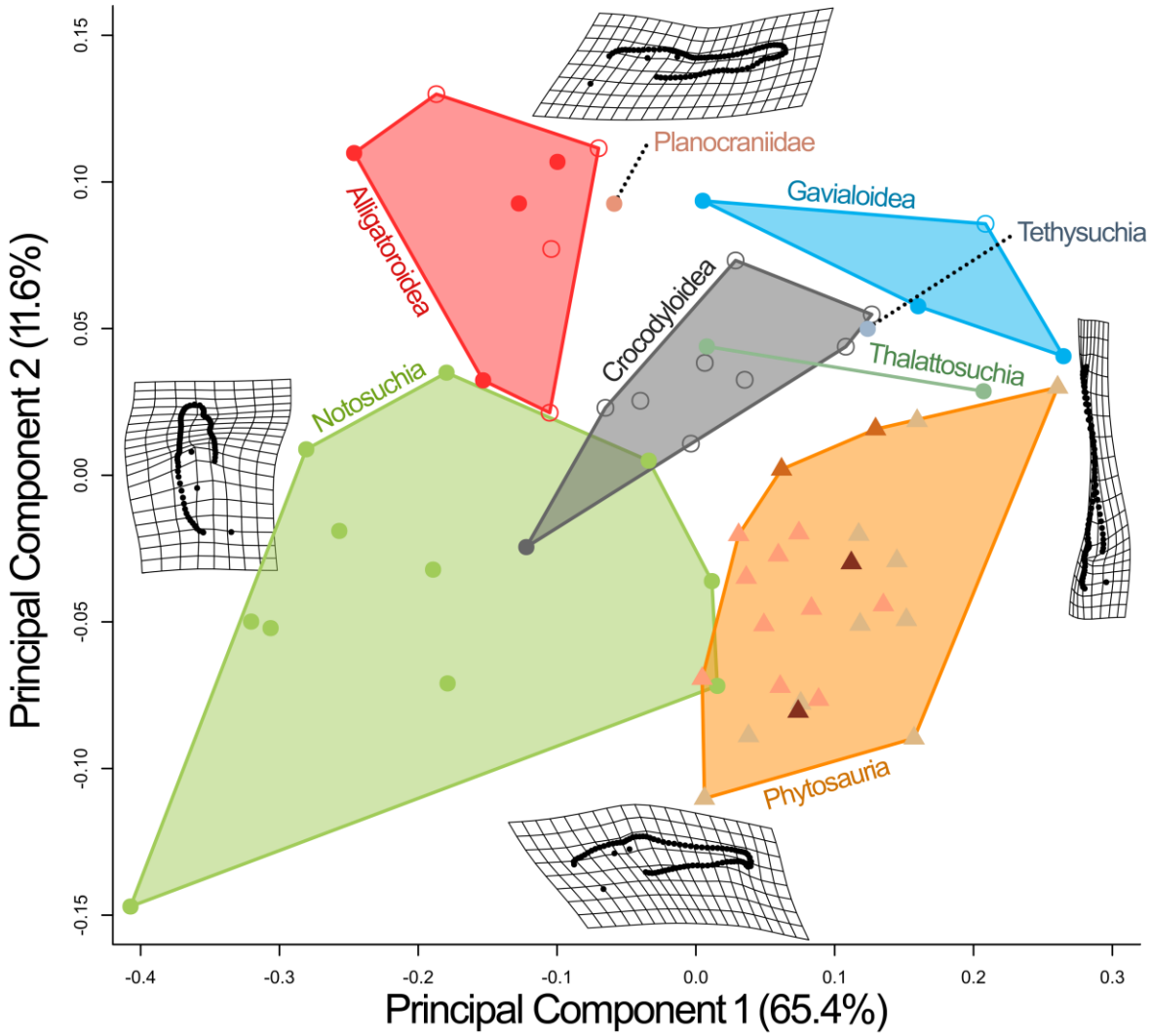

Figure 3.12: Lateral morphospace incorporating Phytosauria and Crocodylomorpha. Convex hulls delimit the morphospace occupation of Phytosauria as a whole, and each individual crocodylomorph group. Morphological reconstructions represent landmark deformation at the extreme ends of PCs 1 and 2.

3.3.4. *Variation in disparity between Phytosauria and crown Crocodylia*

In both the dorsal and lateral datasets there is no statistically significant difference in disparity between phytosaurs and any of the three groups within crown Crocodylia (Phytosauria vs Alligatoroidea [dorsal p=0.84, lateral p=0.96]; Crocodyloidea [dorsal p=0.57, lateral p=0.58]; Gavialoidea [dorsal p=0.46, lateral p=0.12]). However, as may be expected, in both

orientations the entirety of morphological variation within crown Crocodylia is significantly greater than that of Phytosauria (dorsal p=0.007, lateral p=0.006). It therefore appears that while phytosaurs occupy a significantly different area of morphospace to any of the clades within crown Crocodylia (Figures 3.11, 3.12), in terms of their morphological variance they are equivalent to any one of these groups. Within this dataset, in both orientations, none of the clades within crown Crocodylia differ significantly in their disparity.

3.3.5. *Phytosaur morphotypes*

Dorsal view: The maximum variation between the three 'morphotype' groups was summarised by LDA over two axes, the first comprising 99.3% of variation, the second making up the remaining 0.7% (Figure 3.13). The three groups were successfully distinguished in 81.0% of cases, with confusion between 'gracile' and 'moderate', and 'moderate' and 'robust' categories accounting for approximately 9.52% of error each. This result suggests distinct, though not significant, support for groupings within Phytosauria based on dorsal morphology.

Lateral view: The first LD axis summarised 90.8% of the total maximum variation between the three morphotypes, while the second axis summarised 9.2%. Under jackknife cross-validation group membership was correctly predicted 83.3% of the time. Following this initial analysis, it was observed that a specimen of '*Smilosuchus lithodendrorum*' in the 'robust' category was optimised as a member of the 'gracile' group under jackknife validation; interestingly, one of the main causes of error in the dorsal condition was also due to a specimen of '*S. lithodendrorum*'. The lateral view specimen (UCMP 27181) is from a juvenile individual, in which the rostrum is uncrested. It also remains unclear whether '*S.*

lithodendrorum' represents a valid taxon, or a gender-based variant of *Leptosuchus crosbiensis*; due to its morphological/taxonomic uncertainty, and its negative effects on group separation this specimen was removed from this analysis. Following removal of this specimen, the first LD axis accounted for 97.1% of between group variation, and LD axis 2 accounted for the remaining 2.9% (Figure 3.14). The proportion of correct classifications under jackknifing also improved to 87.0%, with all confusion limited to being between the 'moderate' and 'robust' categories. Similar to the situation in dorsal view this proportion is not statistically significant, yet it does add considerable support for the existence of three distinguishable 'morphotypes' within Phytosauria, taking only lateral shape information into account.

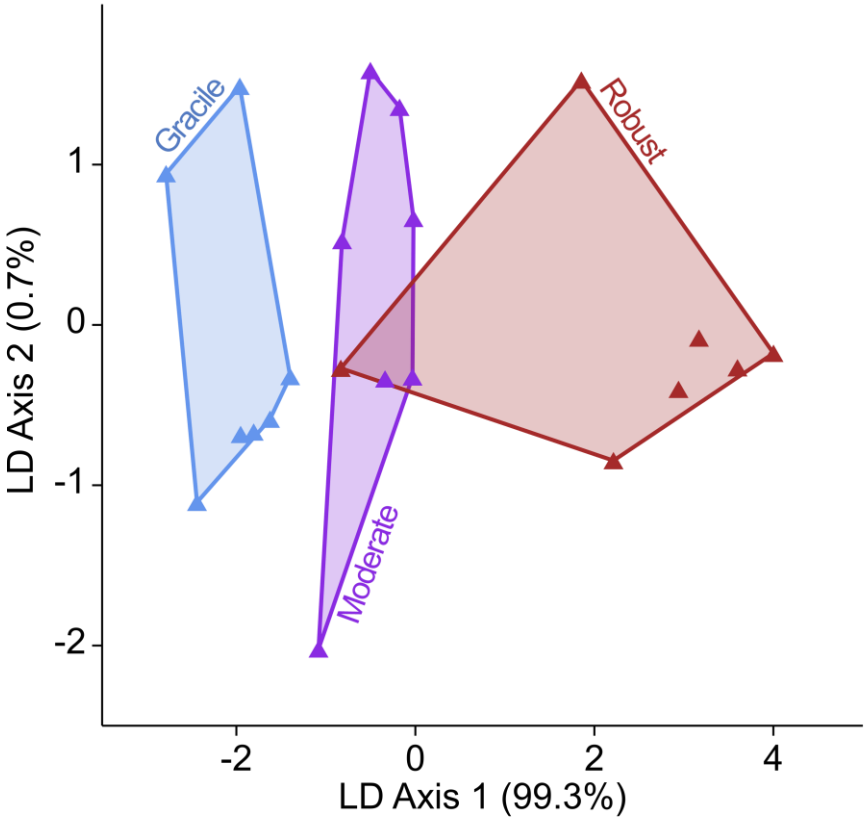

Figure 3.13: Dorsal orientation dataset LDA of maximum separation between gracile, moderate and robust phytosaurs as defined in Table 3.1.

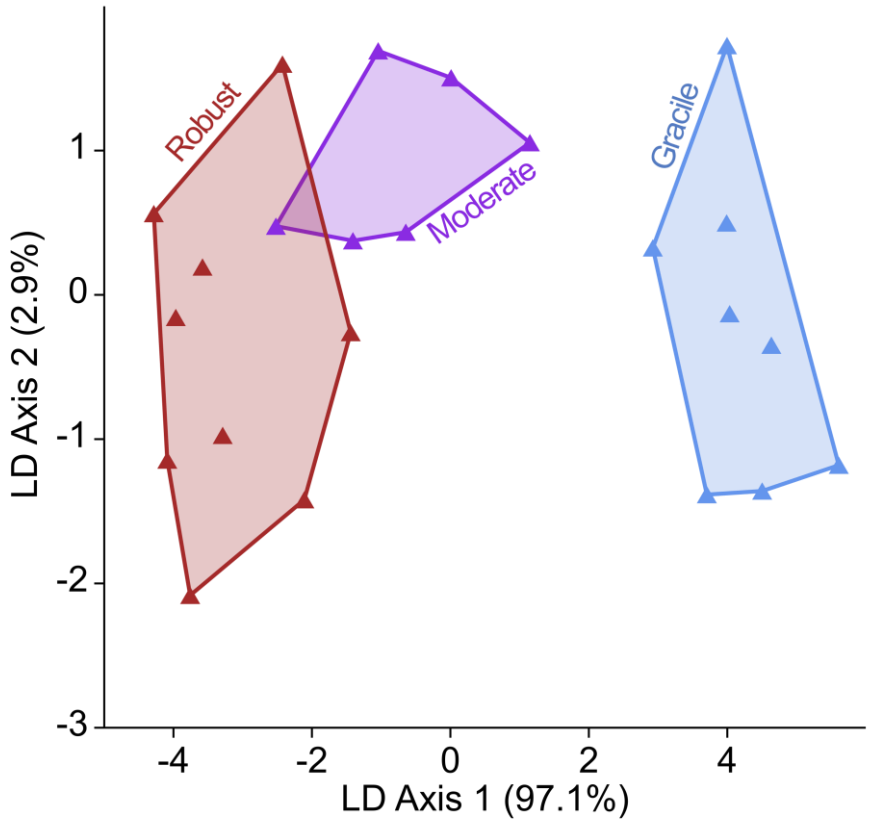

Figure 3.14: Lateral orientation dataset LDA of maximum separation between gracile, moderate and robust phytosaurs as defined in Table 3.1.

To investigate whether the distinction of phytosaur morphotypes achieved separately in dorsal and lateral conditions was compatible (i.e. whether morphotypes can still be identified given a combined dataset representative of 3D morphology) the above datasets were combined and subjected to LDA. The combined dataset was analysed 'as is', such that specimens with data missing for either the dorsal or lateral dataset were retained, as were the gaps; specimens that were present in both dorsal and lateral datasets received a full complement of data. The final combined dataset consisted of 29 specimens and 7 variables. In this condition LD 1 accounted for 96.3% of variation and LD 2 for 3.7% of variation. Correct group classification was achieved in 75.9% of jackknife repeats, with error again occurring

between ‘gracile’ and ‘moderate’ categories (10.34%) and ‘moderate’ and ‘robust’ categories (13.79%), with no overlap between ‘gracile’ and ‘robust’ (Figure 3.15).

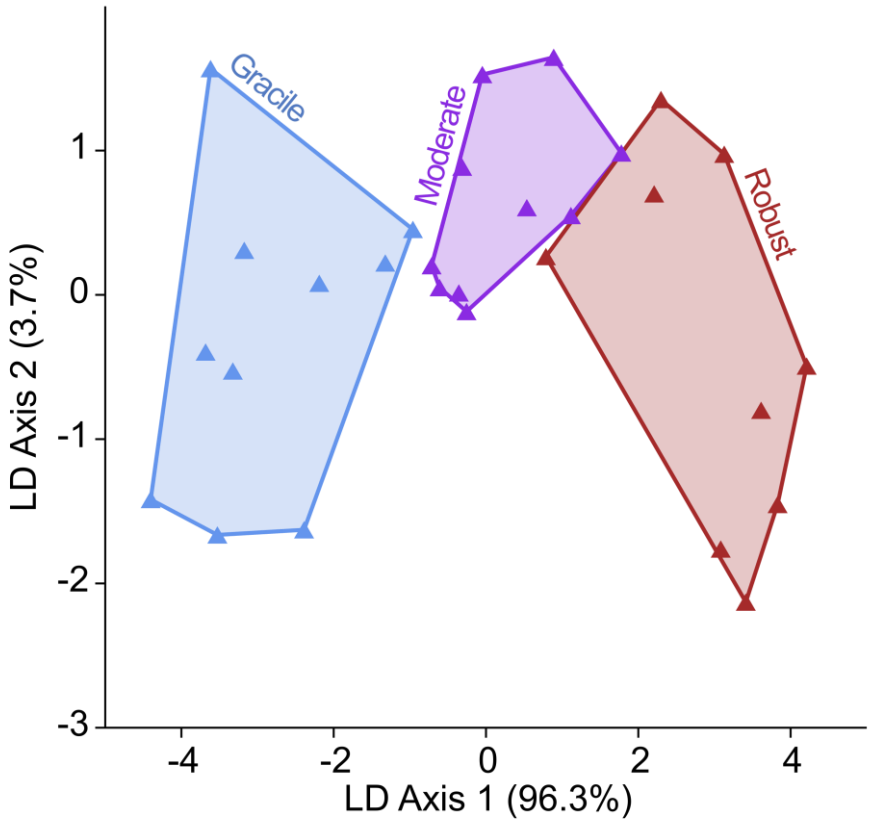

Figure 3.15: Combined LDA using PC scores from the dorsal and lateral datasets. Maximum separation between gracile, moderate and robust phytosaurs as defined in Table 3.1.

This again shows some support for the proposed morphological groupings, but less so than the independent analyses of dorsal and lateral components. It is worth considering, however, that the reduction in correct group assignment may have been due to a high proportion of missing data within the dataset.

In each condition jackknifing recovered incorrect classifications for some taxa:

dorsal – *Ebrachosuchus neukami* [gracile→moderate], '*Paleorhinus*' *sawini* [robust→moderate], '*Smilosuchus lithodendrorum*' PEFO 34852 [robust→moderate] and *Nicrosaurus meyeri* [moderate→gracile];

lateral – '*Paleorhinus*' *sawini* [robust→moderate], '*Smilosuchus lithodendrorum*' PEFO 34852 [robust→moderate] and *Leptosuchus studeri* [moderate→robust];

combined – *Ebrachosuchus neukami* [gracile→moderate], '*Paleorhinus*' *sawini* [robust→moderate], '*Smilosuchus lithodendrorum*' PEFO 34852 & TMM 31173-121 [robust→moderate], *Leptosuchus studeri* [moderate→robust], *Nicrosaurus meyeri* [moderate→gracile] and *Machaeroprosopus pristinus* NMMNHS P-50040 [gracile→moderate].

In an attempt to improve the original model of morphotye classification, LD plots of the dorsal and lateral partitions were assessed visually for the most prominent deviations from original grouping among those listed above, and were sequentially altered until statistical fit of the model no-longer improved, or inaccurate classifications of taxa became incongruent with known specimen morphology.

In the dorsal condition, the reassignment of '*Smilosuchus lithodendrorum*' (PEFO 34852) from robust to moderate, resulted in jackknife resampling finding correct classifications in a significant proportion (95.24%) of cases.

In the lateral condition, the reassignment of '*Smilosuchus lithodendrorum*' (PEFO 34852) from robust to moderate and *Leptosuchus studeri* from moderate to robust, resulted in an increase in correct classifications under jackknife resampling, such that correct classification was achieved in 95.65% of cases. See Table 3.2 for a revised assignment of taxa

to groups, based on the improved morphotype prediction model and Figure 3.16 for revised dorsal and lateral LD plots.

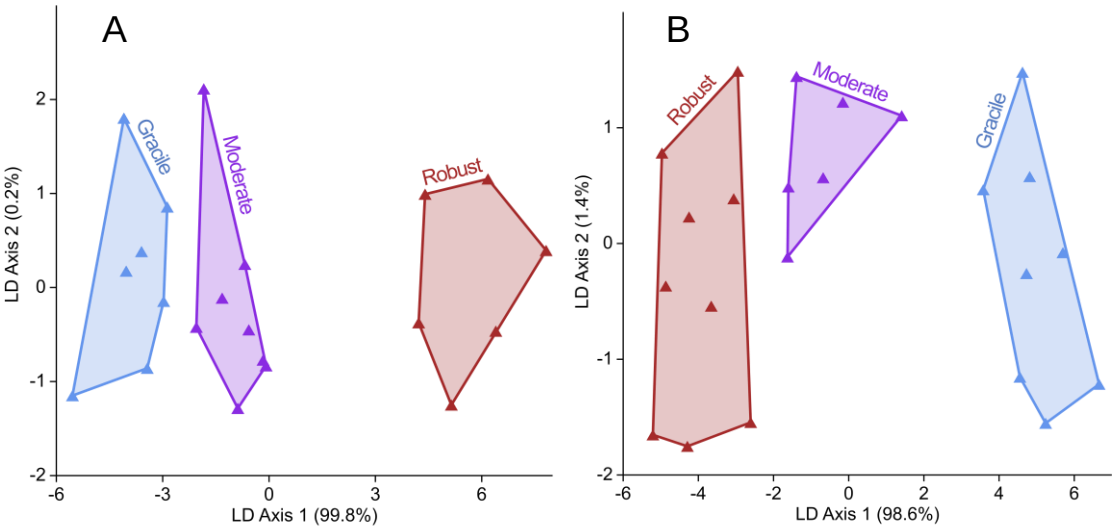

Figure 3.16: Dorsal and lateral phytosaur dataset LDAs, based on the reclassifications of taxa in Table 3.2.

3.3.6. *Changes in rates of morphological evolution*

In this section all significance values are those at the highest 95th percentile; i.e. values under 0.05 denote a situation in which a significant difference in evolutionary rates between groups was found in more than 95% of alternatively time-scaled trees.

When differences were found to be significant in a dataset, pairwise comparisons were used to identify between which groups significant differences occurred. Results of comparisons involving outgroup taxa are not reported here, because of the likelihood that significant rates of evolution are elevated due to the considerable amount of missing taxa that, if included, would provide a more gradual trend of morphological evolution between the outgroup taxa, and between the outgroup and ingroup taxa. Furthermore, the majority of

Table 3.2: Revised phytosaur morphotype classifications.

Taxon/Specimen	Revised Morphotype
Dorsal	
Ebrachosuchus neukami BSPG 1931 X 501	Gracile/Piscivorous
Machaeroprosopus lottorum TTU-P 10076	Gracile/Piscivorous
Machaeroprosopus pristinus MU 525	Gracile/Piscivorous
Machaeroprosopus pristinus NMMNHS P-50040	Gracile/Piscivorous
Machaeroprosopus pristinus PEFO 382	Gracile/Piscivorous
Machaeroprosopus pristinus UCMP 137319	Gracile/Piscivorous
Mystriosuchus planirostris SMNS 9900 & 9134	Gracile/Piscivorous
Leptosuchus crosbiensis TMM 31173-120	Moderate/Generalist
Leptosuchus studeri UMMP 14267	Moderate/Generalist
Mystriosuchus westphali GPIT 261-001	Moderate/Generalist
Nicrosaurus meyeri SMNS 12593 & NHMUK OR42745	Moderate/Generalist
Parasuchus angustifrons ZPAL Ab III 200	Moderate/Generalist
Parasuchus bransoni TMM 31100-101	Moderate/Generalist
Parasuchus bransoni TMM 31100-419	Moderate/Generalist
'Smilosuchus lithodendrorum' PEFO 34852	Moderate/Generalist
'Redondasaurus' ?bermani NMMNHS P-4256	Robust/'Predaceous'
Machaeroprosopus mccauleyi PEFO 31219	Robust/'Predaceous'
Nicrosaurus kapffi SMNS 4379	Robust/'Predaceous'
'*Paleorhinus*' *sawini* TMM 31213-16	Robust/'Predaceous'
Smilosuchus gregorii UCMP 27200	Robust/'Predaceous'
Smilosuchus gregorii AMNH 3060	Robust/'Predaceous'
Lateral	
Machaeroprosopus lottorum TTU-P 10076	Gracile/Piscivorous
Machaeroprosopus pristinus PEFO 382	Gracile/Piscivorous
Machaeroprosopus pristinus UCMP 137319	Gracile/Piscivorous
Machaeroprosopus pristinus UCMP 34249	Gracile/Piscivorous
Machaeroprosopus pristinus MU 525	Gracile/Piscivorous
Machaeroprosopus pristinus AMNH 7222	Gracile/Piscivorous
Mystriosuchus planirostris SMNS 9900 & 9134	Gracile/Piscivorous
Rutiodon carolinensis AMNH 1	Gracile/Piscivorous
Angistorhinus grandis FMNH 631	Moderate/Generalist
Leptosuchus crosbiensis UMMP 7522	Moderate/Generalist
Leptosuchus crosbiensis TMM 31173-120	Moderate/Generalist
Mystriosuchus westphali GPIT 261-001	Moderate/Generalist
Parasuchus hislopi ISIR 42	Moderate/Generalist
'Smilosuchus lithodendrorum' PEFO 34852	Moderate/Generalist
Leptosuchus studeri UMMP 14267	Robust/'Predaceous'
'Redondasaurus' ?bermani NMMNHS P-4256	Robust/'Predaceous'
'Smilosuchus lithodendrorum' TMM 31173-121	Robust/'Predaceous'
'Smilosuchus lithodendrorum' TTU-P 09234	Robust/'Predaceous'
Machaeroprosopus mccauleyi PEFO 31219	Robust/'Predaceous'
Nicrosaurus kapffi SMNS 4379	Robust/'Predaceous'
'*Paleorhinus*' *sawini* TMM 31213-6	Robust/'Predaceous'
Smilosuchus gregorii UCMP 27200	Robust/'Predaceous'
Smilosuchus gregorii AMNH 3060	Robust/'Predaceous'

outgroups contain only a single taxon; therefore, the positions of these taxa morphologically and temporally are unlikely to be representative of their groups.

Among phytosaurs there was no significant change observed in evolutionary rate between any of the groups defined in the phytosaur phylogeny, in either dorsal or lateral orientation (dorsal $p=0.954$; lateral $p=0.668$).

Among crocodylomorphs only there was also no significant difference observed between the evolutionary rates of any of the groups in lateral orientation (lateral $p=1.000$). However, in the dorsal condition a significant difference in evolutionary rate was found (dorsal $p=0.041$); this was found to be associated with significantly lower rates of evolution in Planocraniidae than stem Neosuchia ($p=0.012$), Notosuchia ($p=0.007$), and Thalattosuchia ($p=0.002$). Other groups were also found to possess considerably, but not significantly different evolutionary rates from Planocraniidae; Gavialoidea ($p=0.082$) and Tethysuchia ($p=0.063$). No other significant differences were reported between the groups, with most pairwise comparisons (19 of 28) displaying highly non-significant p-values ($p>0.5$), indicating relatively homogenous evolutionary rates.

When all groups of phytosaurs and crocodylomorphs were compared together, alongside outgroup taxa, no significant differences in evolutionary rates were observed in the lateral orientation ($p=0.999$). However, in the dorsal orientation a significant difference in evolutionary rates was found ($p=0.027$). This corresponded to Planocraniidae possessing the lowest evolutionary rates of all groups, being significantly lower than Alligatoroidea ($p=0.031$), Crocodyloidea ($p=0.001$), stem Neosuchia ($p=0.013$), Notosuchia ($p=0.001$), Tethysuchia ($p=0.034$), Thalattosuchia ($p=0.001$), basal Parasuchidae ($p=0.001$) and Mystriosuchini ($p=0.022$). Planocraniidae was, however, composed of only two taxa

(*Boverisuchus vorax* and *Borealosuchus wilsoni*) that form a 'grade' of Neosuchia in this phylogeny, so the validity of the result may be questionable. These were the only significant differences in evolutionary rates that occurred between groups in over 95% of time-scaled trees; in this condition too, the majority of non-significant differences in evolutionary rates between groups were highly non-significant ($p>0.5$ in 38 of 55 pairwise comparisons). The evolutionary rates of all groups in dorsal and lateral conditions are visualised on their respective trees in Figures 3.17 and 3.18.

In the CalcRates dorsal dataset, no group was found to possess evolutionary rates significantly different to those of the randomised (null) dataset. When comparing the means of the null and observed data, all groups displayed greater mean rates of morphological evolution than in random data, with the exception of Planocraniidae which reported a mean rate approximately an order of magnitude lower than that of the group's random data mean (Table 3.3). Almost all other groups reported slightly elevated means at the same order of magnitude as the null data (with the exception of Tethysuchia). The group displaying least overlap with the null dataset was stem Neosuchia, with a 22% overlap, though this is based on only one taxon; the next lowest overlap was in Tethysuchia (24%), also wherein mean evolutionary rate increased dramatically from 0.008 in the null dataset, to 0.014 in the observed dataset. The majority of rates in the null dataset are relatively equal (between 0.010 and 0.018); as the null rates are calculated without approximately equal morphological change on each branch, large differences in rate are likely due to consistently unequal branch lengths in time-scaling. Planocraniidae is the only group to substantially deviate in its random rates – indicating that its slow rates in Figures 3.17 and 3.18 are at-least in part due to long branch lengths, in comparison to those of other groups.

In the lateral dataset two groups were observed to possess a significantly different

distribution of evolutionary rates than those of the random dataset (Tethysuchia = <1% overlap; Thalattosuchia = 4% overlap). Similarly to stem Neosuchia in the dorsal dataset, Tethysuchia is here only represented by one taxon. In contrast to the dorsal condition, not all mean observed rates are greater than those of the null dataset: all groups in Phytosauria except basal Parasuchidae, Tethysuchia and Crocodyloidea display a decrease in their mean evolutionary rates (in addition the increase in rate in basal Parasuchidae is marginal), Notosuchia, Thalattosuchia and Gavialoidea possess greater mean evolutionary rates than in the null dataset, in Planocraniidae and Alligatoroidea there is no difference in mean rates (Table 3.4). Planocraniidae again displays mean rates approximately an order of magnitude lower than the other taxa, though in the lateral dataset Tethysuchia possesses rates yet another order of magnitude lower. The low rates in Tethysuchia here are partially corroborated by the dorsal dataset, in which rates are also relatively low; however in the lateral dataset tethysuchian rates are entirely based around *Sarcosuchus imperator*, which has generally long branch lengths.

Table 3.3: Results of overlapping analysis between observed dorsal rates of morphological evolution and null rates.

Group	Overlap of random and observed distributions (%)	Mean of random distribution	Mean of observed distribution
Basal Parasuchidae	32	0.013	0.020
Basal Leptosuchomorpha	43	0.013	0.019
Mystriosuchini	54	0.011	0.015
Notosuchia	29	0.010	0.027
Tethysuchia	24	0.008	0.014
Thalattosuchia	58	0.011	0.014
Stem Neosuchia	22	0.018	0.036
Gavialoidea	47	0.010	0.014
Planocraniidae	36	0.001	<0.001 (0.0003)
Crocodyloidea	29	0.011	0.018
Alligatoroidea	38	0.011	0.018

Table 3.4: Results of overlapping analysis between observed lateral rates of morphological evolution and null rates.

Group	Overlap of random and observed distributions (%)	Mean of random distribution	Mean of observed distribution
Basal Parasuchidae	69	0.014	0.015
Basal Mystriosuchinae	31	0.029	0.020
Basal Leptosuchomorpha	46	0.029	0.015
Mystriosuchini	73	0.025	0.023
Notosuchia	32	0.024	0.030
Tethysuchia	<1 (0.007)	<0.001 (0.0008)	<0.001 (0.0002)
Thalattosuchia	4	0.030	0.034
Gavialoidea	24	0.022	0.034
Planocraniidae	80	0.003	0.003
Crocodyloidea	43	0.025	0.016
Alligatoroidea	38	0.028	0.028

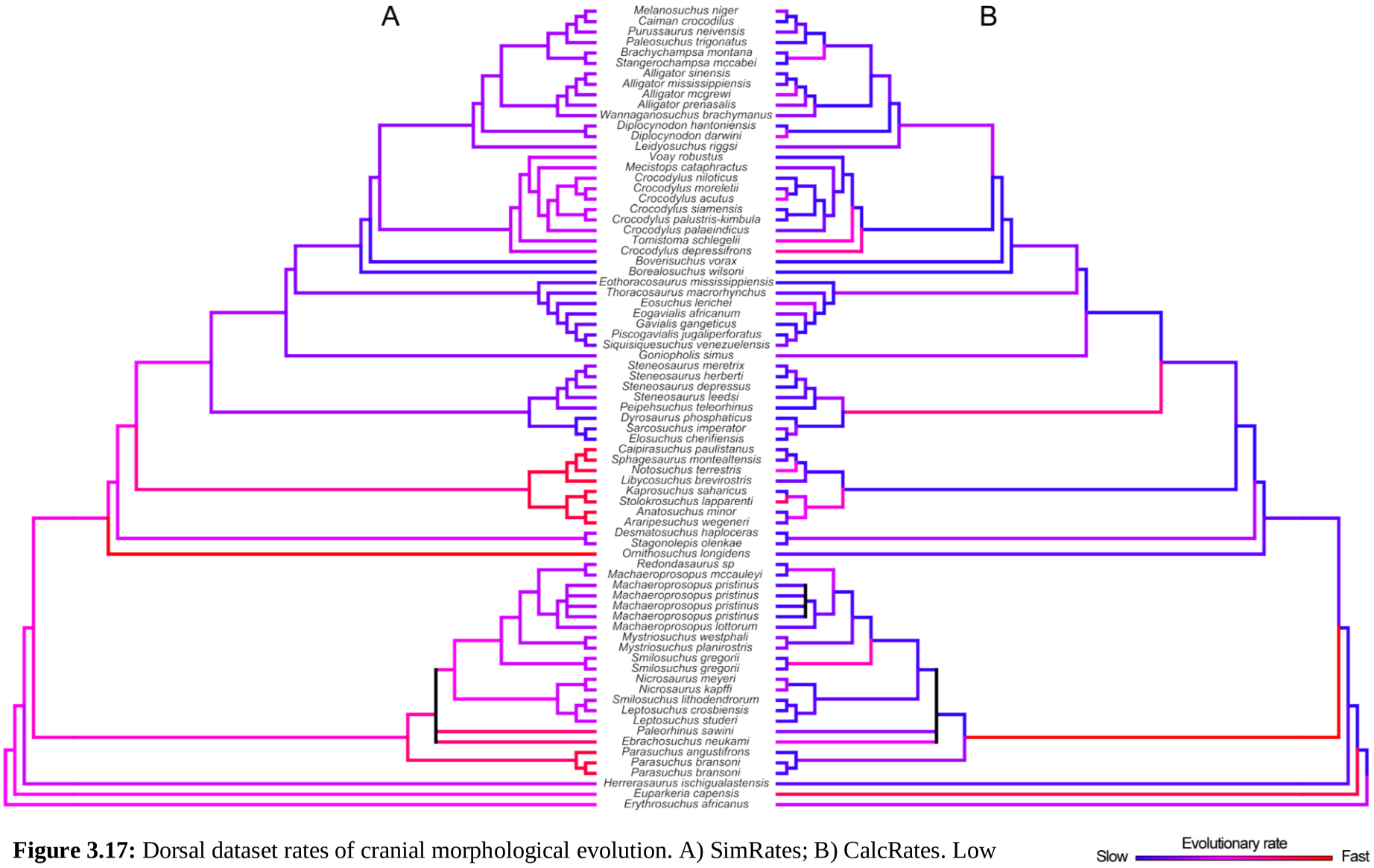

Figure 3.17: Dorsal dataset rates of cranial morphological evolution. A) SimRates; B) CalcRates. Low rates of evolution are coloured blue, high rates are coloured red

Figure 3.18: Lateral dataset rates of cranial morphological evolution. A) SimRates; B) CalcRates. Low rates of evolution are coloured blue, high rates are coloured red

3.4. *Discussion*

3.4.1. *Convergence in patterns of rostral shape variation*

It is clear from my results that whilst phytosaurs and crocodylomorphs remain distinctly separate in morphospace, they do share strikingly similar morphologies in some respects. In extant crocodylians it is rostral morphology that drives the majority of all cranial shape variation (Piras *et al.*, 2013). Although my dataset differs from that of Piras *et al.* (2013) (the majority of my crocodylomorph taxa are extinct, while the dataset of Piras focuses predominantly on crown Crocodylia and only includes three extinct taxa) my data also support this conclusion, as the most dramatic variation observed in PCs 1 and 2 in both dorsal and lateral orientations in crocodylomorph morphospace results from morphological change in the pre-orbital rostrum and the tooth row. I also find this to be the case in phytosaurs; in dorsal view PC 1 (which constitutes over 71% of total variation) is almost entirely limited to shape change within the rostrum (Figure 3.7a), and in lateral view the same is true of PC 1 (53.4% of variation), and is also largely true in PC 2 (14.9%) although some post-rostral variation is also present here (Figure 3.8a).

Whilst the rostrum constitutes the majority of cranial variation in alligatorids and crocodylids, these groups differ in the drivers of this rostral disparity; whereas in crocodylids rostral shape is largely influenced by functional and ecological factors, in alligatorids the rostrum is far more phylogenetically constrained (Sadleir & Makovicky, 2008; Piras *et al.*, 2009, 2013). This is supported by analyses of modularity in alligatorids which confirm a greater covariation in the rostral and post-rostral modules than in the rostral module and the entire skull, as expected if phylogeny has a strong influence (Sadleir & Makovicky, 2008;

Piras *et al*., 2009, 2013). In this aspect of morphology phytosaurs appear to show more similar trends to crocodylids. The variation within phytosaur rostra observed in my analyses largely pertains to a morphological gradient between long, gracile morphologies and shorter, robust morphologies (Figures 3.7, 3.8). However, the different phytosaur taxonomic groupings used (non-Mystriosuchinae parasuchids, non-leptosuchomorph Mystriosuchinae, non-Mystriosuchini leptosuchomorphs, and Mystriosuchini) show no significant differences in morphospace location along the axes of rostral shape variation. Furthermore, at every level of phytosaur phylogeny there are instances of closely related taxa diverging widely in terms of rostral morphology (Figure 3.7b–d). This strongly suggests that the morphology of phytosaur rostra is not closely constrained by phylogeny.

On PC 1 of phytosaur morphological variation in both dorsal and lateral views almost the entirety of variation occurs within the rostrum – there is almost no presence of post-rostral variation (Figures 3.7a, 3.8a). Post-rostral variation in dorsal view is limited to PC 2, which shows almost no component of rostral variation; in lateral view postrostral variation is also missing in PC 1, but does covary with rostral variation in the less variable PCs 2, 3 and 4. The disconnect in covariation between rostral and post-rostral shape in dorsal view, and partially in lateral view is suggestive of the rostrum and post-rostrum being separate modular units in phytosaurs; this would also support the hypothesis that rostral shape in phytosaurs is less constrained by phylogeny, as the majority of phylogenetic characters in phytosaur crania occur post-rostrally.

The disconnect between rostral and post-rostral morphology observed in phytosaurs also appears to be more extreme than in crocodylids; Piras *et al*. (2013) observed some covariation in crown crocodylians between rostral morphology and the structure of the supratemporal fenestrae, among other features. In my analysis of dorsal view in

Crocodylomorpha it is possible to observe this covariation along PCs 1 and 2 (Figure 3.9a). However, in my Phytosauria-only PCA, no such covariation is found. These extrapolations from my analyses are currently only tentative. Under the current dataset it would not be possible to conduct meaningful analyses of modularity due to landmark placement; landmarks were placed to maximise the incorporation of meaningful shape variation in two groups that differ in their cranial construction, similar to McCurry *et al.* (2017a). Although a tentative functional inference can be drawn regarding the phylogenetic disconnect of the rostrum in phytosaurs and its association with rostral shape-based functional partitioning in crocodylids, shape-change alone is not necessarily indicative of functional niche partitioning. Further study into the covariation of functional cranial characters with phytosaur shape-change would lend support to a hypothesis of cranial shape-based niche partitioning. Additional comparative functional analyses, such as FEA on phytosaurs and extant crocodylomorphs, would further clarify any links between form and function. A further interesting avenue of future research would be to thoroughly investigate modularity in the phytosaurian skull alone, allowing the use of sutural contacts and a greater resolution of rostral and post-rostral features, such as the antorbital fenestrae, narial position and squamosal posterior process shape, among others.

3.4.2. *Morphospace occupation*

Looking at Figures 3.11 and 3.12, phytosaurs are significantly morphologically restricted in comparison to the entirety of Crocodylomorpha and crown Crocodylia; however, they are statistically no more or less disparate than any of the three major clades considered within the latter. That phytosaurs occupy less morphospace than crown Crocodylia is not unexpected given their temporal range, which is less than half that of crown Crocodylia (Sues, 1989;

Benton, 2000). However, given the extent of viable morphospace exemplified by crocodylomorphs and the widely accepted success of Phytosauria in the late Triassic, inferred from their almost cosmopolitan global distribution and abundance in fluvial, lacustrine and even marine deposits, it is worth considering whether phytosaur morphospace was constrained. Metoposaurids and capitosauroids are two groups of predatory, aquatic stereospondyls that also were abundant in freshwater ecosystems in the late Triassic; these groups ranged in size from small to large taxa and possessed large, platyrostral, U-shaped skulls. It seems likely that if added to my morphospaces, these groups would overlap considerably with Alligatoroidea, and as hypothesised by Hunt (1989) may have filled the ecological niche of modern alligators. As phytosaurs and metoposaurids share a similar distribution in the late Triassic (Stocker & Butler, 2013), closely linked to the 'summerwet' biome of Sellwood & Valdes (2006), the possibility of competitive niche partitioning appears to be a reasonable hypothesis that could be investigated in future analyses.

While (as previously noted) the vast majority of phytosaur morphological variation relates to the rostrum, the variation that distinguishes phytosaurs from Gavialoidea in dorsal view mostly pertains to the structure of the supratemporal fenestrae. As mentioned above, the morphology of the supratemporal fenestrae appears to lack covariation with rostral morphology and, is the only axis that achieves separation of phytosaurs based on their phylogenetic position. Only non-Mystriosuchinae parasuchids possess dorsally orientated, fully open supratemporal fenestrae, while all members of subsequent phytosaur clades possess depressed fenestrae, with relatively little variation in the proportion of the skull roof they occupy. In comparison to phytosaurs the main difference in cranial variation of gavialids and thalattosuchians is the relative expansion of the supratemporal fenestrae in the latter taxa, and the anterior shifting of the orbits to accommodate this (Figure 3.11). Only one phytosaur

specimen was observed to overlap in range with Gavialoidea, which, unsurprisingly, was a basal parasuchid with dorsally orientated supratemporal fenestrae. Although further analysis is required to test the hypothesis, it is worth considering whether Phytosauria did not evolve into the morphological range of Gavialoidea and Thalattosuchia due to phylogenetic constraints linked to the development of depressed supratemporal fenestrae in Mystriosuchinae.

An additional trend common to both phytosaurs and crocodylomorphs is the repeated divergence into longirostrine and brevirostrine morphologies; the prior assumption in phytosaurs is that these divergent morphologies represent functional divergences, but this has yet to be thoroughly tested. Application of FEA and other functional analyses in a comparative framework between phytosaurs and extant crocodylomorphs may better elucidate the form-function relationship within Phytosauria. Although there is also a clear trend of repeated longirostrine/brevirostrine divergence among crocodylomorphs, care must be taken in its interpretation. There is debate over the phylogenetic positions of *Tomistoma* and Thalattosuchia – both longirostrine forms with adaptations toward piscivory, concerning outgroup choices and the disparity between morphological and molecular phylogeny (Wilberg, 2015; Lee & Yates, 2018); depending on the phylogenetic hypothesis used, a different view of the iterative evolution of longirostry will be found. As the predominant focus of this study is the evolutionary morphological convergence between phytosaurs and crocodylomorphs, rather than dedicated to the morphological relationships of Crocodylomorpha alone, I do not further explore these issues here. If further research was to investigate this, the alternative phylogenetic hypotheses pertaining to *Tomistoma* and Thalattosuchia must be independently addressed to identify the extent to which they affect results.

3.4.3. *Morphotype separation*

The robust, moderate and gracile morphologies highlighted by Hunt (1989) are generally supported by the LDA results, with the LD models based on improved taxon classification achieving correct morphotype classification a significant proportion of the time in both dorsal and lateral partitions.

The combined dataset could not be altered to enable a significant proportion of correct classifications, which suggests that there is a small degree of incongruence between apparent morphotype in dorsal and lateral views. This is consistent with the different morphotype classifications of *Leptosuchus studeri* in dorsal and lateral orientations, which greatly improved the performance of the LDA when assigned to the robust category in lateral view; however if designated as robust in dorsal view, the efficacy of the predictive model dropped from 95.24% to 80.95%.

The splitting of '*Smilosuchus lithodendrorum*' between two morphotypes in the lateral and combined datasets (three morphotypes counting the excluded specimen UCMP 27181) concurs with the suggestions made in Chapter 2 and those of Long & Murry (1995). The current hypodigm of '*S. lithodendrorum*' covers a range of specimens of various sizes, which differ from each other in the extent to which they possess a full rostral crest (Colbert, 1947). As the presence of a continuous rostral crest is the only substantial distinctive feature of the species it is difficult to judge whether it represents a valid taxon, this is hindered further by the poor preservation and fragmentary nature of the holotype (UCMP 26688). '*S. lithodendrorum*' may represent a sexual dimorph of *Leptosuchus crosbiensis*, with which it formed a close relationship in the D and DM trees of Chapter 1. The possibility of the

continuous rostral crest being a sexually selected character has been investigated previously; Camp (1930) argued against this explanation, reasoning that his specimens occurring at different stratigraphic levels possessed consistent rostral morphology. With additional availability of material, Colbert (1947) refuted Camp's argument and found partial support for gender differences within this character, in that a crest was found in all adult specimens, but only in male juveniles. Gender was assumed by Colbert (1947) (and Camp, 1930) on the basis of narial elevation – the justification being essentially that the specimens were divided approximately in half with regards to whether their nares were elevated or not. This evidence does not seem adequate to exclude the more conservative hypothesis of intraspecific variation, which is the view taken here; furthermore, Colbert did not compare '*S. lithodendrorum*' with *L. crosbiensis.* The juvenile specimen of '*S. lithodendrorum*' (referred as a paratype of the species by Camp, 1930) excluded from analysis here (UCMP 27181) is arguably indistinguishable from *L. crosbiensis*, and displays almost the same morphology as the holotype of the latter taxon (UMMP 7522). Large, robust and presumably old individuals of *L. crosbiensis* (TMM 43684, TMM 43684-8) display the same rostral structure as other *L. crosbiensis* specimens, indicating that (if synonymous with '*S. lithodendrorum*') the development of a continuous rostral crest is independent of ontogeny. The disconnect between rostral morphology and ontogeny is also consistent with the presence of both crested juvenile specimens of '*S. lithodendrorum*', and uncrested juvenile specimens that strongly resemble *L. crosbiensis*. An equal possibility is the situation seen in many phytosaur genera, such as *Nicrosaurus, Mystriosuchus, Machaeroprosopus* and *Redondasaurus,* in which there occurs both a robust and a gracile species (or multiple of either). Based on the phylogenetic results from Chapter 1, '*S. lithodendrorum*' may remain a distinct species, but might represent a

robust morph of *Leptosuchus*. A detailed review of '*S. lithodendrorum*' and *L. crosbiensis* would greatly benefit the field of phytosaur systematics in the future.

Although there appears to be validity to the morphotypes of Hunt (1989), it is not possible with only geometric morphometric data to test whether these separate morphotypes represent ecological differences as was suggested by Hunt (1989). To ascertain whether gracile, moderate and robust phytosaur morphologies may have exhibited dietary differences, biomechanical data or ecological correlates such as mechanical advantage, tooth crown aspect ratio, symphyseal length, height of articular condyle etc. would be required (e.g. Stubbs *et al*. 2013).

In their study of pseudosuchian mandibular morphology and biomechanics through the Mesozoic, Stubbs *et al.* (2013) found phytosaurs to overlap with the morphological range of Sphenosuchia (partially), Teleosauridae, Metriorhynchidae, pholidosaurids/stomatosuchids and one specimen of Eusuchia. However, in their biomechanical morphospace, phytosaurs only overlapped in range with Teleosauridae (partially), Metriorhynchidae, one specimen of pholidosaurids/stomatosuchids and one specimen of Eusuchia. In the biomechanical morphospace of Stubbs *et al*. (2013) phytosaurs plot between the midpoint and the negative end of PC 1, indicating a faster, and proportionately less powerful bite; on PC 2 phytosaurs were divided between positive and negative values, though more skewed toward the positive values – indicating a greater resistance to dorsal or lateral bending in the more robust taxa, while negative values associated with more gracile taxa indicated a greater resistance to torsion.

The thalattosuchians included in the present analysis all belong to Teleosauridae, therefore the apparent morphological and biomechanical similarity of metriorhynchids to

phytosaurs found by Stubbs *et al.* cannot be quantified here; however, both groups include more and less longirostrine forms, oreinirostral and gracile snout morphologies and forms with 'pointed' posteriorly projecting squamosals (Young *et al.*, 2010). There are also considerable differences between the crania of the two groups; metriorhynchids (aside from *Rhacheosaurus*) possess comparatively enormous dorsally oriented supratemporal fenestrae, all have large laterally positioned orbits, presumably to provide a wide angle of vision to aid active hunting in a pelagic environment, and include some extremely brevirostrine taxa.

The use of mandibles, rather than crania was argued to be more representative of feeding biomechanics, as crania are co-opted for numerous other functional tasks (Stubbs *et al.*, 2013), therefore the overlap of phytosaur mandibulae with numerous other groups in both morphospace and biomechanical morphospace, in contrast to the relative isolation of phytosaur crania in the morphospace presented here, is not unusual. This may indicate that phytosaurs, metriorhynchids and teleosaurids effected similar biomechanical evolutionary pressures in their mandibulae during feeding, whilst remaining ecologically distinct, whereas other factors formed a greater influence on cranial evolution. One such factor is phylogenetic relatedness; upon testing for the effects of phylogenetic signal on cranial morphology (geomorph: "physignal" function), I found that cranial morphology is highly dependent on phylogeny in my whole dataset (dorsal: $K=0.2244$, $p=0.001$; lateral: $K=0.1915$, $p=0.001$). It may therefore be valid in future to explore more deeply to what extent phylogeny and biomechanics govern the evolution of cranial morphology in pseudosuchian archosaurs more broadly.

Alternatively more direct evidence of diet could be used, such as dental microwear (Purnell *et al.*, 2012, 2013), some aspects of which are explored in the next chapter.

3.4.4. *Rates of morphological evolution*

In the SimRates and CalcRates analyses (Figures 3.17, 3.18), in general the groups within Phytosauria tend to be simulated as evolving much faster under the SimRates analysis, with the exception of non-Mystrioisuchini Leptosuchomorpha in lateral view, which displays low evolutionary rates in both analysis techniques. Conversely, within Crocodylomorpha the SimRates results are a relatively good fit to the CalcRates results; Notosuchia is consistently found to be the fastest evolving group in Crocodylomorpha under SimRates, and the group displays a high proportion of rapidly evolving branches under CalcRates. In all analyses and conditions, Planocraniidae consistently produced the lowest evolutionary rates of all groups.

The results of the CalcRates analyses in dorsal and lateral orientations indicated generally broad overlap between group rates in the observed and null datasets; however, the pattern of evolutionary rates in Figures 3.17 and 3.18, show a variety of branches to possess greatly elevated or decreased rates. Additionally, the groups displaying least overlap of observed and null rates were those composed of the fewest taxa in both dorsal and lateral conditions. Both of these results and the distribution of rates in Figures 3.17 and 3.18 support the hypothesis that rateshifts in these datasets likely occur sporadically in individual taxa, rather than at the taxonomic level at which groups were investigated in the analyses of overlapping. The rate disparity between the individual branches of a taxonomic group are exemplified in the frequency histogram of Thalattouchia in lateral orientation (Figure S2.5); here the distribution is entirely bi-modal, indicating slowly evolving branches that overlap

with the null dataset distribution, and fast evolving branches that greatly exceed any of the null values for Thalattosuchia.

In the lateral orientation dataset the majority of phytosaurs displayed mean evolutionary rates that were slower than the null hypothesis of random evolution (Table 3.4), whereas in the dorsal dataset, morphology generally evolved at a faster rate than the null hypothesis (Table 3.3). These differences are marginal and, as mentioned above, the group treatment here masks the sporadic rate-shifts of individual taxa; however, the disconnect between dorsal and lateral rates of evolution, with lateral morphology being potentially more conserved than dorsal, may partially explain the disconnect observed between dorsal and lateral views in defining morphotypes (Table 3.2).

The most disparate group in my dataset, and one which slightly overlaps with Phytosauria in morphospace in both dorsal and lateral views, is Notosuchia. Results of the SimRates method suggest high evolutionary rates within Notosuchia; CalcRates results generally concur with this in both dorsal and lateral conditions, but indicate that rates are split into a faster evolving clade and a slower evolving clade. Pol & Leardi (2015) identified two 'pulses' of notosuchian diversification, corresponding to the Aptian–Albian and the Cenomanian/Turonian–Santonian.

The faster evolving clade incorporates *Araripesuchus wegeneri*, *Anatosuchus minor*, *Stolokrosuchus lapparenti* and *Kaprosuchus saharicus*, all of which appeared in the primary notosuchian diversification between the Aptian and Albian. I hypothesise that the interaction of two factors led to the rapid evolution reported for this clade (Figure 3.17). First, the taxa within this clade display an enormous range of disparity in both dorsal and lateral conditions (Figures 3.9, 3.10), and second (as argued by Pol and Leardi, 2015), the abruptness of the

Aptian radiation is likely exaggerated due to stratigraphic sampling bias resulting in a lack of any notosuchians from the earliest Cretaceous (Pol *et al.*, 2014). The combined effect of these factors is the sudden diversification of a highly disparate group of notosuchians, and thus rates of morphological evolution that may be artificially inflated.

The second, later, diversification pulse incorporated all taxa from the more slowly evolving clade aside from *Libycosuchus brevirostris*, (*Simosuchus clarki*, *Notosuchus terrestris*, *Sphagesaurus montealtensis*, *Caipirasuchus paulistanus* and *Baurusuchus salgadoensis*) plus two taxa from the faster evolving clade (*Uberabasuchus terrificus* and *Montealtosuchus arrudacamposi*). Likely due to their disparate morphologies, the taxa from the more rapidly evolving clade display greater rates, whereas those of the slower clade either possess long ghost lineages (*Simosuchus clarki*) or form the groups Baurusuchidae and 'advanced notosuchians' (Pol & Leardi, 2015) that, whilst being the main drivers of peak diversity throughout the entire group, are low in morphological disparity. As the stratigraphy prior to the Turonian is well sampled, this event is likely to represent a real diversification (Turner & Sertich, 2010; Pol *et al.*, 2014; Pol & Leardi, 2015), though due to the low disparity, rates of morphological evolution remained relatively stable. The low disparity of these clades also raises questions as to whether the ecological range of the group changed significantly across this diversification. Notosuchia was included in the study of Stubbs *et al.* (2013); the morphological and biomechanical disparity of mandibulae was tracked across the early–late Cretaceous transition, with the authors commenting on the interesting finding that biomechanical disparity was unchanged across this transition, despite the diversification of notosuchians into many mammal-like forms, among others. My results incorporate much fewer taxa, but find that cranial disparity in the late Cretaceous forms is relatively low in comparison to those that diversified in the early Cretaceous, potentially supporting this

finding. Stubbs *et al*. (2013) hypothesised that morphological evolution may instead have continued, but primarily in the development of specialised postcrania and heterodont, mammal-like dentition as seen in numerous late Cretaceous notosuchians.

3.5. *Conclusions*

Phytosaurs were found to occupy a statistically significantly different position in morphospace to all extant crocodylomorphs and the majority of extinct crocodylomorphs (except Thalattosuchia in lateral orientation). The most similar groups to phytosaurs are longirostrine crocodylomorphs such as Gavialoidea and Thalattosuchia; much of the variation separating these taxa from phytosaurs is due to the unique temporal morphology of the latter group. However, it remains unclear whether such differences in temporal morphology would have provoked functional differences, or whether the temporal structure of leptosuchomorph phytosaurs is phylogenetically constrained.

The variation in patterns of rostral and post-rostral morphology of Phytosauria is most similar to that of extent crocodyloids, rather than alligatoroids. In Alligatoroidea, rostral shape is largely constrained by phylogeny; however this does not appear to be true in phytosaurs. Previous studies have found that rostral morphology in crocodyloids is more controlled by function rather than phylogeny – a similar situation may be the case in phytosaurs. Sexual dimorphism may provide an alternative explanation, but does not necessarily preclude sexually dimorphic feeding strategies.

Phytosaurs are statistically no more or less disparate than any group of extant crocodilians, but are significantly less disparate than all groups of crown Crocodylia together. The range of morphology occupied by Phytosauria is unique and is not matched by any extant

crocodylian group; therefore, while extant Crocodylia may not be a perfect morphological proxy for phytosaurs, each group may individually represent a good parallel for morphological (and possibly ecological) variation. In terms of extinct crocodylomorphs Phytosauria shares dorsal morphospace with *Stolokrosuchus lapparenti*, *Elosuchus cherifiensis* and *Piscogavialis jugaliperforatus*; in lateral morphospace, Phytosauria overlaps with *Kaprosuchus saharicus* and remains very close to *Stolokrosuchus*.

The cranium of phytosaurs may be more strongly modular than that of crocodylomorphs. In crocodylomorphs some covariation is observed between rostral morphology and supratemporal structure; however, this covariation is absent in phytosaurs. A dedicated analysis of 3D cranial modularity in Phytosauria is required to test this, and may provide additional insights into phytosaur-crocodylomorph convergence.

Support is found for the three phytosaur morphotypes suggested by Hunt (1989); however, further analyses are required to test his hypotheses of correspondence of these morphotypes to crocodilian 'ecomorphs'. A disconnect is observed between the optimal morphotype classifications of taxa in dorsal and lateral orientations. A similar disconnect is also observed in the morphological evolutionary rates of phytosaurs, suggesting that morphology visible in lateral orientation is more conserved than that visible in dorsal orientation.

Chapter 4 Authorship Statement:

The content of Chapter 4 was produced in collaboration with Jordan Bestwick; Andrew Jones devised the study, collected and processed all phytosaur data, conducted all analyses, produced all figures (excluding Table 4.1, which was taken from Purnell *et al*., 2013) and wrote the entire chapter.

Jordan Bestwick assisted in the planning of experimental design, provided processed crocodylian data and provided training on microwear collection and analysis techniques (excluding canonical variates analysis [CVA]).

Chapter 4: Investigating the diet of phytosaurs and their ecological convergence with extant crocodylomorphs

4.1. *Introduction*

The Triassic Period is often suggested to represent the origin of modern ecosystems (Sepkoski, 1982), in which all modern animal phyla are present for the first time. To understand such ecosystems requires research into the community and evolutionary dynamics of all members, including potential drivers such as niche partitioning, and in turn, their effects on processes such as cladogenesis, diversification and local to global geographical distribution (Rieppel, 1995; Vitt & Pianka, 2005; Ruta *et al.*, 2007; Cisneros & Ruta, 2010; Ezcurra, 2010; Fischer *et al.*, 2012). At the base of our understanding of many aspects of fossil ecosystem dynamics, is an assumption of diet or the trophic interactions between member taxa, that shapes our perception of the ecosystem.

The investigation of food processing, and ultimately diet often relies on dental microtextural analysis, a category of techniques that have previously been successfully applied to a number of extant and extinct taxa, including fish (Purnell *et al.*, 2006, 2007, 2012), mammals (Scott *et al.*, 2005; Ungar *et al.*, 2007, 2008; Goillot *et al.*, 2009; Purnell *et al.*, 2013; Schulz *et al.*, 2013; Gill *et al.*, 2014; Xia *et al.*, 2015) and reptiles (Williams *et al.*, 2009; Whitlock, 2011). Several methods of dental microtextural analysis exist: manual identification and measurement of 'pits' and 'scratches' on 2D dental surfaces; 3D scale-sensitive fractal analysis, and 3D topology-based ISO roughness parameters (International Organization for Standardization, 2012). In this study ISO parameters are used to quantify

microwear, as both ISO parameters and fractal analysis are more robust, repeatable and more resistant to researcher measurement bias than 2D techniques. Although the manual investigation of pits and scratches to attain microwear directionality has functional applications, and can be used to inform researchers about food-processing mechanics (Williams *et al.*, 2009), it is not undertaken here as our primary objective is investigation of diet, rather than precise feeding mechanics.

ISO parameters (ISO 25178-2) are a series of standardised measurements, taken from a scale-limited 3D surface, that together are designed to describe all aspects of surface texture (Table 4.1). For dental microwear applications a roughness profile is extracted from the original 3D surface (scale limiting) by applying a high-pass filter, low pass filter and a form filter to respectively remove large-scale components of the surface such as undulation/waviness, small-scale noise and form-components such as overall surface gradient/tilt. ISO parameters (Table 4.1) are then measured using the resulting roughness profile (scale-limited surface). The resulting ISO measurements are together effectively a multivariate quantitative representation of the 3D surface which can be subjected to multivariate ordination and discrimination techniques such as PCA and LDA, and can be used to investigate hypotheses using standard statistical tests such as ANOVA.

The use of texture to investigate diet has benefits over reliance on gut contents, especially in palaeontological studies; teeth with intact enamel surfaces are much more likely to fossilise, and in greater quantities than gut contents associated with an identifiable taxon, providing a greater sample size both inter- and intraspecifically. Dental texture additionally provides a more long-term signal than gut contents, being accumulated in mammals over periods of days, weeks and occasionally months (Brasch *et al*., 1969; Christensen & Bangerter, 1987; Teaford & Oyen, 1989; Merceron *et al*., 2010) rather than a temporal

'snapshot'. Additionally, due to reptiles' lower metabolic requirements (Andrade *et al.*, 2005) and therefore the less frequent use of the dentition in food processing, dietary signal may take longer to be overwritten and thus may provide a longer-term signal in reptiles than in mammals (Bestwick *et al.*, in prep.). Crocodylians undergo continuous tooth replacement, which may be expected to curtail the amount of wear accumulated on each tooth; however, investigations of tooth replacement rate in captive juvenile and juvenile/subadult *Alligator* indicate replacement rates of 2.7–4.1 months and ~12 months respectively (Edmund, 1962; Erickson, 1996a). *Caiman crocodilus* exhibits rates of ~3.7 months (Erickson, 1996a). Theropod dinosaurs have been shown to display tooth replacement rates between ~9.6 months (adult *Deinonychus*) and ~25.9 months (adult *Tyrannosaurus*) (Erickson, 1996b). Based on these studies I assume similarly slow rates of tooth replacement in phytosaurs, allowing a representative dietary signal to accumulate.

The general hypothesis of phytosaur diet (carnivory/piscivory) is well supported on the basis of tooth morphology, material ostensibly representing gut contents (Hunt, 1991, Chatterjee, 1978; Li *et al.*, 2012; Stocker *et al.*, 2017) and morphological similarity to modern crocodylians. However the diet of many extant crocodylian species is more varied in composition than strict piscivory and carnivory, including varying quantities of tetrapods, fish, arthropods, gastropods and plant-matter (Taylor, 1979; Delany & Abercrombie, 1986; Thorbjarnarson, 1988; Delany, 1990; Sah & Stuebing, 1996; Da Silveira & Magnusson, 1999; Delany *et al.*, 1999; Rice *et al.*, 2005; Wallace & Leslie, 2008; Laverty & Dobson, 2013).

The aim of this chapter is to investigate phytosaur diet using dental microwear as empirical evidence of phytosaur food processing and drawing comparisons with equivalent data for extant crocodylians, with the goal of evaluating phytosaur diet in a more complex real-world context.

In addition to providing more robust evidence for phytosaur dietary composition and presenting a novel view of phytosaur diet, in this chapter a number of hypotheses are also investigated:

1) The three tooth morphologies identified in heterodont phytosaurs by Hungerbühler (2000) represent functional partitioning along the tooth-row, with each tooth morphology adapted to processing a different material component of diet.
2) More robust phytosaurs are more likely to have targeted tetrapod prey, whereas more gracile phytosaurs were primarily piscivorous. This is the view of phytosaurian ecology posited by many previous authors (Hunt, 1989; Parrish, 1989; Hungerbühler, 2000; Heckert *et al.*, 2013).
3) The existence of hypothetical phytosaur 'ecomorphs' as suggested by Hunt (1989), in which robust, moderate and gracile phytosaurs were assigned to different ecological niches, based on morphological comparison with extant crocodylian analogue species.

Table 4.1: ISO textural parameter units, definitions and categories. From Purnell *et al.* (2013): Table S2.

Parameter	Unit	Definition	Category
Sq	µm	Root-Mean-Square height of surface	height
Sp	µm	Maximum peak height of surface	height
Sv	µm	Maximum valley depth of surface	height
Sz	µm	Maximum height of surface	height
Sa	µm	Average height of surface	height
Ssk	-	Skewness of height distribution of surface	height
Sku	-	Kurtosis of height distribution of surface	height
S5z	µm	10 point height of surface	feature
Sdq	-	Root mean square gradient of the surface	hybrid
Sdr	%	Developed interfacial area ratio	hybrid
Sds	$1/mm^2$	Density of summits. Number of summits per unit area making up the surface	hybrid
Ssc	1/µm	Mean summit curvature for peak structures	
Sk	µm	Core roughness depth, Height of the core material	material ratio
Spk	µm	Mean height of the peaks above the core material	material ratio
Svk	µm	Mean depth of the valleys below the core material	material ratio
Smr1	%	Surface bearing area ratio (the proportion of the surface which consists of peaks above the core material)	material ratio
Smr2	%	Surface bearing area ratio (the proportion of the surface which would carry the load)	material ratio
Vmp	$µm^3/mm^2$	Material volume of the peaks of the surface	volume
Vmc	$µm^3/mm^2$	Material volume of the core of the surface	volume
Vvc	$µm^3/mm^2$	Void volume of the core of the surface	volume
Vvv	$µm^3/mm^2$	Void volume of the valleys of the surface	volume
Sal	mm	Auto correlation length. Horizontal distance of the auto correlation function (ACF) which has the fastest decay to the value 0.2. Large value: surface dominated by low frequencies. Small value: surface dominated by high frequencies.	spatial
Str	-	Texture aspect ratio (values range 0-1). Ratio from the distance with the fastest to the distance with the slowest decay of the ACF to the value. 0.2-0.3: surface has a strong directional structure. > 0.5: surface has rather uniform texture.	spatial

4.2. *Materials & Methods*

4.2.1. *Dataset and data partitions*

The ISO dental microwear dataset used in this study is composed of the extant crocodylian and varanid dataset of Bestwick *et al.* (in prep.), and dental microwear collected from phytosaur specimens by A. S. Jones. To test the hypotheses described above and the general diet of phytosaurs the dataset was divided into different sets of partitions (described in the following subsections). When investigating phytosaur tooth position and cranial robusticity only the phytosaur dataset was used for analysis. In the other analyses crocodylians were incorporated but varanids were generally excluded as they are morphologically dissimilar to crocodylians and phytosaurs and are generally terrestrial – performing most activities, including hunting, on land (only one species in this dataset, *Varanus salvator*, incorporates a proportion of fish into its diet), and are therefore subject to different selection pressures on hunting and feeding. Furthermore the degree of heterodonty found in many extant crocodylomorphs and phytosaurs is not present in varanids, which may also affect results.

Phytosaur microwear was collected from premaxillary and maxillary teeth of five species, with 19 total microwear samples included in the present study **(**Table 4.2). Specimens were sampled from the Museum of the University of Texas Tech (TMM) and the Staatliches Museum für Naturkunde, Stuttgart (SMNS), and were chosen to represent a range of taxonomic groups, spanning robust and gracile cranial morphologies, including specimens retaining teeth from varied locations along the tooth row.

The crocodylian and varanid dataset of Bestwick *et al*. (in prep.) includes 96 microwear samples across 13 species (Table 4.3).

Table 4.2: Details of the phytosaur dataset. Each sample represents an individual tooth from which a single texture sample was collected.

Sample No.	Species	Specimen	Tooth Position	Robusticity
1	*Smilosuchus lithodendrorum*	TTU-P 15661	Posterior	Robust
2	*Smilosuchus lithodendrorum*	TTU-P 15661	Posterior	Robust
3	*Smilosuchus lithodendrorum*	TTU-P 15661	Posterior	Robust
4	*Smilosuchus lithodendrorum*	TTU-P 15661	Anterior	Robust
5	*Machaeroprosopus pristinus*	TTU-P 10074	Posterior	Gracile
6	*Machaeroprosopus pristinus*	TTU-P 10074	Mid	Gracile
7	*Machaeroprosopus pristinus*	TTU-P 10074	Mid	Gracile
8	*Nicrosaurus meyeri*	SMNS 91574	Anterior	Gracile
9	*Nicrosaurus meyeri*	SMNS 91574	Anterior	Gracile
10	*Mystriosuchus planirostris*	SMNS 12060	?	Gracile
11	*Mystriosuchus planirostris*	SMNS 12060	Posterior	Gracile
12	*Mystriosuchus planirostris*	SMNS 12060	Posterior	Gracile
13	*Nicrosaurus meyeri*	SMNS 4059	?	Gracile
14	*Nicrosaurus kapffi*	SMNS 13078	Anterior	Robust
15	*Nicrosaurus kapffi*	SMNS 13078	Anterior	Robust
16	*Nicrosaurus kapffi*	SMNS 13078	Mid	Robust
17	*Nicrosaurus kapffi*	SMNS 13078	Mid	Robust
18	*Nicrosaurus kapffi*	SMNS 13078	Mid	Robust
19	*Nicrosaurus kapffi*	SMNS 13078	Mid	Robust

Table 4.3: Details of the crocodylian and varanid dataset of Bestwick *et al.* (in prep.).

Sample No.	Species	Dietary Guild (Bestwick *et al.*, in prep.)
20–27	*Alligator mississippiensis*	Piscivore
28–33	*Caiman crocodilus*	Piscivore
34–40	*Crocodylus acutus*	Hard invertebrate eater
41–44	*Crocodylus niloticus*	Piscivore
45–50	*Crocodylus porosus* Adult	Carnivore
51–55	*Crocodylus porosus* Juvenile	Hard invertebrate eater
56–62	*Gavialis gangeticus*	Piscivore
63–73	*Varanus nebulosus*	Carnivore
74–77	*Varanus komodoensis*	Carnivore
78–85	*Varanus niloticus*	Intermediate invertebrate eater
86–92	*Varanus olivaceus*	Omnivore
93–99	*Varanus prasinus*	Intermediate invertebrate eater
100–107	*Varanus rudicollis*	Carnivore
108–115	*Varanus salvator*	Carnivore

4.2.1.1. *Phytosaur tooth positions*

All phytosaur species exhibit a degree of heterodonty (being less pronounced in gracile taxa) so sampling aimed to represent in each taxon the three phytosaur tooth morphologies identified by Hungerbühler (2000) (Figure 1.3; 4.1). In extremely gracile species such as *Mystriosuchus planirostris* anterior and mid teeth may be confused; to avoid complications in species in which heterodonty is less prominent, dentition was only sampled in situ in these taxa. It was not possible to sample all three tooth positions/morphologies in every taxon due to the sporadic retention of in-situ teeth in phytosaur fossils; teeth are often lost in phytosaurs due to the presence of thecodont tooth insertion with simple cylindrical tooth-roots. When investigating differences in tooth position, samples 10 (*Mystriosuchus planirostris*) and 13 (*Nicrosaurus meyeri*) were excluded as their anteroposterior location along the tooth row was unknown.

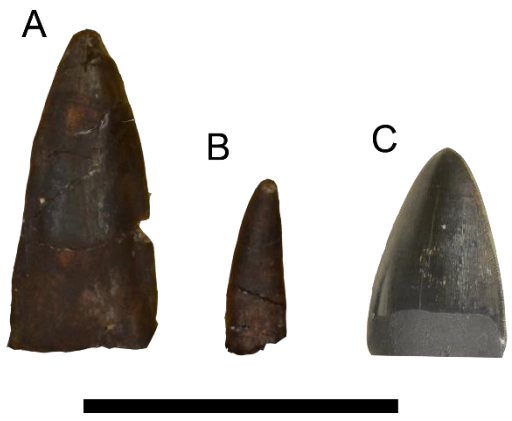

Figure 4.1: Heterodont tooth morphologies along the phytosaur tooth-row. A) Anterior (*Nicrosaurus kapffi*, SMNS 13078), B) mid (*Nicrosaurus kapffi*, SMNS 13078) and C) posterior (‘*Smilosuchus lithodendrorum*’, TTU-P 15661). Scale bar = 5cm.

Three categories were implemented to describe tooth row position/tooth morphology (Table 4.2, Figure 4.1): “Anterior”, corresponding to the anteriormost three/four teeth in the

premaxilla; in addition to their location, these teeth are characterised by their considerable robusticity and apico-basal length which is far greater than most other teeth in the tooth row (Figure 4.1a). In some taxa (e.g. '*Smilosuchus lithodendrorum*', *Smilosuchus gregorii*, *Machaeroprosopus mccauleyi*) an additional set of large teeth occur at the transition between the premaxilla and maxilla; these teeth are more slender than those of the terminal rosette and none were included in this study. "Mid" corresponds to teeth which may or may not be carinated or possess serrations, but are always conical in morphology, with essentially a circular cross-section; these teeth constitute all, or the majority of (see above), the dentition across the mid-section of the tooth row (Figure 4.1b). "Posterior" teeth are characterised by an approximately phylloform morphology with slight to moderate apical recurvature, prominent serrated carinae and a labially convex D-shaped cross-section (Figure 4.1c).

4.2.1.2. *Phytosaur robusticity*

Robust and gracile categories were defined by the membership of the gracile and robust cranial morphologies identified in Chapter 3, section 3.3.5. Specimen membership of these groups is summarised in Table 4.2 and Figure 4.3.

4.2.1.3. *Dietary guilds*

As phytosaur diet was the aim of this investigation, and very little direct evidence of exact phytosaur dietary composition is known, phytosaurs were here classified into their own group "Phytosaurs", which was projected into crocodylian/varanid dietary space.

Crocodylian and varanid specimens were grouped by dietary guild following identical assignments to Bestwick *et al.* (in prep.). In their study each taxon was assigned to a dietary guild, consisting of either carnivore, piscivore, hard-invertebrate eater, intermediate-invertebrate eater or omnivore (Table 4.3). Dietary assignment in their study was based on a reclassification of diet in each taxon, drawing on stomach-content, faecal content and observational studies of crocodylians and varanids (Taylor, 1979; Auffenberg, 1981, 1988; Delany & Abercrombie, 1986; Greene, 1986; Losos & Greene, 1988; Thorbjarnarson, 1988; Delany, 1990; Sah & Stuebing, 1996; Da Silveira & Magnusson, 1999; Delany *et al*., 1999; Rashid, 2004; Rice *et al*., 2005; Wallace & Leslie, 2008; Laverty & Dobson, 2013; Dalhuijsen *et al*., 2014; Rahman *et al*., 2015, 2017). The relative hardness of food items in diet was also taken into account, and the likely contribution of each food type to microwear signal relative to their proportion within diet.

Figure 4.2: Cranial morphology of phytosaur species included in dental microwear analyses. Gracile taxa: A) *Machaeroprosopus pristinus* (UCMP 137319), B) *Mystriosuchus planirostris* (SMNS 9134), C) *Nicrosaurus meyeri* (SMNS 12593). Robust taxa: D) *Smilosuchus lithodendrorum* (UCMP 26688), E) *Nicrosaurus kapffi* (SMNS 4379).

The latter consideration involved the splitting of vertebrate prey into ‘proportion of fish’ and ‘proportion of tetrapods’, and the splitting of invertebrates into proportions of ‘hard’, ‘intermediate’ and ‘soft’ invertebrates in diet. Invertebrate material was subset by Bestwick *et al.* (in prep.) as: Soft = Araneae (spiders), Lepidoptera (butterflies and moths), Myriapoda (centipedes and millipedes) and all invertebrate larvae; Intermediate = Formicidae (ants), Odonata (dragonflies and damselflies) and Orthoptera (grasshoppers and crickets); Hard = Coleoptera (beetles), Crustacea (crabs and crayfish) and Gastropoda (snails). The above classifications into ‘hardness’ categories were based on studies of material properties in invertebrate integuments (Kaliontzopoulou *et al.*, 2012; Runemark *et al*., 2015; Dollion *et al.*, 2017). As I use their dataset as a basis into which phytosaur microwear is projected, the partitions within this dataset correspond exactly with their study. From studies of stomach contents, Bestwick *et al.* (in prep.) calculated the average proportion of diet constituted by total vertebrates, tetrapods, fish, total invertebrates, and hard, intermediate and soft invertebrates. These proportions were later used to test the presence of a correlation between principal component/canonical variate axes and diet (Purnell *et al.*, 2013); essentially a measure of whether significant differences between analysis groups (e.g. pre-assigned dietary guild, species) were actually due to dietary differences or non-dietary variation.

4.2.1.4. *Species groups*

Phytosaurs were not split by species due to the low sample sizes that this would produce. Low sample sizes do not necessarily present a problem in microtextural studies (Purnell *et al.*, 2012, 2013), but dietary differences between phytosaurs were expected to be more related to robusticity than species. Furthermore the low sample sizes would greatly reduce the ability of

statistical tests to find statistical significance, even where differences are large; therefore the cost to statistical power was deemed unnecessary.

Crocodylians and varanids were split into the same species groups as used by Bestwick *et al.* (in prep.). *Crocodylus porosus* was split into an adult and a juvenile group to reflect the presence of both adults and juveniles in the dataset and the presence of an ontogenetic dietary dichotomy between the two (Taylor, 1979; Sah & Stuebing, 1996).

4.2.2. *Cleaning, moulding and casting phytosaur teeth*

Phytosaur teeth were cleaned prior to moulding, to remove dirt and consolidant, and ensure the recovery of microwear detail. A solvent gel, prepared to the specifications set out by Williams & Doyle (2010), was applied to each tooth, ensuring a coating of more than 8 mm thickness was maintained on all sides to allow effective sequestration of consolidant into the gel. Each gel-covered tooth was wrapped with plastic film to limit evaporation of solvents and maintain the position of the gel and its contact with the tooth surface. The solvent gel was allowed to act on the consolidant for at least 20 minutes prior to its removal; following removal, any remaining gel, dirt or other detritus was cleaned from the tooth surface using ethanol and a soft brush, and was allowed to dry.

Tooth moulds were made using Coltène/Whaledent Predident Plus regular body Polyvinylsiloxane (Coltène/Whaledent Ltd., Burgess Hill, West Sussex, UK). This moulding medium has been found to produce highly accurate and precise surface replicas that do not generally differ significantly from reality (Goodall *et al.*, 2015). Two moulds were taken of each tooth; the first mould served to remove loose sediment/dirt that was not removed during the cleaning process, while the second mould was used to create tooth casts.

Casts were made with EpoTek 320 LV Black epoxy resin, which was allowed to cure in a Protima pressure tank (10L) at 2 bar/30psi for 24 hours to minimise the effect of any air incorporated into the resin during mixing and pouring. Finally, casts were sputter-coated with gold (SC650, Bio-Rad, Hercules, CA, USA) to improve light reflectance, in preparation for imaging.

4.2.3. *Imaging of dental texture*

The extraction of dental microwear data from specimen casts followed Purnell *et al*. (2013); for completeness the steps taken are summarised below.

Following visual inspection of labial tooth surface to identify areas of intact enamel, 3D surface-texture files were obtained from the tooth apex (or as close as possible) using an Alicona Infinite Focus microscope G4b (IFM; AliconaGmbH, Graz, Austria; software v. 2.1.2) under 100X magnification, resulting in texture files corresponding to an area of 145 x 110 μm. Imaging was performed at a vertical resolution of 20 nm and lateral resolution of 440 nm. Only areas of tooth surface free from debris, or other features obstructing microwear were used for analysis.

Following imaging, textural data was levelled and manually edited to remove aberrant non-microwear structures, such as dust and anomalous peaks/pits from the 3D reconstruction, within the Alicona software. Surface files were then exported to the software SurfStand (v. 5.0.0 Centre for Precision Technologies, University of Huddersfield, West Yorkshire, UK), in which large scale differences in surface morphology, such as curvature, were removed and non-informative noise was excluded by subjecting the data to a robust Gaussian wavelength filter ($\lambda c = 0.025$ mm) and a fifth-order robust polynomial (Schulz *et al*., 2013; Purnell *et al.*,

2012, 2013). Textural roughness parameters corresponding to ISO 25178-2 (International Organisation for Standardization, 2012) were calculated for the surface dataset in SurfStand; these parameters are summarised in Table 4.1 (Table S2 of Purnell *et al*. [2013]).

4.2.4. *Statistical analyses*

All statistical analyses were carried out in the statistical software JMP 14 (SAS Institute, Cary, NC, USA), with the exception of Benjamini-Hochberg correction (Benjamini & Hochberg, 1995) which was performed using the Microsoft Excel formula sheet of McDonald (2014).

All ISO parameter data displayed right-skewed distributions and were thus log10 transformed prior to data analysis; Ssk was removed from the dataset, being found to exhibit a non-normal distribution, but containing negative values, preventing transformation. The full phytosaur dataset is presented in Table S3.1.

Before statistical comparisons could be made between ISO parameter values of different data partitions (e.g. phytosaur anterior vs mid vs posterior tooth positions), all ISO parameters were separated into the data partitions under investigation and were individually tested for normality using the Shapiro-Wilk W test. Where greater than 5% of the whole dataset indicated a significant result (i.e. non-normality) P-values were subjected to Benjamini-Hochberg correction for multiple comparisons to adjust for increased likelihood of type 1 error (false discovery rate: 0.05). Providing that more than 95% of the dataset was observed to be normally distributed following Benjamini-Hochberg correction, the dataset was accepted for use in further analyses. None of the alternatively partitioned datasets were found to be significantly non-normally distributed following Benjamini-Hochberg correction.

Multiple ANOVAs (as in Purnell *et al.*, 2012, 2013) were used to test for significant differences between analysis partitions (e.g. tooth position) due to ISO parameter values; i.e. finding the aspects of surface roughness that best separate analysis partitions. Where data failed to meet the ANOVA criterion of equality of variances (identified by a significant result in any of the following tests: O'Brien [.5], Brown-Forsythe, Levene, Bartlett or 2-sided F test) separation of groups was instead assessed with Welch's ANOVA. P-values were again adjusted for type 1 error using the Benjamini-Hochberg correction and Tukey-Kramer HSD pairwise comparisons were performed to identify the analysis partitions that differed significantly for each ISO parameter.

The ISO parameters that produced significant separation of the analysis partitions were subjected to principal components analysis (PCA). ISO parameters identified to contain non-significant group-wise variation and/or no significant pairwise differences under Tukey HSD comparisons were excluded from PCA. PC axes were constructed with the correlation matrix (identical results to analysing normalised variables with the covariance matrix) to identify axes of covariation that maximise explained variance; this approach assumes that dietary-related covariation in microwear is the most prevalent in the dataset. The separation of groups along PC axes was investigated using ANOVAs and Tukey HSD tests.

As a priori assumptions are already present within each dataset, e.g. by classifying taxa by dietary guild or by robusticity, and expecting these classifications to explain significant divergences in the data, it is appropriate to also use a supervised dimensionality reduction algorithm, i.e. canonical variates analysis (CVA; a form of LDA) that, by its definition, aims to maximise the separation between user-defined groups. As such it is also arguably a more appropriate technique for directly testing hypotheses of group-based differences in multivariate space than PCA. Initially only significant ISO parameters were

included in CVA, as in PCA; however, CVA may combine multiple parameters containing individually non-significantly separating covariation, in order to produce axes of maximum separation. Therefore, it would not necessarily be expected that an analysis containing only parameters displaying significant variation between groups would perform better than an analysis including all available textural parameters. As such CVAs were also performed that included all textural information, to allow for the possibility of a better result. Separation of groups along CV axes was also investigated with ANOVAs and Tukey HSD tests, with the significance of the contribution of each CV axis to separation of groups analysed with Wilks' Lambda.

In all PCAs and CVAs in which phytosaur dietary reconstruction was based on comparison with extant analogues, the multivariate space was constructed excluding phytosaurs. This resulted in a dietary space in which each axis' relationship to diet could be verified with respect to the known feeding habits of extant taxa. Following construction of the multivariate space, phytosaur datapoints were projected onto it such that their position in dietary space could be evaluated without contributing unknown dietary signal.

The association of PC and CV axes with diet was tested using linear regression of PC/CV scores with the average dietary composition corresponding to the species of each crocodylian/varanid datapoint. Significant positive or negative correlations associated with an axis of variation/separation indicated that a particular component of diet (e.g. total percentage of vertebrates in diet or percentage of hard vertebrates in diet) either increased or decreased with PC/CV values respectively.

4.3. *Results*

4.3.1. *Tooth position*

4.3.1.1. *Significant ISO parameters*

Under ANOVA none of the ISO parameters were found to significantly discriminate between tooth position, following Benjamini-Hochberg correction. A PCA was therefore not performed.

4.3.1.2. *Discriminant analysis of tooth position*

To investigate whether more subtle aspects of covariation between ISO parameters allowed distinction of tooth position, a CVA was conducted including all textural parameters. Both output CV axes found significant differences between tooth position (CV1: F=80.47, P=<0.0001, Tukey tests Mid vs Posterior P=<0.0001, Mid vs Anterior P=<0.0001, Wilks' Lambda=0.03, P=<0.0001; CV2: F=6.77, P=0.0186 [Welch's ANOVA]; Tukey tests Anterior vs Posterior P=0.0012, Anterior vs Mid P=0.0152, Wilks' Lambda=0.39, P=<0.0001). The predictive model was found to misclassify only 17.6% of cases (Figure 4.3).

4.3.1.3. *Association of tooth position and diet*

The presence of significant differences in the dataset, explainable by tooth position, is not necessarily a product of diet. Because dietary composition is unknown for phytosaurs the CV axes could not be regressed against diet to test for this (whereas it could in the crocodylian

dataset). Instead the CV formula that produced significant separation of phytosaur tooth positions in multivariate space was applied to the crocodylian dataset alone, and the resulting crocodylian CV scores were regressed against crocodylian dietary composition. As the hypothesis regarding tooth position specifically proposes the differential use of the three tooth categories in processing different materials, if the hypothesis is correct then the different tooth positions would display different microwear profiles associated with diet.

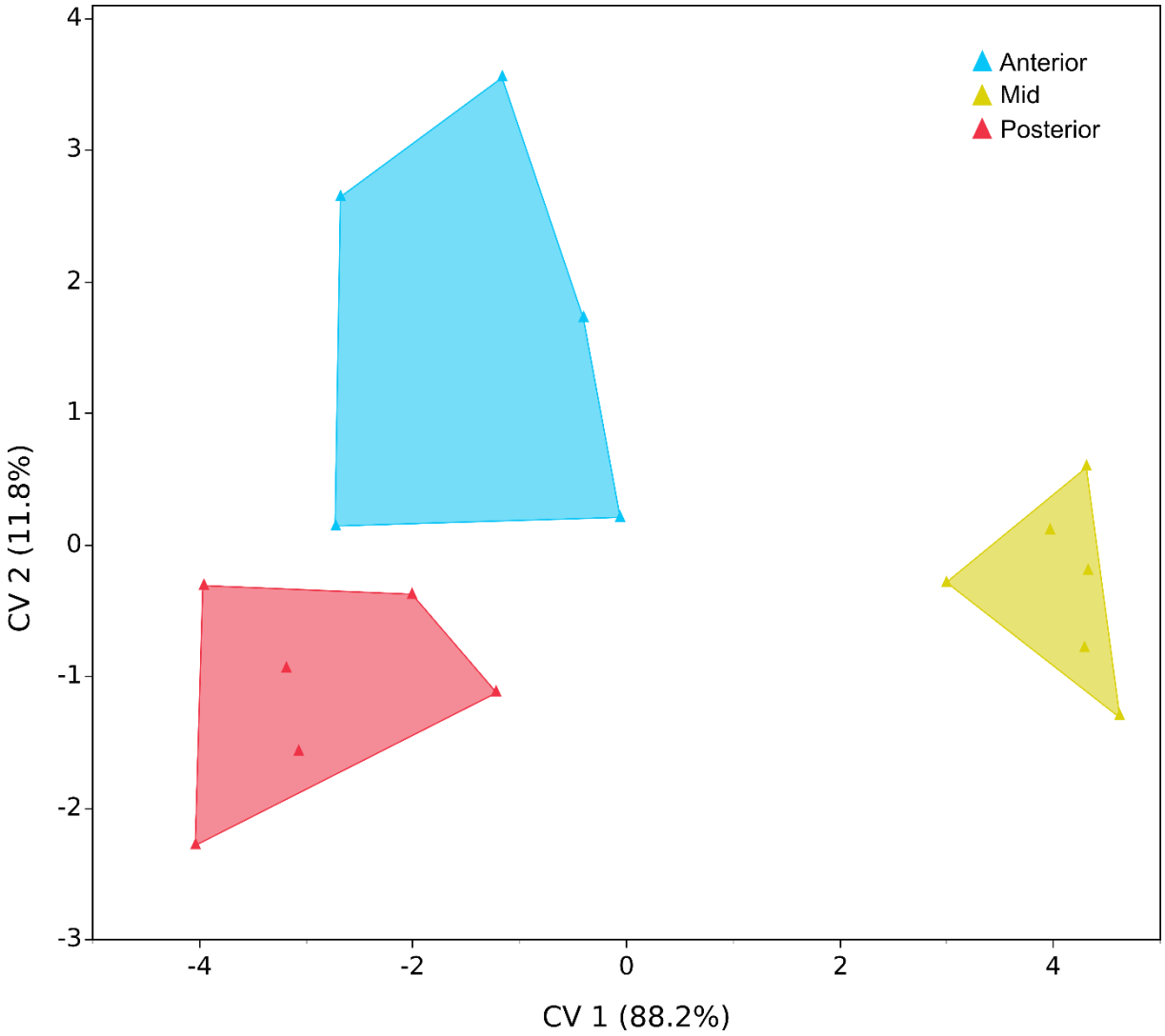

Figure 4.3: CVA multivariate space of phytosaur dental microwear, constructed with all 21 ISO textural parameters, grouped by tooth position.

The extant crocodylian dataset allows the identification of microwear profiles that are verifiably associated with differences in diet, and these profiles are assumed to be consistent among similar taxa. Therefore, if the aforementioned CV formula for phytosaurs produced separation among tooth positions (i.e. diet according to the hypothesis) attributable to dietary composition, then the same should be true in crocodylians.

No significant correlation was observed between crocodylian CV scores and percentage dietary composition in crocodylians. This indicates no significant association between the microwear profiles separating phytosaurs by tooth position, and dietary composition. Furthermore, in none of the analyses discussed below did tooth position categories in phytosaurs produce any statistically significant separation along any PC or CV axes. I therefore find no evidence in support of functional partitioning along the phytosaur tooth row involved in processing different food materials.

4.3.2. *Robusticity*

4.3.2.1. *Significant ISO parameters*

Following Benjamini-Hochberg correction, five ISO parameters produced significant separation robusticity categories in phytosaurs (Sp: F=8.36, P=0.0101; Sz: F=9.91, P=0.0059; Sdq: F=3.10, P=0.0051; Sdr: F=10.27, P=0.0052; S5z: F=7.93, P=0.0119).

4.3.2.2. *PCA and CVA of significant robusticity parameters*

These five parameters were subjected to PCA, from which only PC 1 (76.1% of variation) was found to produce statistically significant separation between gracile and robust

phytosaurs (Figure 4.4) (T-test: t=3.83, P=0.0013). A CVA plotted with these parameters found statistically significant separation of robusticity groups (T-test: t=4.25, P=0.0007), with a very large proportion of variance attributable to between-group differences (Wilks' Lambda=0.48, P=0.0596). Additionally, the CVA mis-classified only 15.8% of cases (i.e. specimens previously defined as gracile being classified as robust, and vice-versa) (Figure 4.5).

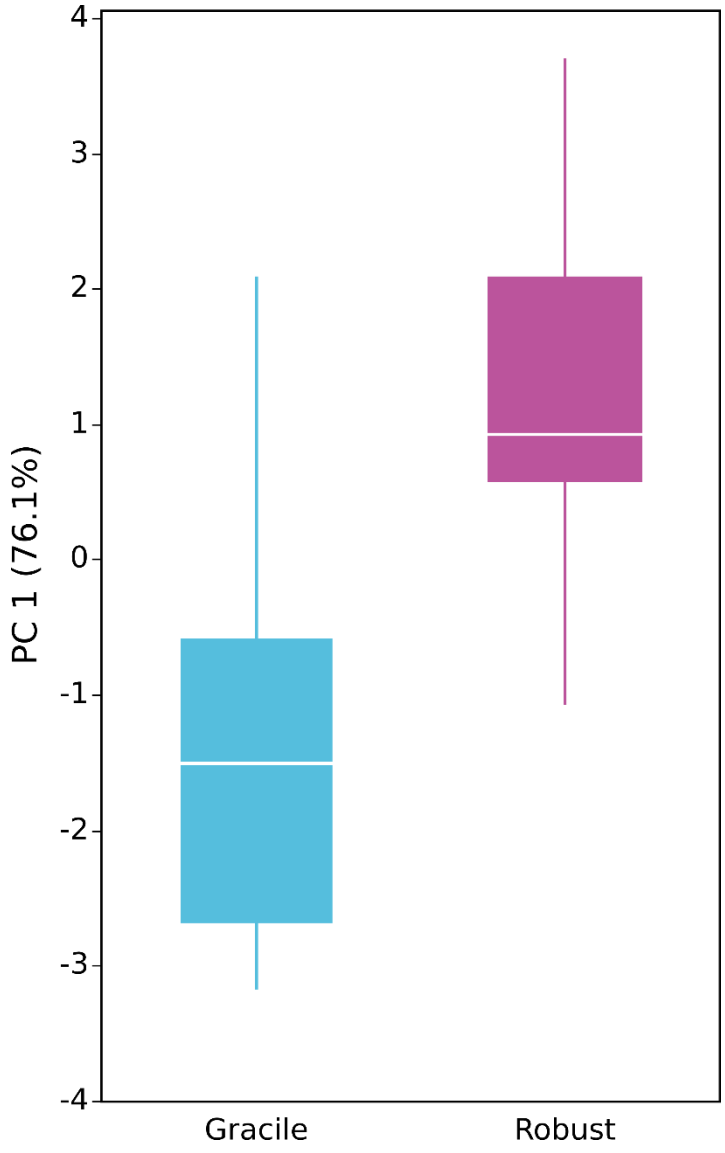

Figure 4.4: PC 1 variation by cranial morphology. PCA constructed with the five ISO parameters significant for cranial morphology (Sp, Sz, Sdq, Sdr, S5z).

Including all textural parameters in the CVA produced a more effective predictive model, misclassifying only 10.5% of cases. It produced significant separation between the robusticity categories, and was significantly attributable to the difference between groups (Figure 4.6) (T-test: t=-50.84, P=<0.0001, Wilks' Lambda=0.007, P=<0.0001).

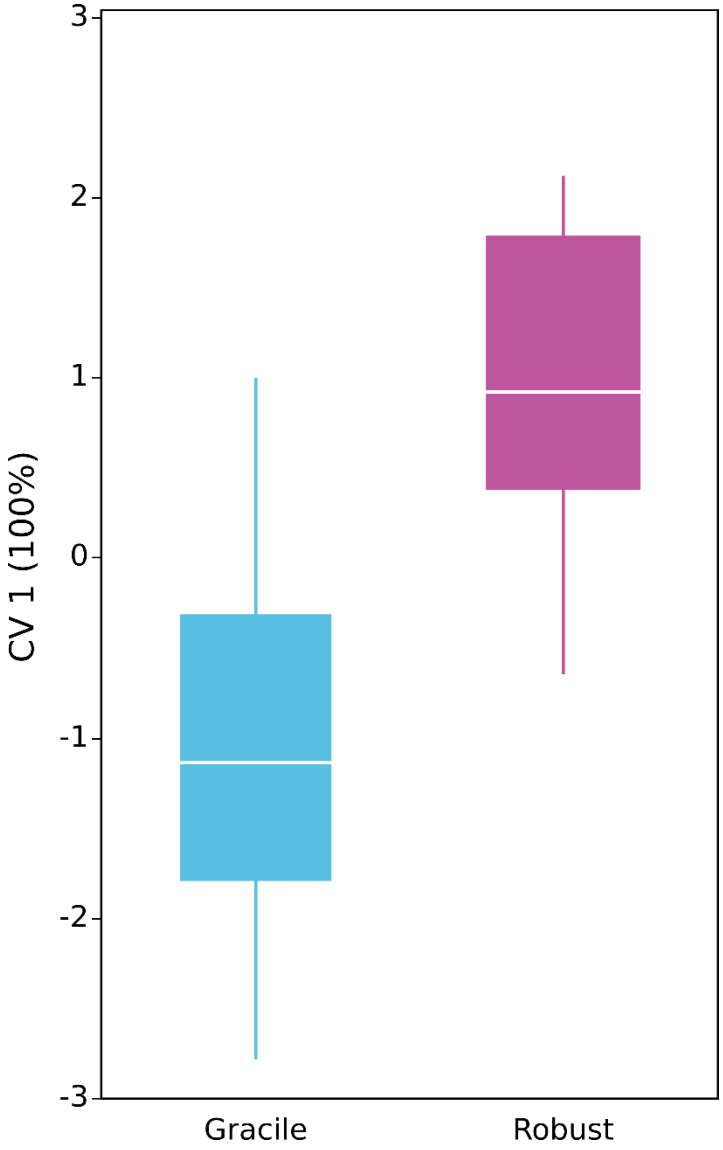

Figure 4.5: CVA of 5 significant ISO parameters (Sp, Sz, Sdq, Sdr, S5z) grouped by cranial morphology. Variation along CV 1.

However, again by applying the PC and CV formulae for maximum variation and separation by cranial robusticity to crocodylians, no significant correlation was observed between crocodylian PC or CV scores and dietary composition, in the multivariate space. Therefore, while there is a significant difference in surface texture between cranially gracile and robust phytosaurs, there is no evidence to suggest that this difference in microwear is due to dietary differences.

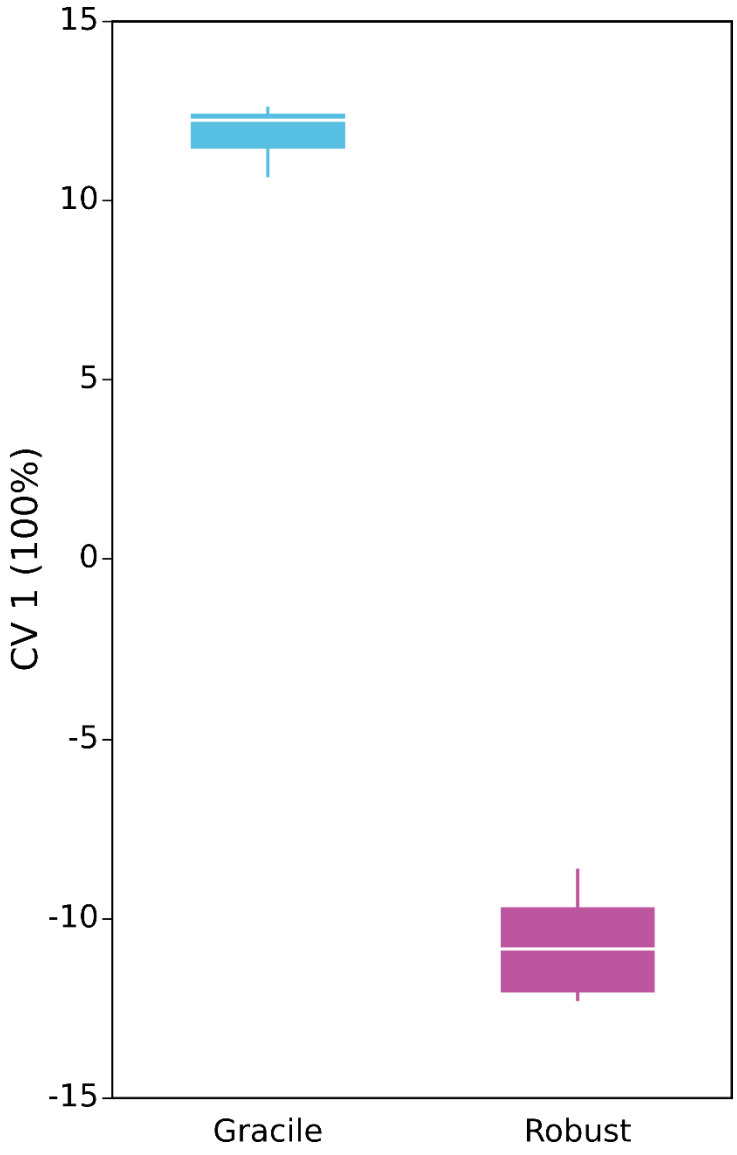

Figure 4.6: CVA of all 21 ISO parameters grouped by cranial morphology. Variation along CV 1.

4.3.3. *Dietary guild*

4.3.3.1. *Significant ISO parameters*

Among crocodylians alone, no ISO parameters produced significant separation by dietary guild. Only when the full reptilian dataset of Bestwick *et al.* (in prep.) was used, including all species of varanids in addition to crocodylians, were any ISO parameters found to significantly discriminate by dietary guild. In this case, four parameters were found to be significant (Sds: F=5.43, P=0.0006; Vmp: F=5.60, P=0.0004; Spk: F=5.47, P=0.0005; Smr1: F=6.28, P=0.0002).

4.3.3.2. *PCA and CVA of significant 'dietary guild' parameters*

These parameters were subjected to PCA and CVA, from both of which the first two axes were found to produce significant differences between pre-defined dietary guilds in multivariate space (PC 1: [Welch's ANOVA] F=3.21, P=0.0182; PC 2: F=4.18, P=0.0016; CV 1: [Welch's ANOVA] F=4.23, P=0.0046, Wilks' Lambda=0.60, P=<0.0001; CV 2: F=4.14, P=0.0017, Wilks' Lambda=1.96, P=0.0456). Tukey HSD significant pairwise differences are presented in Table S3.2. Both analyses display approximately the same results pertaining to phytosaurs, i.e. their separation from omnivorous taxa in multivariate space; however, the CVA finds two additional distinctions over the PCA: phytosaurs are found to be significantly separated from hard-invertebrate eaters and carnivores are significantly distinguished from piscivores (Figures 4.7 and 4.8).

As well as being investigated as a whole group, phytosaurs were again split into gracile and robust categories as a supplementary test of dietary differences in cranial morphology. The results remained identical to those of the combined phytosaur group (in

terms of significance, though exact P values vary) in the PCA, whilst in the CVA the only observed difference was the loss of a significant difference between gracile phytosaurs and hard-invertebrate eaters. Both significant axes of the PCA and CVA were significantly correlated with aspects of dietary composition (Spearman ρ, with Benjamini-Hochberg correction) (significance scores are summarised in Tables S3.3 and S3.4).

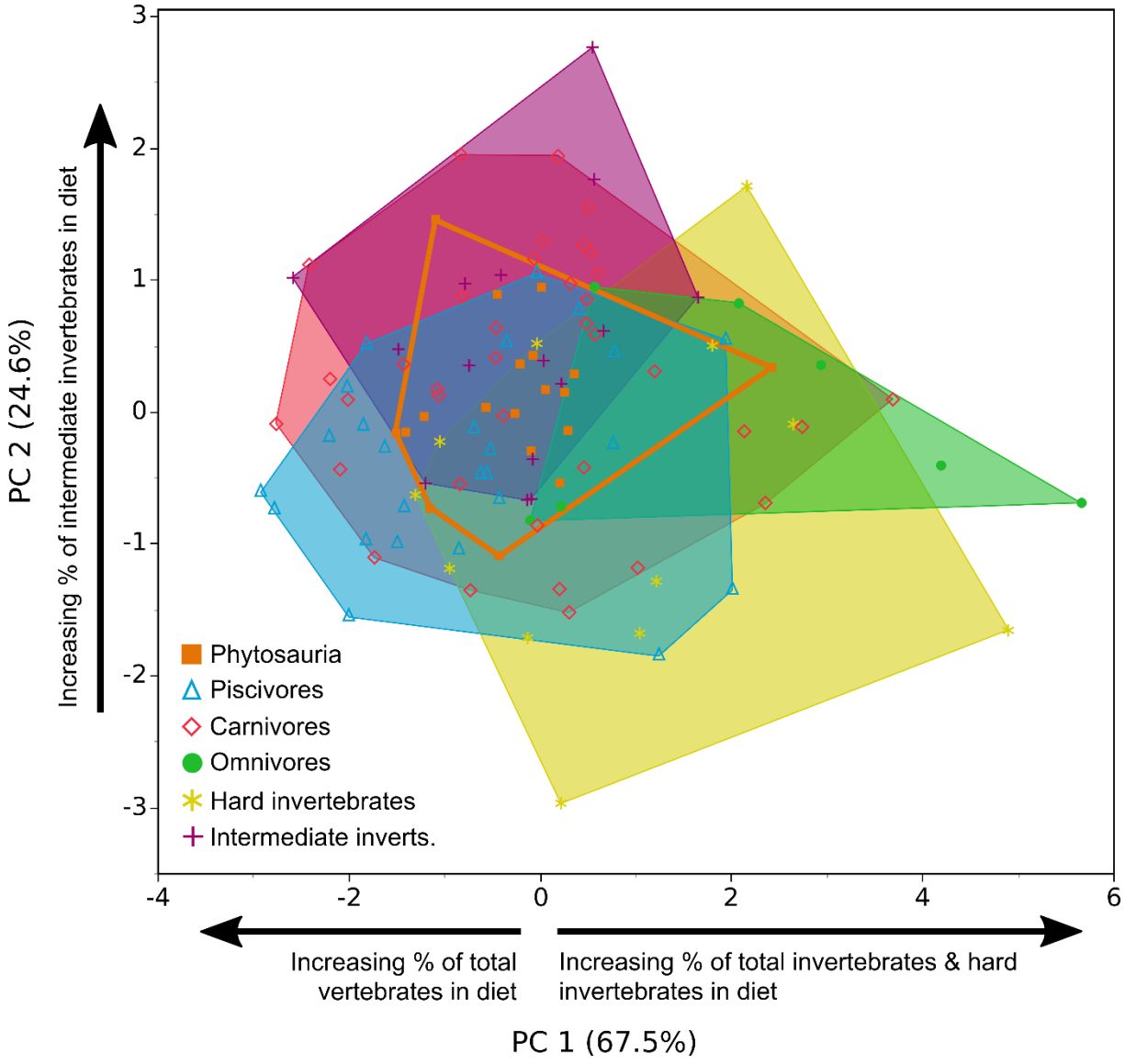

Figure 4.7: PCA of crocodylians and varanids, with phytosaurs projected into the dietary space. PCA constructed with the four significant parameters associated with dietary guild (Sds, Vmp, Spk, Smr1). Convex hulls represent different dietary guilds, plus Phytosauria. Aspects of dietary composition significantly correlated with PC axes are shown with arrows.

The CVA predictive model was found to be highly unreliable – misclassifying 65.6% of cases in the crocodylian+varanid training dataset, therefore whilst it is adequate for achieving statistical separation of groups in multivariate space, the model fails as a robust and consistent predictor of dietary guild in phytosaurs. In this model, 26.3% of phytosaurs were classified as intermediate-invertebrate eaters, 10.5% as hard-invertebrate eaters, 5.3% as omnivores, 31.6% as carnivores and 26.3% as piscivores.

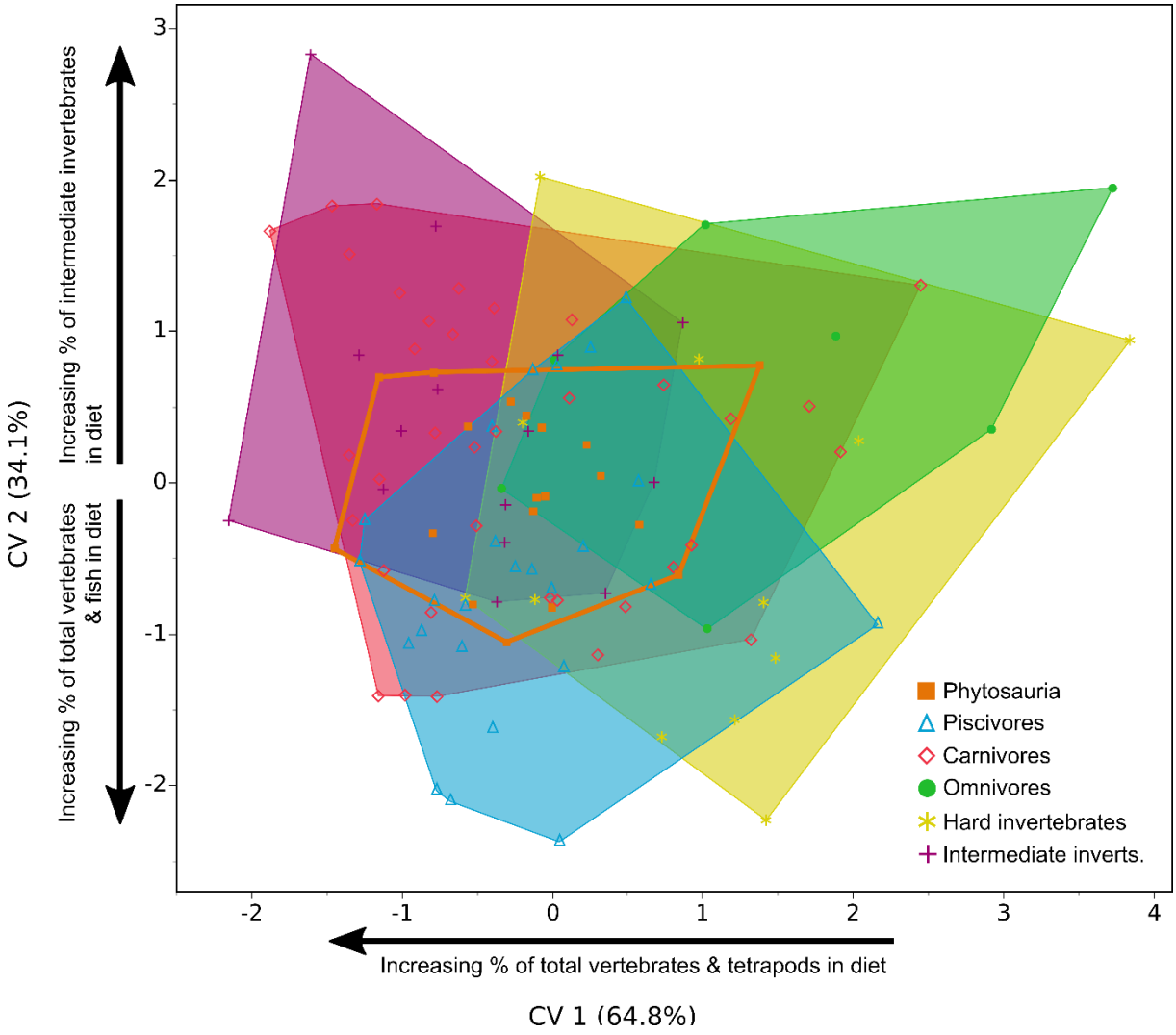

Figure 4.8: CVA of crocodylians and varanids, grouped by dietary guild, with phytosaurs projected into dietary space. CVA constructed with the four significant parameters associated with dietary guild (Sds, Vmp, Spk, Smr1).

4.3.3.3. *CVA by 'dietary guild' using all textural parameters*

The predictive model was improved by the addition of all ISO parameters to the CVA, on top of the original four significant parameters for dietary guild; misclassification was reduced to 42.7% of cases, so remains non-robust. The first three CV axes in this analysis were found to present significant differences between dietary guilds (CV 1: [Welch's ANOVA] F=7.88, P=<0.0001, Wilks' Lambda=0.25, P=0.0151; CV 2: F=8.66, P=<0.0001, Wilks' Lambda=0.53, P=0.7694; CV 3: [Welch's ANOVA] F=5.12, P=0.0012, Wilks' Lambda=0.78, P=0.9896). Tukey HSD significant pairwise differences are presented in Table S3.5. In CVs 2 and 3 only a small quantity of variance was not associated with the separation of dietary groups, but the association between these axes and the discrimination of groups was not significant.

All three axes correlated significantly with aspects of dietary composition (Figures 4.9 and 4.10; significance scores are summarised in Table S3.6). Under this model phytosaurs were classified as: 21.1% intermediate-invertebrate eaters, 15.8% hard-invertebrate eaters, 5.3% omnivorous, 5.3% carnivorous, and 52.6% piscivorous (Table S3.7). In these results, there is a clear favouring of piscivory among the reconstructions of phytosaur dietary guild; the relative proportions of the guilds are similar to the previous model aside from a drop in the proportion of carnivorous estimates and a rise in piscivory. Additionally, phytosaurs are found to be statistically separated from carnivores along CV 3; this result is surprising, as is the wide variation of the carnivorous group, which spans areas of the CV axis corresponding to high proportions of vertebrates in diet, and areas corresponding to high proportions of invertebrates in diet. It is worth considering whether the addition of varanids, which occupy an entirely different ecological niche to crocodylians and phytosaurs (i.e. terrestrial, rather than semi-aquatic) may have resulted in a combined 'carnivores' group that is incompatible

with the crocodylian-only ‘piscivores’ group (the only other group along CV 3 to be distinct from carnivores aside from Phytosauria).

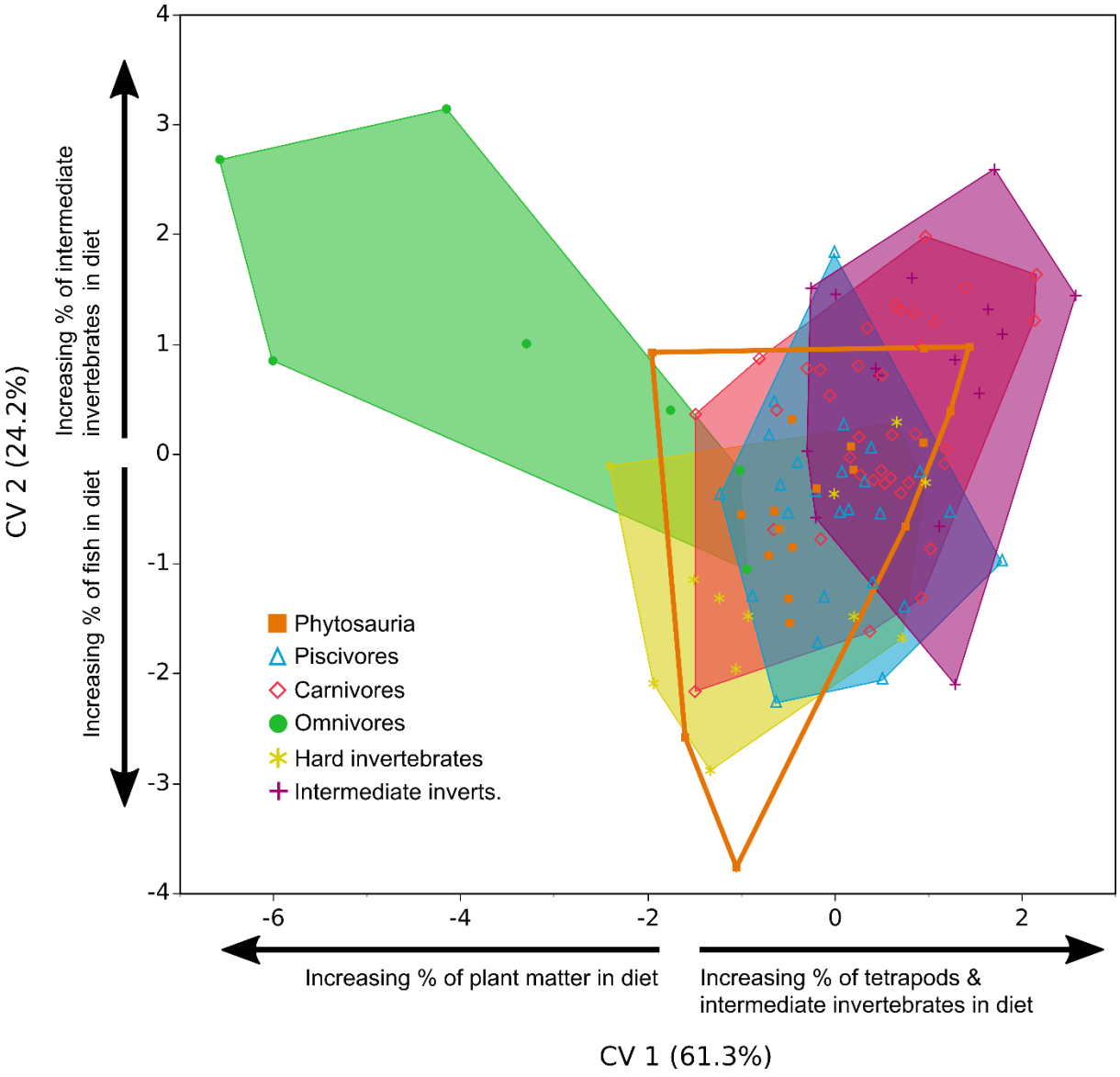

Figure 4.9: CVA of crocodylians and varanids, grouped by dietary guild, with phytosaurs projected into dietary space. CVA constructed with all 21 textural parameters.

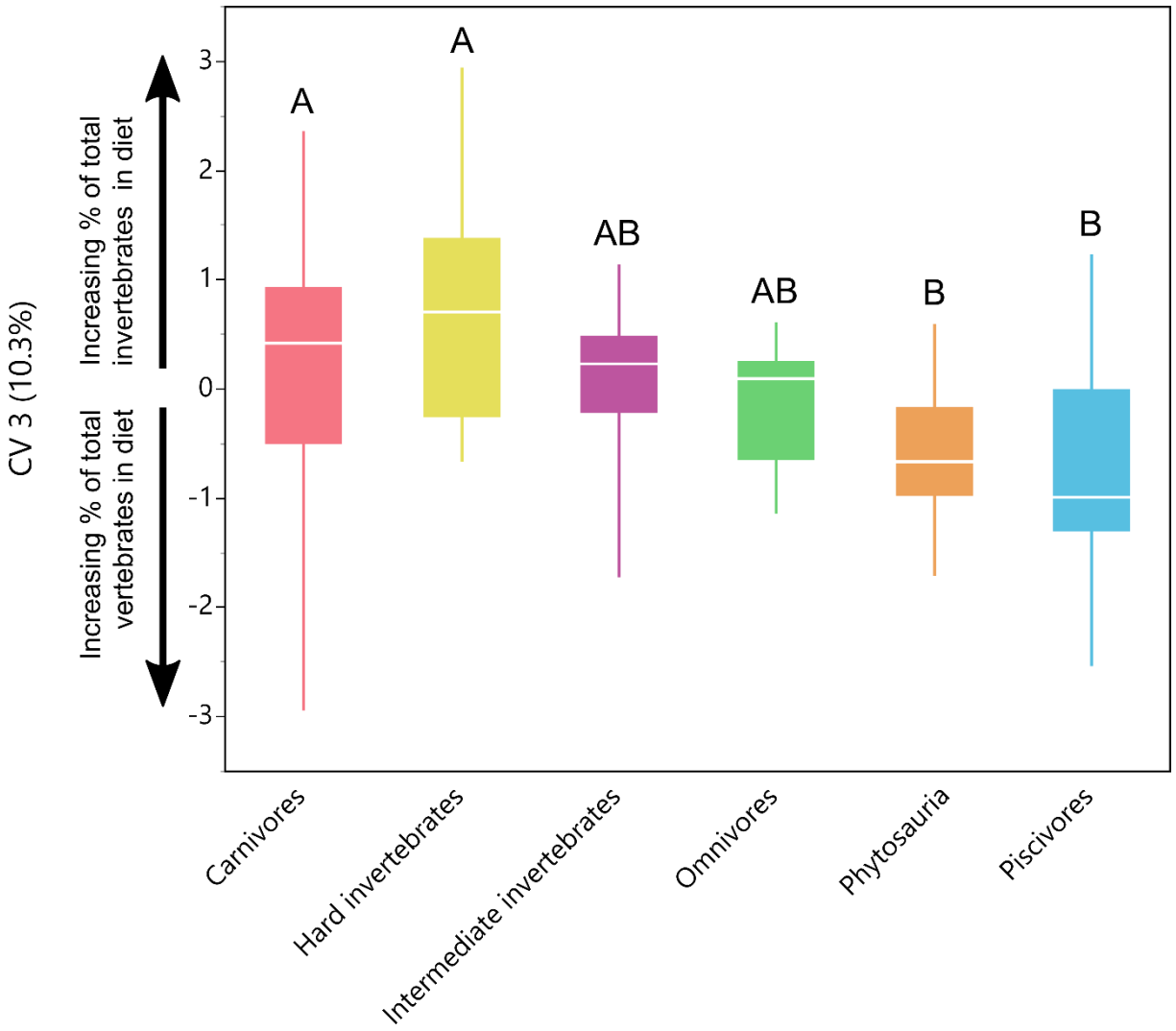

Figure 4.10: Boxplot showing the variance and separation of dietary guilds along CV 3. CVA is the same as that in Figure 4.9.

4.3.3.4. *CVA of 'dietary guild' with all ISO parameters, excluding varanids*

The original aim of comparing phytosaurs to only crocodylians was to provide the closest extant analogue with known dietary information; crocodylians were chosen due to both their striking morphological similarity to phytosaurs and their occupation of semi-aquatic environments. Varanids were originally excluded when searching for significant ISO parameters related to diet (section 4.3.3.1.) but were re-included because no significant ISO

parameters associated with dietary guild were found among crocodylians alone (section 4.3.3.1.); however subsequent analyses displayed unsatisfactory levels of variability within certain dietary groups (e.g. carnivores [Figure 4.10]) and poor robusticity of classification models (sections 4.3.3.2. & 4.3.3.3.). In this section varanids were re-excluded from analysis, but all ISO parameters were included, prompted by their improvement to the classification model.

Both CV axes produced by the analysis allowed significant separation of dietary guilds (CV 1: F=19.27, P=<0.0001, Wilks' Lambda=0.25, P=0.5872; CV 2: F=2.86, P=0.0313, Wilks' Lambda=0.78, P=0.9963); however, only CV 1 displayed significant pairwise differences in Tukey HSD tests (Table S3.8). Although the vast majority of variation in both CV axes apparently contributes to the separation of dietary guilds, this result is non-significant. CV 1 was found to correlate significantly with dietary composition; CV 2 showed strong correlations with multiple aspects of dietary composition in crocodylians, despite displaying no significant differences associated with dietary guild (Figure 4.11, Table S3.9).

Despite relatively poor performance in the separation of dietary guilds in dietary space, this model again improved on those above, misclassifying 27.9% of cases in the crocodylian dataset. Phytosaurs were classified as: 15.8% intermediate-invertebrate eaters, 26.3% carnivores, and 57.9% piscivores (Table S3.10). This further corroborates the findings of the above CVAs, in that there is a prevalence for predicting phytosaurs as piscivorous within both the varanid+crocodylian, and crocodylian only datasets. The consistency of this finding also suggests that the presence/absence of varanids in the dataset did not strongly affect predictions of dietary guild for phytosaurs, but did increase the proportion of mis-classifications. The alternative dietary guild predictions for phytosaurs (i.e. the secondary and occasionally tertiary predictions that occurred with lower frequency than the primary

classification) are also highly suggestive of piscivory or carnivory, constituting 38.1% and 42.9% respectively of all alternative predictions. In contrast, the hard-invertebrate eaters guild was only an alternative prediction in 19.0% of phytosaur cases (Table S3.10).

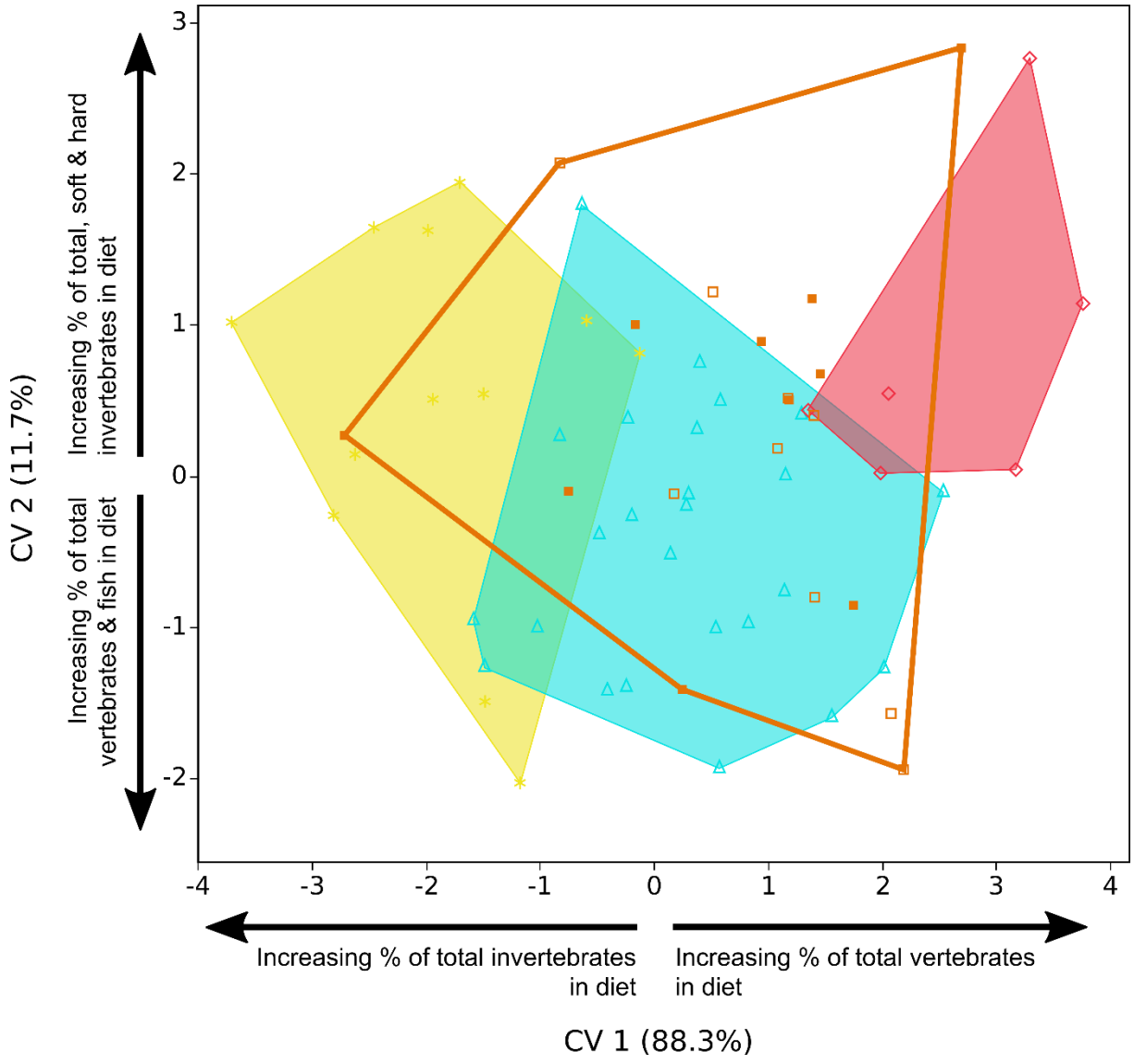

Figure 4.11: CVA of crocodylians only, grouped by dietary guild, with phytosaurs projected into dietary space. Yellow = hard-invertebrate eaters, blue = piscivores, red = carnivores, orange outline = Phytosauria. CVA constructed with all 21 textural parameters.

4.3.4. *Interspecific differences*

Although all species in the previous section were grouped into a number of 'dietary guilds', to summarise the most characteristic component of their diets, it should be remembered that each species exhibits a unique dietary composition, which may be a more biologically accurate grouping factor. Here, species grouping of the crocodylian dataset is used to create a less simplified multivariate space that may better reflect reality.

4.3.4.1. *Significant ISO parameters*

When grouped by species, 12 ISO parameters were found that significantly separated species groups (Sq: F=5.38, P=0.0005; Sdr: [Welch's ANOVA] F=6.24, P=0.0021; Vmp: F=6.11, P=0.0002; Vmc [Welch's ANOVA] F=5.49, P=0.0043; Vvc: [Welch's ANOVA] F=5.06, P=0.0059; Vvv: F=2.87, P=0.0217; Spk: F=5.65, P=0.0003; Sk: [Welch's ANOVA] F=6.76, P=0.0016; Svk: F=2.73, P=0.0274; Smr1: F=5.68, P=0.0003; Smr2: F=3.64, P=0.0063; Sa: F=5.39, P=0.0005).

4.3.4.2. *PCA and CVA using 12 significant ISO parameters for species*

When subjected to PCA the first two PC axes significantly separated species in multivariate space (PC 1: F=5.75, P=<0.0001; PC 2: F=2.91, P=0.0091); CVA on the 12 significant textural parameters resulted in the first two CV axes splitting species groups significantly in multivariate space (CV 1: F=11.19, P=<0.0001, Wilks' Lambda=0.07, P=<0.1539; CV 2: F=3.94, P= 0.001, Wilks' Lambda=0.25, P= 0.8317) (significant Tukey HSD scores are summarised in Table S3.11). Despite the majority of variation in both CVs apparently

contributing to the separation of species groups, they are not significantly associated with group separation. Neither of the significant PC axes correlated significantly with dietary composition; only CV 1 correlated significantly with dietary composition (Figure 4.12, Table S3.12). The predictive CVA model mis-classified 37.2% of cases in the crocodylian training dataset.

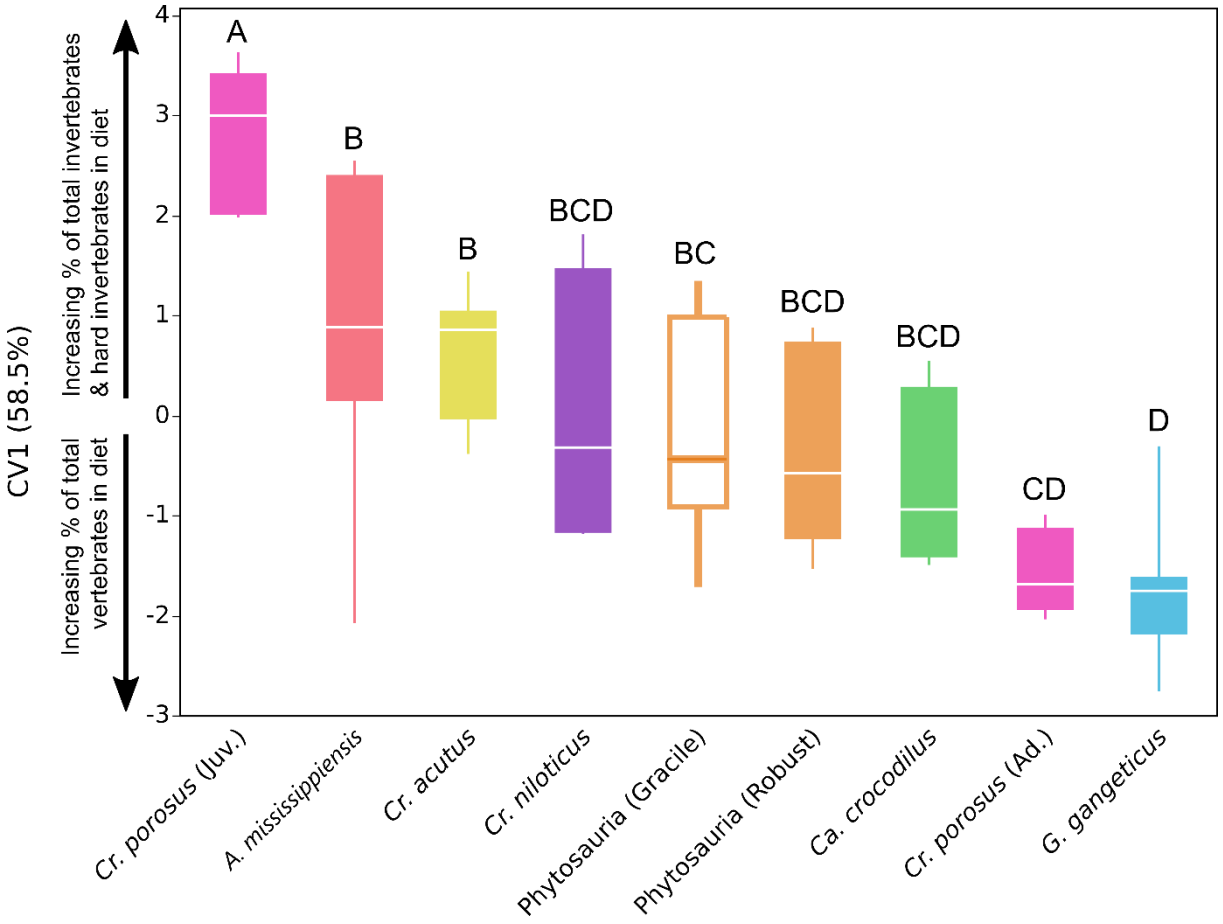

Figure 4.12: Variation and separation of species groups along CV 1. CVA was constructed with crocodylians only, grouped by species, with phytosaurs subsequently projected in. Twelve textural parameters that significantly differed between species were used to construct the CVA (Sq, Sdr, Vmp, Vmc, Vvc, Vvv, Spk, Sk, Svk, Smr1, Smr2, Sa). Non-overlapping letters indicate significant differences.

4.3.4.3. *CVA by species, using all ISO parameters*

When constructed with all textural parameters, the first four CV axes produced significant separation of species groups (CV 1: [Welch's ANOVA] F=14.16, P=<0.0001, Wilks' Lambda=0.006, P=0.2455; CV 2: F=14.54, P=<0.0001, Wilks' Lambda=0.03, P=0.7546; CV 3: F=4.41, P=0.0004, Wilks' Lambda=0.14, P=0.9811; CV 4: F=3.55, P=0.0023, Wilks' Lambda=0.35, P=0.9983), although again Wilks' Lambda suggests that the contributions of these axes to group separation is non-significant.

Only CV axes 2, 3 and 4 correlated significantly with dietary composition (Table S3.13, Figure 4.13); however, CV 3 is not figured here as its only significant correlation is with percentage of plant matter in diet, which is here assumed to be of less importance in phytosaurs due to cranial and tooth morphology. In support of this, on this axis (CV 3) phytosaurs are found to occupy a significantly different position in multivariate space to *Caiman crocodilus* – the only crocodylian taxon in this study with a substantial proportion of plant matter in its diet (18%).

The CVA by species predictive model, including all textural parameters, improves the accuracy of classifications, with only 23.3% of cases mis-classified. As CV 1 does not correlate with diet, only 49.4% of microwear variation separating croc species is actually attributable to diet. Therefore, approximately half of the predictive model is not based on diet, and as such predictions for phytosaurs may be inaccurate. Here phytosaurs are classified as being most similar to: 47.4% *Crocodylus niloticus*, 21.1% *Alligator mississippiensis*, 15.8% *Gavialis gangeticus*, 10.5% *Crocodylus porosus* Adult, and 5.3% *Crocodylus porosus* Juvenile. This is broadly consistent with the observed distribution of species in Figure 4.13, in that phytosaurs predominantly overlap with the ranges of *Crocodylus niloticus*, *Alligator*

misissippiensis, *Gavialis gangeticus* and *Crocodylus porosus* Adult, whilst generally being distinct from the others. This interpretation is also supported by ANOVA results from CVs 2 and 3; however, CV 4 deviates from this (Table S3.14).

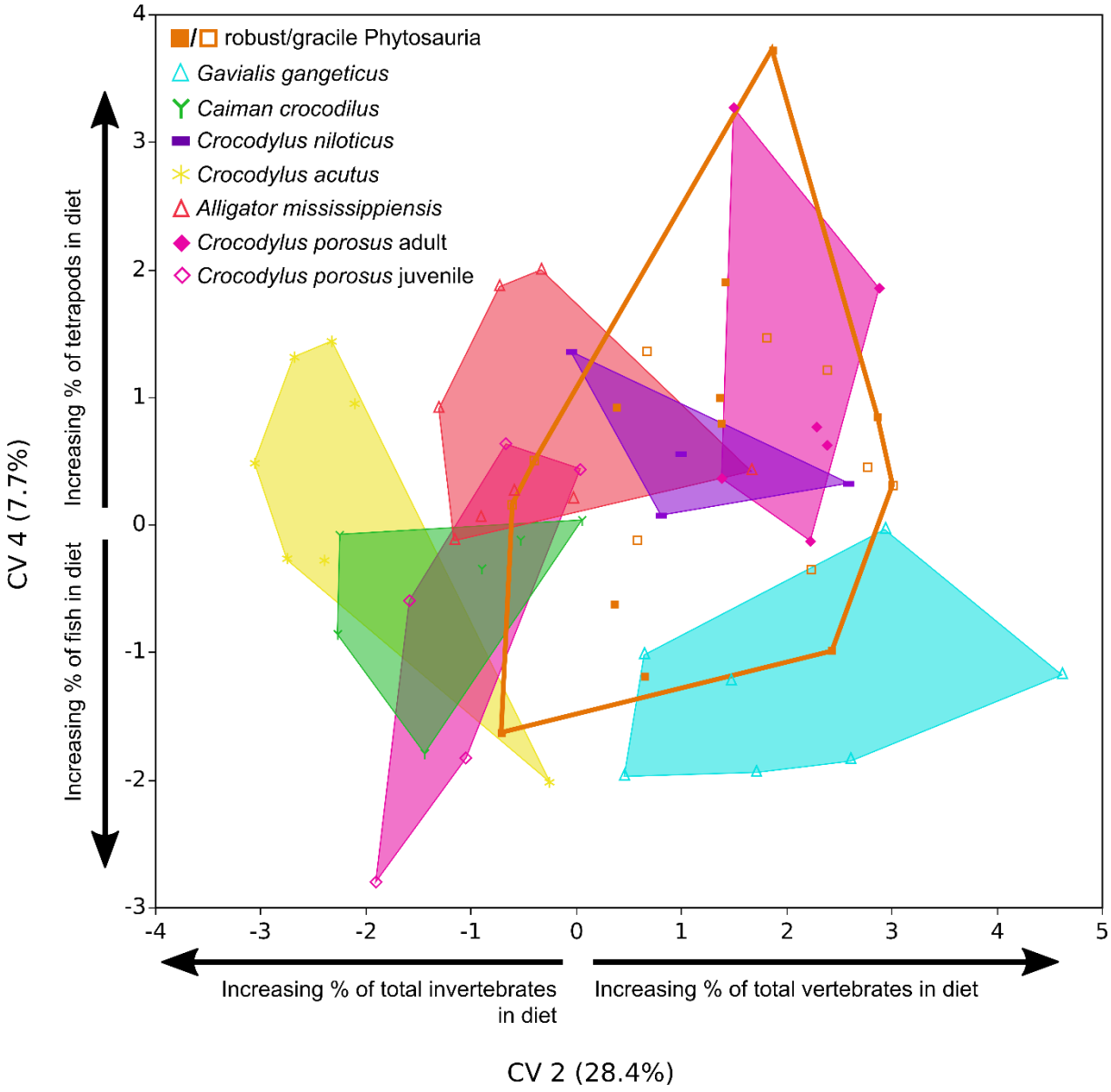

Figure 4.13: CVA of crocodylians only, grouped by species, with phytosaurs projected into dietary space. CVA constructed with all 21 textural parameters.

Phytosaurs are significantly distinct from gharials along the axis predominantly associated with an increased proportion of fish in diet, whilst remaining non-distinct from *Crocodylus porosus* Adult and *Crocodylus niloticus*, and partially *Alligator mississippiensis*; this may suggest that phytosaurs possessed a dietary composition more similar to crocodiles and partially alligators than gharials; however, they are more similar to gharials than taxa with more invertebrate-based diets.

4.4. *Discussion*

4.4.1. *Intra tooth-row functional partitioning*

In his investigation into heterodonty in *Nicrosaurus kapffi*, Hungerbühler (2000) hypothesised a number of functional explanations for the presence of differing tooth morphologies along the phytosaurian tooth row. The analysis presented here investigates an alternative explanation: that heterodonty in phytosaurs was optimised to allow the processing of prey items of differing material properties at each morphologically different region of phytosaur dentition. No evidence is found here in support of tooth-row partitioning for processing different materials; no textural parameters were found to significantly differ among the tooth position categories, and no correlation with extant crocodylian diet was found to be associated with CVA axes of maximum separation.

Although the separation of specimens by tooth row position found here (Figure 4.3) is not associated with diet, the functional hypotheses of Hungerbühler (2000) should not be discounted as an explanation. The large, anteriormost teeth in phytosaurs were hypothesised to have facilitated the seizing and holding of prey items, with their size and resistance to

transverse stresses allowing a forceful killing strike in smaller prey and inflicting considerable damage to larger targets (Hungerbühler, 2000). This would be aided by the presence of denticulate carinae on the anterior teeth, which have been demonstrated to aid in puncturing, slicing and gripping (Frazzetta, 1988; Abler, 1992), and aiding crack propagation in harder materials (Purslow, 1991; Evans & Sanson, 1998). As noted by Hungerbühler (2000), the mid tooth-row dentition forms a cage-like structure due to the lingual curvature of the dental apices, which may have aided the capture of small prey individuals, as is further supported by the presence of infrequent serrations to aid grip, not in continuous orientation with the tooth row. The more posterior maxillary teeth benefitted from increased mechanical advantage, and thus per tooth bite-force, due to their posterior location (Greaves, 1995). In addition to their stout shape, and prominent denticulated antero-posteriorly oriented carinae, these teeth formed a relatively continuous cutting surface in comparison to the other areas of the tooth row, which in combination with the similar posterior teeth of the dentary implies these teeth were adapted to increase the efficiency of food processing (Hungerbühler, 2000). Although the quadrate and glenoid of phytosaurs would not have allowed antero-posterior 'sawing' jaw-motion, Hungerbühler hypothesised that phytosaurs may have employed a scissor-like motion similar to herbivorous iguanids of similar dental morphology (Throckmorton, 1976), or a head-shaking technique similar to carcharhinid sharks in which a continuous row of serrated triangular teeth allows passive cutting due to movements of the food material, rather than the jaw. The former technique in *Uromastix* may involve movement of the quadrate to allow a more 'sawing' shear motion (Throckmorton, 1976), that would not have been possible in phytosaurs due to a lack of cranial kinesis. The latter technique was also proposed in tyrannosaurs (Farlow & Brinkman, 1994) with which the posterior maxillary teeth of phytosaurs share a similar morphology (Hungerbühler, 2000).

These functional hypotheses are not disproven by the results of microwear analysis, but the microwear does not particularly support the hypotheses either. The textural parameters that covaried most strongly with the axis of separation between anterior and posterior teeth (CV 2, Figure 4.14) were:

Sq: Quadratic average of height for the overall textural surface,

Sz: Sum of the highest and lowest point on the surface,

Vvv: Volume of empty space in the material ratio curve, beneath the upper delimitation point for 'dale' features,

Vmp: Volume of the material surface composed of 'peaks'.

The average values of these parameters are essentially homogenous with respect to tooth position, showing no significant differences between position groups as previously mentioned; however, along the axis of separation of anterior to posterior tooth position (CV 2), the more anterior teeth are characterised by a greater volume of peak and dale material and a greater sum of the extremes of height across the surface. The posterior teeth possess a greater quadratic average of height and greater extremes of height. These attributes could be interpreted to mean that anterior teeth are generally rougher in texture with many peaks and pits/scratches, whereas posterior teeth are of a more consistent texture with only a few extremely high or low points (see Figure 4.15 for representative tooth surface textures).

Under the assumption that anterior teeth were used in an opportunistic manner primarily for the initial seizing of prey with considerable and sudden force (due to the increase in speed achieved with distance from the lever fulcrum and increased momentum – the terminal rosette being a weight at the distal end of a lever), a rougher surface would be expected. A forceful impact, potentially with a hard integumentary material, e.g.

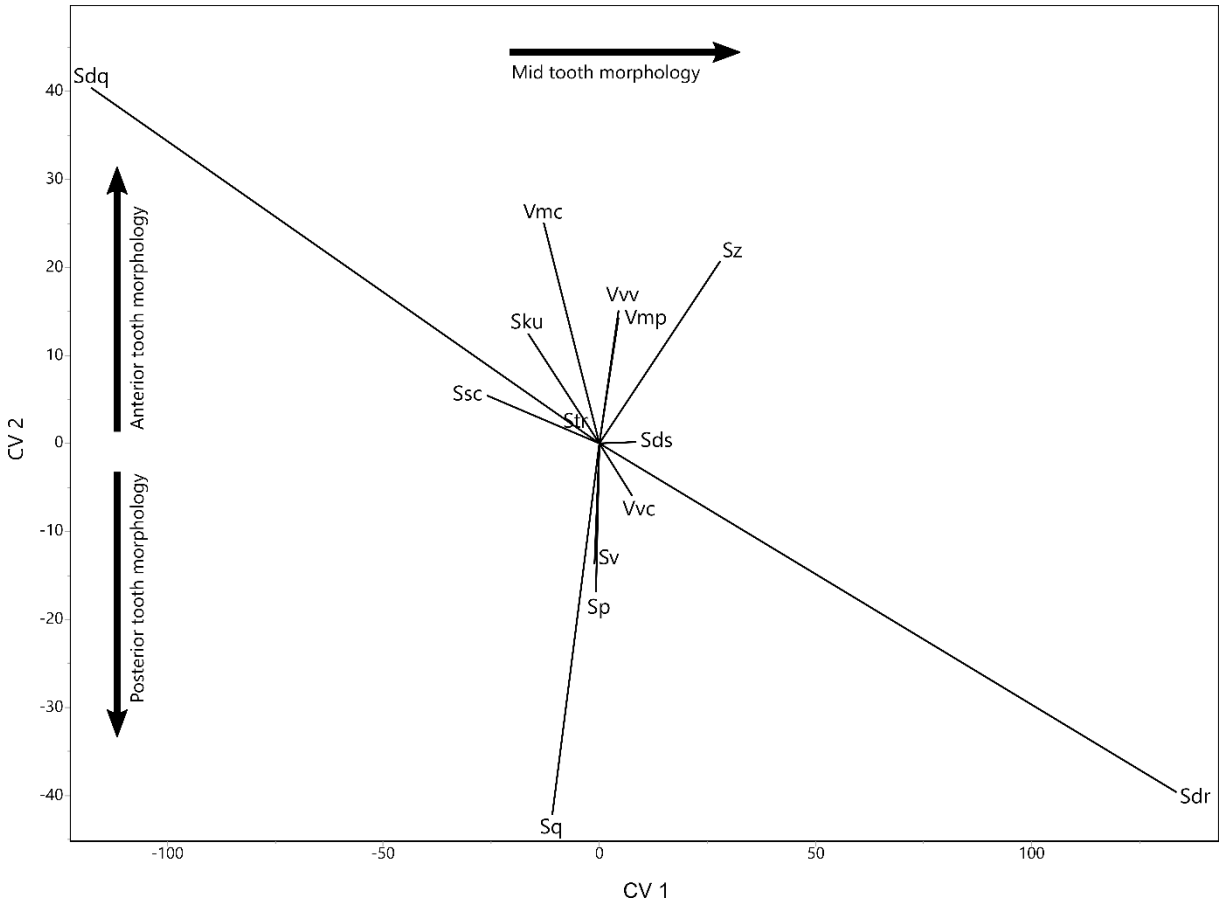

Figure 4.14: CVA biplot corresponding to Figure 4.3, indicating the magnitude of each textural parameter on the CV axes defining maximum separation of tooth position. Rays of the biplot also display the direction of maximum variation for each parameter with respect to both CV axes.

scales/osteoderms (and given the apico-basal length, potentially hard internal structures), is likely to cause greater enamel chipping (Constantino *et al*., 2010) and deeper texture on the enamel surface; due to the use of anterior teeth only in the initial capture, it seems unlikely that sufficient extended abrasion would occur to remove peak material (Blateyron, 2013) before the tooth was shed – therefore a rough surface seems likely. The surface of the posterior teeth would be unlikely to experience the type of sudden impact hypothesised in the anterior teeth due to being further from the initial point of contact – rather the bite would (according to lever mechanics) be slower and more forceful. If a head-shaking or scissor-like

technique was employed to reduce the size of large food items, the resulting microwear would likely be more homogenous due to the comparatively extended time spent performing an abrasive motion with the material in question. This is consistent with the findings of reduced Vmp values in posterior teeth, which is indicative of less peak material potentially due to extended abrasion (Blateyron, 2013) which would allow wear surfaces to become more uniform (especially given the random motion likely produced by a head shaking scenario). The formation of relatively smooth microwear would be aided further in a head-shaking scenario, due to being presumably embedded in soft, less abrasive tissue and posterior teeth being considerably apico-basally shorter than anterior teeth, rather than the repeated initial puncturing of external integument.

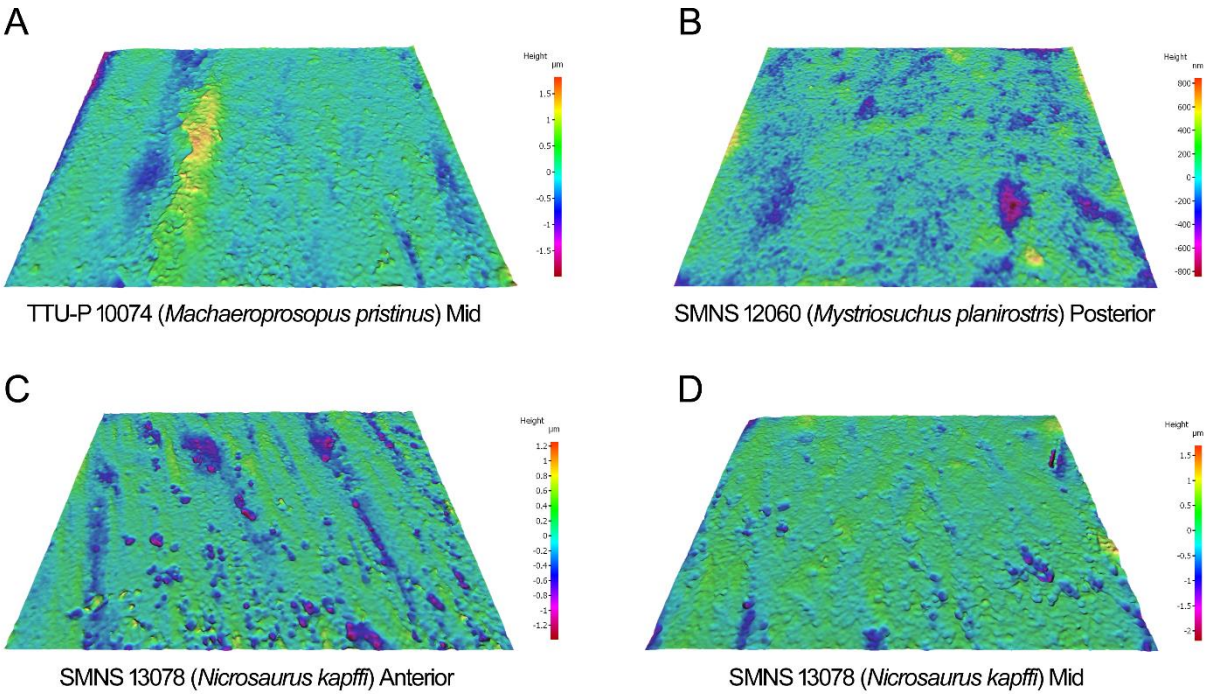

Figure 4.15: Examples of microwear surface textures in gracile (A, B) and robust (C, D) phytosaur taxa. In A, C & D the scale for surface topology is presented in micrometres; in B the scale is in nanometres due to a considerably smoother texture.

The investigation of dental microwear prior to the advent of 3D surface textural analysis included the counting, classification and directional scoring of pits and scratches on dental surfaces (e.g. Williams *et al.* [2009]). As much of the inferences above depend on the presence or absence of forceful directional movement, an analysis into the common directionality of microwear (accepting that the technique may be inapplicable in cases of uniform – non-directional wear [Purnell *et al*., 2012]) may assist in clarifying the above functional hypotheses.

An unrelated, but important practical implication of the dissociation of diet and tooth position is that it validates the pooling of all phytosaur tooth positions in the other analyses. This precludes the necessity for groups such as 'robust phytosaur, anterior tooth', 'gracile phytosaur, mid tooth' etc. and allows analysis groups to contain larger sample sizes, thus being more representative of the whole phytosaur sample within robust statistical testing.

4.4.2. *Dietary partitioning by robusticity*

The question of whether cranial morphology is associated with diet has been previously investigated in crocodylians, in comparison with odontocetes – finding a distinct separation in cranial morphospace between piscivorous taxa and taxa feeding on larger prey, associated with robusticity and the development of a U-shaped cranial cross-section (McCurry *et al.*, 2017a). Significant relationships were also reported between cranial morphology and diet – specifically associated with an increase in rostral, and mandibular symphysis, length in piscivorous taxa (McCurry *et al.*, 2017a). Robust and gracile phytosaurs possess morphological variation consistent with the above, and as such were hypothesised here to fall into two distinct groups, separated by dietary correlated axes of microwear. Significant

separation was achieved in all PCA and CVA tests, though none of the significant axes were correlated with diet.

In addition to diet, robusticity-related cranial morphology has been found to be significantly associated with prey size (Metzger & Herrel, 2005; McCurry *et al*., 2017b), which provides an alternative hypothesis to explain the separation of my data in the absence of a clear dietary association. Robust, rostrally crested phytosaurs are better adapted to accommodate increased dorsoventral bending moments associated with higher bite-forces, and based on osteological fossil evidence (Drumheller *et al.*, 2014) and the conventions of extant taxa, are likely to have targeted larger prey items (Metzger & Herrel, 2005; McCurry *et al*., 2017b). The large, hard parts present in larger prey items are more resistant to dental processing than the small, hard parts in smaller prey items; forceful processing of hard material near an occlusional edge produces chipping of the enamel surface (Chai & Lawn, 2007; Chai *et al*., 2011) rather than the micrometre scale plastic deformation caused by small, hard objects (Lucas *et al.*, 2008). Additionally, the extra force required to process larger, more resistant prey items, and the likely higher force produced by more robust taxa, has been shown to increase the rate at which microwear is formed (Ranjitkar *et al*., 2008), whilst also being associated with higher quantities of chipping (Constantino *et al*., 2010). The thick and columnar enamel apparently present generally in phytosaurs has been inferred as evidence for durophagy (Heckert & Camp, 2007 [although evidence of how taxa were identified was not provided and the sample is small and likely non-representative of the whole group]), and would have allowed the processing of hard materials; however, less robust phytosaurs may have been poorly equipped to accommodate the cranial stresses of processing large, hard material (Lemanis, 2012). On this basis it seems likely that more robust taxa would produce a

‘rougher’, more irregular surface texture than more gracile taxa, simply due to force exerted and likely prey size, irrespective of dietary composition.

The five textural parameters that allow significant separation of robusticity categories are:

Sp: Greatest peak height,

Sz: Sum of highest and lowest points,

Sdq: Gradient of surface points,

Sdr: A measure of surface complexity,

S5z: Average height of the five most prominent peaks and dales.

In PCA (Figure 4.4) all five of these parameters were found to covary positively in the direction of increasing robusticity (Figure 4.16), which supports the above hypothesis of surface texture roughness/complexity in robust taxa. Additional analysis is, however, required in order to robustly test the effects of prey size on microwear in reptiles; therefore, no strict conclusions are drawn here regarding the exact cause of microwear separation by robusticity, but surface texture appearance seems at least consistent with the non-mutually-exclusive possibilities of prey size and bite force.

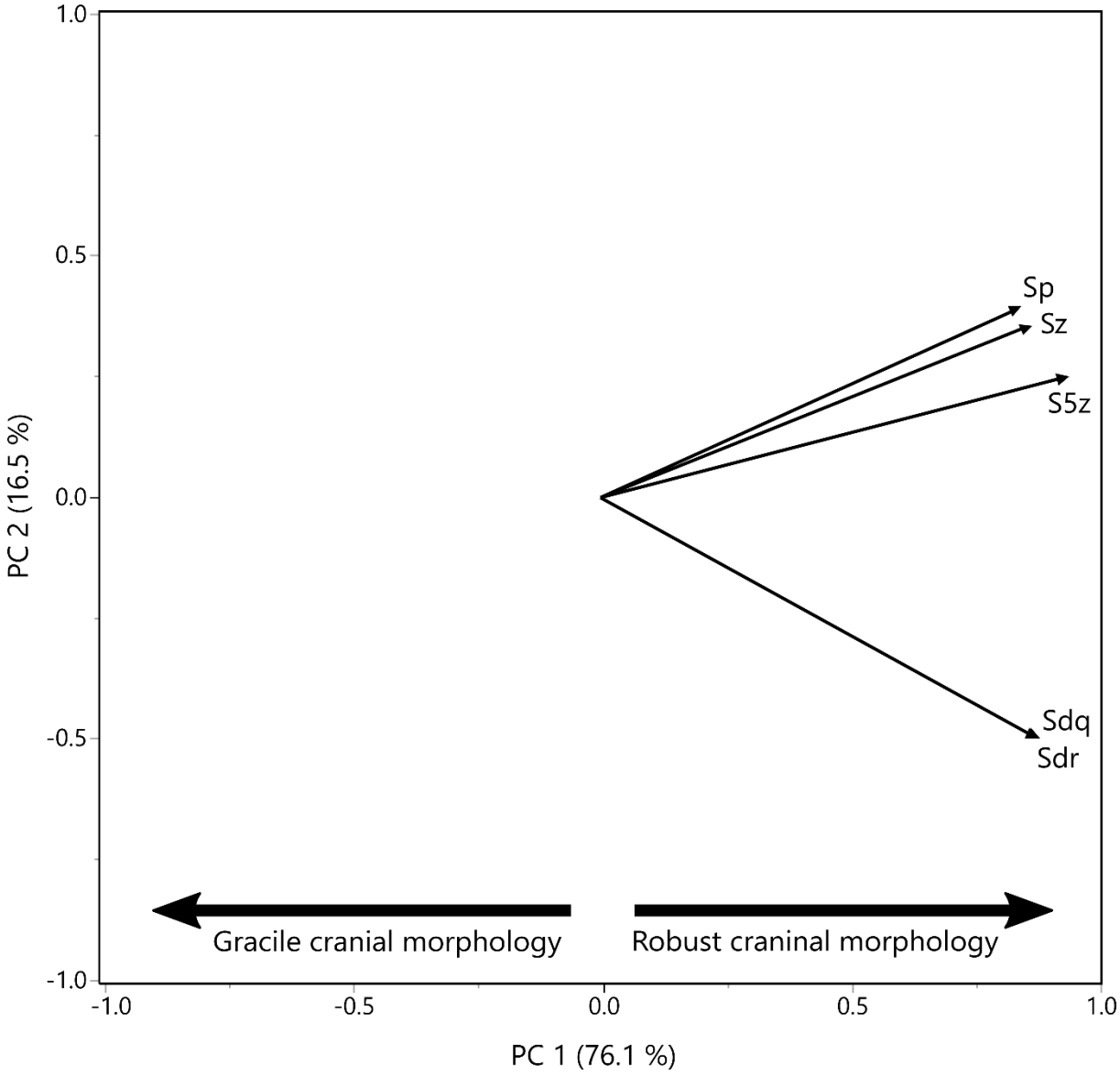

Figure 4.16: PCA biplot for Figure 4.4, showing the textural parameters that describe significant differences between cranial robusticity groups. Biplot rays display the magnitude and direction of variation within each parameter along the PC axes.

4.4.3. *Discrimination of phytosaur diet*

Almost every previous interpretation of phytosaur diet has been based on indirect evidence, and share generally similar assumptions. Parrish (1989) for example, interpreted gracile phytosaurs as most likely to target smaller prey, likely fish, due to the presence of “elongate,

narrow snouts", and robust phytosaurs to feed on larger aquatic prey based on the presence of "broader, less attenuate snouts", possession of a "more heterodont dentition", and "apparent greater absolute size of the adults" (Parrish, 1989 [p238]). Heckert *et al.* (2013) inferred piscivory in more gracile taxa based on non-vertical orientation of tooth crowns/splayed out teeth – inferring a holding/gripping function, similarly to Hungerbühler (2000). As previously mentioned, Hunt (1989) inferred phytosaur ecology based on cranial morphological comparison with extant crocodylian taxa, and erected three phytosaurian 'ecomorphs' based on these comparisons (discussed in Chapter 3). As noted by previous authors (Hungerbühler, 1998b; Stocker & Butler, 2013) this simplified view is not entirely supported by phytosaur stomach contents, wherein three slender-snouted phytosaurs retained temnospondyl, 'prolacertiform' and rhynchosaur remains, and a short-snouted phytosaur preserved fish vertebrae in its gut contents (Chatterjee, 1978; Li *et al.*, 2012; Stocker *et al.*, 2017). More recently, it was noted by Drumheller *et al.* (2014) that narrow, gracile snouts in extant crocodylian taxa do not necessarily equate to obligate piscivory, with taxa such as *Tomistoma schlegelii* and *Crocodylus johnstoni* incorporating tetrapods such as turtles, birds and amphibians, and invertebrates; therefore, conclusions drawn from comparative morphology of crocodylians and phytosaurs should be tentative. This is also the case in the crocodylian dietary composition dataset of Bestwick *et al.* (in prep.); although *Alligator mississippiensis* is categorised as piscivorous, its diet is comprised of 35.8% tetrapods, similarly the diet of the 'carnivorous' *Crocodylus porosus* (adult) is comprised of 34.3% invertebrate material, *Caiman crocodilus* exhibits seasonal piscivory/invertebrate preference but also incorporates 18% plant matter into its diet. Even *Gavialis gangeticus*, which is the usual extant analogue for any hypothetically piscivorous longirostrine extinct taxon, includes tetrapods as 10% of its diet.

The analyses undertaken here used direct evidence of diet, rather than comparative cranial or postcranial morphology. Other studies providing direct dietary evidence for Phytosauria are rare, and (being based on individual feeding occurrences) only provide a temporal snapshot of phytosaur diet (Chatterjee, 1978; Hunt, 1991, Li *et al.*, 2012; Drumheller *et al.*, 2014; Stocker *et al*., 2017). Despite this, my microwear results are entirely congruent with these rare 'gut snapshots', and alongside previous general hypotheses of phytosaur diet, suggest that phytosaur dietary regime consisted predominantly of piscivory and carnivory (Figure 4.11, Table S3.10). I find no significant evidence in support of dietary partitioning between gracile and robust taxa – instead supporting the suggestions of some previous studies (Hungerbühler, 1998b; Stocker & Butler, 2013; Drumheller *et al.*, 2014) that, similarly to extant taxa phytosaur diet was genuinely varied, and that dietary compositions of different phytosaur morphologies would be more complex than is morphologically apparent, as is also indicated by preserved gut contents. Based on the multivariate space occupied by Phytosauria, a reasonable conclusion to draw is that phytosaurs were dietary generalists, and incorporated whatever material was available into their diet. For this reason, the predictions of the CVA model for phytosaur dietary guild (Table S3.10) should not be interpreted as independent categorical reconstructions, but should indicate that some specimens or taxa may indicate a greater proportion of piscivory or carnivory in their diet, with respect to other samples. For example, gracile taxa within the phytosaur dataset have a greater prevalence for being classed as piscivorous (~66%); each gracile taxon (*Machaeroprosopus pristinus*, *Nicrosaurus meyeri*, *Mystriosuchus planirostris*) is composed of three samples – within each species, two of three samples were diagnosed as piscivorous. Conversely, in the six samples pertaining to the robust taxon *Nicrosaurus kapffi*, a carnivorous reconstruction is slightly favoured, being found in three samples (50%) (piscivory in two [~33%], hard invertebrates in

one [~17%]). Surprisingly, in the robust taxon '*Smilosuchus lithodendrorum*' piscivory was reconstructed with greater frequency than carnivory (75%). Again, this supports the conclusion that dietary composition in phytosaurs is likely to be similar to that of extant crocodylians; however, the diet of extant crocodylians is more complex than is often assumed in comparative palaeontological studies.

Regarding the hypotheses of extant phytosaur analogues erected by Hunt (1989), there is, again, no separation between robust and gracile phytosaurs when crocodylian dietary space is devolved to the species-level (Figure 4.12, 4.13). No examples of 'moderate' phytosaur taxa were included in the microwear analyses, though it seems unlikely that this would change the results significantly. The most likely reason why no support is found for the ecomorphs of Hunt (1989) is that we now know that crocodylian, and likely phytosaur diet is much more variable than was perhaps assumed. Phytosaurs span a range of dietary space corresponding to multiple extant crocodylian taxa (Figure 4.13): *Gavialis gangeticus*, *Crocodylus porosus* (adult), *Crocodylus niloticus* and *Alligator mississippiensis*, suggesting a generalist ecology. Conversely, phytosaur specimens rarely overlap with taxa occupying an area of dietary space associated with a high proportion of invertebrates in diet: *Crocodylus porosus* (juvenile), *Crocodylus acutus* and *Caiman crocodilus*.

The presence of *Caiman crocodilus* in the lower left of Figure 4.13 is particularly interesting; this area of morphospace corresponds to an increased proportion of both fish and hard invertebrates in diet. *Ca. crocodilus* was classified into the piscivore dietary guild by Bestwick *et al*. (in prep.), although the diet of this species actually switches between consuming more fish during the wet season, and more hard invertebrates in the dry season (Laverty & Dobson, 2013). The decision of Bestwick *et al.* (in prep.) to classify *Ca. crocodilus* as a piscivore in their study was because all samples of this taxon were taken from

individuals that had died early in the dry season; it was therefore reasoned that the dietary signal of piscivory would remain from the wet season, due to the lower feeding frequency of reptiles (Andrade *et al.*, 2005). Here, by allowing taxa to be grouped by species rather than constraining *Ca. crocodilus* to the piscivorous group (in which dietary signal may be heavily influenced by more specialist piscivores like *Gavialis gangeticus*), it is observed that dietary signal from both the wet and dry season may have been retained, suggesting that this dental microwear technique may be sufficiently sensitive to allow the distinction not only of seasonal diet, but also the transitory period between seasons. This hypothesis is only tentative currently, and requires further investigation with better knowledge of the exact timings of dietary shift.

Throughout the analyses in which phytosaurs are compared with crocodylians, it is evident that the dietary signal of phytosaurs is more poorly constrained than that of crocodylians. An obvious reason for this is that every crocodylian multivariate space is constructed without the input of phytosaurs, which are only projected into the space after it has been constructed: thus, representing an artefact of the analysis technique. However, an alternative possibility relates to the rate at which teeth are replaced in Phytosauria compared to extant crocodylians. It was observed by Heckert & Camp (2007) that the lines of incremental growth in the enamel of phytosaurs corresponded to a shorter period of growth and greater rate of tooth replacement than was observed in the pseudosuchian archosaurs *Revueltosaurus callenderi* and '*Krzyzanowskisaurus hunti*' (=*Revueltosaurus hunti*). The exact rate of tooth replacement is unknown for phytosaurs; however, if greater than extant crocodylians it would result in the accumulation of less microwear texture, and a weaker dietary signal in dietary space.

4.5. *Conclusions*

No evidence is found to support the hypothesis of intra-tooth-row partitioning of different materials in phytosaurs. The structure of dental microwear texture present in phytosaurs that does allow separation of teeth by position is relatively consistent with the hypothesis of functional partitioning of the tooth row; however, the actual differences in tooth texture are statistically very minor.

There was also no association observed between diet and phytosaur robusticity; a better explanation of the separation of these groups by microwear is that of prey size and associated increases in bite force of more robust individuals. These hypotheses are consistent with other avenues of research including enamel structure and thickness, and the relative resistance to biting stress in robust vs gracile phytosaurs; however very few studies have investigated these in relation to phytosaurs, particularly phytosaur enamel structure.

The diet of phytosaurs was reconstructed as a combination predominantly of piscivory and carnivory, in agreement with previous hypotheses, but also with a small proportion of hard invertebrate material. In contrast to most previous hypotheses of phytosaur diet, which assume independent categories of diet based on morphology, it is here assumed that dietary composition is a complex combination of multiple prey types in all taxa, as is actually the case in extant crocodylians, and represents a generalist ecology. There is very weak evidence that fish may have constituted a slightly greater proportion of diet in gracile phytosaurs; however, dietary reconstruction in robust taxa was entirely ambiguous between piscivory and carnivory.

Chapter 5: Conclusions

The phylogenetic analysis presented in Chapter 2 produced two sets of partially conflicting tree topologies, which together broadly support the phylogenetic hypotheses of previous authors (Hungerbühler & Sues, 2001; Hungerbühler, 2002; Parker & Irmis, 2006; Stocker, 2010, 2012, 2013; Hungerbühler *et al.*, 2013; Butler *et al.*, 2014; Kammerer *et al.*, 2015). Many relationships were consistent between all four phylogenetic trees produced: in particular, the taxonomic content of *Parasuchus,* positions of *Wannia scurriensis* and *Diandongosuchus fuyuanensis*, and the synonymy of '*Redondasaurus*' with *Machaeroprosopus* are all in agreement with previous studies (Hungerbühler *et al.*, 2013; Stocker, 2013; Butler *et al.*, 2014 and Stocker *et al.*, 2017). Strong support was also found for a sister relationship between *Rutiodon carolinensis* and *Angistorhinus*.

Current uncertainties were also highlighted, such as the position of *Mystriosuchus*, the monophyly of *Smilosuchus* and the position of *Protome batalaria*. The uncertain phylogenetic position of *Protome* has biostratigraphic implications, meaning that isolated 'leptosuchomorph-type' squamosals may no longer be indicative of non-Mystriosuchini phytosaurs; however, under current biostratigraphic hypotheses of the late Triassic of the western USA, the phylogenetic position of *Protome* is not necessarily problematic. The European genus *Nicrosaurus* was recovered in a less derived position than was previously hypothesised (Parker & Irmis, 2006; Kammerer *et al*., 2015), leading us to revise the definition and internal specifier taxa for Mystriosuchini.

Generally better nodal support and a greater influence on phylogenetic reconstruction was found by using continuous character scoring, rather than geometric morphometric (GM)

scoring. This is a positive result from a practical standpoint as continuous characters are comparatively easier to implement and suffer fewer drawbacks than GM characters. GM characters are hindered by the requirement of undistorted morphology, the potential increase in missing data through their use, difficulty in the interpretation of resulting synapomorphies and the requirement of high computational power/long analysis durations.

In contrast to Chapter 2, wherein geometric morphometrics was applied to phylogeny, in Chapter 3 the discrete character tree of Chapter 2 was applied to geometric morphometric analyses of phytosaur morphology in comparison to crocodylomorphs. Phytosaurs were shown to exhibit repeated evolutionary divergences between robust and gracile areas of morphospace, a pattern that was also found in two groups of crocodylomorphs: Notosuchia and Crocodyloidea.

In terms of dorsal morphology, phytosaurs are significantly distinct from any extant or extinct group of crocodylomorphs; this is also true in lateral orientation, with the exception of Thalattosuchia. The rostral–post-rostral patterns of morphological variation in phytosaurs are more similar to those of crocodylids than alligatorids, being consistent with a stronger link between morphology and function, rather than phylogenetic signal (Sadleir & Makovicky, 2008; Piras *et al*., 2009, 2013). This is also consistent with the greater degree of modularity within the crocodylid skull; my results tentatively suggest greater levels of modularity in the phytosaur skull than that observed in crocodylids, though further analysis is required.

In dorsal view, the morphology of the phytosaur skull is more conservative than the entirety of Crocodylomorpha represented in Chapter 3; however, phytosaurs are no more or less conservative than any individual group of crocodylomorphs. The similarity in levels of disparity is supported by the finding of broadly similar evolutionary rates between

crocodylomorphs and phytosaurs. However, some crocodylomorph groups, such as Notosuchia, displayed generally elevated evolutionary rates matched by high disparity.

It was found that phytosaurs could successfully be separated into three statistically distinct morphological groups, corresponding to gracile, medium and robust phytosaurs, as suggested by Hunt (1989). However, the ecological applicability of these groups could only be investigated with further functional or dietary study.

Further investigation of the phytosaur ecomorphs and extant ecological analogues suggested by Hunt (1989) was undertaken in Chapter 4, using analyses of 3D dental microwear. Investigation into the microwear present within the robusticity categories of Hunt (1989) concluded that it was possible to separate the robust and gracile categories (no members of the 'medium' group were available for sampling) based on dental microwear. However, this separation was not correlated with any aspect of diet/prey type, as implied by Hunt (1989); an alternative hypothesis is that prey items between robusticity categories may have been size-partitioned, based on the association of increasing prey size and skull robusticity in other taxa (Metzger & Herrel, 2005; McCurry *et al*., 2017b), the resistance to stress and bending of more robust skulls (Lemanis, 2012) and the morphology of microwear described here.

There also appears to be little evidence for partitioning of different materials along the heterodont tooth row of phytosaurs. Differences in surfaces may be better explained by functional partitioning of the tooth row, with anterior and mid dentition used for prey capture and restraint, whilst the posterior teeth served a role in processing food items.

The overall diet of phytosaurs was reconstructed as generalist, focussing primarily on fish and tetrapods, though some samples displayed wear more consistent in extant taxa with a

high proportion of hard material in diet, such as invertebrate integument. This estimation of phytosaur diet overlaps with the dietary reconstruction in multivariate space of many extant crocodylomorph species, and is supported by overlapping primarily with generalist, carnivorous and piscivorous species, e.g. *Crocodylus niloticus* and *Crocodylus porosus*, and to a slightly lesser extent *Alligator mississippiensis* and *Gavialis gangeticus.* Very little overlap is observed with taxa primarily associated with a large invertebrate component of diet: *Crocodylus acutus*, *Caiman crocodilus* and juvenile *Crocodylus porosus.*

My results broadly support the conclusion that extant crocodylomorphs are good ecological analogues for phytosaurs, displaying similar morphological and dietary ranges and similar rates of evolution. It should, however, be emphasised that the convergence between the two groups is general; phytosaurs display multiple morphological features that are absent in crocodylomorphs, including the depression of the supratemporal fenestrae, extreme posterior projection of the squamosals, the presence of a mediolaterally narrow but dorsoventrally tall rostrum and the co-occurrence of a gracile 'dolichorostral' anterior snout with a highly robust posterior snout and cranium. Whilst I show that phytosaurs and extant crocodylomorphs fed on a similar array of prey materials that may be attributable to particular prey categories, there is little evidence to justify extrapolating this to the species level, e.g. to infer an ecological similarity between gracile phytosaurs and *Gavialis* or *Tomistoma*, based on their similarity in morphospace. The existence of multiple seemingly specialised phytosaur morphologies, but a generalist feeding signal, may instead indicate that individuals would feed on what prey was available at the time, as is the case in extant crocodylians, based on their diverse dietary compositions.

A consistent pattern within Phytosauria supported by my phylogeny (Chapter 2), and the repeated exploration of particular areas of morphospace reported in Chapter 3, is the

almost ubiquitous co-occurrence of robust and a gracile species within most phytosaur genera. This has prompted suggestions of sexual dimorphism in some of these taxa, with hypothesised synonymy of the species, and the robust species usually interpreted as male and the gracile species as female (Colbert, 1947; Zeigler *et al.*, 2002a, 2003a; Hunt *et al.*, 2006). Sexual dimorphism is argued to be the most parsimonious explanation for the apparent co-occurrence of such taxa in mass death assemblages (Zeigler *et al.*, 2002a, 2003a; Hunt *et al.*, 2006). Valid counter hypotheses have also been proposed to explain this co-occurrence, including dietary niche partitioning and sympatric speciation (Irmis, 2005). My finding of a lack of dietary partitioning between robust and gracile phytosaurs is inconsistent with the hypothesis of niche partitioning, suggesting that two phytosaur species within one ecosystem may be in competition regardless of cranial morphology. On the contrary, allopatry may also be realised through behavioural differences and/or differences in exact prey preference – both of which are difficult to investigate in a palaeontological context and are beyond the scope of the present thesis. The possible incongruence of my result with a broad definition of niche partitioning lends support to the interpretation of these taxa being sexual dimorphs, rather than distinct species; however, very little unambiguous evidence exists regarding sexual dimorphism in phytosaurs, and is an area that requires considerable further investigation. Considerable light may be shed upon the ecological relationships of different phytosaur morphologies by a synthesis of textural microwear with biomechanical methods such as beam-theory and finite element analysis (FEA), and may form a profitable avenue of future research.

The results presented in this thesis prompt a number of other avenues of future research. In Chapter 3 it is hypothesised that phytosaurs may exhibit a high degree of modularity in their crania, and an interesting future approach would be to verify and

investigate modular trends throughout the group's history, potentially as part of a wider investigation. The Triassic was a period of major innovation following the end-Permian mass extinction, wherein many important groups that would dominate Mesozoic ecosystems diversified, such as dinosaurs, pterosaurs and crocodylomorphs. Conducting a 3D geometric morphometric analysis of cranial modularity, in a phylogenetic context, among Triassic archosauromorphs could highlight strongly correlated suites of characters, with potentially wide-ranging impacts on phylogenetic analyses. Furthermore, shifts from a more conservative, integrated cranial structure to a more modular structure, with decoupled, biomechanically characterised functional modules, may aid the identification and phylogenetic placement of key morphological innovations.

The comprehensive phylogeny presented in Chapter 2 enables broader, group-wide analyses to be conducted to aid our understanding of late Triassic ecosystems. For example, a biogeographic analysis of Phytosauria through time could be used to determine the group's dispersal patterns from the Middle–late Triassic. It would be interesting to conduct similar analyses for other groups of large carnivorous taxa throughout the Triassic to produce a combined investigation of faunal turnover, and assess whether geographical partitioning occurred between potential ecological competitors.

It is known that phytosaurs and metoposaurs are broadly found together (Sellwood & Valdes, 2006; Stocker & Butler, 2013) and both represent large, aquatic apex predators that would be expected to be in direct competition. An alternative method of assessing their ecological similarity, that could be combined with future microwear studies is, again, the use of biomechanical techniques, such as FEA to compare the stresses and strains associated with feeding in these two hypothetically ecologically similar, yet morphologically different groups.

Finally, a key goal for future phytosaur research is the inclusion of postcranial material in phylogenetic analyses. This is made challenging by the highly conservative morphology of phytosaur postcranial anatomy; however, this may be where new character coding techniques such as continuous and geometric morphometric methods may be of assistance, e.g. by quantifying subtle differences in the proportions of long bones or the shapes of elements in the pelvic/shoulder girdles. It may also be useful to use linear discriminant analyses (LDA, CVA) on measurements, or landmark configurations of postcranial elements, in order to identify where consistent differences between taxa may occur. This may be a promising starting point with which to greatly enhance systematic reconstructions of Phytosauria.

Appendix: Chapter 2 (phylogenetic analysis)

S1.1. *Taxonomic list*

Institutional abbreviations

AMNH: American Museum of Natural History, New York, USA; **BSPG**: Bayerische Staatssammlung für Paläontologie und Geologie, Munich, Germany; **CMNH**: Carnegie Museum of Natural History, Pittsburgh, USA; **FMNH**: Field Museum of Natural History, Chicago, USA; **GPIT**: Institut für Geologie und Paläontologie Tübingen, Tübingen, Germany; **GR**: Ruth Hall Museum of Paleontology, Ghost Ranch, Abiquiu, USA; **ISI**: Indian Statistical Institute, Kolkata, India; **MB**: Museum für Naturkunde, Berlin, Germany; **MBSN**: Museo Civico di Scienze naturali 'E. Caffi', Bergamo, Italy; **MCZ**: Harvard University Museum of Comparative Zoology, Cambridge, USA; **MNA**: Museum of Northern Arizona, Flagstaff, USA; **MNHN**: Muséum National d'Histoire Naturelle, Paris, France; **MSM**: Arizona Museum of Natural History (previously Mesa Southwest Museum), Mesa, USA; **MU**: University of Missouri, Columbia, Missouri, USA; **NHMUK**: Natural History Museum, London, UK; **NHMW**: Naturhistorisches Museum Wien, Vienna, Austria; **NMC**: Naturkundemuseum Coburg, Coburg, Germany; **NMMNHS**: New Mexico Museum of Natural History and Science, Albuquerque, USA; **OMNH**: Oklahoma Museum of Natural History, Norman, USA; **PEFO**: Petrified Forest National Park, Arizona, USA; **PPHM**: Panhandle Plains Historical Museum West Texas A&M University, Canyon, USA; **SMF**: Forschungsinstitut und Natur-Museum Senckenberg, Frankfurt/Main, Germany; **SMNS**: Staatliches Museum für Naturkunde Stuttgart, Stuttgart, Germany; **TMM**: Texas Memorial Museum, Austin, USA; **TTU-P**: Museum of the University of Texas Tech, Lubbock, USA; **UCM**: University of Colorado Museum, Boulder, USA; **UCMP**: University of California

Museum of Paleontology, Berkeley, USA; **UMMP**: University of Michigan Museum of Paleontology, Ann Arbor, USA; **UMNH**: Natural History Museum of Utah, Salt Lake City, USA; **USNM**: National Museum of Natural History, Washington D.C., USA; **UW**: University of Wisconsin Geological Museum, Madison, USA; **YPM**: Yale Peabody Museum, New Haven, USA; **ZMNH**: Zhejiang Museum of Natural History, Hangzhou, China; **ZPAL**: Instytut Paleobiologii PAN, Warsaw, Poland.

Diandongosuchus fuyuanensis Li *et al.*, 2012

Age: Ladinian (*c.* 242–237 Mya)

Occurrences: Zhuganpo Member, Falang Formation, southeast Fuyuan County, Yunnan Province, China

Holotype: ZMNH M8770, largely complete skeleton missing many caudal vertebrae

Specimen(s) Used for Scoring: ZMNH M8770

Key References: Li *et al.* (2012); Stocker *et al.* (2017)

Most Recent Diagnosis:

Stocker *et al.* (2017) distinguished *D. fuyuanensis* from all other phytosaurs using the following characters: 1) Anterodorsal (nasal) process of premaxilla extending well posterior of external naris; 2) Presence of a fossa expanded in anteroventral corner of external naris; 3) Jugal with pronounced longitudinal ridge on lateral surface; 4) Anterior process of jugal much broader than the posterior process underlying anterior process of quadratojugal; 5) Premaxilla with nine teeth; 6) More than one set of paramedian osteoderms dorsal to the cervical series.

Comments: *D. fuyuanensis* was originally described as a rauisuchian archosaur (Li *et al*., 2012), and was subsequently reassessed as the most basal phytosaur (Stocker *et al*., 2017),

using the following characters: 1) Posterodorsal process of premaxilla strongly sutured to maxilla; 2) More than six premaxillary teeth; 3) Facial portion of maxilla anterior to anterior edge of antorbital fenestra equal in length or longer than portion posterior to anterior edge of fenestra; 4) Entire anterior margin of scapula straight/convex or partially concave; 5) Anterior portion of coracoid distinctly hooked; 6) Ectepicondylar flange of humerus present; 7) Obturator foramen of the pubis modified into a notch that opens medioventrally; 8) medial side of distal tarsal 4 with foramen/foramina; 9) Articular surface for the fibula on the calcaneum convex and hemicylindrical shaped; 10) Osteoderms covering the appendages; 11) Retroarticular process of the articular and surangular well ventral to the articulation with the quadrate; 12) Lateral margin of the humerus straight from midshaft to proximal portion. The hypothesis that *D. fuyuanensis* is the most basal known phytosaur was not explicitly tested by Stocker *et al*. (2017); its position within Phytosauria is assessed for the first time in this study.

Wannia scurriensis (Langston, 1949)

Age: late Carnian–early Norian (*c.* 232–225 Mya)

Occurrences: Camp Springs Formation, Dockum Group, Scurry County, Texas, USA

Holotype: TTU-P 00539, partial skull

Specimen(s) Used for Scoring: TTU-P 00539

Key References: Langston (1949); Stocker (2013)

Most Recent Diagnosis: Stocker (2013) diagnosed *Wannia scurriensis* on the basis of the following proposed autapomorphies: 1) Basitubera that are widely separated mediolaterally; 2) Presence of a ridge on the lateral surface of the jugal; 3) Presence of a thickened shelf along the posteroventral edge of an expanded pterygoid-quadrate wing; 4) ‘Septo-maxillae’ that do not contact one another and do not form part of the internarial septum; 5) Presence of

a nasal swelling posterior to the posterior border of the nares. In addition to these autapomorphies, Stocker (2013) also provided a differential diagnosis outlining non-autapomorphic characters that distinguish *W. scurriensis* from other phytosaurs.

Modified Diagnosis: Here, I diagnose *Wannia scurriensis* using the following unique combination of characters: 1) Presence of an anteroposteriorly oriented ridge on the lateral surface of the jugal, positioned toward the middle or ventral edge of the jugal posterior process; 2) Presence of a nasal swelling posterior to the posterior border of the nares; 3) Posterior rim of nares smooth (not rugose); 4) Absence of paired depressions posterior to the posterior narial rim.

Comments: Some of the characters (1, 2, 3, 5) used by Stocker (2013) to diagnose *Wannia scurriensis* also occur in species of *Parasuchus* and cannot, therefore, be considered autapomorphic. As noted by Stocker (2013), the separation of the basitubera (character 1) is the same as that in *Parasuchus angustifrons*; however, Stocker suggested that the basitubera in *Parasuchus angustifrons* are not as rounded as those of *W. scurriensis*. Based on my examination of specimens of both taxa, this distinction seems subjective and questionable, particularly given that the holotype of *Parasuchus angustifrons* (BSPG 1931 X 502) has been subjected to dorsoventral compression. Stocker (2013) also noted that the narial swelling (charater 5) is also present in *Parasuchus angustifrons* (and is, therefore, also not autapomorphic), although the latter species can be differentiated from *W. scurriensis* as it possesses paired depressions just posterior to the external nares and a rugose posterior narial rim (BSPG 1931 X 502; Butler *et al*. 2014).

The thickened pterygoid-quadrate shelf (character 3) appears to also be present in TMM 31100-101, a specimen referable to *Parasuchus bransoni* on the basis of its narial morphology (see below). Moreover, the majority of the quadrate is missing in *W. scurriensis*,

making character 3 difficult to assess. There are difficulties in scoring character 4 accurately for *W. scurriensis* because interpretative lines have been incorrectly drawn onto the specimen to supposedly mark the positions of the 'septo-maxillae', and the dorsal surface of the septum is damaged. On close side-by-side inspection of the holotype and a cast (TTU-P 14911, which lacks the interpretative lines), the septomaxillae do seem to form a midline contact, and do not therefore differ in any significant regard from those of *Parasuchus hislopi*, *Parasuchus bransoni* and *Parasuchus angustifrons*.

An additional partial skull (TTU-P 11422) was considered referable to *W. scurriensis* by Stocker (2010); however, as noted by Stocker (2013), no characters are preserved that would allow this specimen to be diagnosed, and as such this specimen should be classified as an indeterminate parasuchid excluded from Mystriosuchinae.

The holotype of *W. scurriensis* was previously referred to *Parasuchus bransoni* (Long & Murry, 1995).

Genus: *Parasuchus* Lydekker, 1885

Type species: *Parasuchus hislopi*

Diagnosis: "A 'Paleorhinus-grade' phytosaur that can be distinguished from all other members of this group by the presence of an anterior frontal depression, bifurcated lateral ridge on the squamosal and a row of nodes on the lateral surface of the jugal." (Kammerer *et al.*, 2015).

Parasuchus bransoni (Williston, 1904)

Age: late Carnian–early Norian (*c.* 232–225 Mya)

Occurrences: Popo Agie Formation, Chugwater Group, Wyoming, USA; Colorado City Formation, Dockum Group, Texas, USA

Holotype: FMNH UC 632, skull

Specimen(s) Used for Scoring: FMNH UC 632; TMM 31100-101; TMM 31100-418 and 419 (these two specimens likely represent an associated skull and mandible).

Key References: Williston (1904); Lees (1906); Long & Murry (1995); Butler *et al.* (2014); Kammerer *et al.* (2015)

Most Recent Diagnosis: Long & Murry (1995) diagnosed *Parasuchus bransoni* with the following combination of characters: 1) Skull low; 2) Orbit directed dorsolaterally; 3) Rostrum moderately long, prenarial length equals postnarial length; 4) Maxilla with straight ventral margin; 5) Posterior portion of maxilla not flared laterally; 6) Interpterygoid vacuity small or absent; 7) Homodont dentition; 8) Alveoli circular throughout; 9) Posterior premaxillary alveolae normal; 10) Upper dentition with 36–45 teeth.

Modified Diagnosis: A combination of the three *Parasuchus* characters identified by Butler *et al.* (2014) and Kammerer *et al.* (2015) and one character of Kammerer *et al*. (2015) to distinguish *Parasuchus bransoni* from *Parasuchus hislopi* and *Parasuchus angustifrons*: 1) Presence of an anterior frontal depression; 2) Bifurcated lateral ridge on the squamosal; 3) Row of nodes on the lateral surface of the jugal; 4) Possession of high ‘triangular’ nares.

Comments: Long & Murry (1995) used a combination of nine characters to diagnose *Parasuchus bransoni*. Characters such as their 1, 2, 5, 7 and 9 have been criticized for being subjective, vague and prone to taphonomic distortion (Hungerbühler, 1998a; Stocker, 2010). Character 6 appears to have been generated based on the distorted morphology of the holotype. All non-Mystriosuchinae members of Parasuchidae have an interpterygoid vacuity which extends anteroposteriorly along at least 50% of the palatal vault, and which only

becomes restricted in more derived taxa. This proposed diagnostic character is actually therefore plesiomorphic for Mystriosuchinae. Character 7 is problematic as the assessment of dentition used by Long & Murry (1995) was based on empty alveolae and, therefore, may be unreliable. In any case, some degree of heterodonty has now been recognized in all phytosaurs. Character 9 (here inferred to relate to the increase in size of the posterior two or three premaxillary alveolae in many taxa) is also problematic; although the increase in posterior premaxillary alveolar size is subtler in *Parasuchus bransoni* than in many taxa, it does still occur. Several of the characters) are probably plesiomorphic for Phytosauridae (3, 4, 5, 7, 8, and probably 9) and/or are widespread (1, 2, 8, 10) in basal members of the clade.

Parasuchus hislopi Lydekker, 1885

Age: late Carnian–early Norian (*c.* 232–225 Mya)

Occurrences: Lower Maleri Formation, Pranhita Godavari Valley, Telangana, India; Tiki Formation, Madhya Pradesh, India

Holotype: ISI R 42 (neotype), almost complete skeleton including cranium and mandible.

Specimen(s) Used for Scoring: ISI R 42; ISI R 43

Key References: Lydekker (1885); Chatterjee (1974, 1978); Kammerer *et al.* (2015)

Most Recent Diagnosis: Kammerer *et al*. (2015) diagnosed *Parasuchus hislopi* as follows: a species of *Parasuchus* that is 1) distinguished from *Parasuchus bransoni* by a relatively low narial eminence with a raised, rugose posterior margin of the naris (a ‘narial rim’); 2) Distinguished from *Parasuchus angustifrons* by the absence of paired depressions on the anterior portions of the nasals; 3) Tentatively distinguished from ‘*Paleorhinus magnoculus’* by the posterior confluence of the raised margins of the nares.

Parasuchus angustifrons (Kuhn, 1936)

Age: late Carnian (*c.* 232–228 Mya)

Occurrences: Blasensandstein (lateral equivalent of Hassberge Formation), Middle Keuper Subgroup, northern Bavaria, Germany; Middle Keuper Subgroup, Opole province, Poland

Holotype: BSPG 1931 X 502, partial skull

Specimen(s) Used for Scoring: BSPG 1931 X 502; ZPAL AbIII 111; ZPAL AbIII 200

Key References: Kuhn (1936); Butler *et al.* (2014); Kammerer *et al.* (2015)

Most Recent Diagnosis: Butler *et al.* (2014) diagnosed *Parasuchus angustifrons* on the basis of the following proposed autapomorphies: 1) Stepped lateral rim of external naris that is strongly swollen and rugose at posterior end; 2) Paired depressions on the anterior portions of the nasals (immediately posterior to the external nares) and anterior portions of the frontals; 3) Foramen in ectopterygoid enlarged and subcircular in outline; 4) Suborbital foramen elongate and boomerang-shaped; 5) Large postparietal foramen at junction of supraoccipital and parietal.

Modified Diagnosis: Species of *Parasuchus* with the following autapomorphies: 1) Paired depressions on the anterior portions of the nasals; 2) Large postparietal foramen at junction of supraoccipital and parietal.

Comments: Of the characters proposed by Butler et al. (2014) as autapomorphic for *Parasuchus angustifrons*, characters 1 and 3 are both present in other members of *Parasuchus*: the laterally stepped and posteriorly rugose nares are also present in *Parasuchus hislopi* (ISI R42), while the enlarged ectopterygoid foramen is visible in the holotype of *Parasuchus bransoni* (FMNH UC 632). Character 4, an elongate and boomerang-shaped suborbital foramen, may be variable within the species, given that it appears to be absent in ZPAL AbIII 200. However, the degree of variability of this character among basal phytosaurs

is difficult to assess, given the paucity of well-preserved palates generally within the genus *Parasuchus*. Given this uncertainty, character 4 should not be considered diagnostic until sufficient comparative material is available to assess its usefulness.

Genus: '*Paleorhinus*'

Comments: '*Paleorhinus*' is historically a problematic wastebasket taxon that was previously synonymous with *Parasuchus.* Following recent work (Butler *et al.*, 2014; Kammerer *et al.*, 2015) '*Paleorhinus*' was split into the monophyletic genus *Parasuchus* and a grade of paraphyletic basal phytosaurs, which retained the old genus name. There is currently no valid diagnosis for this genus.

'*Paleorhinus*' *parvus* Mehl, 1928

Age: late Carnian–early Norian (*c.* 232–225 Mya)

Occurrences: Popo Agie Formation, Fremont County, Wyoming, USA

Holotype: MU 530, rostral/mandibular fragments and partial postcrania

Specimen(s) Used for Scoring: MU 530

Key References: Mehl (1928); Kammerer *et al.* (2015)

Most Recent Diagnosis: Mehl (1928) did not provide a list of distinct autapomorphies; however, the morphology of '*Paleorhinus*' *parvus* was discussed in relation to other phytosaurs, and a number of distinctive features were highlighted, which are discussed below.

Modified Diagnosis: Diagnosable on the basis of a unique combination of characters: 1) Anterior tip of the rostrum abruptly downturned; 2) Steep anterodorsally concave curve to the

nares; 3) Anterior border of nares anterior to the antorbital fenestra; 4) Subnarial facial portion of the maxilla is dorsoventrally extensive.

Comments: '*Paleorhinus*' *parvus* was interpreted by Mehl (1928) to possess a proportionately shorter prenarial rostrum than that of *Parasuchus bransoni*. The postnarial portion of the skull of '*Paleorhinus*' *parvus* is not preserved; therefore, Mehl based his calculations on a partial mandible associated with the cranial remains, which he used to estimate total skull length. Mehl's measurements suggest that the snout constituted 42.4% of total cranial length, which is indeed proportionately short compared to *Parasuchus bransoni*, for which values are approximately 50% (TMM 31100-101, 31100-418). This character should be treated with caution, however, as Mehl's calculations of skull length based on the mandible may be somewhat inaccurate. Mehl also suggested that the rostrum of '*Paleorhinus*' *parvus* is more slender than that of *Parasuchus bransoni*; however, it is uncertain whether this is due to mediolateral compression of the former.

The anterior tip of the rostrum was suggested by Mehl (1928) suggested to be more abruptly downturned than in *Parasuchus bransoni*. I concur with this assessment: the rostrum of '*Paleorhinus*' *parvus* is more abruptly downturned than all species of *Parasuchus*, '*Paleorhinus*' *sawini* and *Ebrachosuchus neukami*, and more closely approximates the rostral morphology of *Brachysuchus* and *Angistorhinus*. Mehl also noted that the nares of '*Paleorhinus*' *parvus* are more steeply curved anterodorsally than *Parasuchus bransoni*, but considered the narial development to be suspect and 'not dependable'. However, I concur with Kammerer *et al.* (2015) that there is no reason to suspect that the morphology of the narial region is not genuine, even considering lateral compression. Kammerer *et al.* (2015) also noted that the 'subnarial facial portion of the maxilla' is well preserved and 'has greater

relative height than that of *Parasuchus hislopi*'. I agree with this assessment, and find that this is also true when compared with all other members of *Parasuchus.*

'*Paleorhinus*' *sawini* Long & Murry, 1995

Age: late Carnian–early Norian (*c.* 232–225 Mya)

Occurrences: 'Pre-Tecovas Horizon', Dockum Group, Borden County, Texas, USA

Holotype: TMM 31213-16, skull and possibly associated isolated postcrania

Specimen(s) Used for Scoring: TMM 31213-16

Key References: Long & Murry (1995); Stocker (2010)

Most Recent Diagnosis: Long & Murry (1995) diagnosed '*Paleorhinus*' *sawini* on the basis of the following combination of characters: 1) Skull high; 2) Rostrum short and robust; 3) Prenarial length less than postnarial length; 4) Maxilla with strongly convex ventral margin; 5) Posterior portion of maxilla with prominent lateral flare; 6) Probable heterodont dentition; 7) Posterior maxillary alveoli enlarged and transversely rectangular; 8) Posterior premaxillary enlarged; 9) Upper dentition with 38 teeth.

Modified Diagnosis: A non-leptosuchomorph phytosaur with the following unique character complex: 1) Rostrum short and robust; 2) Prenarial length less than postnarial length; 3) Posterior premaxillary alveoli enlarged; 4) Upper dentition with 38 teeth; 5) Parietal/squamosal bars are medially bowed.

Comments: Characters 1, 4 and 5 of Long & Murry (1995) may be related to general large size and robusticity, but this has yet to be tested through ontogenetic studies of early phytosaurs. In particular, the height of the skull in proportion to its width does not appear to differ considerably from other species of early phytosaur such as *Parasuchus bransoni* (TMM 31100-8, 31100-101) or *Parasuchus angustifrons* (ZPAL Ab III 111, Ab III 200). Characters

6 and 7 are based on incomplete or missing morphology. No teeth remain in the skull, thus estimations of heterodonty are based solely on the shapes and relative sizes of empty alveolae. Given that some degree of heterodonty is present in all phytosaurs and the roots of even mediolaterally compressed phytosaur teeth are approximately circular, it is difficult to make meaningful statements about heterodonty without preservation of the actual dentition. Similarly, the posterior maxillary alveolae are heavily reconstructed with plaster, making character 7 questionable. It is unclear how intraspecifically variable tooth counts are in phytosaurs; however, specimens of *Parasuchus bransoni* and *Parasuchus hislopi* consistently have more than 40 teeth in the upper jaw (TMM 31100-101, 31100-239, ISI R42), whereas *Parasuchus angustifrons* appears to possess a similar number to '*Paleorhinus*' *sawini* (ZPAL Ab III 200). This character is therefore retained, as further study may reveal it to contain taxonomic value.

Stocker (2010) noted two further characters that she proposed distinguish '*Paleorhinus*' *sawini* from *Parasuchus*: 1) Shares medially-bowed parietal-squamosal bars with *Angistorhinus*; 2) The antorbital fossa is highly reduced or absent. It is, however, debatable how reduced in size the antorbital fossa was; upon close examination it appears possible that the fossa may have been broken up to its outer rim, i.e. to the extent of the concavity of the fossa. There is evidence of a thin lamina extending from the interior edge of the purported fenestra in TMM 31213-16, but all of its edges are broken away; this may be the remnants of the original antorbital fossa.

Ebrachosuchus neukami Kuhn, 1936

Age: late Carnian (*c.* 232–228 Mya)

Occurrences: Blasensandstein (lateral equivalent of Hassberge Formation), Middle Keuper Subgroup, northern Bavaria, Germany

Holotype: BSPG 1931 X 501

Specimen(s) Used for Scoring: BSPG 1931 X 501

Key References: Kuhn (1936); Long & Murry (1995); Butler *et al*. (2014)

Most Recent Diagnosis: Butler *et al.* (2014) diagnosed *E. neukami* based on six autapomorphies: 1) Preorbital length more than 3.8 times that of the orbit + postorbital length; 2) More than 50 teeth in the premaxilla and maxilla combined; 3) Pronounced, sharp flange extending along the lateral surface of the dorsal (postorbital) process of the jugal and the ventral (jugal) process of the postorbital that is continuous posteriorly with the lateral margin of the postorbital-squamosal bar; 4) Infratemporal fenestra is substantially longer anteroposteriorly than deep dorsoventrally, terminates anteriorly beneath the midpoint of the orbit; 5) Quadrate foramen very large, approximately two-thirds of width of foramen magnum; 6) Alveolar ridges absent from the anterior maxilla and only poorly developed on the premaxilla.

Rutiodon carolinensis Emmons, 1856

Age: early Norian (*c.* 228–218 Mya)

Occurrences: Cumnock Formation, Deep River Coal Field, near Gulf, North Carolina, USA; Cumnock Formation, New Egypt coal mine, Chatham County, North Carolina, USA

Neotype: USNM PAL 214513 (formerly ‘Williams College unnumbered specimen’)

Specimen(s) Used for Scoring: USNM PAL 214513; USNM V 5373; AMNH 1–5

Key References: Emmons (1856; 1860); Marsh (1896); McGregor (1906); Colbert (1947); Gregory (1962b); Hunt & Lucas (1989); Stocker (2010)

Most Recent Diagnosis: Stocker (2010) suggested the following diagnostic characters with reference to the neotype specimen: 1) Slender rounded premaxillae that lack a rostral crest; 2) Nares placed posteriorly between the antorbital fenestrae with borders above the level of the skull roof. To enable distinction between *Rutiodon carolinensis* and *Angistorhinus*, Stocker added a further character based on preserved temporal regions referred to *Rutiodon carolinensis* in the AMNH collections (AMNH 1–5): 3) Semi-depressed parietal-squamosal bars.

Comments: Hunt & Lucas (1989) designated a neotype for *Rutiodon carolinensis* and proposed four diagnostic characters that were centred around the temporal region of the skull. Stocker (2010) noted that none of the characters included in the diagnosis of Hunt & Lucas (1989) were observable in their designated neotype due to the temporal region not being preserved. Instead, the diagnostic characters appear to be based on USNM and AMNH material that was referred to *Rutiodon carolinensis* by Gregory (1962b).

Characters 1 and 2 of the diagnosis of Stocker (2010) are observable in the neotype; however, if only these characters are considered it is not possible to differentiate *Rutiodon carolinensis* from *Angistorhinus*. Stocker also therefore used the referred AMNH material to provide a further character and a more robust diagnosis.

It should be noted that the elevation of the nares (character 2 of Stocker, 2010) may not be entirely reliable, as the orbital and narial portions of the neotype do not articulate together meaning there is no way to be certain that the nares would have been elevated above the level of the skull roof. Furthermore, Gregory (1962b) noted that in the neotype the nares were inferred to be elevated, while those of AMNH 1 are not, suggesting a degree of variability in this feature.

Genus: ***Angistorhinus*** Mehl, 1913

Type species: *Angistorhinus grandis*

Diagnosis: "Posterior process of squamosal incipient; cleft between posterior and descending process of squamosal variable; supratemporal fenestra large, relatively wide, but not approaching posterolateral corner of squamosal; postorbital portion of skull abbreviated; parietals short and wide with much of posterior portion not fused; occiput with moderately deep, wide posterior emargination; postfrontal not in contact with supratemporal fenestra; opisthotic process elongate." (Long & Murry, 1995).

Stocker (2010) presented a clearer, but informal diagnosis, in supplementary information: "Angistorhinus is distinguished by lack of a rostral crest, elevated nares into a 'crater' or 'volcano' above the level of the skull roof, and parietal-squamosal bars that are at the level of the skull roof, mediolaterally wide, possess a medial curvature, and are less than half the length of the parietals (the parietals remain united for more than half their length)."

Angistorhinus talainti Dutuit, 1977b

Age: late Carnian–early Norian (*c.* 232–225 Mya)

Occurrences: Timezgadiouine Formation, Western Moroccan Atlas, Morocco

Holotype: MNHN TAL 1–11 (syntypes), three skulls plus four partial mandibles and mandibular fragments

Specimen(s) Used for Scoring: MNHN TAL 1; MNHN TAL 2

Key References: Mehl (1913); Dutuit (1977b); Long & Murry (1995)

Most Recent Diagnosis: Long & Murry (1995) felt the placement of *A. talainti* within the genus *Angistorhinus* was unjustified and therefore considered it as referable to a new and currently unnamed genus within the subfamily 'Angistorhininae' Camp, 1930. They considered it to be diagnosed by the following combination of characters: 1) Supratemporal fenestra extremely elongate and narrow, crescentic in dorsal view and extending to posterolateral corner of squamosal; 2) Postorbital portion of the skull elongate with parietals long, narrow and fused for most of their length; 3) Postfrontal not in contact with supratemporal fenestra; 4) Occiput with shallow posterior emargination; 5) Posterior process of squamosal well developed and terminally convex; 6) Parietal extensions not present; 7) Opisthotic process short and paddle shaped.

Modified Diagnosis: *A. talainti* can be diagnosed from other phytosaurs using a combination of characters that includes generic *Angistorhinus* characters and characters recognized in previous studies (Dutuit, 1977b; Long & Murry, 1995): 1) Parietal/squamosal bars equal to, or greater than the thickness of the postorbital/squamosal bars; 2) Parietal/squamosal bars curve medially; 3) Supratemporal fenestrae narrow and short; 4) Postorbital portion of the skull elongate with parietals long, narrow and fused for most of their length; 5) Posterior process of squamosal well developed and terminally convex; 6) Posterolaterally curving groove extends from the supratemporal fenestra to the posterolateral corner of the squamosal; 7) Prominent ridge runs along the anterior dorsolateral edge of the postorbital-squamosal bar; 8) Parietals diverge posterior to the main vacuity of the supratemporal fenestra.

Comments: The interpretation of the supratemporal fenestra of *A. talainti* in character 1 of Long & Murry (1995) contradicts the description of Dutuit (1977b), who stated in his diagnosis that the supratemporal fenestrae are narrow and short. The figures in Dutuit (1977b) superficially show an elongate fenestra, as suggested by Long & Murry (1995); however,

Long & Murry did not distinguish between the dorsal opening of the fenestra and a posterior groove which grades from the posterior corner of the fenestra onto the posterolateral corner of the squamosal. It is difficult to delimit the fenestra due to the presence of this groove, but I agree with Dutuit (1977b), that the actual opening of the fenestra is relatively short. Characters 3 and 4 of Long & Murry (1995) appear to be shared by all members of *Angistorhinus* observed in this study, and character 5 is present in multiple specimens from Texas and New Mexico, such as TMM 31100-1332, TMM 31100-164, TMM 31100-298 and NMMNHS-P 4781. Character 6 is difficult to interpret - the terms 'parietal extensions' and 'horizontal parietal extensions' are used in Long & Murry's revised diagnosis of 'Angistorhininae'; however, no further explanation of these features is given. I assume that this terminology refers to the posterior thickening of the parietal/squamosal bars that is observed throughout *Angistorhinus*. The parietals of *A. talainti* are expanded posteriorly in a horizontal plane to a greater extent than other species and specimens of *Angistorhinus* mentioned by Long & Murry (1995).

Angistorhinus grandis Mehl, 1913

Age: late Carnian–early Norian (*c.* 232–225 Mya)

Occurrences: Popo Agie Formation, between Squaw and Baldwin Creeks, Fremont County, Wyoming, USA

Holotype: FMNH UC 631, Skull and associated partial mandible

Specimen(s) Used for Scoring: FMNH UC 631

Key References: Mehl (1913); Long & Murry (1995)

Most Recent Diagnosis: Long & Murry (1995) diagnosed *A. grandis* as a species of *Angistorhinus* with the following characters: 1) Posterior process of squamosal very short, but deep with straight posterior margin; 2) No cleft between posterior process and descending process of the squamosal; 3) Parietal extension ?short; 4) Rostrum delicate; 5) Alveoli circular throughout with posterior premaxillary alveoli not enlarged (this region of snout is not swollen); 6) Ventral margin of maxilla not laterally flared; 7) Orbits directed more dorsally than laterally.

Modified Diagnosis: I diagnose *A. grandis* as a species of *Angistorhinus* with the following unique character combination: 1) Ventral margin of maxilla not laterally flared; 2) Supratemporal fenestrae wide and triangular in shape; 3) Lateral temporal fenestra large and more sub-triangular than rectangular; 4) U-shaped emargination between the supratemporal fenestrae at the posterior border of the parietals in dorsal view.

Comments: I suggest that characters 1 and 2 of Long & Murry (1995) should be treated with caution, or potentially rejected, as the posterior process of the squamosal is not actually preserved in *A. grandis*. The morphology of the posterior process was reconstructed in plaster from a supposed impression of the medial surface of the process preserved in the matrix with the skull; however, no photographs or diagrams exist of this impression, and its described morphology differs from the rounded morphology of the posterior process of the squamosal observed in all other specimens of *Angistorhinus.*

Characters 3 and 4 of Long & Murry (1995) are phrased ambiguously and are therefore difficult to objectively assess. Alongside character 5, these characters are also present in all other specimens of *Angistorhinus* that were examined, and are therefore not useful for a diagnosis at specific level. Character 7 reports the orientation of the orbit; however, phytosaur skulls are often mediolaterally or dorsoventrally compressed meaning that

the orientation of the orbits can vary widely both inter- and intraspecifically, and should not be used for diagnostic or phylogenetic purposes (Chatterjee, 1978; Hungerbühler, 1998a).

Genus: *Smilosuchus* Long & Murry, 1995

Type species: *Smilosuchus gregorii*

Diagnosis: *Leptosuchus*-grade phytosaurs with the following derived characters: 1) Extreme heterodonty; 2) Posterior premaxillary teeth (except last three) abruptly and very greatly enlarged, causing a swelling of the premaxilla in this region; 3) Tooth pattern posteriorly shifted; 4) Ventral margin of the maxilla greatly flared laterally; 5) Rostral crest fully developed; 6) Anterior portion of rostrum very heavy and massive; 7) Posterior portion of the skull considerably wider than in *Leptosuchus*, with lateral temporal fenestra facing dorsolaterally; 8) Orbit directed dorsolaterally. (Long & Murry, 1995).

Comments: The genus *Smilosuchus* was erected by Long & Murry (1995) to accommodate only *S. gregorii*; because the genus was monotypic the diagnosis given was the same for both genus and species. Subsequently more species have been placed in *Smilosuchus* (Stocker, 2010), though the character-based diagnosis has not been amended. Of these characters, 4, 6 and 7 are likely to be size-correlated, which has previously been noted to be undesirable and problemateic (Irmis, 2005), 7 and 8 are highly prone to taphonomic distortion and the wording of character 3 conveys little useful information and is very difficult to interpret. Of the remaining characters, 2 and 5 are consistently present only in *S. gregorii* and may be useful in defining the species. This, however leaves only character 1 (extreme heterodonty) as a valid character to define the genus *Smilosuchus*.

Stocker (2010) suggests a number of differences between *Smilosuchus* and *Leptosuchus*, which may assist in producing a stronger diagnosis for *Smilosuchus*: 1) The jugal is excluded from the AOF in *S. gregorii*, *S. lithodendrorum* and *S. adamanensis*, contrary to *Leptosuchus*. However this feature is known to be greatly variable within a single species (e.g. *Nicrosaurus kapffi*) and is likely to be equally variable in other species (Hungerbühler, 1998). 2) The articulation of the postorbital/squamosal bar in *Leptosuchus* is slot-like whereas in *Smilosuchus* it is diagonal. 3) The length of the posterior process of the squamosal in comparison to postorbital length of the skull, measured to the tip of the squamosal, is moderate in *Smilosuchus* and long in *Leptosuchus*. Although the difference is relatively minor, it occurs consistently in multiple specimens of each genus. 4) The squamosal/postorbital bar slightly overhangs the supratemporal fenestra in *Smilosuchus* and creates a subtle medial flange. 5) The posterior edge of the opisthotic process of the squamosal in *Smilosuchus* is smoothly curved. This appears to be generally true, however the right squamosal of the holotype of *S. adamanensis* features a sharp angle between the straight, horizontal ventral border of the squamosal posterior process and the ventrally oriented opisthotic, suggesting this feature may be more variable than previously thought. 6) In *Smilosuchus* the medial squamosal fossa extends to the posterior edge of the squamosal, whereas it does not in *Leptosuchus*.

Revised Diagnosis: In this study *Smilosuchus* is therefore diagnosed as a leptosuchomorph phytosaur possessing the following features: 1) Postorbital/squamosal suture diagonal; 2) Posterior process of the squamosal moderately anteroposteriorly elongated; 3) Small medial flange of postorbital/squamosal bar present; slightly obscures supratemporal fenestra in dorsal view; 4) Medial squamosal fossa extends to posterior edge of squamosal.

Smilosuchus gregorii (Camp, 1930)

Age: early Norian (*c.* 225–220 Mya)

Occurrences: Blue Mesa Member, Chinle Formation, near Round Rock, Apache County, Arizona, USA

Holotype: UCMP 27200, slightly dorsoventrally compressed skull and mandibles

Specimen(s) Used for Scoring: UCMP 27200; AMNH D.VP. 3060

Key References: Camp (1930); Colbert (1947); Long & Murry (1995)

Most recent diagnosis: Long & Murry (1995) diagnosed the new genus *Smilosuchus* and the sole species that they referred to it, *S. gregorii*, based on the following character combination: 1) Extreme heterodonty; 2) Posterior premaxillary teeth (except last three) abruptly and very greatly enlarged, causing a swelling of the premaxilla in this region; 3) Tooth pattern posteriorly shifted; 4) Ventral margin of the maxilla greatly flared laterally; 5) Rostral crest fully developed; 6) Anterior portion of rostrum very heavy and massive; 7) Posterior portion of the skull considerably wider than in *Leptosuchus*, with lateral temporal fenestra facing dorsolaterally; 8) Orbit directed dorsolaterally.

Modified Diagnosis: *S. gregorii* is diagnosed on the basis of the following unique character combination: 1) Full rostral crest; 2) Greatly dorsoventrally expanded posterior process of the squamosal.

Comments: Characters 4, 6 and 7 of Long & Murry (1995) may be size-correlated, which is both undesirable and problematic (Irmis, 2005); 7 and 8 are highly prone to taphonomic distortion and the phrasing of character three is ambiguous.

Of the remaining characters, 2 and 5 are consistently present only in *S. gregorii* rather than '*S*'. *adamanensis* or '*S*'. *lithodendrorum* and may therefore be useful in defining the species.

Character 1 (extreme heterodonty) is present in all current species of *Smilosuchus* and is therefore not of diagnostic use for *S. gregorii*.

'*Smilosuchus*' *adamanensis* (Camp, 1930)

Age: early Norian (*c.* 225–220 Mya)

Occurrences: Blue Mesa and lower Sonsela Members, Chinle Formation, Petrified Forest National Park, Apache County, Arizona, USA

Holotype: UCMP 26699, skull and mandibles

Specimen(s) Used for Scoring: UCMP 26699; UCMP 170166

Key References: Camp (1930); Long & Murry (1995); Stocker (2010)

Most Recent Diagnosis: Long & Murry (1995) differentiated '*S'. adamanensis* from other *Leptosuchus*-grade phytosaurs on the basis the following character combination: 1) Posterior process of squamosal is a deep vertical plate with moderate posterior elongation beyond paroccipital process; 2) Post-fenestral portion of squamosal wide and abruptly truncated when viewed dorsally, though the extra-fenestral portion of the bar is narrow.

Comments: Both characters of Long & Murry are accurate; however, character 1 is somewhat variable in other early leptosuchomorph taxa e.g. *Leptosuchus crosbiensis* (UMMP 7522, TMM 31173-120), and character 2 is based on heavily distorted morphology in the holotype. The lack of either a rostral or narial crest in '*S.*' *adamanensis* distinguishes it from other putative members of the genus *Smilosuchus* and members of *Leptosuchus*, though it is unclear whether or not this feature is plesiomorphic.

'*S.*' *adamanensis* suffers the same problem as '*S*'. *lithodendrorum* (see below); the majority of material referred to this species by Camp (1930) was referred based on geographical and stratigraphical proximity. As such, previous definitions of the taxon may be

chimeric; subsequent analyses should therefore treat referred specimens with caution or rely only on the holotype. A thorough re-examination and redescription of the holotype of '*S'. adamanensis* may bring further diagnostic characters to light; however, such work is beyond the scope of the current study.

'*Smilosuchus*' *lithodendrorum* (Camp, 1930)

Age: Norian (*c.* 219–217 Mya)

Occurrences: Lot's Wife beds, Sonsela Member, Chinle Formation, Petrified Forest National Park, Navajo County, Arizona, USA; Tecovas Formation, Dockum Group, Crosby County, Texas, USA

Holotype: UCMP 26688, poorly preserved, fragmentary and compressed left half of skull, and almost complete mandibles.

Specimen(s) Used for Scoring: UCMP 26688; TMM 31173-121

Key References: Camp (1930); Long & Murry (1995); Stocker (2010); Parker & Martz (2011)

Most Recent Diagnosis: Stocker (2010) proposed that '*Smilosuchus*' *lithodendrorum* should be diagnosed as a species of *Smilosuchus* with the following characters: 1) A highly angled rostrum that continues anteroventrally in a smooth descent; 2) The posterior process of the squamosals grade anteroventrally into the opisthotic process; 3) Very slight medial flange on the dorsal edge of the squamosal.

Comments: The validity of '*S*'. *lithodendrorum* has previously been questioned; it was synonymized with *Leptosuchus crosbiensis* by Long & Murry (1995) with no justification given. Stocker (2010) suggested that this may have been due to the narrow postorbital/squamosal bar, which is a prominent feature of *Leptosuchus crosbiensis* and

Leptosuchus studeri. It is also possible that the synonymization was due to extensive morphological variation exhibited in the specimens referred to '*S*'. *lithodendrorum* by Camp (1930). Camp's assignments of lectotypes and referred specimens were based on geographical and stratigraphical proximity of specimens to the holotype, rather than morphology; as a result, a number of smaller, non-crested skulls (between 678 and 965 mm in length) were assigned to this species as juveniles of '*S.*' *lithodendrorum* (UCMP 26684, 26719, 27179, 27181). These specimens lack the full rostral crest reported in larger individuals of '*S.*' *lithodendrorum*, instead their crests extend anterior of the nares before descending to form tubular rostra close to the most anterior extent of the maxillae. This morphology, combined with the size range of the specimens and aforementioned similarities between *L. crosbiensis* and '*S.*' *lithodendrorum*, seemingly makes them indistinguishable from the holotype of *L. crosbiensis.* Conversely, the crest morphology in larger specimens of both '*S.*' *lithodendrorum* and *L. crosbiensis* does differ substantially. In larger specimens of '*S*'. *lithodendrorum* (e.g. UCMP 26688; TMM 31173-121) the rostrum is fully crested, with the crest forming a straight diagonal gradient from the nares to the tip of the premaxillae. However, in larger specimens of *L. crosbiensis* (e.g. TMM 43684, 43684-8) the morphology remains unchanged from smaller specimens such as TMM 31173-120, with a partial rostral crest extending from the nares to the most anterior extent of the maxillae, and a separate premaxillary crest at approximately the mid-point of the premaxillae. A more detailed examination of all material potentially referable to these taxa may help to quantify the morphological variation associated with these taxa, and disentangle their diagnoses. Stocker (2010) did tentatively identify some subtle differences between '*S.*' *lithodendrorum* and *L. crosbiensis*, although her diagnosis does not take into account the intermediate morphologies

present in some specimens. However, a full redescription and re-evaluation of the species is beyond the remit of this paper. I therefore use the diagnosis of Stocker (2010).

The holotype of '*S.*' *lithodendrorum* was previously referred to '*S.*' *adamanensis* and *Leptosuchus crosbiensis* (Long & Murry, 1995).

'*Phytosaurus*' *doughty* Case, 1920

Age: early Norian (*c.* 225–220 Mya)

Occurrences: Tecovas Formation, Dockum Group, Texas, USA

Holotype: AMNH FR. 4919, right posterior portion of skull

Specimen(s) Used for Scoring: AMNH FR. 4919

Key References: Case (1920); Stocker (2010)

Most Recent Diagnosis: Case (1920) was able to identify two characters to separate '*Phytosaurus*' *doughtyi* from other *Leptosuchus*-grade phytosaurs: 1) No evidence of the opisthotic process posterior to the quadrate; 2) The nares rise at their posterior rim.

Comments: Character 2 of Case (1920) is present in referred specimens of *Leptosuchus crosbiensis* (TMM 31173-120 and TTU-P 09230); despite this, Stocker (2010) tentatively suggested the referral of MSM 92-023.001 to '*Phytosaurus*' *doughtyi* based in part on the presence of a deep saddle between the orbits and external nares. It may therefore be the case that the differences in this character are more nuanced between *L. crosbiensis* and '*Phytosaurus*' *doughtyi*, rather than being simply present or absent. Character 1 of Case (1920) appears to be an autapomorphy of '*Phytosaurus*' *doughtyi*, and this is supported by my first-hand study of the holotype specimen.

Genus: *Leptosuchus* Case, 1922

Type species: *Leptosuchus crosbiensis*

Diagnosis: "Rutiodontine more derived than *Rutiodon* in the following characters: squamosal with moderate posterior process extending well beyond paroccipital process; dorsal rim of post-temporal arch well below level of skull roof; moderate heterodonty; partial rostral crest, at least in adults; snout with inverted "V" shape in cross-section; anterior portion of snout heavy; orbit laterally directed". (Long & Murry, 1995).

Comments: The definition of Long & Murry (1995) is based on a hypodigm of *Leptosuchus* that includes specimens now belonging to *Smilosuchus adamanensis*. In a detailed re-analysis of *Leptosuchus*, Stocker (2010) reassigned '*L.*' *adamanensis* to *Smilosuchus*, but did not redefine the genus *Leptosuchus*. Node 7 in the phylogeny of Stocker (2010) defines the currently understood monophyly of *Leptosuchus* taxa (*L. crosbiensis* & *L. studeri*) and is supported by one synapomorphy: "distal end of paroccipital process of opisthotic rounded, distal edge is curved rather than straight". Another synapomorphy was found under DELTRAN: "jugal contributing to antorbital fenestra".

Specimens pertaining to the currently monophyletic understanding of *Leptosuchus* (Stocker, 2010) were included to represent the genus in this study, though no revised diagnosis of *Leptosuchus* is presented.

Leptosuchus studeri Case & White, 1934

Age: early Norian (*c.* 225–220 Mya)

Occurrences: Tecovas Formation, Dockum Group, Cerita de la Cruz Creek, Potter County, Texas USA; Blue Mesa Member, Chinle Formation, Arizona, USA

Holotype: UMMP 14267, skull

Specimen(s) Used for Scoring: UMMP 14267

Key References: Case & White (1934); Stocker (2010)

Most Recent Diagnosis: Stocker (2010) used two characters to diagnose *L. studeri*: 1) Posterior edges of the posterior processes [of the squamosals] curl inwards in *L. studeri*, differing from the straight posterior processes of *L. crosbiensis*; 2) Small dorsally convex area on the dorsal surface of the mid-premaxillae.

Comments: At the time of writing the holotype and referred specimens of *L. studeri* were unavailable to study, so my observations are tentative and brief. It seems possible that character 1 of Stocker (2010) could be due to taphonomic distortion, although the morphology is present on both posterior processes, and to the same degree. Character 2 of Stocker (2010) is also present in *Leptosuchus crosbiensis*, appearing in a line-drawing of the holotype (Case, 1922), and is visible in multiple other specimens (TMM 31173-120, 43684, 43684-8; TTU-P 00902, 09230, 09234, 10001). The shape of the premaxillary crest does, however, appear to be different to that of *L. crosbiensis*. The crest of *L. crosbiensis* is anteroposteriorly symmetrical and forms a smooth 'hump', whereas in *L. studeri* the anterior portion of the crest slopes gently and the posterior slightly more steeply; the apex of the crest is therefore sharper. A partially prepared specimen at Petrified Forest National Park (field no. RLG 11/07-3) also displays this crest morphology, and the posterior process of the squamosal is also identical in lateral view to *L. studeri*.

The holotype of *L. studeri* was previously referred to *L. crosbiensis* (Long & Murry, 1995).

Leptosuchus crosbiensis Case, 1922

Age: early Norian (*c.* 225–220 Mya)

Occurrences: Tecovas Formation, Dockum Group, Crosby County, Texas, USA

Holotype: UMMP 7522, skull

Specimen(s) Used for Scoring: UMMP 7522; TMM 31173-120; USNM V 15841; TTU-P 09230

Key References: Case (1922); Long & Murry (1995); Stocker (2010)

Most Recent Diagnosis: Stocker (2010) listed diagnostic features of *L. crosbiensis* in comparison to other *Leptosuchus*-grade taxa: 1) An overall slenderness of the skull; 2) Supratemporal fenestrae that are completely visible in dorsal view; 3) Supratemporal fenestrae are bounded anterolaterally by mediolaterally narrow dorsal edges of the squamosals.

Modified Diagnosis: 1) An overall slenderness of the skull; 2) Supratemporal fenestrae that are completely visible in dorsal view; 3) Supratemporal fenestrae are bounded anterolaterally by mediolaterally narrow dorsal edges of the squamosals; 4) Dorsally rounded crest on the anterior portion of the premaxilla; 5) Partial rostral crest extends approximately level from the nares and descends at a point level with the anterior-most extent of the maxillae.

Comments: I suggest two additional characters (4 and 5 in the above modified diagnosis), to reinforce the diagnosis of *L. crosbiensis*. See '*Smilosuchus*' *lithodendrorum* for further discussion of this taxon.

Pravusuchus hortus Stocker, 2010

Age: Norian (*c.* 219–217 Mya)

Occurrences: White 'hoodoo' sandstone, Kellogg Butte Sandstone, Sonsela Member, Chinle Formation, Devil's Playground, Petrified Forest National Park, Arizona, USA; ?Monitor Butte Member, Chinle Formation, Fry Canyon, Utah, USA

Holotype: AMNH FR. 30646, dorsoventrally crushed postnarial portion of skull and separate mediolaterally compressed right half of rostrum

Specimen(s) Used for Scoring: AMNH FR. 30646; PEFO 31218; PEFO 34239

Key References: Stocker (2010); Parker & Martz (2011); McCormack & Parker (2017)

Most Recent Diagnosis: Stocker (2010) identified one autapomorphy for *Pravusuchus hortus* (the 'septomaxilla' forms part of the lateral rim of the external nares) and a unique character combination: 1) Absence of antorbital fossa; 2) broad and rounded interpremaxillary fossa; 3) Alveolar ridges visible in lateral view; 4) Fully crested rostrum; 5) Long posterior process of squamosal; 6) Posterior process of squamosal is greatly dorsoventrally expanded; 7) Possession of a subsidiary opisthotic process of the squamosal; 8) Supratemporal fenestrae partially depressed; 9) Supratemporal fenestrae that are mostly visible in dorsal view.

Comments: In relation to the 'septomaxillary' autapomorphy of *Pravusuchus hortus* Stocker (2010) stated that 'dorsal examination of the narial region shows a possible dorsolateral process of the 'septomaxilla' on the lateral border of the naris'. Upon first-hand examination of the holotype and other specimens I suggest that a lateral extension of the 'septomaxilla' is unlikely; rather, the suture identified by Stocker may represent the lateral border of the paranasal, as described by Hungerbühler *et al*. (2013). As noted in the holotype by Stocker (2010), 'iron oxide covers potential 'septomaxilla'-premaxilla sutures'; however, amongst the iron oxide a distinct groove extends from the anterior narial border, occupying the same position as the 'septomaxillary' suture in most phytosaurs. Therefore, I suggest that *Pravusuchus hortus* is diagnosed using only the unique character combination proposed by Stocker (2010), until the lateral extent of the 'septomaxillae' can be unambiguously verified in additional specimens.

Genus: ***Nicrosaurus*** Fraas, 1866

Type species: *Nicrosaurus kapffi*

Diagnosis: Moderately large genus (maximum skull length c. 900 mm) of Phytosauridae showing the following characters: usually at least a short prenarial crest present; nares below the level of the skull roof, anterior rim of the naris at or somewhat behind the level of the anterior rim of the antorbital fenestra; supratemporal fenestra moderately wide, subrectilinear with rounded anterior margin; descending squamosal processes of the parietals meet in an angle ("inverted V"-shape of previous authors); parieto-squamosal bar depressed below the level of the skull roof for a distance of approximately 20 to 25% of the skull height; postorbitosquamosal bar relatively broad and short, dorsoventrally thin; medial part of the postorbito-squamosal bar overhangs the lateral half of the supratemporal fenestra; vertical component of the squamosal narrow; posterior process of the squamosal moderately long, not continuously tapering in dorsal view; suborbital opening long and slit-like; dentition moderately to strongly heterodont. (Hungerbühler & Hunt, 2000).

Nicrosaurus kapffi (Meyer, 1860)

Age: middle–late Norian (*c.* 216–209 Mya)

Occurrences: Löwenstein Formation (middle Stubensandstein), Middle Keuper Subgroup, Baden-Württemburg, Germany

Holotype: SMNS 4060/4060a, poorly preserved rostral fragment and associated symphyseal-postsymphyseal mandibular fragment, uncat. No. 15, left maxillary and jugal fragment that fits with 4060, SMNS 54708, anterior fragment of left premaxilla (syntype series)

Specimen(s) Used for Scoring: SMNS 4378; SMNS 4379; SMNS 5726; SMNS 5727; NHMUK OR42743

Key References: Meyer (1860, 1861, 1863, 1865); Hungerbühler (1998a); Hungerbühler & Hunt (2000)

Most Recent Diagnosis: Hungerbühler (1998a) presented a unique character combination for *N. kapffi* based largely on characters from Long & Murry (1995) and Ballew (1989). The unique combination is composed of the following two characters: 1) Presence of a continuous prenarial crest reaching just behind the downturned tip of the snout; 2) Top of prenarial crest straight or slightly convex.

Nicrosaurus meyeri Hungerbühler & Hunt (2000)

Age: middle–late Norian (*c.* 216–209 Mya)

Occurrences: Löwenstein Formation (middle Stubensandstein), Middle Keuper Subgroup, Baden-Württemburg, Germany

Holotype: SMNS 12593, dorsoventrally compressed skull in two pieces

Specimen(s) Used for Scoring: SMNS 12593; SMNS 4059; NHMUK OR38038; NHMUK OR42745; GPIT 2070.001

Key References: Meyer (1861); Hunt (1994b); Hungerbühler (1998a); Hungerbühler & Hunt (2000)

Most Recent Diagnosis: Hungerbühler & Hunt (2000) identified *N. meyeri* as a species of *Nicrosaurus*, differentiated from *N. kapffi* on the basis of the following characters: 1) Rostrum slender and gracile; 2) Prenarial crest absent or over posterior part of the snout only; 3) Septomaxilla terminates at the level of the anterior tip of the nasal; 4) Anterior part of the internasal septum may be prominent and visible in lateral view; 5) Sculpture of the pre-orbital

region prominent; 6) Cheek region (quadratojugal + jugal) always with a well developed longitudinal depression; 7) Craniomandibular facet of the quadrate less wide and lateral condyle offset from the cheek; 8) Postorbito-squamosal bar broader; 9) Supratemporal fenestra less wide; 10) In dorsal view the posterior process of the squamosal is continuously broad, the medial rim is angular; 11) Posterior process of the squamosal terminates with a pointed tip; 12) Paroccipital process of the squamosal ('hooklike process') small; 13) Alveolar ridges more prominent, prechoanal part of the vomers mostly slender and tapering; 14) Upper jaw dentition moderately heterodont; 15) Premaxillary teeth set more laterally; 16) Mandibular symphysis equals ~50% of the total mandibular length (rather than 40% as in *Nicrosaurus kapffi*).

Coburgosuchus goeckeli Heller, 1954

Age: middle–late Norian (*c.* 216–209 Mya)

Occurrences: Upper Burgsandstein (lateral equivalent of the Löwenstein Formation), Untersiemau, Baden-Wurttemburg, Germany

Holotype: NMC 15436, postnarial portion of skull

Specimen(s) Used for Scoring: NMC 15436

Key References: Heller (1954)

Most Recent Diagnosis: Heller (1954) originally described this specimen in German; however, since then this taxon has been largely ignored. Heller (1954) diagnosed the genus as a phytosaur of similar size to *Nicrosaurus kapffi*, though differentiated by an even greater development of the squamosals and more laterally oriented orbits.

Comments: As with many other diagnoses, I doubt the utility of orbital orientation as a reliable diagnostic character; however, the substantially more pronounced lateral curvature of

the squamosals does appear to be valid and distinguishes *Coburgosuchus goeckeli* from *Nicrosaurus kapffi*. I am currently preparing a redescription of *Coburgosuchus*, and as such I do not present further diagnostic characters at this time.

Genus: *Machaeroprosopus* Mehl, 1916

Type species: *Machaeroprosopus buceros*

Diagnosis: Differs from all other phytosaurs in possessing the following synapomorphies: strongly developed medial lamella of postorbito-squamosal bar with the supratemporal fenestra reduced to slit (Hungerbühler, 2002: character 19) and visible in dorsal view; rounded top of the parieto-supraoccipital complex (Hungerbühler, 2002: character 24); dorsal portion of squamosals mediolaterally expanded forming a shelf level with the parietal and postorbital; lamina of the squamosal extends onto the paroccipital process forming the ventrolateral border of the posttemporal fenestra (unknown in *Machaeroprosopus jablonskiae*) (Hungerbühler, 2002: character 38). Differs from '*Redondasaurus*' and *Mystriosuchus* in possessing a posttemporal fenestra less than three times wider than high (Hungerbühler, 2002: character 41). Differs from '*Redondasaurus*' in having a supratemporal fenestra that is visible in dorsal view. (Parker & Irmis, 2006).

Comments: The above characters were originally intended to diagnose '*Pseudopalatus*' (Parker & Irmis, 2006); they are used here to diagnose *Machaeroprosopus* as Parker *et al.* (2012) re-erected the genus *Machaeroprosopus* to contain all valid (at the time) members of '*Pseudopalatus*'. Parker *et al.* (2012) do not give a new diagnosis for *Machaeroprosopus* as the taxonomic content of the genus remained the same as '*Pseudopalatus*'.

The genus *Machaeroprosopus* has a long and complex history (Parker *et al.*, 2012), which, during its first 15 years was assigned three species currently referred to *Smilosuchus* (*S. gregorii*, *S. adamanensis* and *S. lithodendrorum*) (Camp, 1930), one species ('*M. andersoni*') variably synonymised with *M. pristinus* (Long & Murry, 1995), another currently referred to the nomen dubium '*Phytosaurus*' ('*Phytosaurus*' *doughtyi*) (Camp, 1930), and '*M.*' *zunii*, which was recently found to occupy a position far outside of Mystriosuchini (Stocker, 2010). Historically, therefore, the diagnosis of the genus has been problematic and was further complicated by the loss of the 'type' specimen (*Machaeroprosopus validus*), rendering the genus invalid. Parker *et al.* (2012) subsequently found *M. validus* to have been incorrectly named as the type species – reinstating the genus with the correct type species (*Machaeroprosopus buceros*).

Although the genus is now well taxonomically defined, lingering traces of its difficult past persist, in the form of tentatively referred specimens in need of proper redescription and phylogenetic testing ('*M.*' *zunii*, '*M. andersoni*', '*M. tenuis*').

'*Machaeroprosopus*' *zunii* Camp, 1930

Age: early Norian (*c.* 225–220 Mya)

Occurrences: Blue Mesa Member, Chinle Formation, Arizona, USA

Holotype: UCMP 27036, partial braincase and postcrania

Specimen(s) Used for Scoring: UCMP 27159

Key References: Camp (1930); Stocker (2010)

Most Recent Diagnosis: Camp (1930) produced a diagnosis of '*M*'. *zunii* based on various referred specimens. Due to the arbitrary referral of many of the specimens (see below) the characters presented may constitute a mosaic from multiple species: 1) Rostrum very long,

slender; 2) Nasals large, extending forward beyond nares and entering dorsal border of antorbital fenestra; 3) Posterior squamosal process very large, broad, flat, and expanded vertically; 4) Parietals small, anterior suture lies well behind posterior border of orbits; 5) Posterior parietal process Y-shaped; 6) Anterior border of supratemporal fenestra very wide and not excavated forward to or nearly to middle of parietals; 7) Postorbito-squamosal bar narrow.

Comments: Camp (1930) presented the holotype of '*M*'. *zunii* as a partial braincase and postcrania, thus containing little to no material of diagnostic utility. However, a number of specimens containing cranial material, such as UCMP 27048, 27189, 27159 were also referred to '*M*'. *zunii*, of which UCMP 27159 was also used in the matrix of Stocker (2010). As the type material is undiagnostic the rest of the referred specimens are referred on the basis of stratigraphic and geographic proximity to the type and should therefore be treated cautiously or altogether excluded. Additionally, inspection of the holotype specimen suggests that the braincase belongs to a smaller individual than the postcrania, and likely belongs to a taxon less derived than basal leptosuchomorph phytosaurs, suggesting that the holotype specimen may also be chimaeric (Axel Hungerbühler, pers. comm. to ASJ, 2018). '*M*'. *zunii* is included here and scored based on only one of Camp's referred specimens. A specimen in the Smithsonian Institute (USNM V17098) is catalogued as '*M*'. *zunii* and appears to share a similar morphology to that of the specimens referred by Camp; I include this specimen as a separate OTU to test the credibility of its referral and this taxon in general, to judge whether it warrants more detailed investigation.

The holotype of '*M.*' *zunii* was previously referred to '*Smilosuchus*' *adamanensis* (Long & Murry, 1995).

Protome batalaria Stocker, 2012

Age: early Norian (*c.* 220–218 Mya)

Occurrences: Upper Lot's Wife beds, Sonsela Member, Chinle Formation, Petrified Forest National Park, Arizona, USA

Holotype: PEFO 34034, pre-narial rostrum with narial fragments, post-narial skull roof with squamosals, basioccipital and left mandible.

Specimen(s) Used for Scoring: PEFO 34034

Key References: Stocker (2012)

Most Recent Diagnosis: Stocker (2012) presented three autapomorphies and a unique character combination for *Protome batalaria*. Due to the length of the unique character combination I only present the autapomorphies here: 1) Presence of a flat ventral surface on the basitubera; 2) Posterior prongs from the exoccipitals dorsal to the foramen magnum; 3) Fossa surrounding the anterior corner of the external mandibular fenestra.

Modified Diagnosis: The unique character combination of Stocker (2012), plus the two autapomorphies: 1) Presence of a flat ventral surface on the basitubera; 2) Fossa surrounding the anterior corner of the external mandibular fenestra.

Comments: Autapomorphies 1 and 3 of Stocker (2012) appear valid; however, the posterior exoccipital prongs mentioned in character 2 appear to also be present in *Coburgosuchus*, but further study is required to verify this. These prongs were also noticed by Hungerbühler *et al.* (2013) in *Machaeroprosopus lottorum* and were identified as the proatlantes; this feature is also present in multiple other specimens referable to *Machaeroprosopus*, '*Redondasaurus*' and potentially other taxa, although a thorough review is required (Axel Hungerbühler, pers. comm. to ASJ, 2018).

‘*Machaeroprosopus*’ *andersoni* Mehl, 1922

Age: late Norian (*c.* 218–208 Mya)

Occurrences: Bull Canyon Formation, Dockum Group, near Santa Rosa, Guadalupe County, New Mexico, USA

Holotype: FMNH UC 396, heavily reconstructed skull

Specimen(s) Used for Scoring: FMNH UC 396

Key References: Mehl (1922); Long & Murry (1995)

Most Recent Diagnosis: Mehl (1922) suggested that ‘*M*’. *andersoni* shares a close affinity with ‘*Machaeroprosopus validus*’ and distinguished it using the following characters: 1) Postero-median border of supra-temporal fenestrae not completely depressed; 2) Anterior border of nares not elevated; 3) Terminal expansion of rostrum gradual; 4) Nasals extending some distance in front of anterior border of nares; 5) Greatest length of maxillae at alveolar margin; 6) Approximately ninety-four teeth in upper dentition; 7) Four large teeth in terminal expansion of rostrum; 8) Alveolae not crowded; 9) Lateral expansion of rostrum at posterior end of premaxillae.

Comments: ‘*M*’. *andersoni* was synonymized with *Machaeroprosopus buceros* by Long & Murry (1995); however, upon inspection of their diagnosis of *Machaeroprosopus buceros* it is clear that many characters are inappropriate for, or are not preserved in the holotype (and only specimen) of ‘*M*’. *andersoni*. Two characters pertain to the squamosals, which are not preserved in ‘*M*’. *andersoni*, three characters are unnecessarily used to describe the same morphology of the pre-narial crest, and the majority of the remaining characters do not distinguish either taxon from many others, even when the characters are taken in combination.

Aside from the problem that the characters of Mehl (1922) may not differentiate ‘*M*’. *andersoni* from all current species of *Machaeroprosopus*, they are also based on comparison

with '*Machaeroprosopus validus*' which has subsequently been lost and also found not to be the type species of *Machaeroprosopus* (Parker *et al.*, 2012). This taxon requires reanalysis and thorough comparison to *Machaeroprosopus buceros* (the valid type species) and other members of *Machaeroprosopus*; however, this is beyond the scope of the current study.

Machaeroprosopus jablonskiae Parker & Irmis, 2006

Age: late Norian (*c.* 218–216 Mya)

Occurrences: Jim Camp Wash beds, Sonsela Member, Chinle Formation, Petrified Forest National Park, Arizona, USA

Holotype: PEFO 31207, skull roof with squamosals

Specimen(s) Used for Scoring: PEFO 31207

Key References: Parker & Irmis (2006); Parker & Martz (2011)

Most Recent Diagnosis: Parker & Irmis (2006) noted a single autapomorphy of *Machaeroprosopus jablonskiae*: Distinct smooth bevelled edge on the antero-medial edge of the postorbito-squamosal bar that forms a supratemporal fossa lateral to the supratemporal fenestra. This feature has subsequently also been identified in *Machaeroprosopus lottorum* (Hungerbühler *et al.*, 2013); however, *Machaeroprosopus lottorum* is distinguishable as the bevelled edge effectively closes the supratemporal fenestra in dorsal view, whereas the fenestra remains visible in *Machaeroprosopus jablonskiae*. Alongside this they presented a unique character combination as follows: 1) Apomorphic characters for *Pseudopalatus* [*Machaeroprosopus*] clade; 2) Squamosal tips that are not knob-like as in *Machaeroprosopus buceros* + *Machaeroprosopus pristinus*; 3) Thin oar-like paroccipital process of the opisthotic that is fused to the internal squamosal process as in *Machaeroprosopus buceros* + *Machaeroprosopus mccauleyi*; 4) Anterior process of the squamosal enters the lateral wall of

the braincase as in *Mystriosuchus westphali* and *S. gregorii*; 5) No lateral groove or ridge on the squamosal; 6) Squamosals are strongly anteroposteriorly shortened.

Machaeroprosopus mccauleyi (Ballew, 1989)

Age: late Norian–early Rhaetian (*c.* 213–207 Mya)

Occurrences: Upper Petrified Forest Member, Chinle Formation, Billings Gap, Apache County, Arizona, USA

Holotype: UCMP 126999, skull missing anterior rostrum, mandibles present

Specimen(s) Used for Scoring: UCMP 126999; PEFO 31219; PEFO 34853

Key References: Ballew (1989); Hunt *et al*. (2006)

Most Recent Diagnosis: Ballew (1989) diagnosed *Machaeroprosopus mccauleyi* based on the following autapomorphies: 1) Squamosal with distinct triangular outline without knob-like process; 2) Lateral portion of opisthotic thin and elongate; 3) Posttemporal fenestra large because of a medial expansion; 4) Basioccipital head relatively large; 5) Basioccipital neck relatively short.

Modified Diagnosis: 1) Squamosal with distinct triangular outline without knob-like process; 2) rostrum is completely crested in lateral view; 3) Ventral expansion of the alveolar rim at the border of the premaxillae and maxillae 4) Pre-infratemporal shelf does not extend under the posterior corner of the antorbital fenestra; 5) Anteroposterior corners of the antorbital fenestra rounded; 6) Anteromedial portion of the supratemporal fenestrae remain visible in dorsal view.

Comments: Characters 2, 3, 4 and 5 of Ballew (1989) do not appear to be different to those in other specimens of *Machaeroprosopus*. Character 1 does appear to be valid, but may be subject to intraspecific variability; PEFO 31219 (referred by Stocker, 2010) does possess a

short, robust terminal knob on the posterior process of the squamosal, though in all other respects greatly resembles UCMP 126999 (the holotype).

Hunt *et al*. (2006) referred three specimens from Bull Canyon, New Mexico to *Machaeroprosopus mccauleyi* and cited three characters which link them to the holotype. Of the three skulls referred, I tentatively accept only one assignment (YPM 3293 [although the considerable robusticity of the specimen in comparison to the holotype complicates assignment]); I consider NMMNHS P-4256 to more likely represent '*Redondasaurus*' *bermani* while NMMNHS P-4239 was not figured and was not examined here. Regardless, the suggested characters are relevant to *Machaeroprosopus mccauleyi* and differentiate this taxon from many other members of *Machaeroprosopus*, albeit not from '*Redondasaurus*' *bermani*. Given the sparsity of robust phylogenetic characters given by Ballew (1989), the character suggestions of Hunt *et al.* (2006) are worth investigating. The first character is the same as character 1 of Ballew (1989), the others are: 2) In posterior view, the lateral margins of the skull flare at about 60°; 3) In lateral view, the rostrum is completely crested (inferred from the gradient of the holotype of *Machaeroprosopus mccauleyi* which lacks the distal rostrum). Character 2 of Hunt *et al*. (2006) is not diagnostic, being present in all robust species of *Machaeroprosopus* and may be prone to taphonomic distortion, and/or ontogenetic changes. Character 3 is useful as no other current species of *Machaeroprosopus* share this character. Neither character 1 of Ballew (1989), nor character 3 of Hunt *et al.* (2006) allow distinction of *Machaeroprosopus mccauleyi* from '*Redondasaurus*' *bermani*; therefore, I suggest four further characters (my characters 3–6) to allow this differentiation.

Machaeroprosopus buceros (Cope, 1881)

Age: late Norian–early Rhaetian (*c.* 213–207 Mya)

Occurrences: Petrified Forest Member, Chinle Formation, Orphan Mesa, New Mexico, USA; Upper Petrified Forest Member, Chinle Formation, Canjilon Quarry, New Mexico, USA; Upper Petrified Forest Member, Chinle Formation, Snyder Quarry, New Mexico, USA; Upper Cooper Canyon Formation, Dockum Group, Garza County, Texas, USA

Holotype: AMNH FR. 2318, poorly preserved skull missing anterior end of rostrum

Specimen(s) Used for Scoring: AMNH FR. 2318; TTU-P 11423; UCMP 34250; NMMNHS-P 39700

Key References: Cope (1881); Ballew (1989); Long & Murry (1995); Lucas *et al.* (2002); Zeigler *et al*. (2003a, b)

Most Recent Diagnosis: Long & Murry (1995) diagnosed *Machaeroprosopus buceros* as a 'heavy-skulled' 'pseudopalatine' with the following combination of characters: 1) Squamosal with posterior process elongated, but deeper and shorter than that of *Pseudopalatus* [*Machaeroprosopus pristinus*], tapering into a blunt apex; 2) Descending process of squamosal large; 3) Rostrum partially crested; 4) Length shorter than posterior portion of skull; 5) Snout does not descend abruptly immediately anterior to external nares; 6) The latter are raised above the level of the skull roof as in *Pseudopalatus* [*Machaeroprosopus pristinus*]; 7) Crest sharp-edged with no sculpturing; 8) Dentition heterodont; 9) Alveoli closely spaced; 10) Enlarged anteriormost teeth and with dagger-like teeth at mid-length of premaxilla; 11) Crest deepest posteriorly.

Modified Diagnosis: In this study, I diagnose *Machaeroprosopus buceros* on the basis of the following unique character combination: 1) Posterior process of the squamosal is elongate and knob-like; 2) Tubular anterior portion of the rostrum has a triangular, rather than semi-circular, cross-section (amended from Ballew [1989] character 56); 3) Rostrum partially crested; 4) Snout does not descend abruptly immediately anterior to external nares.

Comments: Characters 1, 2, 4, 6, 8 and 9 of Long & Murry (1995) present problems; characters 1 and 2 describe morphologies that vary between specimens of *Machaeroprosopus buceros* (AMNH FR. 2318, TTU-P 11423, UCMP 34250). The morphologies described by characters 4 and 6 disagree with the first-hand observations made in this study; with the rostrum measured from the most anterior point of the snout to the anterior border of the nares, no specimens observed here possessed a rostrum shorter in length than the narial + postnarial region of the skull - including even the holotype in which the most anterior section of the snout is lost. As in other species of *Machaeroprosopus* such as *Machaeroprosopus pristinus* and *Machaeroprosopus mccauleyi*, I found no evidence for the nares exceeding the height of the skull roof. Characters 8 and 9 describe features that are common to some extent in many, if not most, leptosuchomorph phytosaurs, and within *Machaeroprosopus* they are shared with *Machaeroprosopus mccauleyi*.

In their revision of North American phytosaurs, Long & Murry (1995) erected the new genus '*Arribasuchus*', referring to it both *Machaeroprosopus buceros* and *Machaeroprosopus mccauleyi*. In a similar manner to their diagnosis of *Smilosuchus* the diagnostic character combination for the genus '*Arribasuchus*' is the same as that for the type species, in this case *Machaeroprosopus buceros*. *Machaeroprosopus mccauleyi* was tentatively retained in '*Arribasuchus*' by Long & Murry (1995), despite characters such as 'rostrum partially crested' being directly inconsistent with the species diagnosis of *Machaeroprosopus mccauleyi* given by Ballew (1989) (also used by Long & Murry to diagnose *Machaeroprosopus mccauleyi*).

Subsequent analyses have suggested that '*Arribasuchus*' is paraphyletic (Hungerbühler, 2002; Hungerbühler *et al*., 2013; Parker & Irmis, 2006), and should be considered a junior synonym of *Machaeroprosopus* (Hungerbühler *et al*., 2013).

Macheroprosopus pristinus (Mehl, 1928)

Age: late Norian–early Rhaetian (*c.* 213–207 Mya)

Occurrences: Chinle Formation, Apache County, Arizona, USA; Upper Petrified Forest Member, Chinle Formation, Canjilon Quarry, New Mexico, USA; Upper Petrified Forest Member, Chinle Formation, Snyder Quarry, New Mexico, USA

Holotype: MU 525, skull with many areas of plaster restoration

Specimen(s) Used for Scoring: MU 525; AMNH FR. 7222; NMMNHS-P 50040; PEFO 382; UCMP 137319; UCMP 27018 ('*Machaeroprosopus tenuis*' holotype)

Key References: Mehl (1928); Long & Murry (1995); Zeigler *et al.* (2002b, 2003a, b)

Most Recent Diagnosis: Stocker (2010) used the following characters to diagnose *Machaeroprosopus pristinus*: 1) Supratemporal fenestrae nearly completely closed in dorsal view by medially expanded postorbital-squamosal bars, and the fenestrae are completely depressed below the level of the skull roof; 2) Squamosal process of the parietals immediately posterior to the main body of the parietals drop ventrally before continuing on to articulate with the parietal processes of the squamosals; 3) The posterior processes of the squamosals are expanded posteriorly as in *Leptosuchus*; however, there is no dorsoventral expansion of this posterior process, which is usually described as 'knob-like' in this taxon.

Modified Diagnosis: I use a combination of characters from Stocker (2010), one modified from Ballew (1989), and other novel characters: 1) Proportionally long rostrum (ratio of pre-narial to narial + post-narial length [measured to the posterior extremity of the parietals] greater than or equal to 2.2); 2) Subtriangular antorbital fenestra; anterior corner is pointed/acutely rounded and posterior border is taller and straight/gently rounded; 3) Rostrum descends immediately anterior to external nares and remains low and tubular for the majority

of its length; 4) Tubular portion of rostrum is semi-circular in cross-section; 5) Weak heterodonty.

Comments: In her phylogenetic analysis, Stocker (2010) did not score *Machaeroprosopus pristinus* using the holotype, and instead used UCMP 27159 and NMMNHS-P 31292. UCMP 27159 is a referred specimen of '*M*'. *zunii* (Camp, 1930) and was used as a referred specimen to phylogenetically score '*M*'. *zunii* in Stocker's analysis; however, Stocker reported the same specimen number as the holotype of *Machaeroprosopus tenuis*, which was referred to, and used to score *Machaeroprosopus pristinus*. I assume this was a typographical error, and that Stocker actually scored and referred UCMP 27018 (actual holotype of '*Machaeroprosopus tenuis'*) to *Machaeroprosopus pristinus*, as UCMP 27159 is clearly different from *Machaeroprosopus pristinus* and UCMP 27018, based both on morphology and preservation. The choice to refer, and use NMMNHS-P 31292 for scoring is puzzling; the skull displays a partial rostral crest which rises above the level of the nares and abruptly descends approximately at the midpoint of the external nares. No other referred specimen of *Machaeroprosopus pristinus* has a rostral crest, and the crest morphology is unknown in any other species of phytosaur. The specimen has previously been referred to *Machaeroprosopus buceros* (Zeigler *et al.*, 2002b), to which *Machaeroprosopus pristinus* was also referred as a junior synonym and may explain the use of NMMNHS-P 31292 to define *Machaeroprosopus pristinus* by Stocker. However, Stocker clearly stated that her analysis would not investigate the synonymy of these species, and in accordance used the proposed junior synonym '*Machaeroprosopus pristinus*' in her analysis, demonstrating that no synonymy was assumed. Furthermore, Zeigler *et al*. (2002b) attributed the unusual crest of NMMNHS-P 31292 to post-mortem deformation; however, upon close study I believe the morphology to be genuine,

which if true, casts uncertainty over the referral of this specimen to any currently known species.

The analysis of Hungerbühler *et al.* (2013) agreed with the hypothesis of these taxa being conspecific, with morphological differences due to sexual dimorphism; however no synapomorphies were given in support of this, and is therefore difficult to interpret. Hungerbühler *et al.* (2013) ultimately decided not to synonymise the taxa and urged against this action without "substantial supporting evidence".

The diagnosis of Stocker (2010) does not allow differentiation of *Machaeroprosopus pristinus* and *Machaeroprosopus buceros*; in my revised diagnosis I therefore highlight that *Machaeroprosopus pristinus* possesses only weak heterodonty, whereas *Machaeroprosopus buceros* is strongly heterodont. This feature, however, is not included in my analysis character matrix.

Machaeroprosopus lottorum Hungerbühler *et al*., 2013

Age: late Norian (*c.* 218–208 Mya)

Occurrences: Upper Cooper Canyon Formation, Dockum Group, Texas, USA

Holotype: TTU-P 10076, skull

Specimen(s) Used for Scoring: TTU-P 10076; TTU-P 10077

Key References: Hungerbühler *et al*. (2013)

Most Recent Diagnosis: Hungerbühler *et al*. (2013) diagnosed *Machaeroprosopus lottorum* with the following characters: 1) Lateral rim of the naris broad, flat and rugose; 2) Supratemporal fenestra fully closed in dorsal aspect, forming a shallow semi-circular indentation into the skull roof, with a strongly bevelled rim that continues onto the parietal; 3) Free section of the postorbital/squamosal bar short; 4) Strongly developed horizontal medial

laminae of palatines, that almost close the posterior section of the palatal vault in ventral view.

Modified Diagnosis: 1) Lateral rim of the naris broad, flat and rugose; 2) Supratemporal fenestra fully closed in dorsal aspect, forming a shallow semi-circular indentation into the skull roof, with a strongly bevelled rim that continues onto the parietal; 3) Strongly developed horizontal medial laminae of palatines, that almost close the posterior section of the palatal vault in ventral view.

Comments: I generally agree with the characters proposed by Hungerbühler *et al*. (2013), with the exception of their character 3. In TTU-P 10076 character 3 holds true i.e. the free section of postorbital/squamosal bar is proportionately shorter than in almost all other phytosaur specimens studied. However, in TTU-P 10077 the length of the free section of postorbital/squamosal bar is greater than in some specimens of *Machaeroprosopus pristinus* (UCMP 34249, 27231, 34228) including the holotype (MU 525), but shorter than other referred specimens (NMMNHS P-50040; PEFO 382; AMNH FR 7222); this character is also shorter in the majority of specimens of *Mystriosuchus planirostris*. This suggests the feature may be more variable than previously realized in *Machaeroprosopus lottorum* and is therefore removed from the diagnosis.

Genus: '*Redondasaurus*' Hunt & Lucas, 1993

Type species: '*Redondasaurus*' *gregorii*

Diagnosis: Parasuchid that differs from all other members of the family in having supratemporal fenestrae concealed in dorsal view, reduced antorbital fenestrae, a prominent pre-infratemporal shelf at the anteroventral margin of the lateral temporal fenestra,

septomaxillae that wrap around the outer margin of the external narial opening, a thickened orbital margin, an inflated posterior nasal behind the external narial opening and thickened dorsal osteoderms. (Spielmann & Lucas, 2012).

'*Redondasaurus*' *gregorii* Hunt & Lucas, 1993

Age: Rhaetian (*c.* 208.5–201.3 Mya)

Occurrences: Redonda Formation, Dockum Group, Shark Tooth Hill, Quay County, New Mexico, USA

Holotype: YPM 3294, poorly preserved and compressed skull missing left quadrate area, dorsal narial area and tip of rostrum

Specimen(s) Used for Scoring: YPM 3294

Key References: Gregory (1972); Hunt & Lucas (1993); Hungerbühler *et al*. (2013)

Most Recent Diagnosis: Spielmann & Lucas (2012) built on the original diagnosis of Hunt & Lucas (1993) and diagnosed *Redondasaurus gregorii* using the following character combination: 1) Supratemporal fenestrae concealed in dorsal view; 2) Reduced antorbital fenestrae; 3) A prominent pre-infratemporal shelf at the anteroventral margin of the lateral temporal fenestra; 4) Septomaxillae that wrap around the outer margin of the external narial opening; 5) A thickened orbital margin; 6) An inflated posterior nasal behind the external narial opening; 7) Thickened dorsal osteoderms.

Modified Diagnosis: I retain most of the characters proposed by Spielmann & Lucas (2012) but reword them for more precise interpretation: 1) Supratemporal fenestrae concealed in dorsal view; 2) Antorbital fenestra with a distinct sharp corner at the anterior-most and posterior-most extremities; 3) Pre-infratemporal shelf projects anteriorly as a lobe reaching beneath the posterior corner of the antorbital fenestra, and dorsally joins with a ventrally

descending flange of the postorbital; 4) Posterior border of the orbit equal to- or thicker than the dorsoventrally thinnest part of the posterior process of the jugal; 5) An inflated posterior nasal behind the external narial opening; 6) Postorbital/squamosal bars wide; 7) Thickened dorsal osteoderms.

Comments: I find issues with characters 2 and 4 of the diagnosis of Spielmann & Lucas (2012). The reduction of the antorbital fenestra in '*Redondasaurus*' appears to be subjective based on the relative size of the antorbital fenestra when compared to the robusticity and size of the skull. In large specimens such as NMMNHS P-4256 and NMMNH P-31094 that have previously been referred to '*Redondasaurus*', the antorbital fenestra appears small; however, in the holotype of '*Redondasaurus*' *gregorii* (YPM 3294) the antorbital fenestra appears of similar proportions relative to the skull as in other phytosaurs such as *Mystriosuchus planirostris* or *Machaeroprosopus pristinus*. I suggest instead that the shape of the antorbital fenestra is unique in '*Redondasaurus*' as both its anterior and posterior apices are sharp, rather than rounded; the antorbital fenestra only appears to be relatively small in specimens of '*Redondasaurus*' *bermani* and is therefore used as a character for that species only. Although this is a generic feature of '*Redondasaurus*' it is retained in this species diagnosis in case '*Redondasaurus*' is synonymized with *Machaeroprosopus.* In such a scenario this character would be useful as part of a character combination to differentiate the species from almost all other members of the genus. I find no evidence for 'septomaxillae' that wrap around to the lateral side of the nares; Stocker (2010) found this feature to be present in both '*Redondasaurus*' and *Pravusuchus hortus*; however, in the holotype of the latter this area is covered with iron oxide and may actually be the paranasal suture, which was identified in *Machaeroprosopus lottorum* by Hungerbühler *et al.* (2013). Given the phylogenetic proximity of *Machaeroprosopus lottorum* and '*Redondasaurus*' it is likely that the feature described in

‘*Redondasaurus*’ may also be the paranasal; as the feature is currently ambiguous it is excluded from the diagnosis given here.

The holotype of ‘*R.*’ *gregorii* has previously been referred to *Machaeroprosopus pristinus* (Long & Murry, 1995).

‘*Redondasaurus*’ *bermani* Hunt & Lucas, 1993

Age: Rhaetian (*c.* 208.5–201.3 Mya)

Occurrences: ‘siltstone member’, Chinle Formation, *Coelophysis* Quarry, New Mexico, USA

Holotype: CMNH 69727, skull

Specimen(s) Used for Scoring: NMMNHS-P 4983

Key References: Hunt & Lucas (1993); Hunt *et al.* (2006); Hungerbühler (2002); Hungerbühler *et al.* (2013)

Most Recent Diagnosis: Hunt & Lucas (1993) diagnosed ‘*Redondasaurus*’ *bermani* as a ‘*Redondasaurus* species that differs from others in possessing a rostrum with a partial crest’.

Modified Diagnosis: A species of ‘*Redondasaurus*’ with the following characters: 1) Full rostral crest extending from nares to the terminal rosette of the premaxilla; 2) Antorbital fenestra reduced in size relative to other taxa of similar size and robuusticity; 3) Length of the symphyseal portion of the mandible approximately half that of the post-symphyseal region.

Comments: ‘*Redondasaurus*’ *bermani* was synonymized with *Machaeroprosopus buceros* by Long & Murry (1995) as mentioned above, and was also synonymized with ‘*Redondasaurus*’ *gregorii* by Spielmann & Lucas (2012) who concluded that it was the male sexual dimorph. Due to the lack of evidence for synonymy I tentatively retain ‘*Redondasaurus*’ *bermani* as a distinct species, but a thorough re-description of the species would be of great benefit.

Hungerbühler (2002) used a silhouette of NMMNHS-P 4256 in their phylogeny to denote '*Redondasaurus*' *bermani*, but referred to as 'NMMNHS-P 5246'. This appears to be a typographical mistake. NMMNHS-P 4256 is included as a separate OTU to '*Redondasaurus*' in this study so its affinities can be tested.

The holotype of '*R.*' *bermani* has previously been referred to *Machaeroprosopus buceros* (Ballew, 1989).

Genus: *Mystriosuchus* Fraas, 1896

Type species: *Mystriosuchus planirostris*

Diagnosis: "Rostrum strongly elongated, ratio of rostral to narial plus postnarial length exceeds 2´2; interpremaxillary fossa reduced to a slit in the anterior part of the premaxilla; deep sculpture of the skull roof and the narial region; presence of a pre-orbital depression; anterior border of the supratemporal fenestra raised; dorsoventrally thick posterior section of the parieto-squamosal bar with a triangular crosssection; sharp lateral ridge of the squamosal; posterior process of the squamosal reduced; posttemporal fenestra strongly reduced" (Hungerbühler, 2002).

Mystriosuchus westphali (Hungerbühler & Hunt 2000)

Age: middle–late Norian (*c.* 216–209 Mya)

Occurrences: Löwenstein Formation (middle Stubensandstein), Middle Keuper Subgroup, Baden-Württemburg, Germany

Holotype: GPIT 261/001, skull with left side slightly distorted

Specimen(s) Used for Scoring: GPIT 261/001; AMNH 10644

Key References: Huene (1909; 1911); Hungerbühler (1998a; 2002); Hungerbühler & Hunt (2000)

Most Recent Diagnosis: Hungerbühler (2002) listed eight autapomorphies for *Mystriosuchus westphali* as follows: 1) Discrete snout crest at midlength of the premaxillae; 2) Semicylindrical alveolar ridges; 3) Posterior process of the squamosal absent; 4) Squamosal contacts the prootic anteriorly; 5) Supraoccipital reaches the post-temporal fenestra and borders its dorsomedial half; 6) Lobate extension of the vertically descending squamosal process of the parietal; 7) Post-temporal fenestra is reduced to a narrow slit; 8) Presence of a discrete ossification (orbitosphenoid) anterior to the laterosphenoid.

Modified Diagnosis: 1) Discrete snout crest at midlength of the premaxillae; 2) Squamosal contacts the prootic anteriorly; 3) Supraoccipital reaches the post-temporal fenestra and borders its dorsomedial half; 4) Post-temporal fenestra is reduced to a narrow slit; 5) Presence of a discrete ossification (orbitosphenoid) anterior to the laterosphenoid; 6) A sharp corner of bone extends into the antorbital fenestra at approximately the midpoint of the posterior border, giving the posterior border a ‘stepped’ appearance.

Comments: Based on subsequent analyses and first-hand examination of specimens, I exclude characters 2, 3 and 6 of Hungerbühler (2002) from this diagnosis. Character 2 is present in almost all phytosaurs; characters 3 and 6 are both observed in the holotype of *Mystriosuchus westphali*. However, a specimen found in the collections of the AMNH (AMNH 10644), which is referable to *Mystriosuchus westphali* (as a species of *Mystriosuchus* that possesses a distinct sharp crest at the midlength of the premaxilla and lacks the abrupt concave rise of the rostrum into a narial crest), differs in displaying neither of these states. In AMNH 10644 the posterior process of the squamosal shares the same morphology as *Mystriosuchus planirostris* and the ‘lobate extensions’ on the squamosal process of the

parietal are absent. Furthermore, these lobate extensions have been found in an indeterminate specimen of *Machaeroprosopus* (either *Machaeroprosopus pristinus*, *Machaeroprosopus buceros* or *Machaeroprosopus lottorum*) by Hungerbühler *et al*. (2013), but not in any others, suggesting this state is likely intraspecifically variable in multiple taxa. A further character, relating to the antorbital fenestra, is added which is found in both the holotype and AMNH 10644 but in no specimens of *Mystriosuchus planirostris*.

Mystriosuchus planirostris (Meyer, 1863)

Age: middle–late Norian (*c.* 216–209 Mya)

Occurrences: Löwenstein Formation (middle Stubensandstein), Middle Keuper Subgroup, Baden-Württemburg, Germany; Zorzino Limestone, Lombardy, Italy

Holotype: MCZ 1018, fragment of right pre-orbital (lectotype); MCZ 1019A, 1019B, 1019C; MCZ 1022A, 1022B, rostral and skull fragments, partial caudal centrum (paralectotypes)

Specimen(s) Used for Scoring: SMNS 10260; SMNS 9900; SMNS 9134; SMNS 13240; SMNS 91574

Key References: Meyer (1863); Fraas (1896); Hungerbühler (1998a; 2002); Hungerbühler & Hunt (2000)

Most Recent Diagnosis: Hungerbühler (2002) listed six autapomorphic characters to distinguish *Mystriosuchus westphali* from *Mystriosuchus planirostris*: 1) The rostrum is extremely elongated; 2) A subvertical slope results in a concave profile of the prenarial area from side to side; 3) The external nasal opening is subdivided into a posterior section facing dorsally, and a strongly inclined anterior section that opens anteriorly; 4) The raised anterior border of the supratemporal fenestra extends along the medial rim of the squamosal; 5) The

parieto-squamosal bar is depressed by more than 30 per cent of the skull height; 6) A larger quadrate foramen is present in a round recess formed by quadratojugal and quadrate.

Comments: Hungerbühler (2002) provided a detailed and useful discussion of characters previously used to diagnose *Mystriosuchus planirostris*, giving reasons why they should now be excluded.

Specimen-level OTUs

NMMNHS-P 4781

Age: early Norian (*c.* 225–218 Mya)

Occurrence: Los Esteros Member, Santa Rosa Formation, Santa Fe County, New Mexico, USA

Notes: This specimen consists of the right orbital plus postorbital region of a skull, though lacking any of the interior or posterior elements such as the braincase, occipitals or palatines. Hunt *et al.* (1993) assigned this specimen to *Angistorhinus* sp. based on a combination of features: 1) Supratemporal fenestrae at the level of the skull roof; 2) Squamosals project posteriorly; 3) Squamosal process (parietal/squamosal bar) is rounded.

This specimen was included in order to test its phylogenetic affinities with *Angistorhinus*, as the specimen was found in younger rocks (early Norian [225–218 Mya]) than all other *Angistorhinus* specimens included here (Carnian to early Norian [232–225 Mya]). Furthermore, very few specimens potentially referable to *Angistorhinus* have previously been included in phylogenetic analyses of Phytosauria, therefore more '*Angistorhinus*' specimens are included more generally in this study, to assist in future research in producing a more well defined character diagnosis for the genus.

TMM 31100-1332

Age: late Carnian–early Norian (*c.* 232–225 Mya)

Occurrence: 'Otis Chalk Quarry 3', Colorado City Formation, Dockum Group, Howard County, Texas, USA

Notes: Stocker (2013) mentioned this specimen in reference to '*Angistorhinus*-like specimens from the Otis Chalk localities'. The specimen consists of a complete cranium, infilled with sediment, though lacking an associated mandible. Although the surface preservation is relatively good, there are many cracks through the skull, which cause slight displacements in areas such as the rostrum. The temporal region of the skull is slightly compressed dorsoventrally, causing the squamosal posterior processes and parietal/squamosal bars to curve posteroventrally.

This specimen was included in this analysis to test its affinities with *Angistorhinus* as suggested by Stocker (2013) and, as above, to better characterise the genus.

USNM v 21376

Age: late Carnian–early Norian (*c.* 232–225 Mya)

Occurrence: Base of the Dockum Group, three miles North of Otis Chalk, Howard County, Texas, USA

Notes: This specimen was figured in lateral view by Stocker & Butler (2013) (Figure 5d), as an example of the genus *Angistorhinus*. The preorbital portion of the specimen is preserved, as is an area of skull roof including the prefrontals, frontals and the anterior parts of the postfrontals and parietals. The posterior processes of the squamosals are also preserved, as is the occipital condyle and ventral parts of the quadrates; however almost all of the postorbitals,

jugals, quadratojugals and anterior and ventral parts of the squamosals are modelled with plaster. Due to the plaster reconstruction, the orientation of the supratemporal fenestrae is incorrect; the proximal remnants of the parietal/squamosal bars preserved on the squamosals have been aligned with the reconstructed postorbital/squamosal bars, whilst the parietal/squamosal bars are reconstructed entirely from plaster mimicking the depressed temporal morphology of *Mystriosuchus* or *Machaeroprosopus*. The specimen also preserves the symphysial region of the mandible, the anterior portions of the two rami including approximately the anterior third of the mandibular fenestra, and part of the left articular and retroarticular process. The nares appear to be elevated well above the level of the skull roof, although their posterior extremity appears to be damaged and the skull roof may be slightly crushed. The specimen may also be slightly mediolaterally compressed.

Like the above specimens, this was included to test its affinities to *Angistorhinus* and to better characterise the genus.

PEFO 34852

Age: early Norian (*c.* 225–220 Mya)

Occurrence: Blue Mesa Member, Chinle Formation, Petrified Forest National Park, Arizona, USA

Notes: This specimen consists of a complete cranium which has been crushed laterally at an oblique angle such that the external elements of the left half of the skull retain their original morphology, whereas the right half is strongly dorsoventrally compressed.

Griffin *et al*. (2017) referred this specimen to *Smilosuchus adamanensis* based on the following characters from the matrix of Kammerer *et al*. (2015): 1) An antorbital fossa is absent (3-3); 2) A rostral crest is present but not continuous (18-1); 3) The interorbital-nasal

area is concave (21-1); 4) There is a moderate posterior process of the squamosal (24-1); 5) The posterior process of the squamosal is expanded in lateral view, but not rounded (25-1); 6) The squamosal fossa extends to the posterior edge of the squamosal (30-0); 7) The supratemporal fenestrae are partially depressed (32-1); 8) The supratemporal fenestrae are mostly visible in dorsal view (33-1).

However, upon first-hand comparison of these character scorings with the holotype of *S. adamanensis* and specimens of other non-Mystriosuchini leptosuchomorph taxa, I find that all the above character scorings, aside from number 5, may equally refer to *Leptosuchus crosbiensis.* Furthermore, I find that the score for character 2 does not reflect the rostral morphology of either the holotype of *S. adamanensis* or my referred specimen UCMP 170166; in both specimens there is no evidence of any rostral crest, i.e. the rostrum forms an unbroken, straight slope from the posterior border of the nares to the premaxillae, whereupon the rostrum becomes tubular. However, in PEFO 34852, previously referred specimens of *L. crosbiensis* (USNM 15481, TMM 31173-120, TTU-P 09230), the holotype of *L. crosbiensis* (subtly) and the holotype of *Leptosuchus studeri* (the sister taxon to *L. crosbiensis* in the analysis of Stocker (2010)), the narial openings extend horizontally from their posterior border, and directly anterior to the nares the rostrum either continues horizontally or slopes slightly ventrally, before dipping more strongly ventrally and levelling out to form a tubular rostrum. Therefore, from the characters presented it is unclear whether this specimen actually represents *S. adamanensis*; for this reason I include the specimen here as a separate OTU so its affinities can be tested phylogenetically.

NMMNHS-P 4256

Age: late Norian (*c.* 218–208 Mya)

Occurrence: lower Bull Canyon Formation, Dockum Group, Barranca Badlands, Quay County, New Mexico, USA

Notes: This specimen consists of a large skull, missing the majority of its right postnarial region, the entire palate and the posterior section of the right mandibular ramus. Similarly to PEFO 34852, the skull has been compressed at an oblique dorsolateral angle leaving the left half relatively free from deformation, whilst the right half is strongly compressed and sheared dorsally.

According to Heckert *et al.* (2001) this specimen was originally referenced in the PhD thesis of Hunt (1994a) as a 'robust morph' of '*Redondasaurus*' *gregorii*. Subsequently it was used in the phylogeny of Hungerbühler (2002) to exemplify '*Redondasaurus*' *bermani*, rather than the (at the time) unnumbered Carnegie Museum specimen assigned as the holotype of '*Redondasaurus*' *bermani* by Hunt & Lucas (1993) (CMNH 69727). Hunt *et al.* (2006) then referred this specimen to *Machaeroprosopus mccauleyi*, as a male sexual dimorph of the species due to the difference in skull size and rostral robusticity between this specimen and the holotype of *Machaeroprosopus mccauleyi.* Their species referral was based on three characters: 1) Posterior squamosal process is sub-triangular and lacks a knob-like termination; 2) In posterior view, the lateral margins of the skull flare at about 60 degrees; 3) In lateral view the rostrum is completely crested. All of these characters (regardless of their legitimacy or usefulness) can also be found in '*Redondasaurus*' *bermani*; however, Hunt *et al.* also based their identification on an assumption that two species of 'brachyrostral' phytosaurs were unlikely to have occurred simultaneously geographically and temporally. As detailed earlier, the genus '*Redondasaurus*' was redefined by Spielmann & Lucas (2012), and more diagnostic characters were added; again, disregarding the legitimacy of these characters, many of them

are applicable to NMMNHS-P 4256, suggesting the need for the placement of this specimen to be tested more thoroughly.

USNM v 17098

Age: early Norian (*c.* 221–219 Mya)

Occurrence: ?Bluewater Creek Member, Chinle Formation, Apache County, Arizona, USA

Notes: USNM v 17098 is a poorly preserved partial skull and mandible that are dorsoventrally compressed. The skull lacks most of the left lateral postnarial elements, though preserves much of the right half, the palate and braincase. The mandible is largely complete, though aspects are fragmentary and lacks the anterior-most portion of the terminal rosette.

This specimen was referred to *Leptosuchus* sp. by Long & Murry (1995) and again by Heckert & Lucas (2003); however, the label with the specimen identifies it as *Machaeroprosopus zunii*, though no justification has been provided for any of these three identifications. By scoring this specimen phylogenetically it may be possible to more definitively constrain its position and investigate whether the specimen can legitimately be referred to '*M.*' *zunii*, and simultaneously find whether this specimen adds support to the case for '*M.*' *zunii* being considered a legitimate taxon.

NMMNHS-P 31094

Age: Rhaetian (*c.* 208.5–201.3 Mya)

Occurrence: Redonda Formation, Dockum Group, Apache Canyon, Quay County, New Mexico, USA

Notes: This specimen consists of an extremely robust cranium, missing the majority of the premaxillae and the anterior extremities of the maxillae. The skull is slightly dorsoventrally

crushed and slightly sheared. Heckert *et al.* (2001) provided a short description of the skull, referring the specimen to '*Redondasaurus*' sp. on the basis of comparisons with other taxa, which I summarize as four characters: 1) Supratemporal fenestrae that are depressed and concealed in dorsal view; 2) Antorbital fenestra 'tiny' relative to narial length; 3) Postorbital/squamosal bars are anteroposteriorly short; 4) Postorbital/squamosal bars are broad.

I include this specimen to test its referral to the genus '*Redondasaurus*', and as an additional '*Redondasaurus*' OTU, it may help to elucidate whether the genus is monophyletic or not.

MB.R. 2747

Age: Rhaetian (*c.* 208.5–201.3 Mya)

Occurrence: lower Exter Formation, near Salzgitter, Lower Saxony, Germany

Notes: MB.R. 2747 represents the largest phytosaur specimen found in Europe, and consists of a strongly deformed skull preserved in 11 articulating and non-articulating fragments, a partial mandible preserved in four articulating fragments, multiple vertebrae and centra, partial scapulae and coracoids, a humerus, and a set of articulated osteoderms. The skull retains the majority of the rostrum up to the anterior corner of the antorbital fenestrae, the posterior process of the right maxilla and the main bodies of the left and right jugals with the anterior corners of the lateral temporal fenestrae, a postnarial portion of the skull roof including a section of the posterior narial border and a dorsal part of the right orbital rim, a relatively complete, but crushed, braincase with dorsal portions of the parietals preserved and a fragment of the left postorbital/squamosal bar. The mandible consists of a short posterior section of the symphysis, from which the two rami bifurcate; the left ramus extends

posteriorly such that part of the mandibular fenestra is preserved, whilst the right ramus does not extend as far as the beginning of the fenestra. The surface preservation of the material is generally good, but is extensively fractured making sutures difficult to discern.

This specimen was originally described by von Huene (1922) and was referred to the species '*Angistorhinopsis ruetimeyeri*'. This referral was based entirely on stratigraphic age and the size of the specimen, as the holotype of '*A. ruetimeyeri*' consists of a partial phytosaur basioccipital, mandibular and postcranial fragments from a bonebed in Switzerland - none of which are diagnostic. The taxon '*A. ruetimeyeri*' is therefore a nomen dubium; furthermore, MB.R. 2747 has never before been included in a phylogenetic analysis of phytosaurs. Its inclusion here will therefore provide a phylogenetic placement that may be useful in any future redescription of the specimen.

NHMW 1986 0024 0001

Age: middle–late Norian (*c.* 216–209 Mya)

Occurrence: Dachsteinkalk, Totes Gebirge, Styria, Austria

Notes: This specimen is an undescribed right half of a phytosaur skull from Austria, with a possibly associated partial mandible and ilium, that was referred to *Mystriosuchus planirostris* by Buffetaut (1993). Aside from the anterior tip of the snout and the quadratojugal, the half skull is relatively complete and well preserved with some sutures discernible; however, it may be somewhat mediolaterally compressed. The mandible is more poorly preserved; its dorsal surface is heavily weathered and the posterior half of the left ramus is missing, although the ventral surface is retained, allowing a more accurate estimate of skull length. Approximately the posterior quarter of the right ramus is missing. Similarly to MB.R. 2747, this specimen

has never before been analysed phylogenetically, and its inclusion may assist future descriptive work.

S1.2. *Character list*

It is important to note here that when incorporating continuous and geometric morphometric character scorings for analysis, the format of the TNT data file requires these characters to be presented first in the file. This differs from how the characters are ordered in the character list below. My character list presents characters in the order in which they occur for the base discrete matrix; where a character possesses a continuous or GM variant this is flagged next to that character, as indicated below. It should also be noted that characters in a TNT file begin at zero, whereas I shift my characters such that the list begins at one.

[NEW] Character was devised for this study, rather than being modified or taken from a previous study

*** Character possesses a corresponding continuous variant**

† Character possesses a corresponding/partially corresponding GM variant

1) Anterior end of premaxillae [from Stocker 2010, character 7]

0: In anteroposterior plane of posterior rostrum

1: downturned

Although the distal terminus of the rostrum is downturned in all phytosaurs, in some such as *Parasuchus* and some specimens of *Machaeroprosopus pristinus*, there is dorsoventral constriction of the rostrum just posterior to the terminal rosette subsequent to which the rostrum deepens again such that the ventral edge is approximately level with the downturned anterior tip.

2) Interpremaxillary fossa [Hungerbühler 2002, character 43; Stocker 2010, character 8]

0: Absent

1: Present, broad and rounded

2: Present, narrow slit

Only species of *Mystriosuchus* display a narrow, slit-like fossa between the alveolar ridges; all other phytosaurs possess a broadly rounded fossa.

3) Alveolar ridges [modified from Stocker 2010, character 9]

0: Continuously visible in lateral view

1: Inconsistently visible, or entirely hidden in lateral view

Modified such that the state differences reflect the development of any kind of ventral overhang of the ventral rostral margin, rather than separating only those taxa in which such a ventral overhang is complete from those that display either an intermediate state or no overhang.

4) Ventral alveolar bulge between premaxilla and maxilla [modified from Hungerbühler *et al.* 2013, character 2]

0: Absent

1: Present

Wording modified for clarity. This ventral bulge of the tooth-row is consistently visible in *Smilosuchus gregorii* and most robust members of *Machaeroprosopus*. In some other taxa such as

Smilosuchus lithodendrorum, *Pravusuchus hortus* and '*Redondasaurus*' *gregorii* the bulge is not present in all specimens.

5) Alveolar rim of maxilla [modified from Hungerbühler 2002, character 3; Stocker 2010, character 10]

0: Horizontal or subconvex

1: Strongly ventrally convex

Wording altered slightly for clarity.

6) Premaxillary crest [modified from Hungerbühler 2002, character 48]

0: Absent

1: Present, rounded

2: Present, sharp

In the majority of phytosaurs an isolated premaxillary crest is absent, however *Mystriosuchus westphali* possesses a premaxillary crest with a sharp dorsal edge, giving the rostrum a more triangular coronal cross-section through the crest. *Leptosuchus studeri* and *crosbiensis* both also display an isolated premaxillary crest, however the dorsal edge is rounded, maintaining a curved dorsal profile in cross-section. This character is modified here to account for the different crest morphologies.

7) Rostral crest [modified from Stocker 2010, characters 17, 18, 19]

0: Absent

1: Narial crest a relatively abrupt rise to the nares interrupting a straight profile from rostrum to orbit

2: A straight steep slope from the nares to the premaxilla

3: Extends horizontally level from the nares for the majority of the crest with a terminal anterior slope

4: Extends horizontally level from nares for less than half the rostral length then descends and becomes tubular

This character was previously three separate characters, the first of which pertained to the morphology of the premaxilla, while the subsequent two scored the presence or absence of a 'rostral crest' and its morphology. Putting aside disputes over the cladistic usefulness of crest characters, these characters appear to overlap, risking artificial inflation of the influence of some traits. From the character state descriptions in the second and third characters, the 'rostral crest' appears to refer to the crest across both the premaxilla and maxilla. State zero of the first character (premaxilla dorsoventrally taller than mediolaterally wide) therefore directly overlaps with the second state of the next character (presence of a rostral crest). State one of the first character (tube-like morphology of the premaxilla) does not completely correlate with state zero of the next character (absence of rostral crest - rostrum tube-like for entire length) as morphologies exist (e.g. *Leptosuchus crosbiensis* and *studeri*) where the premaxilla is slender, but rises into a crest posterior to its contact with the maxilla; this would be described by a combination of state one in the first character, and state zero in the second. This morphology is, however, given a distinct state of its own in the third character: state zero (rostral crest partial or undulating from nares to terminal rosette); this state correlates exactly with a combination of states of the previous two characters. Furthermore, the third character is only applicable to taxa with rostral crests; un-crested taxa must therefore be scored as inapplicable which is treated as uncertainties during character optimization, resulting in their morphologies being 'estimated' for a trait they do not possess. Here I present a multi-state combination of the previously used characters, in which states are mutually exclusive and that is applicable to all taxa. An example of character state one is the abrupt rise to the nares in *Mystriosuchus planirostris*; state two is exemplified by *Smilosuchus gregorii*; state three is autapomorphic for *Nicrosaurus kapffi* and state four applies to taxa such as *Leptosuchus crosbiensis* and *studeri*.

*** [ORDERED] 8) Transverse width of the rostrum between the antorbital fenestrae in dorsal view [modified from Butler *et al.* 2014, character 46]**

0: Less than or equal to 1.20

1: 1.21 to 1.59

2: Greater than or equal to 1.60

States are here modified to represent the greater range of morphologies measured in this study. Measured as the ratio of the width of the rostrum between the antorbital fenestrae at their midpoint, and the interorbital distance at its shortest point. State zero corresponds to a narrow width, state one to moderate, and state two to a large width.

9) Suture between maxilla, premaxilla and nasal [from Hungerbühler 2002, character 2]

0: Slopes anteroventrally

1: Dorsally convex lobe

10) Posterior portion of maxilla lateral outline in dorsal view [from Hungerbühler 2002, character 4]

0: Straight/subconcave

1: Convex

*** [ORDERED] 11) Ratio of rostral to narial plus post narial length [modified from Hungerbühler 2002, character 1; Stocker 2010, character 14]**

0: Less than or equal to 1.50

1: 1.51 to 1.99

2: Greater than or equal to 2.00

In previous analyses this character used the pre-orbital and orbital + post-orbital lengths; however, orbital + post-orbital length was measured to the posterior process of the squamosal - the morphology of which is highly variable, and the subject of a number of other characters in their matrices. To avoid mixing the signal of this character with those of characters pertaining to the squamosal, I use the posterior extremity of the parietals as my posterior measuring point. The nares are used here rather than the orbits as phylogenetic signal is either unclear or lost when pre-orbital length is compared to the orbital + postorbital length to the posterior tip of the parietals. This suggests that much of the signal previously found in this character may be linked to variation in the squamosals, combined with rostral variation. The position of the nares does shift between phytosaurs belonging to, and excluded from Mystriosuchinae and thus presents a partial correlation with one other character pertaining to this change in position. However this is here judged to be a more favourable option than correlation with the squamosals, which are far more variable than the position of the nares, are the subject of more characters and have traditionally been used as one of the main diagnostic features for different groups of phytosaurs.

12) Narial openings [from Hungerbühler 2002, character 50]

0: Dorsally or anterodorsally

1: Anterior section opens forward, posterior upward

13) Narial openings B [from Sereno 1991, character P; Stocker 2010, character 1]

0: Directed laterally

1: Directed dorsally

[ORDERED] 14) Position of nares [from Hungerbühler 2002, character 10; Stocker 2010, character 2]

0: Terminal

1: Non-terminal, posterior rim of nares in front of anterior rim of antorbital fenestra

2: Non-terminal, posterior rim of nares behind anterior rim of antorbital fenestra

15) Anterior extent of septomaxillae [from Stocker 2010, character 12]

0: Anterior to anterior tip of nasal

1: Posterior to or at level with anterior tip of nasal

16) Narial outlets [from Hungerbühler *et al.* 2013, character 10]

0: Absent

1: Present

This character refers to grooves exiting the anterior extremity of the external nares, often resulting from the anterior convergence of the lateral narial borders. Narial outlets are almost entirely pervasive throughout non-leptosuchomorph phytosaurs, but only occur in a handful of more derived taxa; specifically in *Machaeroprosopus lottorum* and some specimens of *Nicrosaurus meyeri*, *Mystriosuchus planirostris* and *westphali* and *Machaeroprosopus pristinus*.

17) Dorsal rim of nares [from Hungerbühler 2002, character 9; Stocker 2010, character 20]

0: At or below level of skull roof

1: Above level of skull roof

18) Narial wing [from Hungerbühler *et al.* 2013, character 11]

0: Present

1: Absent, narial opening closed anteriorly

State zero refers to a raised lateral rim of the external nares, which descends prior to the anterior border of the nares, often abruptly, leaving a roughly 90 degree corner at the anterodorsal point of the lateral narial rim, exemplified in *Mystriosuchus planirostris*.

19) Interorbital nasal area lateral view [modified from Hungerbühler 2002, character 14; Stocker 2010, character 21]

0: Flat from orbit to nares

1: Posterior border of nares and anterior border of orbits dip down into a concavity

This character and the subsequent one were previously a single character, describing the morphology of the interorbital-nasal area. However the original description of the character and its states are confusing: 'Interorbitonasal area: flat (0); convex (1). The area between the nares and the orbits is primitively flat and broad. In derived phytosaurs, the area is narrower, transversely round, and saddle-shaped because of the elevation of the nares and the orbital rims.' Hungerbühler (2002). The character initially appears to be describing only the transverse profile of the interorbital-narial area, however at

the end the phrase ‘saddle-shaped’ is used in relation to the concavity seen in some phytosaurs in lateral view caused by the raised posterior border of the nares and anterior border of the orbits. This suggests the character should be aimed at describing the full three-dimensional morphology of the area, however this laterally visible morphology is not represented in the character states. The character is split here, in order to allow representation of both the laterally visible profile (character 19) and transverse morphology (character 20).

Additionally, whilst the states of character 20 are roughly similar to their original wording, their applicability to some taxa is different. Previously all derived taxa were stated to possess an interorbital-nasal area that ‘is narrower, transversely round’; however all members of Mystriosuchini excluding *Mystriosuchus* (and *Nicrosaurus* if included within Mystriosuchini) possess a much broader area between the nares and orbits than the more basal taxa, which is transversely flat, prior to its lateral descent. The cross section of this morphology is roughly rectangular in dorsal profile, rather than the inverted U-shape present in *Leptosuchus*-like phytosaurs, *Rutiodon* and *Angistorhinus*. In *Parasuchus*-grade phytosaurs, the large anteroposterior extent of the interorbital-nasal area results in a varied transverse morphology depending on the position at which it is sampled. I therefore tentatively exclude *Parasuchus*-grade phytosaurs from this character

20) Interorbital nasal area cross section [modified from Hungerbühler 2002, character 14; Stocker 2010, character 21]

0: Flat and broad

1: Dorsally curved in cross section

[See notes for character 19]

21) Infranasal recess [from Hungerbühler 2002, character 11]

0: Absent

1: Present

[ORDERED] 22) Antorbital fossa [from Hungerbühler 2002, character 12; Stocker 2010: character 3; Butler *et al.* 2014, character 3]

0: Present lacrimal jugal and maxillary fossae touching

1: Present but reduced lacrimal jugal and maxillary fossae in contact dorsally but not ventrally

2: Present but reduced lacrimal jugal and maxillary fossae not touching

3: Absent

23) Discrete row of anteroposteriorly extending nodes on the lateral surface of the jugal [from Butler *et al.* 2014, character 44]

0: Absent

1: Present

24) Jugal and antorbital fenestra [from Stocker 2010, character 4]

0: Excluded from antorbital fenestra

1: Contributing to antorbital fenestra

*** [ORDERED] 25) Length of antorbital fenestra [modified from Hungerbühler *et al*. 2013, character 13]**

0: Less than 1.9 times naris length

1: Greater than or equal to 1.9 times naris length

Modified to reflect the range of morphology sampled in this study. Measured as the ratio between the length of the antorbital fenestra and the length of the external nares. State zero scores a relatively shorter antorbital fenestra, while state one scores a relatively longer antorbital fenestra.

26) Broad median depression on dorsal surface of frontals near border with nasals [from Kammerer *et al.* 2015, character 47]

0: Absent

1: Present

27) Posterolateral margins of nares [modified from Kammerer *et al.* 2015, character 48]

0: Relatively low without ornamentation or derived features

1: Swollen and rugose creating a distinct narial rim

2: Distinctly raised in lateral view forming a sharp triangular peak well above the surrounding skull roof

State two is added here to reflect the morphology of *Parasuchus bransoni*, which deviates from the previous two states with the dorsally pronounced morphology of its posterior narial rim.

28) Pre-orbital depression [from Hungerbühler 2002, character 15]

0: Absent

1: Present

29) Depression and flange in postorbital bar [from Hungerbühler *et al.* 2013, character 14]

0: Absent

1: Small elongate depression posterior rim of postorbital may create a small flange behind orbit

2: Strong elongate depression posterior rim of postorbital bar forms a distinct flange merging with po/sq bar

30) Jugal and orbit [from Stocker 2010, character 5]

0: Excluded from orbit

1: Contributing to orbit

In *Nicrosaurus kapffi*, both states of this character are present, with both states represented in individual specimens in some cases **(Hungerbühler, 1998a)**.

31) Medial margins of orbits [from Stocker 2010, character 6]

0: Flat with skull roof

1: Raised into orbital ridges

32) Deep sculpture of the skull roof [from Hungerbühler 2002, character 17]

0: Absent

1: Present

33) Sutural articulation of squamosal and postorbital in dorsal view [from stocker 2010, character 22]

0: Slot like, posterior process of po fits into slot in sq

1: Diagonal, sq forms anteromedial portion of po/sq bar and po forms posterolateral portion

2: Approximately transverse

[ORDERED] 34) Most anterior extent of infra-temporal fenestra [from Butler *et al.* 2014, character 45]

0: Beneath the posterior corner of the orbit

1: Extended anteriorly, reaches below the middle or anterior half of the orbit

2: Anteroventral corner distinctly in front of anterior rim of orbit

35) Pre-infratemporal shelf [from Hungerbühler 2002, character 18]

0: Absent

1: Present

The 'pre-infratemporal shelf' is an anteriorly convex, crescent-shaped ridge slightly anterior of the anterior border of the antero-ventral corner of the infratemporal fenestra. This morphology is present in all members of *Mystriosuchus*, *Machaeroprosopus* and '*Redondasaurus*' to some degree, and also in some specimens of *Nicrosaurus*.

36) Lateral ridge from post-orbital/squamosal bar [modified from Stocker 2010, character 23; Butler *et al*. 2014, character 23]

0: Absent

1: Continues posteriorly onto squamosal as a horizontal ridge forming a shelf overhanging the infratemporal fenestra

2: Bifurcates into two small ridges on lateral surface of squamosal

The morphology of any ridge on the lateral surface of the postorbital/squamosal bar has previously been scored with considerable subjectivity. The original character on which this is based possesses a number of states which may be equally applicable to multiple taxa depending on interpretation. Here, the character is simplified to reflect the morphologies that were recognized in this study, including the absence of a ridge.

37) Lateral ridge of postorbital squamosal bar continues as ridge onto posterior process of squamosal [from Hungerbühler *et al.* 2013, character 19]

0: Absent

1: Present

*** [ORDERED] 38) Length of posterior process of squamosal in relation to postorbital length [modified from Hungerbühler 2002, character 31; Stocker 2010, character 24]**

0: Absent or extremely short, posterior edge of squamosal does not extend or barely extends posteriorly beyond the distal end of the paroccipital process of the opisthotic

1: Less than 3.60

2: 3.60 to 4.99

3: Greater than, or equal to 5.00

Modified to reflect the measurements made for the greater range of taxa included in this study. The character is measured as the ratio of the distance from the posterior border of the orbit to the posteriormost point of the squamosal, and the distance from the posterior border of the paroccipital process to the tip of the squamosal. State one scores a long posterior process, state two a moderate process, and state three a short process.

† 39) Posterior process of squamosal [modified from Hungerbühler 2002, character 32; Stocker 2010, character 25]

0: Greatly dorsoventrally expanded

1: Moderately dorsoventrally expanded

2: Terminal knob

Ballew (1989), character 50 references the presence of a 'knob-like' posterior process of the squamosal in *Machaeroprosopus pristinus* and *Machaeroprosopus buceros*; this then became the 'terminal knob' of Hungerbühler (2002) and was subsequently used to describe this morphology. This character is modified to use this terminology, which is assumedly referenced by the 'dorsally compressed' state, used in previous versions of this character. Using this terminology makes the character less ambiguous.

† 40) Terminal knob of the squamosal [modified from Hungerbühler 2002, character 32; Hungerbühler *et al.* 2013, character 24]

0: Terminal knob raised distally above po/sq bar

1: Terminal knob in plane of po/sq bar

In some specimens the distal region of the terminal knob-like process of the squamosal is inflexed dorsally. The previous version of this character mentioned the posterior raising of the posterior process of the squamosal in reference to a greatly dorsoventrally expanded posterior process. This morphology was not recognized in any specimens in this study, whereas it was noted to be relatively common among individuals possessing a terminal knob.

41) Dorsal edge of squamosal [from Hungerbühler 2002, character 33; Stocker 2010, character 26]

0: Straight and narrow, no medial expansion

1: Expanded medially

This character essentially scores the presence or absence of any size of medial flange of the postorbital/squamosal bar.

42) Dorsal edge of squamosal B [from Stocker 2010, character 27]

0: Mediolaterally flat

1: Ventral depression between medial and lateral edges of the dorsal edge of the squamosal

*** [ORDERED] 43) Length of free postorbital/squamosal bar [modified from Hungerbühler *et al.* 2013, character 17]**

0: Less than 2.90

1: 2.90 to 3.39

2: Greater than or equal to 3.40

Modified to reflect the measurements made for the greater range of morphologies in this study. The character is measured as the ratio between the distance from the most anterior point of the supratemporal fenestra and the posteriormost point of the squamosal, to the shortest distance between the posterior border of the orbit and the most anterior point of the supratemporal fenestra. State zero corresponds to ‘short’, one corresponds to ‘moderate’ and two to ‘long’.

44) Medial extent of squamosal [modified from Hungerbühler 2002, character 30]

0: To mid length of parieto squamosal bar

1: Enters base of supraoccipital shelf wedged between parietal and supraoccipital

The character state ‘Enters rim of supraoccipital shelf dorsal to parietal’ has been removed as it was not recognized in any of the specimens examined in this study.

45) Cross section of posterior half of postorbito squamosal bar [from Hungerbühler 2002, character 22]

0: Low, dorsoventrally compressed

1: High, triangular

† 46) Ventral margin of squamosal [from Stocker 2010, character 28]

0: Gently sloping anteroventrally from posterior edge of posterior process to opisthotic process

1: Distinct horizontal ventral edge between posterior edge of posterior process and opisthotic process

47) Subsidiary opisthotic process of squamosal [from Hungerbühler 2002, character 35; Stocker 2010, character 29]

0: Absent

1: Present

48) Extent of squamosal fossa [from Stocker 2010, character 30]

0: Extends to posterior edge of sq

1: Does not reach posterior edge of sq

[ORDERED] 49) Orientation of supratemporal fenestra [from Stocker 2010, character 32]

0: Dorsally expressed parietal squamosal bar at level with skull roof

1: Partially depressed parietal process of squamosal below level of skull roof

2: Fully depressed posterior process of parietal and entire parietal squamosal bar below level of skull roof

† 50) Mediolateral expansion of posterior process of squamosal [modified from Hungerbühler *et al*. 2013, character 25]

0: Tip of squamosal tapers strongly posteriorly

1: Tip of squamosal tapers with a smooth lateral deflection distally

51) Face of medial rim of squamosal along supratemporal fenestra and posterior process [modified from Hungerbühler *et al*. 2013, character 23]

0: Entire rim rounded or sharp

1: Rim entirely or in part squared

52) Extent of squaring of the squamosal rim [modified from Hungerbühler *et al*. 2013, character 23]

0: Squared in posterior section

1: Entire rim squared

53) Ridge around anterior and or medial edge of supratemporal fenestra [modified from Hungerbühler 2002, character 20]

0: Absent

1: Present, medial only

2: Present, anterior and medial

The terminology used in the original character is quite vague 'Anterior border of supratemporal fenestra… raised above skull roof'. This character is a reinterpretation of the original, with more specific terms. In state one, the ridge would only be present on the parietal ledge, whereas in state two the ridge may extend to the anterior border of the supratemporal fenestra.

*** † [ORDERED] 54) Width of squamosal [modified from Hungerbühler *et al.* 2013, character 18]**

0: Less than or equal to 3.80

1: Greater than 3.80

Modified to reflect the greater range of morphologies measured in this study. Scored as the ratio between the length of the squamosal from the anteriormost point of the supratemporal fenestra to the posterior-most extent of the posterior process, and the width of the postorbital/squamosal bar at its approximate mid-point, or the point most representative of its general width. State zero corresponds to a wide postorbital/squamosal bar, state one denotes a relatively less wide bar.

† 55) Outline of medial rim of squamosal along supratemporal fenestra and posterior process [modified from Hungerbühler 2002, character 29]

0: Sinuous

1: Angular

2: Straight

3: Curved

Character state three has here been added to represent the morphologies found in *Nicrosaurus* and *Coburgosuchus*, which I feel were not adequately described by the previous character states.

56) Path of parietal/squamosal bars [from Stocker 2010, character 34]

0: Trending straight posteriorly to attachment on squamosals

1: Curved medially convex before attaching on squamosals

[ORDERED] 57) Visibility of supratemporal fenestrae in dorsal view [modified from Hungerbühler 2002, character 19; Stocker 2010, character 33]

0: Visible, STF completely open dorsally

1: Mostly visible, posterolateral portions of STF covered in dorsal view

2: Mostly covered dorsally, at most only anteromedial corners or medial slit of STF visible in dorsal view

3: Lamella merges with parietal, STF obliterated in dorsal view

This character combines those of Hungerbühler and Stocker. The wording used by Stocker is more inherently understandable, as Hungerbühler describes the visibility of the fenestra via the expansion of the squamosal, which is technically correct, but less intuitive. The final state of Hungerbühler's character is, however, missing from Stocker's and is useful in describing the morphology found in some extremely robust members of *Machaeroprosopus* and most specimens of '*Redondasaurus*'.

58) Parietal/squamosal bars [from Stocker 2010, character 35]

0: Slender, narrower than the width of po/sq bars

1: Wide, approximately the same mediolateral width as po/sq bars

[ORDERED] 59) Dorsal edge of parietal/squamosal bar [from Hungerbühler 2002, character 26]

0: Horizontal

1: Gently sloping

2: Steeply sloping

3: Either entirely, or in parts vertical

*** [ORDERED] 60) Parietal ledge, ratio of width to length [modified from Hungerbühler *et al.* 2013, character 30]**

0: Less than 1.30

1: 1.30 to 2.10

2: Greater than 2.10

Modified to reflect the greater range of morphologies sampled in this study. Width is measured either at the mid-point of the ledge, or the point that is most representative of its general width. Length is measured from the posterior-most extent of the ledge to the anterior-most point of the supratemporal fenestra (in phytosaurs where the parietal/squamosal bars are at the level of the skull roof, the posterior-most point of the ledge is measured at the midline of the parietals). State zero corresponds to a parietal ledge that is generally more anteroposteriorly prominent, whereas state two is very wide and hardly projects posteriorly.

61) Medial half of parieto squamosal bar lateral wall of supraoccipital shelf [from Hungerbühler 2002, character 37]

0: High and thin

1: Low, continuously thin

2: Low, basally thickened

62) Lobate extension on the vertical rim of the squamosal processes of the parietal [from Hungerbühler 2002, character 53]

0: Absent

1: Present

63) Depth and shape of supraoccipital shelf [from Hungerbühler 2002, character 36]

0: Shallow, longitudinal axis of shelf vertical

1: Deep, axis of shelf straight and horizontal

2: Deep axis of shelf with steep slope anteriorly and terminal horizontal deflection of shelf

64) Top of parieto supraoccipital complex formed by squamosal processes of parietals [from Ballew 1989, character 19; Hungerbühler 2002, character 24]

0: Angular, inverted V shape

1: Rounded, inverted U shape

2: Rectangular

65) Parietal prongs [from Hungerbühler 2002, character 25]

0: Absent

1: Present

66) Posttemporal fenestra [from Hungerbühler 2002, character 41]

0: Moderately wide and tall

1: Moderately wide and compressed

2: Extremely reduced in width and height to a slit

67) Lateral border of posttemporal fenestra [Hungerbühler 2002, character 38; Stocker 2010, character 37]

0: Formed by contact of the parietal process of the squamosal and the paroccipital process of the opisthotic

1: Formed laterally only by the paroccipital process

2: Formed laterally and slightly ventrally by process of squamosal that extends onto paroccipital process

68) Shape of quadratojugal [modified from Sereno 1991, character Q; Stocker 2010, character 31]

0: L shaped, anterior suture trends anteroventrally

1: Subtriangular

2: L shaped, anterior suture trends anterodorsally

69) Anterior border of parabasisphenoid contribution to basitubera [from Stocker 2010, character 39]

0: Basitubera separated widely

1: Basitubera separated narrowly with a ridge along their anterior border

2: Basitubera connected tubera form a sharp ridge along their anterior border

70) Morphology of basioccipital between tubera [from Stocker 2010, character 40]

0: Concave depression

1: Anteroposteriorly oriented ridge on the midline

71) Lateral extent of basitubera compared to basipterygoid processes in ventral view [from Stocker 2010, character 41]

0: Lateral extent of basitubera even with lateral extent of basipterygoid processes

1: Lateral extent of basitubera more laterally expanded compared to basipterygoid processes

72) Length of interpterygoid vacuity [from Chatterjee 1978, phenetic feature 7; Hungerbühler 2002, character 47]

0: Long, more than 50 per cent of length of palatal vault

1: Tiny oval indentation at posterior rim of conjoined pterygoids

73) Suborbital foramen [from Hungerbühler 2002, character 46; Stocker 2010, character 43]

0: Elongated, wide

1: Elongated, slit-like

2: Reduced to a single oval fenestra or subdivided into two or more small openings

74) Anterior extent of the palatine [from Hungerbühler 2002, character 44]

0: Tip located behind the posterior rim of choana

1: Tip extends forward beyond the posterior rim of choana

2: Tip extends forward beyond the anterior rim of choana

75) Palatal ridge [from Hungerbühler *et al.* 2013, character 40]

0: Low, rounded longitudinal elevation

1: Prominent, sharp ventrally to ventromedially directed crest

76) Medial edge of palatine below posterior part of palatal vault [from Hungerbühler *et al.* 2013, character 41]

0: Sloping or vertical

1: Horizontal flange may restrict the opening of the palatal vault significantly

77) Dorsal surface of surangular [from Mateus *et al.* 2014]

0: Gently convex

1: Gently concave rising to apex just posterior to dentary contact

78) Shape of retroarticular process in lateral view [from Mateus *et al.* 2014]

0: Distally sharply pointed or curved into a posterodorsally oriented hook

1: Distally rounded or blunt

[NEW] 79) Snout dorsal surface cross sectional shape

0: Rounded, dorsal surface of snout is curved from side to side

1: Triangular, sides of the snout are straight and slope up to the midline

[NEW] 80) Anterior separation of the septomaxillae

0: Septomaxillae separate posterior to level with the anterior narial border

1: Septomaxillae separate distinctly anterior of the anterior narial border

[NEW] † 81) Shape of antorbital fenestra

0: Ellipsoid

1: Approximately a geometric ‘stadium’ shape

2: Approximately triangular

3: Approximately triangular - point posteriormost

[NEW] 82) Lateral surface of maxilla and jugal ventral/posteroventral to AOF

0: Flat/laterally convex

1: Concavity running along the length of the element

[NEW] 83) Lateral surface of main body of jugal

0: Generally flat, element forms one dorsolaterally facing plane between its ventral and dorsal extremities

1: Anteroposteriorly directed ridge running from below AOF towards ventral border of subTF splits jugal into a dorsolaterally facing facet and a laterally facing facet

2: Anteroposterior ridge running along the centre of the jugal posterior process

3: Anteroposterior ridge running toward ventral border of jugal posterior process

[NEW] 84) Anterior extension of the pre-infratemporal shelf

0: Anteriormost border of shelf is posterior to the posteriormost border of the antorbital fenestra

1: Anteriormost border of shelf terminates anterior of the posteriormost corner of the antorbital fenestra

[NEW] 85) Dorsal extension of pre-infratemporal shelf

0: Merges dorsally into lateral surface of jugal

1: Continues dorsally contributing to the posterior edge of the postorbital descending process

[NEW] 86) Jugal foramen in anteroventral corner of the infra-temporal fenestra

0: Visible only in medial view, not visible in lateral view

1: Visible in lateral view

[NEW] * [ORDERED] 87) Relative robusticity of the jugal

0: Less than 7.30 (Robust)

1: 7.30-8.40 (Moderate)

2: Greater than 8.40 (Slender)

This ratio is calculated as the distance from the posterolateral-most corner of the quadrate to the anteroventral corner of the infra-temporal fenestra, divided by the thickness of the posterior process of the jugal at its thinnest point below the infra-temporal fenestra (measured perpendicular to the long axis of the element, i.e. approximately dorsoventrally).

[NEW] 88) Proximal section of postorbital descending process where posterior border of orbit meets skull roof

0: Flares anteroposteriorly creating a wide triangular connection

1: Posterior border of orbit remains thin until it reaches skull roof

[NEW] * † [ORDERED] 89) Infra-temporal fenestra diagonal aspect ratio

0: Less than or equal to 2.30

1: Greater than 2.30

Measured as the distance from the anteroventral corner, to the posterodorsal corner of the infra-temporal fenestra, divided by the distance from the anterodorsal corner, to the posteroventral corner of the infra-temporal fenestra.

[NEW] 90) Additional ridge on lateral surface of posterior process of squamosal below ridge or rugosity from po/sq bar

0: Absent

1: Present

[NEW] † 91) Posterior border of quadrate in lateral view

0: Straight anterodorsal line for majority of element

1: Ventral section of border is anteroposteriorly concave

[NEW] 92) Internarial septum

0: Restricted to between, or extends slightly anterior of the external nares

1: Extends anterior of the nares by approximately the narial length

[NEW] 93) Triangular projection ventro-medial to the glenoid of the articular

0: Anterior border is straight, trending posteroventrally

1: Ventral half of anterior border possesses an anteriorly projecting process

[NEW] * [ORDERED] 94) Relative length of mandibular symphysis

0: Less than 1.00 (Short)

1: Greater than or equal to 1.00 (Long)

Measured as the anteroposterior length of the mandibular symphysis, divided by the anteroposterior length of the post-symphyseal region.

S1.3. ***Nodal synapomorphies***

This list presents all synapomorphic character changes at every node of each of the four data treatments: discrete, discrete + continuous, discrete + GM, and discrete + continuous + GM.

Discrete tree

1) No synapomorphies

2) 13: 0→1
   22: 0→1

3) 36: 0→1
   69: 0→1

4) 23: 0→1
   26: 0→1
   50: 0→1

5) 82: 0→1
   91: 0→1

6) 1: 0→1
   22: 1→2
   73: 0→1

83: 1→0

7) 9: 0→1

14: 1→2

19: 0→1

29: 0→1

36: 1→0

38: 0→2

69: 1→2

72: 0→1

74: 1→2

80: 0→1

81: 0→2

8) 22: 2→1

60: 1→0

92: 0→1

9) 56: 0→1

58: 0→1

10) 42: 0→1

51: 0→1

11) 12: 0→1

17: 0→1

66: 0→1

70: 0→1

12) 69: 2→1

13) 8: 0→2

16: 1→0

25: 0→1

41: 0→1

44: 0→1

49: 0→1

57: 0→1

59: 0→1

88: 1→0

14) 81: 2→1

15) 90: 0→1

16) 19: 1→0

20: 0→1

39: 0→1

17) 7: 0→4

18) 48: 0→1

19) 3: 0→1

7: 4→2

33: 0→2

20) 21: 0→1

29: 1→0

21) 49: 1→2

53: 2→0

54: 1→0

57: 1→2

67: 0→2

22) 38: 2→3

23) 49: 1→2

24) 35: 0→1

43: 2→0

54: 1→0

75: 0→1

87: 0→1, 2

25) 59: 1, 2→3

84: 0→1

85: 1→0

26) 2: 1→2

20: 0→1

27) 88: 0→1

28) 65: 0→1

29) 3: 0→1

4: 0→1

7: 1→4

46: 1→0

47: 0→1

30) 25: 1→0

48: 0→1

31) 30: 1→0

36: 0→1

51: 0→1

60: 1→2

32) 3: 1→0

4: 1→0

48: 0→1

90: 0→1

33) 7: 4→1

8: 2→1

89: 0→1

34) 7: 4→2

22: 2→3

35) 11: 1→0

36) 48: 1→0

53: 1→0

37) 19: 1→0

57: 2→3

59: 2→3

63: 1→0

38) 89: 0→1

Discrete + continuous tree

1) No synapomorphies

2) 13: 0→1

22: 0→1

3) 36: 0→1

69: 0→1

4) 23: 0→1

26: 0→1

50: 0→1

54: 0.525-0.545 → 0.353-0.420

5) 25: 0.452-0.470 → 0.409-0.446

82: 0→1

91: 0→1

6) 1: 0→1

11: 0.459-0.484 → 0.490-0.686

22: 1→2

25: 0.452-0.470 → 0.514

73: 0→1

83: 1→0

89: 0.244-0.272 → 0.457-0.520

7) 9: 0→1

14: 1→2

29: 0→1

36: 1→0

60: 0.060-0.090 → 0.036-0.038

69: 1→2

72: 0→1

74: 1→2

80: 0→1

8) 19: 0→1

22: 2→1

25: 0.514 → 0.503

92: 0→1

9) 56: 0→1

58: 0→1

87: 0.106-0.110 → 0.103

10) 42: 0→1

51: 0→1

11) 8: 0.240-0.253 → 0.274

12: 0→1

17: 0→1

66: 0→1

70: 0→1

12) 69: 2→1

13) 5: 0→1

16: 1→0

25: 0.514 → 0.684-0.718

41:0→1

88: 1→0

90: 0→1

14) 57: 0→1

87: 0.106-0.110 → 0.117-0.132

15) 10: 0→1

79: 0→1

16) 11: 0.678-0.686 → 0.729

54: 0.525-0.545 → 0.395-0.406

17) 48: 0→1

89: 0.457 → 0.462

18) 21: 0→1

29: 1→0

19) 49: 1→2

54: 0.395-0.406 → 0.270

57: 1→2

67: 0→2

20) 54: 0.270 → 0.159

89: 0.457 → 0.615-0.833

21) 19: 0→1

20: 1→0

22) 33: 0→1

38: 0.281 → 0.457

54: 0.525-0.545 → 0.494

67: 0→2

90: 1→0

23) 49: 1→2

54: 0.494 → 0.383-0.399

24) 43: 0.106-0.118 → 0.070

53: 2→1

54: 0.383-0.399 → 0.213

61: 0→2

65: 0→1

25) 59: 1→2

60: 0.098-0.102 → 0.125

26) 60: 0.125 → 0.236-0.267

27) 48: 0→1

28) 35: 0→1

38: 0.457-0.751 → 0.325-0.442

89: 0.507 → 0.550-0.582

29) 22: 3→2

75: 0→1

30) 39: 1→0

53: 1→2

31) 3: 1→0

4: 1→0

32) 39: 1→2

90: 0→1

33) 43: 0.070 → 0.034-0.043

48: 1→0

59: 2→3

86: 0→1

34) 25: 0.439-0.514 → 0.113

34: 1→2

53: 1→0

54: 0.180-0.197 → 0.039-0.095

89: 0.550-0.620 → 0.710

35) 84: 0→1

87: 0.338-0.401 → 0.574-0.577

36) 7: 1→2

53: 1→2

57: 2→3

37) 57: 2→1

61: 2→1

85: 1→0

38) 2: 1→2

20: 0→1

39) 19: 0→1

88: 0→1

Discrete + GM tree (excluding landmark 'state changes')

1) [39, 40, 46]: LANDMARK

[50, 54, 55]: LANDMARK

81: LANDMARK

89: LANDMARK

91: LANDMARK

2) 13: 0→1

22: 0→1

[39, 40, 46]: LANDMARK

[50, 54, 55]: LANDMARK

81: LANDMARK

89: LANDMARK

91: LANDMARK

3) 36: 0→1

[39, 40, 46]: LANDMARK

[50, 54, 55]: LANDMARK

69: 0→1

81: LANDMARK

89: LANDMARK

91: LANDMARK

4) 23: 0→1

26: 0→1

[39, 40, 46]: LANDMARK

[50, 54, 55]: LANDMARK

81: LANDMARK

89: LANDMARK

91: LANDMARK

5) [39, 40, 46]: LANDMARK

[50, 54, 55]: LANDMARK

81: LANDMARK

82: 0→1

89: LANDMARK

91: LANDMARK

6) 1: 0→1

22: 1→2

[39, 40, 46]: LANDMARK

[50, 54, 55]: LANDMARK

81: LANDMARK

83: 1→0

89: LANDMARK

91: LANDMARK

7) 11: 0→1,2

34: 0→1

42: 1→0

[39, 40, 46]: LANDMARK

[50, 54, 55]: LANDMARK

81: LANDMARK

89: LANDMARK

91: LANDMARK

8) [39, 40, 46]: LANDMARK

[50, 54, 55]: LANDMARK

81: LANDMARK

89: LANDMARK

91: LANDMARK

9) 9: 0→1

14: 1→2

[39, 40, 46]: LANDMARK

[50, 54, 55]: LANDMARK

80: 0→1

81: LANDMARK

89: LANDMARK

91: LANDMARK

10) 19: 0→1

22: 2→1

[39, 40, 46]: LANDMARK

81: LANDMARK

89: LANDMARK

91: LANDMARK

92: 0→1

11) [39, 40, 46]: LANDMARK

56: 0→1

58: 0→1

81: LANDMARK

89: LANDMARK

91: LANDMARK

12) 42: 0→1

[39, 40, 46]: LANDMARK

51: 0→1

81: LANDMARK

89: LANDMARK

91: LANDMARK

13) 12: 0→1

17: 0→1

66: 0→1

70: 0→1

81: LANDMARK

14) 69: 2→1

81: LANDMARK

15) 5: 0→1

16: 1→0

25: 0→1

[39, 40, 46]: LANDMARK

49: 0→1

[50, 54, 55]: LANDMARK

57: 0→1

59: 0→1

81: LANDMARK

89: LANDMARK

91: LANDMARK

16) 41: 0→1

[39, 40, 46]: LANDMARK

[50, 54, 55]: LANDMARK

81: LANDMARK

89: LANDMARK

91: LANDMARK

17) [39, 40, 46]: LANDMARK

48: 0→1

[50, 54, 55]: LANDMARK

81: LANDMARK

89: LANDMARK

90: 0→1

91: LANDMARK

18) [39, 40, 46]: LANDMARK

[50, 54, 55]: LANDMARK

81: LANDMARK

89: LANDMARK

91: LANDMARK

19) 3: 0→1

33: 0→2

[39, 40, 46]: LANDMARK

[50, 54, 55]: LANDMARK

81: LANDMARK

89: LANDMARK

91: LANDMARK

20) 29: 1→0

33: 0→1

[39, 40, 46]: LANDMARK

[50, 54, 55]: LANDMARK

81: LANDMARK

89: LANDMARK

91: LANDMARK

21) 38: 2→3

[39, 40, 46]: LANDMARK

[50, 54, 55]: LANDMARK

60: 0→1

67: 0→2

81: LANDMARK

89: LANDMARK

91: LANDMARK

22) [39, 40, 46]: LANDMARK

49: 1→2

[50, 54, 55]: LANDMARK

81: LANDMARK

89: LANDMARK

91: LANDMARK

23) 9: 1→0

33: 1→2

[39, 40, 46]: LANDMARK

53: 2→1

[50, 54, 55]: LANDMARK

75: 0→1

81: LANDMARK

89: LANDMARK

91: LANDMARK

24) [39, 40, 46]: LANDMARK

[50, 54, 55]: LANDMARK

57: 1→2

81: LANDMARK

89: LANDMARK

90: 0→1

91: LANDMARK

25) 33: 2→0

[39, 40, 46]: LANDMARK

53: 1→0

[50, 54, 55]: LANDMARK

81: LANDMARK

89: LANDMARK

91: LANDMARK

26) 38: 3→2

43: 2→0

[39, 40, 46]: LANDMARK

[50, 54, 55]: LANDMARK

64: 0→1

81: LANDMARK

87: 0→1, 2

89: LANDMARK

91: LANDMARK

27) [39, 40, 46]: LANDMARK

[50, 54, 55]: LANDMARK

59: 1, 2→3

81: LANDMARK

84: 0→1

85: 1→0

89: LANDMARK

91: LANDMARK

28) 2: 1→2

[39, 40, 46]: LANDMARK

[50, 54, 55]: LANDMARK

81: LANDMARK

89: LANDMARK

91: LANDMARK

29) 19: 0→1

[39, 40, 46]: LANDMARK

[50, 54, 55]: LANDMARK

81: LANDMARK

88: 0→1

89: LANDMARK

91: LANDMARK

30) 29: 0→1

[39, 40, 46]: LANDMARK

[50, 54, 55]: LANDMARK

65: 0→1

81: LANDMARK

89: LANDMARK

91: LANDMARK

31) 3: 0→1

4: 0→1

7: 1→4

[39, 40, 46]: LANDMARK

47: 0→1

[50, 54, 55]: LANDMARK

81: LANDMARK

89: LANDMARK

91: LANDMARK

32) [39, 40, 46]: LANDMARK

48: 0→1

[50, 54, 55]: LANDMARK

81: LANDMARK

89: LANDMARK

91: LANDMARK

33) 19: 0→1

[39, 40, 46]: LANDMARK

[50, 54, 55]: LANDMARK

81: LANDMARK

89: LANDMARK

91: LANDMARK

34) 30: 1→0

[39, 40, 46]: LANDMARK

[50, 54, 55]: LANDMARK

60: 1→2

81: LANDMARK

89: LANDMARK

91: LANDMARK

35) 3: 1→0

4: 1→0

[39, 40, 46]: LANDMARK

[50, 54, 55]: LANDMARK

81: LANDMARK

89: LANDMARK

90: 0→1

91: LANDMARK

36) 7: 4→1

8: 2→1

[39, 40, 46]: LANDMARK

[50, 54, 55]: LANDMARK

81: LANDMARK

89: LANDMARK

91: LANDMARK

37) 7: 4→2

22: 2→3

[39, 40, 46]: LANDMARK

[50, 54, 55]: LANDMARK

81: LANDMARK

89: LANDMARK

91: LANDMARK

38) 11: 1→0

[39, 40, 46]: LANDMARK

[50, 54, 55]: LANDMARK

81: LANDMARK

89: LANDMARK

91: LANDMARK

39) [39, 40, 46]: LANDMARK

48: 1→0

53: 1→0

[50, 54, 55]: LANDMARK

81: LANDMARK

89: LANDMARK

91: LANDMARK

40) 19: 1→0

[39, 40, 46]: LANDMARK

[50, 54, 55]: LANDMARK

57: 2→3

59: 2→3

63: 1→0

81: LANDMARK

89: LANDMARK

91: LANDMARK

41) [39, 40, 46]: LANDMARK

[50, 54, 55]: LANDMARK

81: LANDMARK

89: LANDMARK

91: LANDMARK

Discrete + Continuous + GM tree (excluding landmark 'state changes')

1) [39, 40, 46]: LANDMARK

[50, 54, 55]: LANDMARK

81: LANDMARK

89: LANDMARK

91: LANDMARK

2) 13: 0→1

22: 0→1

[39, 40, 46]: LANDMARK

[50, 54, 55]: LANDMARK

81: LANDMARK

89: LANDMARK

91: LANDMARK

3) 36: 0→1

[39, 40, 46]: LANDMARK

[50, 54, 55]: LANDMARK

69: 0→1

81: LANDMARK

89: LANDMARK

91: LANDMARK

4) 23: 0→1

26: 0→1

[39, 40, 46]: LANDMARK

[50, 54, 55]: LANDMARK

81: LANDMARK

89: LANDMARK

91: LANDMARK

5) 25: 0.452-0.470 → 0.409-0.446

[39, 40, 46]: LANDMARK

[50, 54, 55]: LANDMARK

81: LANDMARK

82: 0→1

89: LANDMARK

91: LANDMARK

6) 1: 0→1

11: 0.459-0.484 → 0.490

22: 1→2

25: 0.452-0.470 → 0.514

[39, 40, 46]: LANDMARK

[50, 54, 55]: LANDMARK

81: LANDMARK

83: 1→0

89: LANDMARK

91: LANDMARK

7) 8: 0.178-0.219 → 0.253-0.616

11: 0.490 → 0.686-0.800

34: 0→1

42: 1→0

43: 0.126-0.150 → 0.104-0.106

[39, 40, 46]: LANDMARK

[50, 54, 55]: LANDMARK

81: LANDMARK

89: LANDMARK

91: LANDMARK

8) [39, 40, 46]: LANDMARK

[50, 54, 55]: LANDMARK

81: LANDMARK

89: LANDMARK

91: LANDMARK

9) 9: 0→1

14: 1→2

[39, 40, 46]: LANDMARK

[50, 54, 55]: LANDMARK

80: 0→1

81: LANDMARK

89: LANDMARK

91: LANDMARK

10) 19: 0→1

22: 2→1

25: 0.514 → 0.503

[39, 40, 46]: LANDMARK

81: LANDMARK

89: LANDMARK

91: LANDMARK

92: 0→1

11) [39, 40, 46]: LANDMARK

58: 0→1

81: LANDMARK

87: 0.106-0.132 → 0.103

89: LANDMARK

91: LANDMARK

12) 42: 0→1

[39, 40, 46]: LANDMARK

51: 0→1

81: LANDMARK

89: LANDMARK

91: LANDMARK

13) 12: 0→1

17: 0→1

66: 0→1

70: 0→1

81: LANDMARK

14) 69: 2→1

81: LANDMARK

15) 5: 0→1

16: 1→0

25: 0.514 → 0.684-0.718

41: 0→1

[39, 40, 46]: LANDMARK

[50, 54, 55]: LANDMARK

81: LANDMARK

89: LANDMARK

90: 0→1

91: LANDMARK

16) [39, 40, 46]: LANDMARK

[50, 54, 55]: LANDMARK

57: 0→1

81: LANDMARK

89: LANDMARK

91: LANDMARK

17) 10: 0→1

[39, 40, 46]: LANDMARK

[50, 54, 55]: LANDMARK

79: 0→1

81: LANDMARK

87: 0.117-0.132 → 0.145

89: LANDMARK

91: LANDMARK

18) 11:0.686-0.690 → 0.729

43: 0.104-0.106 → 0.103

[39, 40, 46]: LANDMARK

[50, 54, 55]: LANDMARK

81: LANDMARK

89: LANDMARK

91: LANDMARK

19) [39, 40, 46]: LANDMARK

48: 0→1

[50, 54, 55]: LANDMARK

81: LANDMARK

89: LANDMARK

91: LANDMARK

20) 21: 0→1

29: 1→0

[39, 40, 46]: LANDMARK

[50, 54, 55]: LANDMARK

81: LANDMARK

89: LANDMARK

91: LANDMARK

21) [39, 40, 46]: LANDMARK

49: 1→2

53: 2→0

[50, 54, 55]: LANDMARK

57: 1→2

67: 0→2

81: LANDMARK

89: LANDMARK

91: LANDMARK

22) 38: 0.251 → 0.521

[39, 40, 46]: LANDMARK

[50, 54, 55]: LANDMARK

81: LANDMARK

89: LANDMARK

91: LANDMARK

23) 19: 0→1

20: 1→0

[39, 40, 46]: LANDMARK

[50, 54, 55]: LANDMARK

81: LANDMARK

89: LANDMARK

91: LANDMARK

24) 33: 0→1

38: 0.218 → 0.442-0.457

[39, 40, 46]: LANDMARK

[50, 54, 55]: LANDMARK

67: 0→2

81: LANDMARK

89: LANDMARK

90: 1→0

91: LANDMARK

25) 3: 0→1

4: 0→1

[39, 40, 46]: LANDMARK

49: 1→2

[50, 54, 55]: LANDMARK

81: LANDMARK

89: LANDMARK

91: LANDMARK

26) 43: 0.106-0.118 → 0.070

[39, 40, 46]: LANDMARK

[50, 54, 55]: LANDMARK

73: 1→2

76: 0→1

81: LANDMARK

89: LANDMARK

91: LANDMARK

27) [39, 40, 46]: LANDMARK

53: 2→1

[50, 54, 55]: LANDMARK

70: 0→1

81: LANDMARK

89: LANDMARK

91: LANDMARK

28) [39, 40,46]:

[50, 54, 55]: LANDMARK

59: 1→2

60: 0.098-0.102 → 0.125

81: LANDMARK

89: LANDMARK

91: LANDMARK

29) [39, 40, 46]: LANDMARK

[50, 54, 55]: LANDMARK

60: 0.124 → 0.236-0.267

81: LANDMARK

89: LANDMARK

91: LANDMARK

30) [39, 40, 46]: LANDMARK

48: 0→1

[50, 54, 55]: LANDMARK

81: LANDMARK

89: LANDMARK

91: LANDMARK

31) 35: 0→1

[39, 40, 46]: LANDMARK

[50, 54, 55]: LANDMARK

81: LANDMARK

89: LANDMARK

91: LANDMARK

32) 3: 1→0

4: 1→0

7: 2→1

[39, 40, 46]: LANDMARK

[50, 54, 55]: LANDMARK

75: 0→1

81: LANDMARK

89: LANDMARK

91: LANDMARK

33) 38: 0.442-0.457 → 0.077-0.319

[39, 40, 46]: LANDMARK

[50, 54, 55]: LANDMARK

81: LANDMARK

89: LANDMARK

90: 0→1

91: LANDMARK

34) 19: 1→0

[39, 40, 46]: LANDMARK

[50, 54, 55]: LANDMARK

81: LANDMARK

89: LANDMARK

91: LANDMARK

35) [39, 40, 46]: LANDMARK

48: 1→0

[50, 54, 55]: LANDMARK

81: LANDMARK

86: 0→1

89: LANDMARK

91: LANDMARK

36) 25: 0.325-0.439 → 0.113

34: 1→2

[39, 40, 46]: LANDMARK

53: 1, 2→0

[50, 54, 55]: LANDMARK

81: LANDMARK

89: LANDMARK

91: LANDMARK

37) [39, 40, 46]: LANDMARK

[50, 54, 55]: LANDMARK

81: LANDMARK

84: 0→1

87: 0.338-0.401 → 0.574-0.577

89: LANDMARK

38) 7: 1→2

[39, 40, 46]: LANDMARK

[50, 54, 55]: LANDMARK

57: 2→3

81: LANDMARK

89: LANDMARK

91: LANDMARK

39) [39, 40, 46]: LANDMARK

[50, 54, 55]: LANDMARK

57: 2→1

61: 2→1

81: LANDMARK

85: 1→0

89: LANDMARK

91: LANDMARK

40) 2: 1→2

20: 0→1

[39, 40, 46]: LANDMARK

[50, 54, 55]: LANDMARK

81: LANDMARK

89: LANDMARK

91: LANDMARK

41) 19: 0→1

[39, 40, 46]: LANDMARK

[50, 54, 55]: LANDMARK

81: LANDMARK

88: 0→1

89: LANDMARK

91: LANDMARK

Table S1.1: Number of characters and proportion of missing data in each data block.

Character type	Number of characters *[Number of discretely scored counterparts]*	Proportion of missing data *[Proportion missing in discretely scored counterparts]*
Discrete	94 *[N/A]*	32.5% *[N/A]*
Continuous	10 *[10]*	34.3% *[31.7%]*
GM (Landmark)	5 *[9]*	41.4% *[38.4%]*

Table S1.2: Percentage of missing data in the discrete data block for each OTU.

OTUs	Missing discrete character scores	Percentage missing data
Machaeroprosopus_lottorum	5	5.3
Machaeroprosopus_pristinus	5	5.3
Mystriosuchus_planirostris	7	7.4
Nicrosaurus_kapffi	7	7.4
Machaeroprosopus_mccauleyi	8	8.5
Machaeroprosopus_buceros	9	9.6
Nicrosaurus_meyeri	10	10.6
Angistorhinus_talainti	13	13.8
Smilosuchus_gregorii	13	13.8
Mystriosuchus_westphali	14	14.9
Leptosuchus_crosbiensis	17	18.1
Parasuchus_angustifrons	17	18.1
Parasuchus_bransoni	17	18.1
Redondasaurus_gregorii	19	20.2
Smilosuchus_adamanensis	19	20.2
Ebrachosuchus_neukami	21	22.3
Rutiodon_carolinensis	22	23.4
Pravusuchus_hortus	23	24.5

Parasuchus_hislopi	24	25.5
Leptosuchus_studeri	25	26.6
Redondasaurus_bermani	27	28.7
NMMNHS_P4256	28	29.8
Euparkeria_capensis	28	29.8
Smilosuchus_lithodendrorum	29	30.9
TMM_31100_1332	29	30.9
Paleorhinus_sawini	31	33.0
PEFO_34852	31	33.0
NMMNHS_P31094	32	34.0
USNM_v_17098	38	40.4
Diandongosuchus_fuyuanensis	39	41.5
Machaeroprosopus_andersoni	44	46.8
Angistorhinus_grandis	46	48.9
Protome_batalaria	48	51.1
NHMW_1986_0024_0001	48	51.1
Phytosaurus_doughtyi	49	52.1
Coburgosuchus_goeckeli	50	53.2
Wannia_scurriensis	50	53.2
USNM_v_21376	57	60.6
MB.R._2747	59	62.8
Machaeroprosopus_zunii	65	69.1
Machaeroprosopus_jablonskiae	66	70.2
NMMNHS_P4781	74	78.7
Paleorhinus_parvus	79	84.0

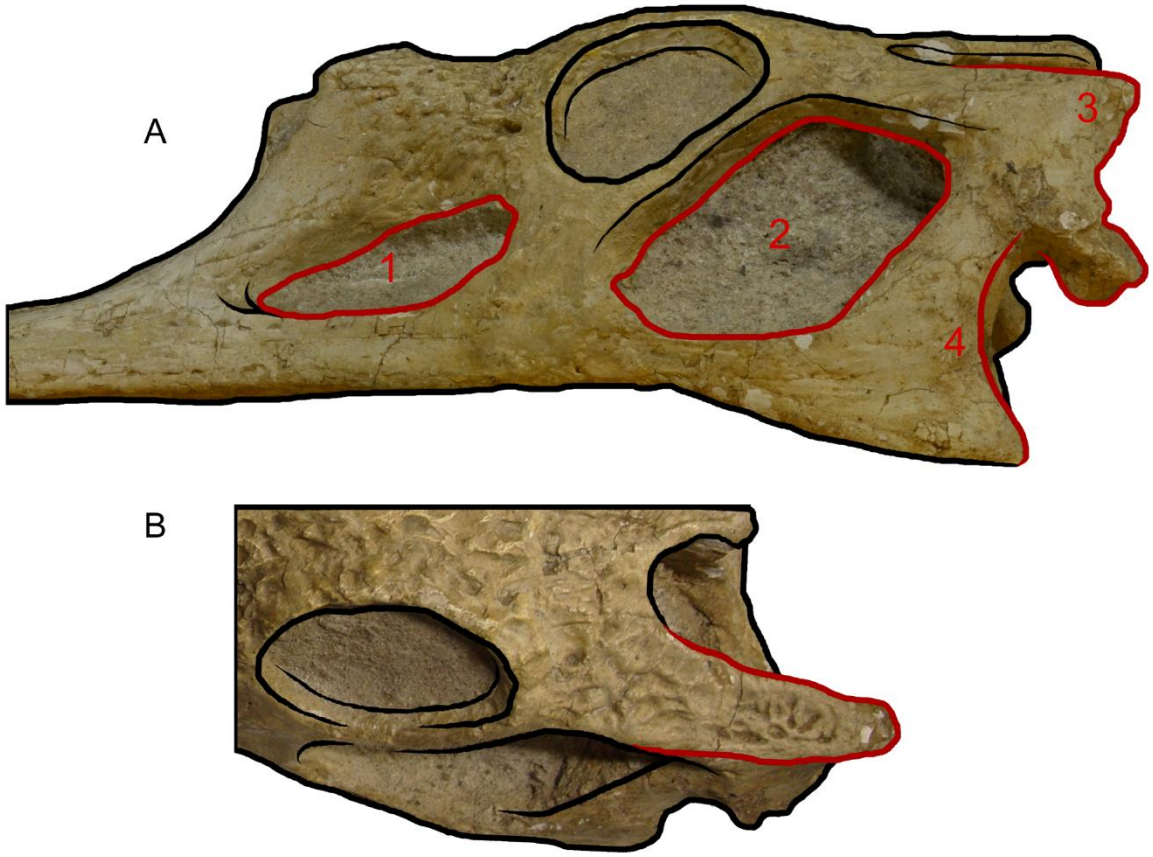

Figure S1.1: The five aspects of cranial morphology subjected to GM character scoring. Pathways along which semilandmarks were plotted are drawn in red; these correspond to A)1 shape of the antorbital fenestra, 2 shape of the lateral temporal fenestra, 3 shape of the posterior process of the squamosal in lateral view, 4 posterior curvature of the quadrate and B) shape of the postorbital/squamosal bar and the posterior process of the squamosal in dorsal view.

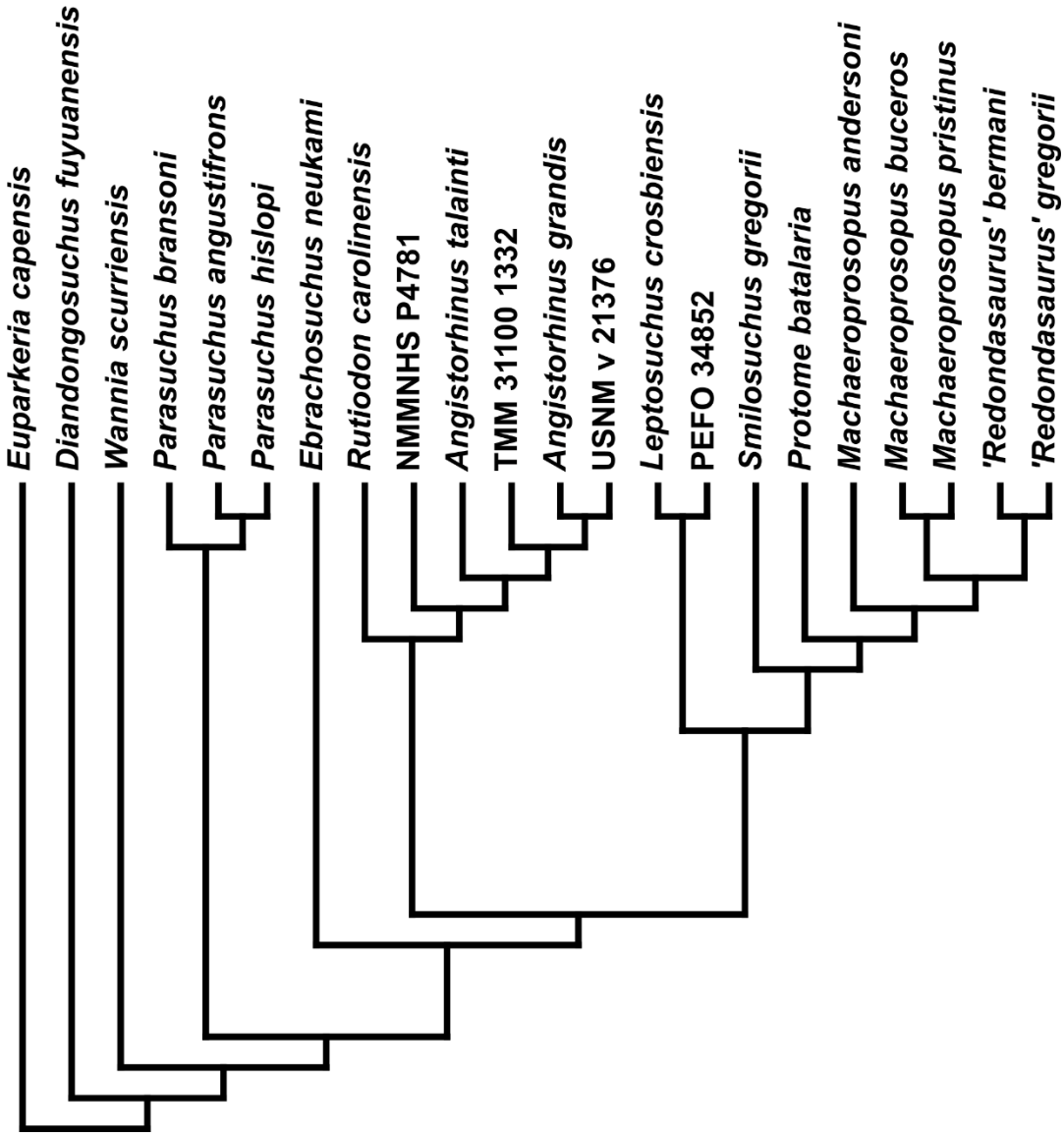

Figure S1.2: Maximum agreement subtree showing consistent relationships between D, DC, DM & DCM trees; taxa expressing conflicting relationships have been pruned.

Appendix: Chapter 3 (geometric morphometrics)

Table S2.1: Dorsal view geometric morphometric dataset of phytosaurs and crocodylians. Table includes the group classification assigned to each taxon and used to construct convex-hulls in morphospaces. Specimen number is included for samples based on photos; references are included for samples based on specimens figured in the literature.

	Dorsal	
Taxon	Group for analysis	Specimen No. (and literature reference if specimen image was derived from a previous study)
Alligator mcgrewi	Crocodylia: Alligatoroidea	FMNH P 26242
Anatosuchus minor	Notosuchia	MNN-GAD17
Araripesuchus wegeneri	Notosuchia	MNN-GAD19
Crocodylus depressifrons	Crocodylia: Crocodyloidea	HLMD-Me7499a
Brachychampsa montana	Crocodylia: Alligatoroidea	UCMP-133901
Caipirasuchus paulistanus	Notosuchia	MPMA-67-0001-00
Crocodylus acutus	Crocodylia: Crocodyloidea	NHMUK 1975-997
Mecistops cataphractus	Crocodylia: Crocodyloidea	NHMUK 1862-6-30-8
Crocodylus moreletii	Crocodylia: Crocodyloidea	NHMUK 1861-4-1-4
Crocodylus niloticus	Crocodylia: Crocodyloidea	NHMUK 1959-1-8-55
Crocodylus palaeindicus	Crocodylia: Crocodyloidea	NHMUK 39795
'Crocodylus palustris-kimbula'	Crocodylia: Crocodyloidea	NHMUK 1897-12-31-1
Crocodylus siamensis	Crocodylia: Crocodyloidea	NHMUK 1921-4-1-168
Diplocynodon darwini	Crocodylia: Alligatoroidea	HLMD-Be233
Diplocynodon hantoniensis	Crocodylia: Alligatoroidea	TN-907
Dyrosaurus phosphaticus	Tethysuchia	KX 15904
Elosuchus cherifiensis	Tethysuchia	MNHN-R-MRS-340–25
Eogavialis africanum	Crocodylia: Gavialoidea	SMNS 11785
Gavialis gangeticus	Crocodylia: Gavialoidea	NHMUK 1935-6-4-1
Goniopholis simus	Stem Neosuchia	NHMUK OR41098
Kaprosuchus saharicus	Notosuchia	MNN-IGU12
'Leidyosuchus riggsi'	Crocodylia: Alligatoroidea	FMNH-P-15582
Libycosuchus brevirostris	Notosuchia	BSPG-1912-VIII-574a,b
Melanosuchus niger	Crocodylia: Alligatoroidea	NHMUK 45-8-25-125
Notosuchus terrestris	Notosuchia	MACN-RN-1037
Peipehsuchus teleorhinus	Thalattosuchia	IVPP-V10098
Piscogavialis jugaliperforatus	Crocodylia: Gavialoidea	SMNK-PAL-1282
Boverisuchus vorax	Stem Crocodylia	FMNH-PR399
Purussaurus neivensis	Crocodylia: Alligatoroidea	UCMP 39704
Sarcosuchus imperator	Tethysuchia	MNHN.F1973-9GDF662
Sphagesaurus montealtensis	Notosuchia	MPMA_68-0003-12

Steneosaurus depressus	Thalattosuchia	OUMNH J.01420
Steneosaurus herberti	Thalattosuchia	MNHN.F_1890-13
Steneosaurus leedsi	Thalattosuchia	NHMUK PV R3806
Steneosaurus meretrix	Thalattosuchia	OUMNH J.29850
Stolokrosuchus lapparenti	Notosuchia	Cast of MNN GDF 600
Thoracosaurus macrorhynchus	Crocodylia: Gavialoidea	MNHN.F1897-15
Tomistoma schlegelii	Crocodylia: Crocodyloidea	NHMUK 1860-11-6-8
Voay robustus	Crocodylia: Crocodyloidea	NHMUK PV R36685
Alligator mississippiensis	Crocodylia: Alligatoroidea	AMNH R-71621
Alligator prenasalis	Crocodylia: Alligatoroidea	AMNH 1015 Mook (1932)
Alligator sinensis	Crocodylia: Alligatoroidea	AMNH R-23898
Borealosuchus wilsoni	Stem Crocodylia	USNM V 12990
Caiman crocodilus	Crocodylia: Alligatoroidea	AMNH 43291
Eosuchus lerichei	Crocodylia: Gavialoidea	IRSNB R 48
Eothoracosaurus mississippiensis	Crocodylia: Gavialoidea	MSU 3293 Brochu (2004)
Paleosuchus trigonatus	Crocodylia: Alligatoroidea	AMNH R-93812
Siquisiquesuchus venezuelensis	Crocodylia: Gavialoidea	MBLUZ-P-5050 Brochu & Rincón (2004)
Stangerochampsa mccabei	Crocodylia: Alligatoroidea	RTMP.86.61.1 Wu *et al.* (1996)
Wannaganosuchus brachymanus	Crocodylia: Alligatoroidea	SMM P76.28.247 Erickson (1982)
Ebrachosuchus neukami	Basal Parasuchidae (non-Mystriosuchinae Parasuchidae)	BSPG 1931 X 501
Leptosuchus crosbiensis	Basal Leptosuchomorpha (non-Mystriosuchini Leptosuchomorpha)	TMM 31173-120
'Redondasaurus' ?bermani	Mystriosuchini	NMMNHS-P4256
Machaeroprosopus lottorum	Mystriosuchini	TTU-P10076
Machaeroprosopus mccauleyi	Mystriosuchini	PEFO 31219
Machaeroprosopus pristinus	Mystriosuchini	MU 525
Machaeroprosopus pristinus	Mystriosuchini	NMMNHS-P50040
Machaeroprosopus pristinus	Mystriosuchini	PEFO 382
Machaeroprosopus pristinus	Mystriosuchini	UCMP 137319
'Smilosuchus lithodendrorum'	Basal Leptosuchomorpha (non-Mystriosuchini Leptosuchomorpha)	PEFO 34852
Smilosuchus gregorii	Basal Leptosuchomorpha (non-Mystriosuchini Leptosuchomorpha)	UCMP 27200
Smilosuchus gregorii	Basal Leptosuchomorpha (non-Mystriosuchini Leptosuchomorpha)	AMNH 3060

Nicrosaurus kapffi	Basal Leptosuchomorpha (non-Mystriosuchini Leptosuchomorpha)	SMNS 4379
Nicrosaurus meyeri	Basal Leptosuchomorpha (non-Mystriosuchini Leptosuchomorpha)	Combined morphology of SMNS 12593 & NHMUK OR42745
Mystriosuchus westphali	Mystriosuchini	GPIT 261-001
Mystriosuchus planirostris	Mystriosuchini	Combined morphology of SMNS 9900 & 9134
Paleorhinus sawini	Basal Parasuchidae (non-Mystriosuchinae Parasuchidae)	TMM 31213-16
Parasuchus angustifrons	Basal Parasuchidae (non-Mystriosuchinae Parasuchidae)	ZPAL AbIII 200
Parasuchus bransoni	Basal Parasuchidae (non-Mystriosuchinae Parasuchidae)	TMM 31100-101
Parasuchus bransoni	Basal Parasuchidae (non-Mystriosuchinae Parasuchidae)	TMM 31100-419
Leptosuchus studeri	Basal Leptosuchomorpha (non-Mystriosuchini Leptosuchomorpha)	UMMP 14267 Case & White (1934)
Erythrosuchus africanus	Archosauromorpha (non-archosaur archosauromorph)	Cranial reconstruction Gower (2003)
Desmatosuchus haploceras	Aetosauria	Cranial reconstruction Small (2002)
Stagonolepis olenkae	Aetosauria	Cranial reconstruction Sulej (2010)
Ornithosuchus longidens	Ornithosuchia	Cranial reconstruction Walker (1964)
Herrerasaurus ischigualastensis	Dinosauria	Cranial reconstruction based on PVSJ 407 Sereno & Novas (1994)
Euparkeria capensis	Archosauromorpha (non-archosaur archosauromorph)	Cranial reconstruction Ewer (1965)

Table S2.2: Lateral view geometric morphometric dataset of phytosaurs and crocodylians. Table composition as in Table S3.1.

Lateral		
Taxon	Group for analysis	Specimen No. (and literature reference if specimen image was derived from a previous study)
Alligator mcgrewi	Crocodylia: Alligatoroidea	AMNH 7905
Anatosuchus minor	Notosuchia	MNN GAD17
Araripesuchus wegeneri	Notosuchia	MNN GAD19
Baurusuchus salgadoensis	Notosuchia	MPMA 62-0001-02
Caipirasuchus_paulistanus	Notosuchia	MPMA 67-0001-00 Iori & Carvalho (2011)
Crocodylus palaeindicus	Crocodylia: Crocodyloidea	NHMUK OR39795
Crocodylus acutus	Crocodylia: Crocodyloidea	NHMUK 1975-997
Mecistops cataphractus	Crocodylia: Crocodyloidea	NHMUK 1862-6-30-8
Crocodylus moreletii	Crocodylia: Crocodyloidea	NHMUK 1861-4-1-4
Crocodylus niloticus	Crocodylia: Crocodyloidea	NHMUK1959-1-8-55
'Crocodylus palustris-kimbula'	Crocodylia: Crocodyloidea	NHMUK 1897-12-31-1
Crocodylus siamensis	Crocodylia: Crocodyloidea	NHMUK 1921-4-1-168
Gavialis gangeticus	Crocodylia: Gavialoidea	NHMUK 1935-6-4-1
Melanosuchus niger	Crocodylia: Alligatoroidea	NHMUK 45-8-25-125
Tomistoma schlegelii	Crocodylia: Crocodyloidea	NHMUK 1860-11-6-8
Diplocynodon darwini	Crocodylia: Alligatoroidea	HLMD-Me 7500
Diplocynodon hantoniensis	Crocodylia: Alligatoroidea	CAMSM TN 907
Kaprosuchus saharicus	Notosuchia	MNN IGU12
Libycosuchus brevirostris	Notosuchia	BSPG 1912 VIII 574a,b
Montealtosuchus arrudacamposi	Notosuchia	MPMA 16-0007-04
Notosuchus terrestris	Notosuchia	MACN-RN 1037
Pelagosaurus typus	Thalattosuchia	SMNS 91.102
Piscogavialis jugaliperforatus	Crocodylia: Gavialoidea	SMNK PAL 1282
Boverisuchus vorax	Stem Crocodylia	FMNH PR 399
Sarcosuchus imperator	Tethysuchia	MNHN.F 1973-9 GDF 662
Simosuchus clarki	Notosuchia	Cast of UA 8679
Steneosaurus herberti	Thalattosuchia	MNHN.F 1890-13
Stolokrosuchus lapparenti	Notosuchia	Cast of MNN GDF 600
Uberabasuchus terrificus	Notosuchia	CPP 0630
Voay robustus	Crocodylia: Crocodyloidea	NHMUK PV R36685
Wannaganosuchus brachymanus	Crocodylia: Alligatoroidea	SMM P76.28.247 Erickson (1982)
Paleosuchus trigonatus	Crocodylia: Alligatoroidea	AMNH R-93812
Alligator sinensis	Crocodylia: Alligatoroidea	IVPP 1335 Cong *et al.* (1998)

Eogavialis africanum	Crocodylia: Gavialoidea	SMNS 11785
Eosuchus lerichei	Crocodylia: Gavialoidea	IRSNB R 48
Paleosuchus_palpebrosus	Crocodylia: Alligatoroidea	AMNH R-58136
Leptosuchus crosbiensis	Basal Leptosuchomorpha (non-Mystriosuchini Leptosuchomorpha)	TMM 31173-120
Machaeroprosopus lottorum	Mystriosuchini	TTU-P 10076
'Redondasaurus' ?bermani	Mystriosuchini	NMMNHS-P4256
Machaeroprosopus mccauleyi	Mystriosuchini	PEFO 31219
Machaeroprosopus pristinus	Mystriosuchini	PEFO 382
Machaeroprosopus pristinus	Mystriosuchini	UCMP 137319
Machaeroprosopus pristinus	Mystriosuchini	UCMP 34249
Mystriosuchus westphali	Mystriosuchini	GPIT 261-001
Mystriosuchus planirostris	Mystriosuchini	Combined morphology of SMNS 9900 & 9134
Nicrosaurus kapffi	Basal Leptosuchomorpha (non-Mystriosuchini Leptosuchomorpha)	SMNS4379
Paleorhinus sawini	Basal Parasuchidae (non-Mystriosuchinae Parasuchidae)	TMM 31213-16
Parasuchus hislopi	Basal Parasuchidae (non-Mystriosuchinae Parasuchidae)	ISIR 42
Smilosuchus gregorii	Basal Leptosuchomorpha (non-Mystriosuchini Leptosuchomorpha)	UCMP 27200
'Smilosuchus lithodendrorum'	Basal Leptosuchomorpha (non-Mystriosuchini Leptosuchomorpha)	PEFO 34852
'Smilosuchus lithodendrorum'	Basal Leptosuchomorpha (non-Mystriosuchini Leptosuchomorpha)	TMM 31173-121
'Smilosuchus lithodendrorum'	Basal Leptosuchomorpha (non-Mystriosuchini Leptosuchomorpha)	TTU-P 09234
'Smilosuchus lithodendrorum'	Basal Leptosuchomorpha (non-Mystriosuchini Leptosuchomorpha)	UCMP 27181
Machaeroprosopus pristinus	Mystriosuchini	MU 525
Smilosuchus gregorii	Basal Leptosuchomorpha (non-Mystriosuchini Leptosuchomorpha)	AMNH 3060
Rutiodon carolinensis	Basal Mystriosuchinae (non-leptosuchomorph Mystriosuchinae)	AMNH 1
Machaeroprosopus pristinus	Mystriosuchini	AMNH 7222
Angistorhinus grandis	Basal Mystriosuchinae (non-leptosuchomorph Mystriosuchinae)	FMNH 631
Leptosuchus crosbiensis	Basal Leptosuchomorpha (non-Mystriosuchini Leptosuchomorpha)	UMMP 7522 Case (1922)

Leptosuchus studeri	Basal Leptosuchomorpha (non-Mystriosuchini Leptosuchomorpha)	UMMP 14267 Case & White (1934)
Erythrosuchus africanus	Archosauromorpha	BP / 1 / 5207 Foth *et al.* (2016) Bernard Price Institute for Palaeontological Research,University of the Witswatersrand, Johannesburg, SouthAfrica
Desmatosuchus haploceras	Aetosauria	Cranial reconstruction Small (2002)
Stagonolepis olenkae	Aetosauria	Cranial reconstruction Sulej (2010)
Ornithosuchus longidens	Ornithosuchia	Cranial reconstruction Walker (1964)
Postosuchus kirkpatricki	'Rauisuchia'	Cranial reconstruction Chatterjee (1985)
Euparkeria capensis	Archosauromorpha	Cranial reconstruction Ewer (1965)
Herrerasaurus ischigualastensis	Dinosauria	Cranial reconstruction based on PVSJ 407 Sereno & Novas (1994)

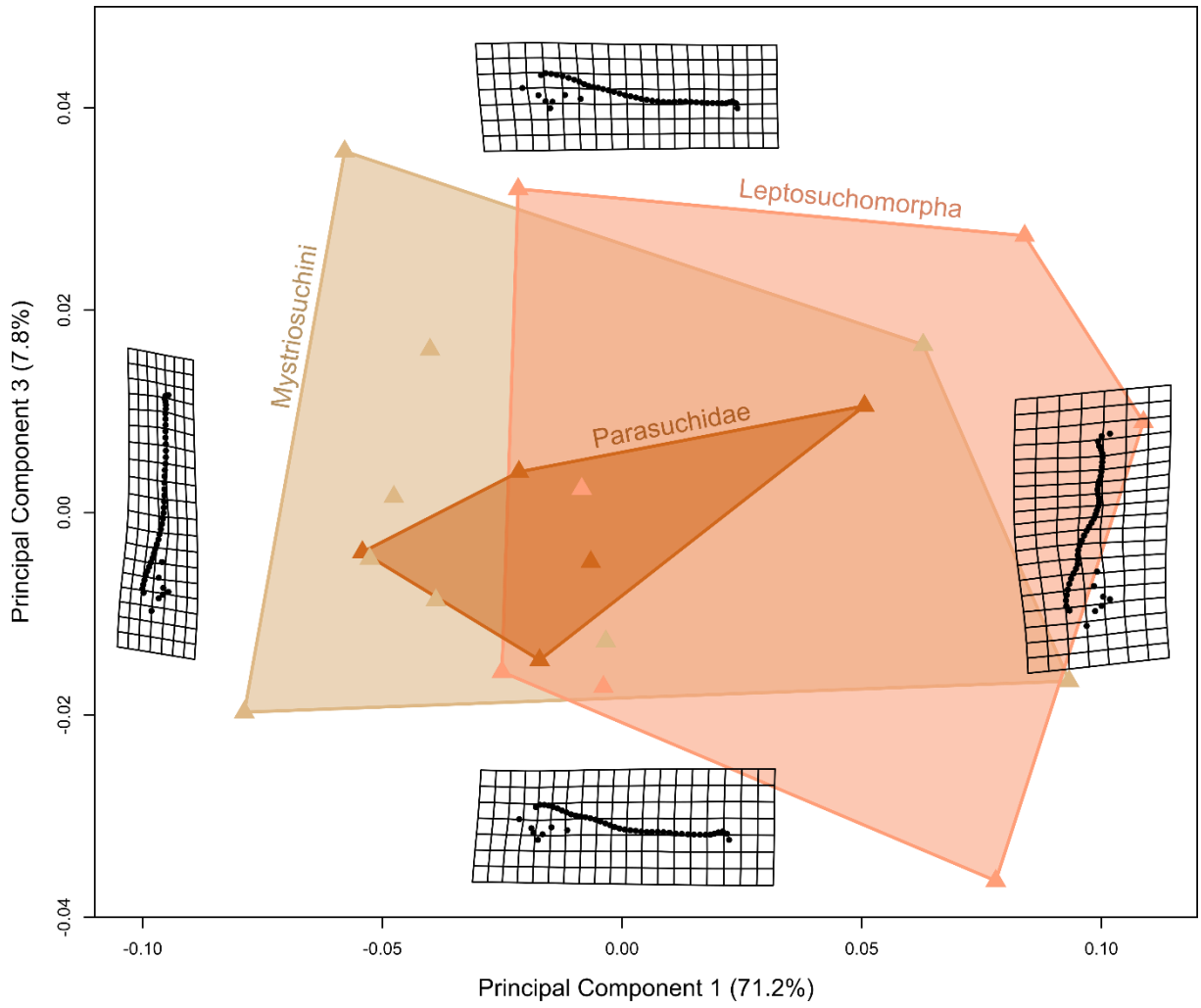

Figure S2.1: Dorsal view morphospace of Phytosauria; PC 1 vs PC 3. PC 3 describes subtle changes in the location of the orbit and position of the supratemporal fenestra in relation to the posterior quadrate extremity.

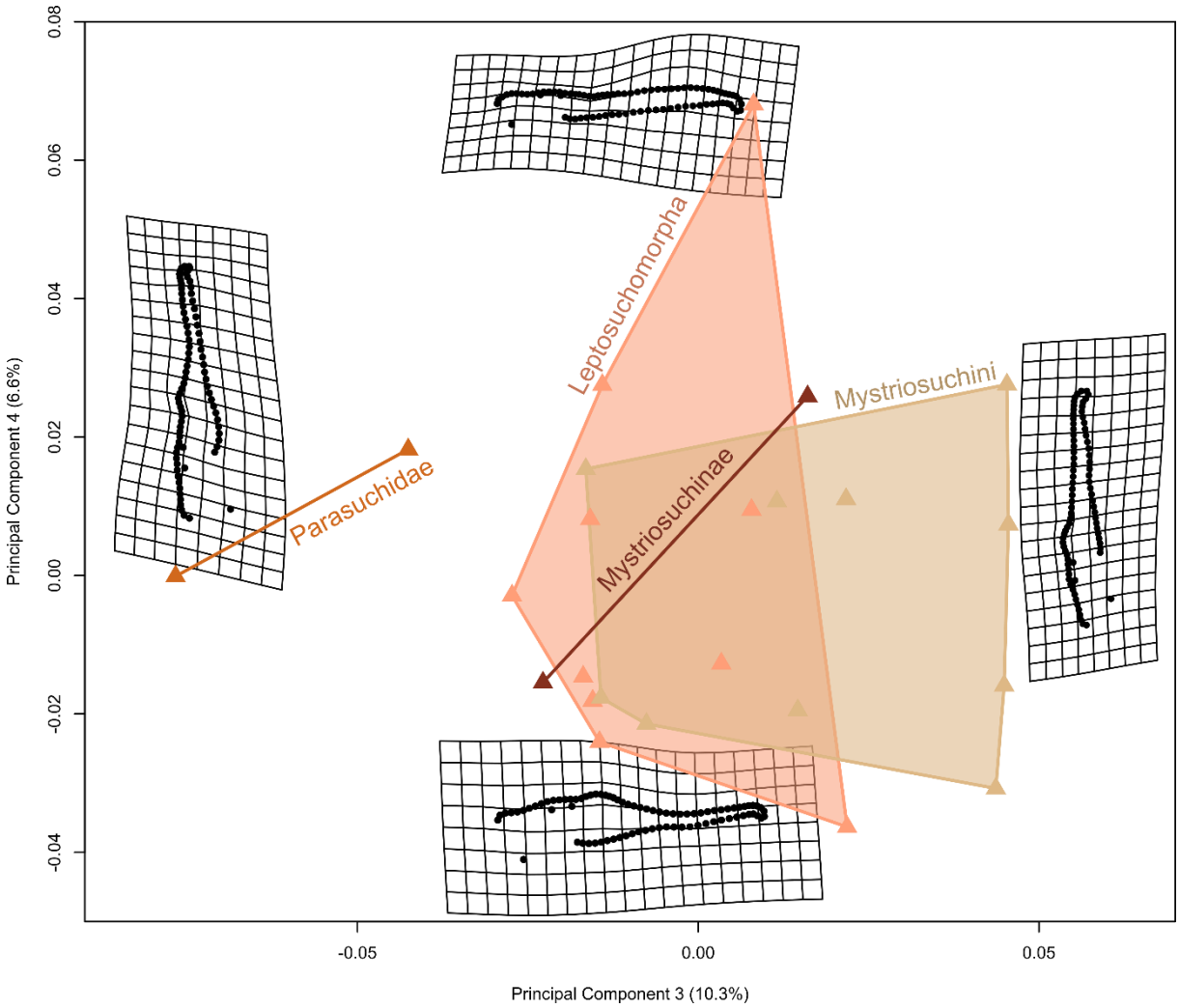

Figure S2.2: Lateral view morphospace of Phytosauria; PC 3 vs PC 4. PC 3 describes the anteroposterior shifting of the external nares, from a basal parasuchid to mystriosuchine morphology, and anteroposterior extension of the posterior process of the squamosals. PC 4 describes a shift between gracile and robust rostral morphology; the robust morphology on PC 4 is specific to *Nicrosaurus kapffi*.

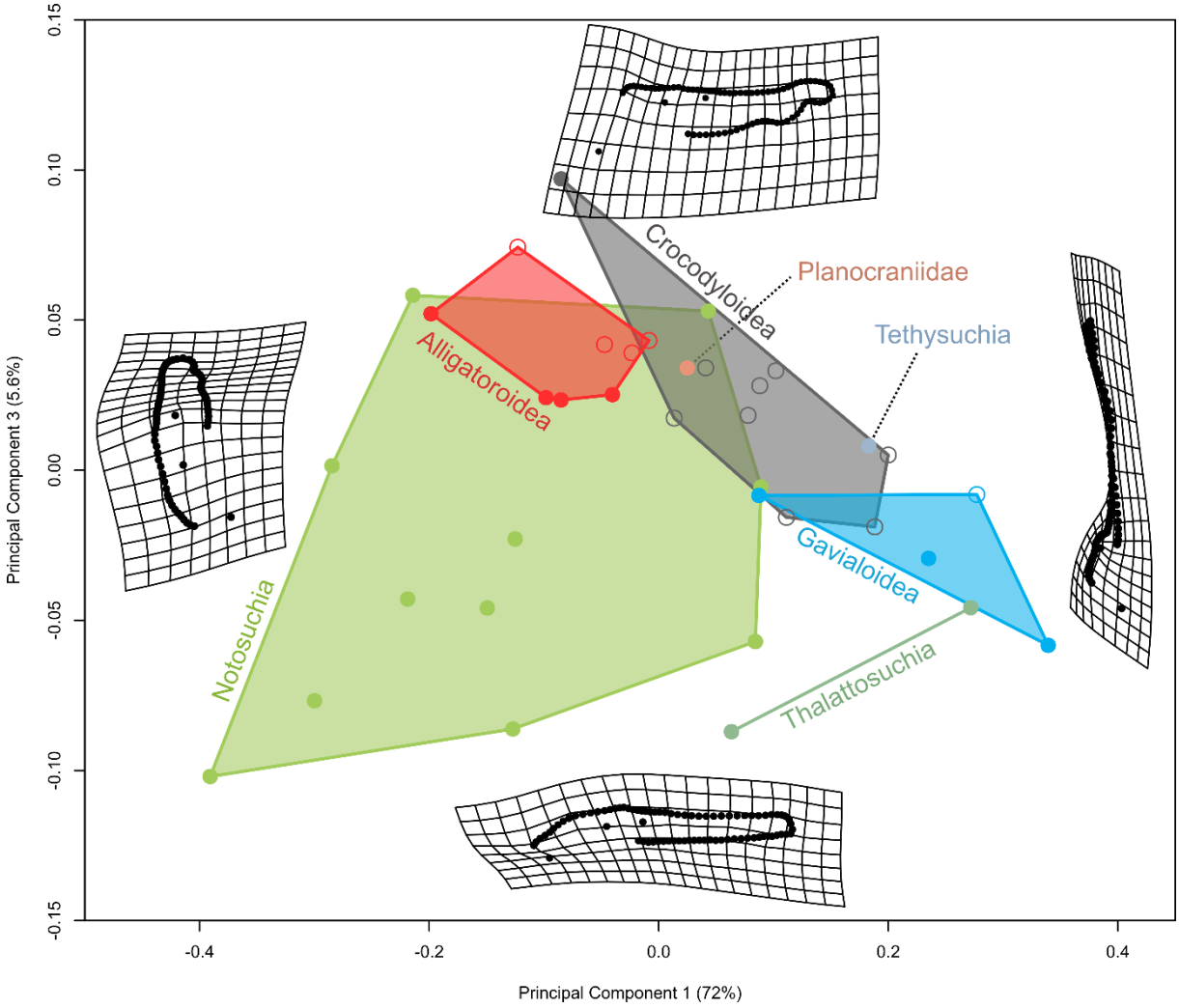

Figure S2.3: Lateral view morphospace of Crocodylomorpha; PC 1 vs PC 3. PC 3 describes a simultaneous increase in the robusticity of the cranial tooth row, development of the terminal rosette, increase in the dorsoventral height of the squamosals and posterior movement of the quadrate condyle.

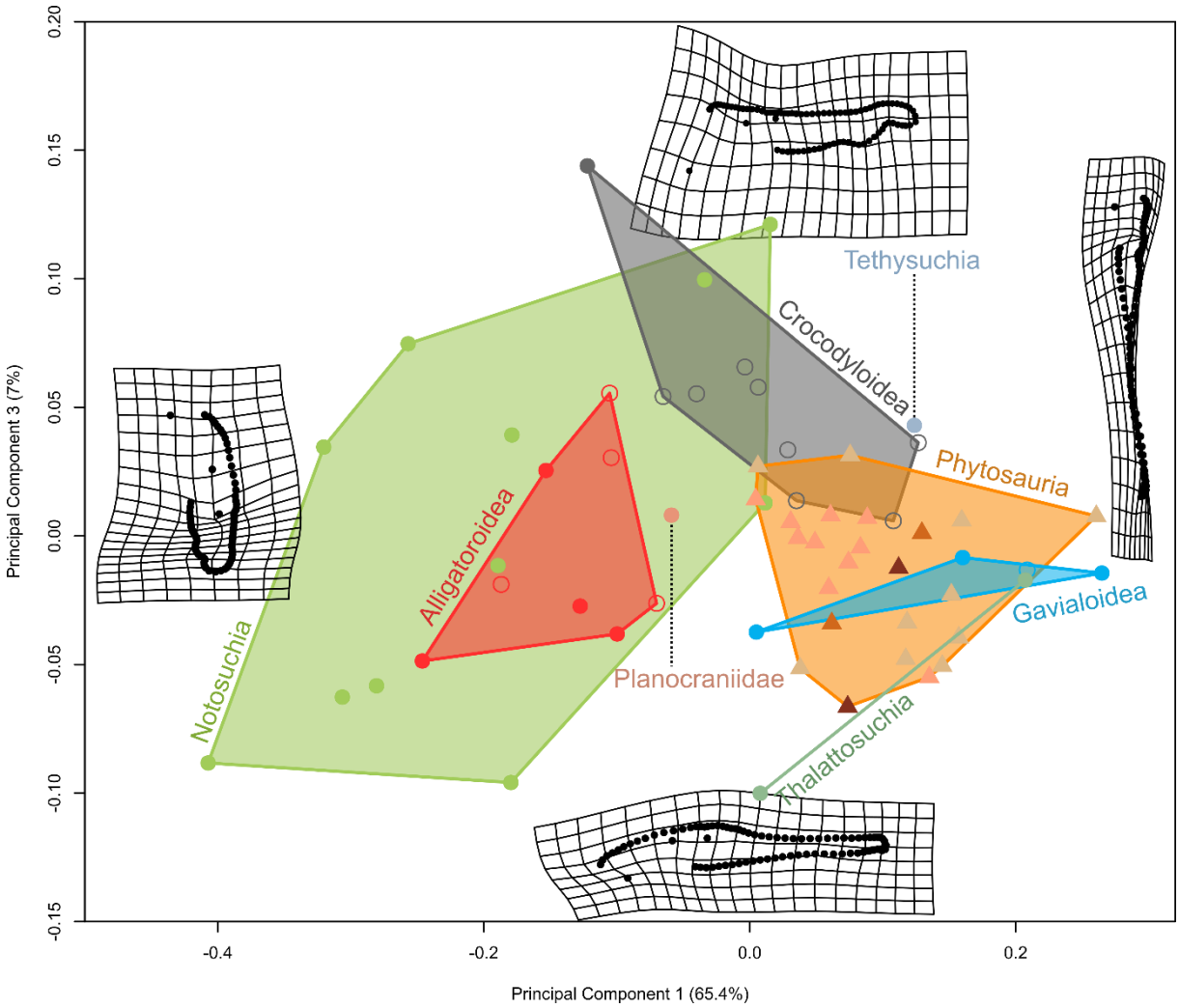

Figure S2.4: Lateral view morphospace of Phytosauria and Crocodylomorpha; PC 1 vs PC 3. Variation described by PC 3 remains approximately identical to that of the crocodylomorph-only morphospace in Figure S3.3.

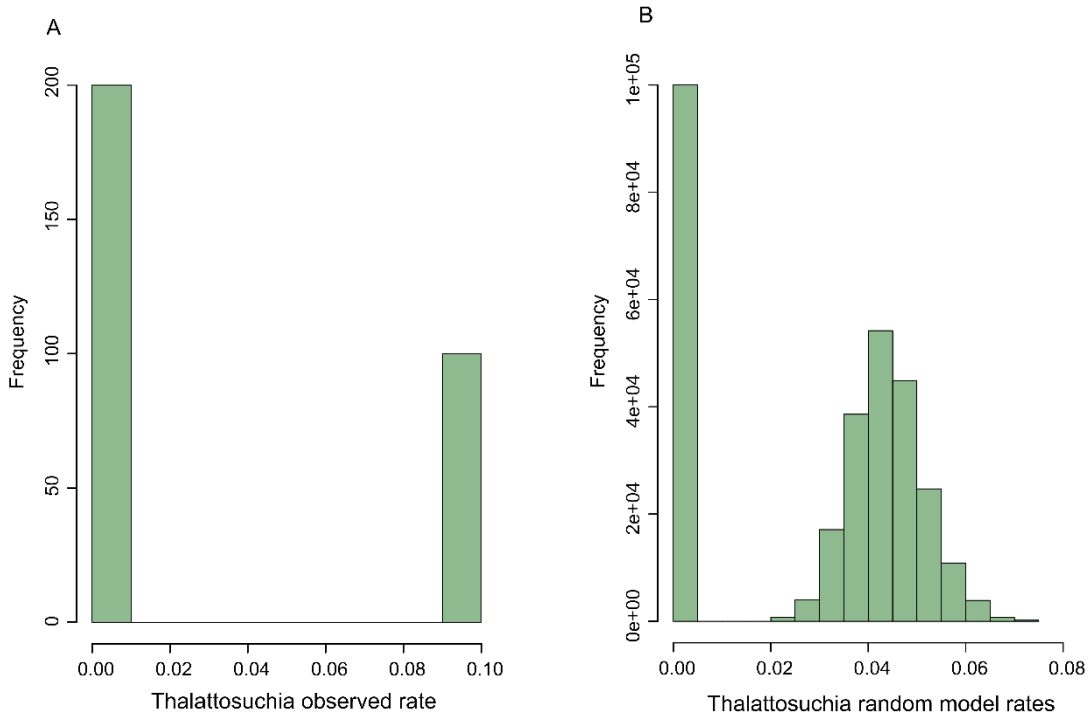

Figure S2.5: Frequency histograms of morphological evolutionary rates in every branch of Thalattosuchia, from the CalcRates analysis. A) Observed rates calculated from the morphological dataset; B) rates calculated from branches of the random evolutionary rates tree. The observed rates display a bimodal distribution, which overlaps considerably with low values of the random dataset; however the observed dataset contains rates exceeding any found in the random dataset.

Table S3.1: All log-transformed ISO textural parameter values for the phytosaur dataset, also including species, specimen, cranial robusticity and tooth position information.

Species	Specimen	Cranial morphology	Tooth position	Sq	Sku	Sp	Sv
'Smilosuchus lithodendrorum'	TTU-P 15661	Robust	Posterior	-1.4524	4.39666	0.25387	1.4681
'Smilosuchus lithodendrorum'	TTU-P 15661	Robust	Posterior	-1.5847	2.28554	0.62111	0.52295
'Smilosuchus lithodendrorum'	TTU-P 15661	Robust	Posterior	-1.0556	2.19355	0.85015	0.71638
'Smilosuchus lithodendrorum'	TTU-P 15661	Robust	Anterior	-1.6713	2.10071	0.42003	0.08066
Machaeroprosopus pristinus	TTU-P 10074	Gracile	Posterior	-2.0099	1.7258	-0.0398	-0.251
Machaeroprosopus pristinus	TTU-P 10074	Gracile	Mid	-1.7545	1.79625	-0.1839	0.07881
Machaeroprosopus pristinus	TTU-P 10074	Gracile	Mid	-1.1973	2.16722	0.59056	0.69863
Nicrosaurus meyeri	SMNS 91574	Gracile	Anterior	-1.7779	2.4177	0.33647	0.14323
Nicrosaurus meyeri	SMNS 91574	Gracile	Anterior	-1.6094	2.30698	-0.159	0.47063
Mystriosuchus planirostris	SMNS 12060	Gracile	?	-1.7545	2.00701	0.16721	-0.2536
Mystriosuchus planirostris	SMNS 12060	Gracile	Posterior	-1.666	1.81743	-0.2033	0.08984
Mystriosuchus planirostris	SMNS 12060	Gracile	Posterior	-1.959	1.6825	-0.1649	-0.1708
Nicrosaurus meyeri	SMNS 4059	Gracile	?	-1.7148	1.71434	0.13976	0.22314
Nicrosaurus kapffi	SMNS 13078	Robust	Anterior	-1.4482	1.54841	0.26005	0.30528
Nicrosaurus kapffi	SMNS 13078	Robust	Anterior	-1.6246	1.60944	0.02859	0.48181
Nicrosaurus kapffi	SMNS 13078	Robust	Mid	-1.8079	1.8345	0.19639	0.01587
Nicrosaurus kapffi	SMNS 13078	Robust	Mid	-1.4961	2.18538	0.22873	0.61085
Nicrosaurus kapffi	SMNS 13078	Robust	Mid	-1.3823	2.13298	0.54812	0.7715
Nicrosaurus kapffi	SMNS 13078	Robust	Mid	-1.7373	2.28564	0.68006	0.05543

Table S3.1: Continued.

Sz	Sds	Str	Sdq	Ssc	Sdr	Vmp	Vmc	Vvc	Vvv	Spk	Sk	Svk
1.72793	12.1118	-0.7593	-1.5847	0.02567	0.73621	9.10609	11.6613	12.0137	10.3156	-1.6348	-1.1117	-0.7487
1.26638	12.1281	-1.0134	-1.4439	0.36949	0.99251	9.41735	11.835	12.1756	10.3222	-1.3243	-0.9623	-1.0413
1.47865	12.1653	-0.4416	-1.3056	0.45171	1.25647	9.84161	12.2877	12.5062	11.0477	-0.9138	-0.5586	-0.3425
0.9582	12.0782	-1.5325	-1.5279	0.16042	0.83595	9.51044	11.7981	12.0552	10.2036	-1.2588	-1.0328	-1.2658
0.55331	12.1495	-0.5108	-1.682	-0.0726	0.54581	9.19928	11.5425	11.9382	9.61581	-1.5896	-1.2483	-1.8708
0.64972	12.1118	-2.6037	-1.5559	0.02567	0.76361	8.97335	11.7118	11.9316	10.3766	-1.8079	-1.1332	-1.0906
1.3392	12.1227	-1.9661	-1.4482	0.52295	0.99103	10.4312	12.0436	12.4913	10.5532	-0.47	-0.8255	-0.851
0.93766	12.2453	-0.4829	-1.8264	-0.129	0.24764	9.3501	11.5806	11.8914	10.1503	-1.461	-1.204	-1.214
0.89772	12.0257	-0.7765	-1.7373	-0.3092	0.42723	9.44936	11.7753	12.1335	10.3156	-1.3626	-1.0272	-0.9808
0.67192	12.2453	-0.8699	-1.7148	0.12663	0.47375	9.51044	11.7598	12.1007	9.90848	-1.3168	-1.0217	-1.6045
0.64658	12.0839	-1.4917	-1.9105	-0.3257	0.08893	9.54681	11.813	12.1653	10.1386	-1.2801	-0.9782	-1.2694
0.52532	12.3327	-0.5798	-1.7838	-0.1098	0.33433	9.05719	11.6082	11.9316	9.78695	-1.726	-1.1584	-1.666
0.87547	12.1281	-1.0079	-1.4439	0.2799	0.98395	9.05017	11.8636	12.1335	10.1773	-1.6874	-0.9163	-1.2658
0.97607	12.1281	-1.7898	-1.2946	0.32642	1.26751	9.15377	12.1756	12.3283	10.5558	-1.5799	-0.6812	-0.9623
0.9738	12.0317	-0.5692	-1.3243	0.17731	1.22495	9.09941	11.9954	12.221	10.2819	-1.666	-0.8324	-1.2208
0.8029	12.1118	-1.3665	-1.666	-0.0877	0.55618	9.36734	11.6952	11.9829	10.0432	-1.4065	-1.1332	-1.4106
1.13076	12.1653	-2.333	-1.4653	0.37018	0.94934	9.36734	12.0137	12.3588	10.3385	-1.3903	-0.7744	-1.0134
1.35892	11.9704	-0.8747	-1.3168	-0.0812	1.16907	9.36734	12.0895	12.3104	10.669	-1.3665	-0.7487	-0.7593
1.10889	12.1227	-1.328	-1.6145	0.0944	0.65752	9.48037	11.7199	12.0725	10.0257	-1.291	-1.0877	-1.4439

Table S3.1: Continued.

Smr1	Smr2	S5z	Sa
2.4248	4.50092	0.89077	-2.0956
2.4248	4.47961	1.08586	-1.9661
2.23001	4.44969	1.37877	-1.4653
2.29253	4.45899	0.82549	-2.025
2.5177	4.4987	0.46938	-2.3126
2.23001	4.44265	0.61464	-2.0956
2.59525	4.4613	1.16315	-1.6451
2.35138	4.4762	0.82812	-2.1893
2.45101	4.483	0.84027	-2.0025
2.40695	4.48864	0.58501	-2.0794
2.43361	4.48639	0.60922	-2.0025
2.35138	4.49424	0.35977	-2.2538
2.23001	4.47961	0.74432	-2.0099
2.04122	4.44383	0.87838	-1.726
2.19722	4.45899	0.85484	-1.9105
2.35138	4.46591	0.70754	-2.1456
2.43361	4.48864	0.96241	-1.8326
2.23001	4.45202	1.18906	-1.7316
2.45959	4.4762	0.93295	-2.0956

Table S3.2: Significant pairwise differences between dietary guilds along PC and CV axes 1 and 2 of the PCA and CVA for the full crocodylian and varanid dataset by dietary guild, using the four parameters significant to dietary guild (Sds, Vmp, Spk & Smr1).

PC 1	P values
Omnivore ~ Piscivore	<0.0001
Omnivore ~ Phytosaur	0.0014
Omnivore ~ Intermediate invertebrates	0.0023
Omnivore ~ Carnivore	0.0015
Hard invertebrates ~ Piscivore	0.0144
PC 2	
Intermediate invertebrates ~ Hard invertebrates	0.0038
Carnivore ~ Hard invertebrates	0.0146
Intermediate invertebrates ~ Piscivore	0.0302
CV 1	
Omnivore ~ Intermediate invertebrates	0.0002
Omnivore ~ Carnivore	0.0004
Omnivore ~ Piscivore	0.0012
Omnivore ~ Phytosaur	0.0026
Hard invertebrates ~ Intermediate invertebrates	0.0009
Hard invertebrates ~ Carnivore	0.0016
Hard invertebrates ~ Piscivore	0.0061
Hard invertebrates ~ Phytosaur	0.0148
CV 2	
Omnivore ~ Piscivore	0.0229
Intermediate invertebrates ~ Piscivore	0.0165
Carnivore ~ Piscivore	0.0125

Table S3.3: PCA of all crocodylian and varanid taxa, using the four textural parameters significant for dietary guild (Sds, Vmp, Spk & Smr1): Spearman ρ correlations of PC axes 1 and 2 against dietary composition percentages. Significant correlations after Benjamini-Hochberg correction highlighted in green.

Principal Component axis	vs. % of 'x' in diet	Spearman ρ	P value
PC1	Total verts	-0.3762	0.0002
PC1	Tetrapods	-0.0942	0.3615
PC1	fish	-0.2481	0.0148
PC1	Total inverts	0.3232	0.0013
PC1	Soft inverts	0.0784	0.4478
PC1	Inter inverts	0.1703	0.0971
PC1	Hard inverts	0.2733	0.007
PC1	Plant matter	0.0825	0.4243
PC2	Total verts	-0.0724	0.4835
PC2	Tetrapods	0.2188	0.0322
PC2	fish	-0.1815	0.0768
PC2	Total inverts	0.0841	0.4151
PC2	Soft inverts	0.0451	0.6624
PC2	Inter inverts	0.3007	0.0029
PC2	Hard inverts	0.0432	0.6759
PC2	Plant matter	-0.0934	0.3656

Table S3.4: CVA of all crocodylian and varanid taxa, grouped by dietary guild, using the four textural parameters significant for dietary guild (Sds, Vmp, Spk & Smr1): Spearman ρ correlations of CV axes 1 and 2 against dietary composition percentages. Significant correlations after Benjamini-Hochberg correction highlighted in green.

Canonical Variate axis	vs. % of 'x' in diet	Spearman ρ	P value
CV1	Total verts	-0.2752	0.0067
CV1	Tetrapods	-0.2998	0.003
CV1	fish	-0.0321	0.7566
CV1	Total inverts	0.2039	0.0463
CV1	Soft inverts	-0.0379	0.7139
CV1	Inter inverts	-0.104	0.3131
CV1	Hard inverts	0.1833	0.0738
CV1	Plant matter	0.2097	0.0403
CV2	Total verts	-0.2551	0.0121
CV2	Tetrapods	0.1118	0.2783
CV2	fish	-0.2719	0.0074
CV2	Total inverts	0.2163	0.0343
CV2	Soft inverts	0.0657	0.5246
CV2	Inter inverts	0.3459	0.0006
CV2	Hard inverts	0.1799	0.0794
CV2	Plant matter	0.0083	0.9358

Table S3.5: Significant pairwise differences between dietary guilds along CV axes 1, 2 and 3 of the CVA for the full crocodylian and varanid dataset by dietary guild, using all 21 textural parameters.

CV 1	P values
Omnivore ~ Piscivore	<0.0001
Omnivore ~ Phytosaur	<0.0001
Omnivore ~ Intermediate invertebrates	<0.0001
Omnivore ~ Carnivore	<0.0001
Omnivore ~ Hard invertebrates	<0.0001
Intermediate invertebrates ~ Hard invertebrates	0.001
Intermediate invertebrates ~ Phytosaur	0.0151
Carnivore ~ Hard invertebrates	0.0137
CV 2	
Omnivore ~ Hard invertebrates	0.0003
Omnivore ~ Piscivore	0.0101
Omnivore ~ Phytosaur	0.0156
Intermediate invertebrates ~ Phytosaur	0.0096
Intermediate invertebrates ~ Hard invertebrates	<0.0001
Intermediate invertebrates ~ Piscivore	0.0044
Carnivore ~ Piscivore	0.0321
Carnivore ~ Hard invertebrates	0.0005
CV 3	
Hard invertebrates ~ Piscivore	0.0013
Hard invertebrates ~ Phytosaur	0.0041
Carnivore ~ Piscivore	0.0126
Carnivore ~ Phytosaur	0.0469

Table S3.6: CVA of all crocodylian and varanid taxa, grouped by dietary guild, using all 21 textural parameters: Spearman ρ correlations of CV axes 1, 2 and 3 against dietary composition percentages. Significant correlations after Benjamini-Hochberg correction highlighted in green.

Canonical Variate axis	vs. % of 'x' in diet	Spearman ρ	P value
CV1	Total verts	0.091	0.3781
CV1	Tetrapods	0.3373	0.0008
CV1	fish	-0.0604	0.5589
CV1	Total inverts	0.0143	0.8901
CV1	Soft inverts	0.1129	0.2733
CV1	Inter inverts	0.3591	0.0003
CV1	Hard inverts	-0.1052	0.3077
CV1	Plant matter	-0.3095	0.0022
CV2	Total verts	-0.2382	0.0195
CV2	Tetrapods	0.1813	0.0772
CV2	fish	-0.3053	0.0025
CV2	Total inverts	0.1717	0.0944
CV2	Soft inverts	0.1542	0.1335
CV2	Inter inverts	0.494	0.0001
CV2	Hard inverts	0.0762	0.4606
CV2	Plant matter	0.0824	0.4251
CV3	Total verts	-0.2556	0.0119
CV3	Tetrapods	0.1367	0.1842
CV3	fish	-0.2304	0.0239
CV3	Total inverts	0.3041	0.0026
CV3	Soft inverts	0.197	0.0544
CV3	Inter inverts	0.223	0.029
CV3	Hard inverts	0.1797	0.0798
CV3	Plant matter	-0.2162	0.0344

Table S3.7: Phytosaur dietary predictions based on the CV predictive model constructed with all crocodylian and varanid taxa, grouped by dietary guild and using all 21 textural parameters.

#	Species	Predicted dietary guild	Probability	Other predictions
1	*Smilosuchus lithodendrorum*	piscivore	0.7873	hard invertebrates 0.19
2	*Smilosuchus lithodendrorum*	piscivore	0.5195	carnivore 0.14 hard invertebrates 0.30
3	*Smilosuchus lithodendrorum*	intermediate invertebrates	0.4722	carnivore 0.38 piscivore 0.11
4	*Smilosuchus lithodendrorum*	piscivore	0.6827	carnivore 0.18 hard invertebrates 0.10
5	*Machaeroprosopus pristinus*	piscivore	0.7124	hard invertebrates 0.16
6	*Machaeroprosopus pristinus*	piscivore	0.5769	carnivore 0.22 hard invertebrates 0.16
7	*Machaeroprosopus pristinus*	omnivore	0.4450	hard invertebrates 0.27 piscivore 0.16
8	*Nicrosaurus meyeri*	piscivore	0.5285	carnivore 0.27 intermediate invertebrates 0.15
9	*Nicrosaurus meyeri*	hard invertebrates	0.6653	piscivore 0.30
10	*Mystriosuchus planirostris*	intermediate invertebrates	0.4639	carnivore 0.30 piscivore 0.22
11	*Mystriosuchus planirostris*	hard invertebrates	0.3649	carnivore 0.23 piscivore 0.33
12	*Mystriosuchus planirostris*	intermediate invertebrates	0.5104	carnivore 0.32 piscivore 0.16
13	*Nicrosaurus meyeri*	piscivore	0.5403	carnivore 0.25 intermediate invertebrates 0.13
14	*Nicrosaurus kapffi*	intermediate invertebrates	0.4699	carnivore 0.44
15	*Nicrosaurus kapffi*	piscivore	0.5431	carnivore 0.15 hard invertebrates 0.11 intermediate invertebrates 0.20
16	*Nicrosaurus kapffi*	piscivore	0.5508	carnivore 0.23 hard invertebrates 0.16
17	*Nicrosaurus kapffi*	carnivore	0.4812	hard invertebrates 0.20 intermediate invertebrates 0.10 piscivore 0.22
18	*Nicrosaurus kapffi*	hard invertebrates	0.4172	carnivore 0.19 piscivore 0.34
19	*Nicrosaurus kapffi*	piscivore	0.4105	carnivore 0.32 hard invertebrates 0.20

Table S3.8: Significant pairwise differences between dietary guilds along CV 1 of the CVA for the crocodylian dataset by dietary guild, using all 21 textural parameters.

CV 1	P values
Carnivore ~ Hard invertebrates	<0.0001
Carnivore ~ Piscivore	0.0002
Carnivore ~ Robust phytosaurs	0.0069
Hard invertebrates ~ Robust phytosaurs	<0.0001
Hard invertebrates ~ Gracile phytosaurs	<0.0001
Hard invertebrates ~ Piscivore	<0.0001

Table S3.9: CVA of crocodylian taxa, grouped by dietary guild, using all 21 textural parameters: Spearman ρ correlations of CV axes 1 and 2 against dietary composition percentages. Significant correlations after Benjamini-Hochberg correction highlighted in green.

Canonical Variate axis	vs. % of 'x' in diet	Spearman ρ	P value
CV1	Total verts	0.4735	0.0013
CV1	Tetrapods	0.3276	0.032
CV1	fish	0.2208	0.1547
CV1	Total inverts	-0.4228	0.0047
CV1	Soft inverts	-0.0448	0.7755
CV1	Inter inverts	0.0903	0.5646
CV1	Hard inverts	-0.261	0.0909
CV1	Plant matter	0.1443	0.3558
CV2	Total verts	-0.3792	0.0121
CV2	Tetrapods	0.141	0.3672
CV2	fish	-0.5028	0.0006
CV2	Total inverts	0.4501	0.0025
CV2	Soft inverts	0.35	0.0214
CV2	Inter inverts	0.0065	0.9672
CV2	Hard inverts	0.5205	0.0003
CV2	Plant matter	-0.1597	0.3064

Table S3.10: Phytosaur dietary predictions based on the CV predictive model constructed with crocodylian taxa, grouped by dietary guild and using all 21 textural parameters.

#	Species	Predicted dietary guild	Probability	Other predictions
1	*Smilosuchus lithodendrorum*	piscivore	0.7838	hard invertebrates 0.17
2	*Smilosuchus lithodendrorum*	piscivore	0.5111	carnivore 0.18 hard invertebrates 0.31
3	*Smilosuchus lithodendrorum*	piscivore	0.6312	carnivore 0.36
4	*Smilosuchus lithodendrorum*	carnivore	0.7413	piscivore 0.25
5	*Machaeroprosopus pristinus*	piscivore	0.7031	carnivore 0.28
6	*Machaeroprosopus pristinus*	piscivore	0.7770	carnivore 0.15
7	*Machaeroprosopus pristinus*	hard invertebrates	0.6090	carnivore 0.24 piscivore 0.15
8	*Nicrosaurus meyeri*	piscivore	0.5236	carnivore 0.47
9	*Nicrosaurus meyeri*	hard invertebrates	0.6420	piscivore 0.36
10	*Mystriosuchus planirostris*	carnivore	0.6303	piscivore 0.37
11	*Mystriosuchus planirostris*	piscivore	0.5782	hard invertebrates 0.42
12	*Mystriosuchus planirostris*	piscivore	0.7173	carnivore 0.28
13	*Nicrosaurus meyeri*	piscivore	0.5534	carnivore 0.42
14	*Nicrosaurus kapffi*	carnivore	0.6692	piscivore 0.33
15	*Nicrosaurus kapffi*	carnivore	0.6582	piscivore 0.33
16	*Nicrosaurus kapffi*	piscivore	0.5741	carnivore 0.39
17	*Nicrosaurus kapffi*	hard invertebrates	0.5802	piscivore 0.42
18	*Nicrosaurus kapffi*	piscivore	0.7391	hard invertebrates 0.25
19	*Nicrosaurus kapffi*	carnivore	0.6084	piscivore 0.37

Table S3.11: Significant pairwise differences between species groups along PC and CV axes 1 and 2 of the PCA and CVA for the crocodylian dataset by species, using the 12 textural parameters significant for species (Sq, Sdr, Vmp, Vmc, Vvc, Vvv, Spk, Sk, Svk, Smr1, Smr2 & Sa).

PC 1	P values
Crocodylus porosus Juvenile ~ *Caiman crocodilus*	0.0001
Crocodylus porosus Juvenile ~ *Gavialis gangeticus*	0.0004
Crocodylus porosus Juvenile ~ *Crocodylus porosus* Adult	0.0021
Crocodylus porosus Juvenile ~ Gracile phytosaurs	0.0155
Alligator mississippiensis ~ Caiman crocodilus	0.0067
Alligator mississippiensis ~ Gavialis gangeticus	0.0193
PC 2	
Crocodylus porosus Juvenile ~ *Gavialis gangeticus*	0.0151
CV 1	
Crocodylus porosus Juvenile ~ *Gavialis gangeticus*	<0.0001
Crocodylus porosus Juvenile ~ *Crocodylus porosus* Adult	<0.0001
Crocodylus porosus Juvenile ~ *Caiman crocodilus*	<0.0001
Crocodylus porosus Juvenile ~ Robust phytosaurs	<0.0001
Crocodylus porosus Juvenile ~ Gracile phytosaurs	0.0002
Crocodylus porosus Juvenile ~ *Crocodylus niloticus*	0.0037
Crocodylus porosus Juvenile ~ *Crocodylus acutus*	0.0156
Crocodylus porosus Juvenile ~ *Alligator mississippiensis*	0.0487
Alligator mississippiensis ~ Gavialis gangeticus	0.0001
Alligator mississippiensis ~ Crocodylus porosus Adult	0.0007
Crocodylus acutus ~ Gavialis gangeticus	0.0012
Crocodylus acutus ~ Crocodylus porosus Adult	0.0062
Gracile phytosaurs ~ Gavialis gangeticus	0.0323
CV 2	
Robust phytosaurs ~ *Crocodylus acutus*	0.0008
Robust phytosaurs ~ *Caiman crocodilus*	0.0101
Crocodylus porosus Juvenile ~ *Crocodylus acutus*	0.0417

Table S3.12: CVA of crocodylian taxa, grouped by species, using the 12 textural parameters significant for species (Sq, Sdr, Vmp, Vmc, Vvc, Vvv, Spk, Sk, Svk, Smr1, Smr2 & Sa): Spearman ρ correlations of CV axes 1 and 2 against dietary composition percentages. Significant correlations after Benjamini-Hochberg correction highlighted in green.

Canonical Variate axis	vs. % of x in diet	Spearman ρ	P value
CV1	Total verts	-0.4328	0.0037
CV1	Tetrapods	-0.2526	0.1022
CV1	fish	-0.3024	0.0487
CV1	Total inverts	0.4145	0.0057
CV1	Soft inverts	-0.0339	0.8293
CV1	Inter inverts	0.0387	0.8053
CV1	Hard inverts	0.4406	0.0031
CV1	Plant matter	-0.0831	0.5964
CV2	Total verts	0.267	0.0835
CV2	Tetrapods	0.0226	0.8856
CV2	fish	0.0828	0.5975
CV2	Total inverts	-0.2062	0.1847
CV2	Soft inverts	-0.1195	0.4454
CV2	Inter inverts	0.1742	0.2639
CV2	Hard inverts	0.0915	0.5596
CV2	Plant matter	-0.1767	0.2571

Table S3.13: CVA of crocodylian taxa, grouped by species, using all 21 textural parameters: Spearman ρ correlations of CV axes 1, 2, 3 and 4 against dietary composition percentages. Significant correlations after Benjamini-Hochberg correction highlighted in green.

Canonical Variate axis	vs. % of x in diet	Spearman ρ	P value
CV1	Total verts	0.1717	0.271
CV1	Tetrapods	-0.1078	0.4913
CV1	fish	0.0343	0.8273
CV1	Total inverts	-0.124	0.4282
CV1	Soft inverts	-0.2271	0.143
CV1	Inter inverts	0.3226	0.0349
CV1	Hard inverts	0.2221	0.1524
CV1	Plant matter	-0.3108	0.0425
CV2	Total verts	0.6469	0.0001
CV2	Tetrapods	0.2419	0.1181
CV2	fish	0.3566	0.0189
CV2	Total inverts	-0.5799	0.0001
CV2	Soft inverts	-0.1227	0.4332
CV2	Inter inverts	0.2129	0.1704
CV2	Hard inverts	-0.3064	0.0457
CV2	Plant matter	-0.0963	0.5392
CV3	Total verts	-0.1648	0.291
CV3	Tetrapods	-0.2787	0.0703
CV3	fish	-0.0208	0.8945
CV3	Total inverts	0.1006	0.5208
CV3	Soft inverts	-0.2342	0.1307
CV3	Inter inverts	0.0387	0.8053
CV3	Hard inverts	0.2153	0.1655
CV3	Plant matter	0.4362	0.0035
CV4	Total verts	-0.1059	0.4991
CV4	Tetrapods	0.4642	0.0017
CV4	fish	-0.4085	0.0065
CV4	Total inverts	0.2006	0.1971
CV4	Soft inverts	0.3702	0.0145
CV4	Inter inverts	0.1936	0.2136
CV4	Hard inverts	0.3097	0.0433
CV4	Plant matter	-0.098	0.5318

Table S3.14: Significant pairwise differences between species groups along CV axes 2, 3 and 4 of the CVA for the crocodylian dataset by species, using all 21 textural parameters.

CV 2	P values
Crocodylus acutus ~ *Crocodylus porosus* Adult	<0.0001
Crocodylus acutus ~ *Gavialis gangeticus*	<0.0001
Crocodylus acutus ~ Gracile phytosaurs	<0.0001
Crocodylus acutus ~ Robust phytosaurs	<0.0001
Crocodylus acutus ~ *Crocodylus niloticus*	0.0003
Crocodylus acutus ~ *Alligator mississippiensis*	0.0481
Caiman crocodilus ~ *Crocodylus porosus* Adult	<0.0001
Caiman crocodilus ~ *Gavialis gangeticus*	<0.0001
Caiman crocodilus ~ Gracile phytosaurs	0.0008
Caiman crocodilus ~ Robust phytosaurs	0.0017
Caiman crocodilus ~ *Crocodylus niloticus*	0.0385
Crocodylus porosus Juvenile ~ *Crocodylus porosus* Adult	0.0004
Crocodylus porosus Juvenile ~ *Gavialis gangeticus*	0.0003
Crocodylus porosus Juvenile ~ Gracile phytosaurs	0.0050
Crocodylus porosus Juvenile ~ Robust phytosaurs	0.0101
Alligator mississippiensis ~ *Crocodylus porosus* Adult	0.0018
Alligator mississippiensis ~ *Gavialis gangeticus*	0.0012
Alligator mississippiensis ~ Gracile phytosaurs	0.0269
CV 3	
Caiman crocodilus ~ *Crocodylus acutus*	0.0010
Caiman crocodilus ~ *Gavialis gangeticus*	0.0045
Caiman crocodilus ~ Gracile phytosaurs	0.0218
Caiman crocodilus ~ Robust phytosaurs	0.0321
Caiman crocodilus ~ *Alligator mississippiensis*	0.0312
Crocodylus porosus Juvenile ~ *Crocodylus acutus*	0.0395
CV 4	
Crocodylus porosus Adult ~ *Gavialis gangeticus*	0.0057
Alligator mississippiensis ~ *Gavialis gangeticus*	0.0206
Gracile phytosaurs ~ *Gavialis gangeticus*	0.0342
Robust phytosaurs ~ *Gavialis gangeticus*	0.0414

References

Abel, O. 1922. Die Schnauzenverletzungen der Parasuchier und ihre biologische Bedeutung. *Paläontologische Zeitschrift*, **5**, 26–57 DOI: 10.1007/BF03041524

Abler, W. L. 1992. The serrated teeth of tyrannosaurid dinosaurs, and biting structures in other animals. *Paleobiology*, **18**, 161–183.

Adams, D.C. 2014. Quantifying and comparing phylogenetic evolutionary rates for shape and other high-dimensional phenotypic data. *Systematic Biology*, **63**, 166–177.

Adams, D. C., & Otárola-Castillo, E. 2013. Geomorph: an R package for the collection and analysis of geometric morphometric shape data. *Methods in Ecology and Evolution*, **4**, 393–399 DOI: 10.1111/2041-210X.12035

Adams, D. C., Collyer, M. L., & Kaliontzopoulou, A. 2018. Geomorph: Software for geometric morphometric analyses. R package version 3.0.6. https://cran.r-project.org/package=geomorph.

Anderson, H. T. 1936. The jaw musculature of the phytosaur, *Machaeroprosopus*. *Journal of Morphology*, **59**, 549–587.

Andrade, D. V., Cruz-Neto, A. P., Abe, A. S., & Wang, T. 2005. Specific Dynamic Action in Ectothermic Vertebrates: A Review of the Determinants of Postprandial Metabolic Response in Fishes, Amphibians, and Reptiles. Pp. 306–324 in Starck, J. M., & Wang, T. (eds) *Physiological and Ecological Adaptations to Feeding in Vertebrates*. Enfield, New Hampshire: Science Publishers.

Auffenberg, W. 1981. *The behavioral ecology of the Komodo monitor*. Florida, USA, University Presses of Florida.

Auffenberg, W. 1988. *Gray's Monitor Lizard*. Florida, USA, University Presses of Florida.

Ballew, K. L. 1989. *A phylogenetic analysis of Phytosauria (Reptilia: Archosauria) from the late Triassic of the western United States*. Unpublished MA thesis, University of California, Berkeley, 73 pp.

Bapst, D. W. 2012. paleotree: an R package for paleontological and phylogenetic analyses of evolution. *Methods in Ecology and Evolution*, **3**, 803–807. DOI: 10.1111/j.2041-210X.2012.00223.x

Beaulieu, J. M., Jhwueng, D. C., Boettiger, C., & O'Meara, B. C. 2012. Modeling stabilizing selection: expanding the Ornstein–Uhlenbeck model of adaptive evolution. *Evolution: International Journal of Organic Evolution*, **66**, 2369-2383 DOI: 10.1111/j.1558-5646.2012.01619.x

Bell, M. A., & Lloyd, G. T. 2014. strap: an R package for plotting phylogenies against stratigraphy and assessing their stratigraphic congruence. *Palaeontology*, **58**, 379–389 DOI: 10.1111/pala.12142

Benjamini, Y., & Hochberg, Y. 1995. Controlling the False Discovery Rate: A Practical and Powerful Approach to Multiple Testing. *Journal of the Royal Society Series B (Methodological)*, **57**, 289–300.

Benton, M. J. 2000. *Vertebrate Palaeontology*, 2nd edn. Malden, MA., Blackwell Science, Inc.

Benton, M. J., & Storrs, G. W. 1994. Testing the quality of the fossil record: paleontological knowledge is improving. *Geology*, **22**, 111–114 DOI: 10.1130/0091-7613(1994)022<0111:TTQOTF>2.3.CO;2

Benton, M. J., Hitchin, R., & Wills, M. A. 1999. Assessing congruence between cladistic and stratigraphic data. *Systematic Biology*, **48**, 581–596.

Bestwick, J., Unwin, D. M., & Purnell, M. A. In Prep. First evidence of dietary discrimination in modern reptiles from 3D dental microwear textural analysis.

Blateyron, F. 2013. The areal field parameters; Pp. 15–43 in Leach, R. (ed) *Characterisation of areal surface texture*. Springer, Berlin, Heidelberg.

Bolt, J. R. 1974. Evolution and functional interpretation of some suture patterns in Paleozoic labyrinthodont amphibians and other lower tetrapods. *Journal of Paleontology*, **48**, 434–458.

Bookstein, F. L. 1996. Landmark methods for forms without landmarks: localizing group differences in outline shape. *Mathematical Methods in Biomedical Image Analysis, 1996, Proceedings of the Workshop on Mathematical Methods in Biomedical Image Analysis*, 279–289.

Bookstein, F. L. 1997. Landmark methods for forms without landmarks: morphometrics of group differences in outline shape. *Medical Image Analysis*, **1**, 225–243.

Brasch, S. V., Lazarou, J., Van Abbe, N. J., & Forrest, J. O. 1969. The assessment of dentifrice abrasivity in vivo. *British Dental Journal*, **127**, 1513–1518.

Brochu, C. A. 2004. A new Late Cretaceous gavialoid crocodylian from eastern North America and the phylogenetic relationships of thoracosaurs. *Journal of Vertebrate Paleontology*. **24**, 610–633.

Brochu, C. A., & Rincón, A. D. 2004. A gavialoid crocodylian from the Lower Miocene of Venezuela. *Special Papers in Palaeontology, Fossils of the Miocene Castillo Formation, Venezuela: Contributions in Neotropical Palaeontology*, **71**, 61–79.

Brochu, C. A. 2012. Phylogenetic relationships of Palaeogene ziphodont eusuchians and the status of *Pristichampsus* Gervais, 1853. *Earth and Environmental Science Transactions of the Royal Society of Edinburgh*, **103**, 521–550.

Brochu, C. A., Parris, D. C., Grandstaff, B. S., Denton Jr, R. K., & Gallagher, W. B. 2012. A new species of *Borealosuchus* (Crocodyliformes, Eusuchia) from the Late Cretaceous—early Paleogene of New Jersey. *Journal of Vertebrate Paleontology*, **32**, 105–116.

Bronzati M., Montefeltro FC., Langer MC. 2012. A species-level supertree of Crocodyliformes. *Historical Biology*, **24**, 598–606. DOI: 10.1080/08912963.2012.662680

Bronzati, M., Montefeltro, F. C., Langer, M. C. 2015. Diversification events and the effects of mass extinctions on Crocodyliformes evolutionary history. *Royal Society Open Science*, **2**, 140385.

Brusatte, S. L., Benton, M. J., Desojo, J. B., & Langer, M. C. 2010. The higher-level phylogeny of Archosauria (Tetrapoda: Diapsida). *Journal of Systematic Palaeontology*, **8**, 3–47.

Brusatte, S. L., Butler, R. J., Niedźwiedzki, G., Sulej, T., Bronowicz, R., & Satkūnas, J. 2013. First record of Mesozoic terrestrial vertebrates from Lithuania: phytosaurs (Diapsida: Archosauriformes) of probable late Triassic age, with a review of phytosaur biogeography. *Geological Magazine*, **150**, 110–122 DOI: 10.1017/S0016756812000428

Buffetaut, E. 1993. Phytosaurs in time and space. *Paleontolol Lombarda Nuova serie*, **2**, 39–44.

Buffetaut, E., & Ingavat, R. 1982. Phytosaur remains (Reptilia, Thecodontia) from the Upper Triassic of north-eastern Thailand. *Geobios*, **15**, 7–17.

Busbey, A. B. 1995. The structural consequences of skull flattening in crocodilians; Pp. 173–192 in Thomason, J. J. (ed) *Functional Morphology in Vertebrate Paleontology*. Cambridge, Cambridge University Press.

Butler, M. A., & King, A. A. 2004. Phylogenetic comparative analysis: a modeling approach for adaptive evolution. *The American Naturalist*, **164**, 683–695 DOI: 10.1086/426002

Butler, R. J., Rauhut, O. W., Stocker, M. R., & Bronowicz, R. 2014. Redescription of the phytosaurs *Paleorhinus* (‘*Francosuchus*’) *angustifrons* and *Ebrachosuchus neukami* from Germany, with implications for late Triassic biochronology. *Zoological Journal of the Linnean Society*, **170**, 155–208 DOI: 10.1111/zoj12094

Butler, R. J., Jones, A. S., Buffetaut, E., Mandl, G. W., Scheyer, T., Schultz, O. In review. A new species of *Mystriosuchus* (Archosauriformes, Phytosauria) from the late Triassic of Austria. *Zoological Journal of the Linnean Society*.

Camp, C. L. 1930. A study of the phytosaurs with description of new material from western North America. *Memoirs of the University of California*, **10**, 1–174.

Case, E. C. 1920. Preliminary description of a new suborder of phytosaurian reptiles with a description of a new species of *Phytosaurus*. *The Journal of Geology*, **28**, 524–535 DOI: 10.1086/622732

Case, E. C. 1922. New reptiles and stegocephalians from the Upper Triassic of western Texas. *Carnegie Institute of Washington Publication*, **321**, 1–84.

Case, E. C. 1929. Description of the skull of a new form of phytosaur: with notes on the characters of described North American phytosaurs. *University of Michigan Studies, Memoirs of the University of Michigan Museums*, **2**, 1–56.

Case, E. C., & White, T. E. 1934. Two new specimens of phytosaurs from the Upper Triassic of western Texas. *Contributions from the Museum of Paleontology, University of Michigan*, **4**, 133–142.

Catalano, S. A., Goloboff, P. A., & Giannini, N. P. 2010. Phylogenetic morphometrics (I): the use of landmark data in a phylogenetic framework. *Cladistics*, **26**, 539–549 DOI: 10.1111/j.1096-0031.2010.00302.x

Catalano, S. A., Ercoli, M. D., & Prevosti, F. J. 2015. The more, the better: the use of multiple landmark configurations to solve the phylogenetic relationships in musteloids. *Systematic Biology*, **64**, 294–306.

Chai, H., & Lawn, B. R. 2007. A universal relation for edge chipping from sharp contacts in brittle materials: a simple means of toughness evaluation. *Acta Materialia*, **55**, 2555–2561.

Chai, H., Lee, J. J. W., & Lawn, B. R. 2011. On the chipping and splitting of teeth. *Journal of the Mechanical Behavior of Biomedical Materials*, **4**, 315–321.

Chappill, J. A. 1989. Quantitative characters in phylogenetic analysis. *Cladistics*, **5**, 217–234 DOI: 10.1111/j.1096-0031.1989.tb00487.x

Chatterjee, S. 1974. A Rhynchosaur from the Upper Triassic Maleri Formation of India. *Philosophical Transactions of the Royal Society of London Series B*, **267**, 209-261 DOI: 10.1098/rstb.1974.0001

Chatterjee, S. 1978. A primitive parasuchid (phytosaur) reptile from the Upper Triassic Maleri Formation of India. *Palaeontology*, **21**, 83–127.

Chatterjee, S. 1985. *Postosuchus*, a new thecodontian reptile from the Triassic of Texas and the origin of tyrannosaurs. *Philosophical Transactions of the Royal Society of London B*, **309**, 395–460.

Chatterjee, S. 2001. *Parasuchus hislopi* Lydekker, 1885 (Reptilia, Archosauria): Proposed replacement of the lectotype by a neotype. *Bulletin of Zoological Nomenclature*, **58**, 34–36.

Christensen, R. P., & Bangerter, V. W. 1987. Immediate and long-term in vivo effects of polishing on enamel and dentin. *Journal of Prosthetic Dentistry*, **57**, 150–160.

Cisneros, J. C., & Ruta, M. 2010. Morphological diversity and biogeography of procolophonids (Amniota: Parareptilia). *Journal of Systematic Palaeontology*, **8**, 607–625.

Colbert, E. H. 1947. Studies of the phytosaurs *Machaeroprosopus* and *Rutiodon*. *Bulletin of the American Museum of Natural History*, **88**, 53–96.

Cong, L., Hou, L., Wu, X. C., & Hou, J. F. 1998. The gross anatomy of *Alligator sinensis* Fauvel. *Beijing: CIP, China.*

Congreve, C. R., & Lamsdell, J. C. 2016. Implied weighting and its utility in palaeontological datasets: a study using modelled phylogenetic matrices. *Palaeontology*, **59**, 447–462 DOI: 10.1111/pala.12236

Constantino, P. J., Lee, J. J. W., Chai, H., Zipfel, B., Ziscovici, C., Lawn, B. R., & Lucas, P. W. 2010. Tooth chipping can reveal the diet and bite forces of fossil hominins. *Biology letters*, rsbl20100304.

Cope, E. D. 1881. *Belodon* in New Mexico. *American Naturalist*, **15**, 922–923.

Cranston, P. S., & Humphries, C. J. 1988. Cladistics and computers: a chironomid conundrum? *Cladistics*, **4**, 72–92 DOI: 10.1111/j.1096-0031.1988.tb00469.x

Crisp, M. D., & Weston, P. H. 1987. Cladistics and legume systematics, with an analysis of the Bossiaeeae, Brongniartieae and Mirbelieae. *Advances in Legume Systematics*, **3**, 65–130.

Da Silveira, R., & Magnusson, W. E. 1999. Diets of spectacled and black caiman in the Anavilhanas Archipelago, Central Amazonia, Brazil. *Journal of Herpetology*, **33**, 181–192.

Dalhuijsen, K., Branch, W. R., & Alexander, G. J. 2014. A comparative analysis of the diets of *Varanus albigularis* and *Varanus niloticus* in South Africa. *African Zoology*, **49**, 83–93.

Delany, M. F. 1990. Late summer diet of juvenile American alligators. *Journal of Herpetology*, **24**, 418–421.

Delany, M. F., & Abercrombie, C. L. 1986. American alligator food habits in northcentral Florida. *The Journal of Wildlife Management*, **50**, 348–353.

Delany, M. F., Linda, S. B., & Moore, C. T. 1999. Diet and Condition of American Alligators in 4 Florida Lakes. *Proceedings of the Annual Conference of the Southeastern Association of Fisheries and Wildlife Agencies*, **53**, 375–389.

Dodson, P. 1975. Taxonomic implications of relative growth in lambeosaurine hadrosaurs. *Systematic Biology*, **24**, 37–54 DOI: 10.1093/sysbio/24.1.37

Dollion, A. Y., Measaey, J., Cornette, R., Carne, L., Tolley, K. A., Da Silva, J. M., Boistel, R., Fabre, A. C., & Herrel, A. 2017. Does diet drive the evolution of head shape and bite force in chameleons of the genus *Bradypodion*? *Functional Ecology*, **31**, 671–684.

Drevermann, F. 1918. Ein Parasuchier-Schädel aus dem schwäbischen Stubensandstein. *Bericht der Senckenbergischen Naturforschenden Gesellschaft in Frankfurt am Main*, **47**, 120-123.

Drumheller, S. K., Stocker, M. R., & Nesbitt, S. J. 2014. Direct evidence of trophic interactions among apex predators in the late Triassic of western North America. *Naturwissenschaften*, **101**, 975–987.

Dutuit, J. M. 1977a. *Paleorhinus magnoculus*, phytosaure du Trias supérieur de l'Atlas marocain. *Géologie Méditerranéenne*, **4**, 255–268.

Dutuit, J. M. 1977b. Description du crâne de *Angistorhinus talainti* n. sp: un nouveau Phytosaure du Trias atlasique marocain. *Bulletin du Museum National d'Histoire Naturelle*, **489**, 297–336.

Dutuit, J. M. 1978. Description de quelques fragments osseux provenant de la région de Folakara (Trias supérieur malgache). *Bulletin de Museum Nationale d'Histoire naturelle, Paris. Series III*, **516**, 79–89.

Dzik, J. 2001. A new *Paleorhinus* fauna in the early late Triassic of Poland. *Journal of Vertebrate Paleontology*, **21**, 625–627.

Eaton, T. H. Jr 1965. A new Wyoming phytosaur. *The University of Kansas Paleontological Contributions*, **2**, 1–6.

Edmund, A. G. 1962. Sequence and rate of tooth replacement in the Crocodilia. *Royal Ontario Museum, Life Sciences Division Contribution*, **56**, 1–42.

Emmons, E. 1856. *Geological report of the midland counties of North Carolina*. George P. Putnam and Co. New York: XX + 352 pp., 8 pls.

Emmons, E. 1860. *Manual of geology: designed for the use of colleges and academies. Second edition*. A. S. Barnes and Burr. New York: XI + 297 pp.

Erickson, B. R. 1982. *Wannaganosuchus*, a new alligator from the Paleocene of North America. *Journal of Paleontology*, **56**, 492–506.

Erickson, G. M. 1996a. Daily deposition of dentine in juvenile *Alligator* and assessment of tooth replacement rates using incremental line counts. *Journal of Morphology*, **228**, 189–194.

Erickson, G. M. 1996b. Incremental lines of von Ebner in dinosaurs and the assessment of tooth replacement rates using growth line counts. *Proceedings of the National Academy of Sciences*, **93**, 14623–14627.

Erickson, G. M., Lappin, A. K., & Vliet, K. 2003. The ontogeny of bite-force performance in American alligator (*Alligator mississippiensis*). *Journal of Zoology*, **260**, 317–327.

Erickson, G. M., Lappin, A. K., Vliet, K., Brueggen, J., Kledzik, D., & Webb, G. 2005. Comparative bite-force performance of extant and fossil crocodilians: a window into evolutionary feeding biomechanics. *Journal of Vertebrate Paleontology*, **25**, 54A.

Erickson, G. M., Gignac, P. M., Steppan, S. J., Lappin, A. K., Vliet, K. A., Brueggen, J. D., Inouye, B. D., Kledzik, D., & Webb, G. J. W. 2012. Insights into the ecology and evolutionary success of crocodilians revealed through bite-force and tooth-pressure experimentation. *PLoS One*, **7**, e31781.

Evans, A. R., & Sanson, G. D. 1998. The effect of tooth shape on the breakdown of insects. *Journal of Zoology*, **246**, 391–400.

Ewer, R. F. 1965. The anatomy of the thecodont reptile *Euparkeria capensis* Broom. *Philosophical Transactions of the Royal Society of London B*, **248**, 379–435.

Ezcurra, M. D. 2010. Biogeography of Triassic tetrapods: evidence for provincialism and driven sympatric cladogenesis in the early evolution of modern tetrapod lineages. *Proceedings of the Royal Society of London B: Biological Sciences*, **277**, rspb20100508.

Ezcurra, M. D. 2016. The phylogenetic relationships of basal archosauromorphs, with an emphasis on the systematics of proterosuchian archosauriforms. *PeerJ*, **4**, e1778 DOI: 10.7717/peerj.1778

Fara, E., & Hungerbühler, A. 2000. *Paleorhinus magnoculus* from the Upper Triassic of Morocco: a juvenile primitive phytosaur (Archosauria). *Comptes Rendus de l'Académie des Sciences-Series IIA-Earth and Planetary Science*, **331**, 831–836 DOI: 10.1016/S1251-8050(00)01481-6

Farlow, J. O., & Brinkman, D. L. 1994. Wear surfaces on the teeth of tyrannosaurs. *The Paleontological Society Special Publications*, **7**, 165–176.

Farris, J. S. 1970. Methods for computing Wagner trees. *Systematic Biology*, **19**, 83–92 DOI: 10.1093/sysbio/19.1.83

Farris, J. S. 1990. Phenetics in camouflage. *Cladistics*, **6**, 91–100 DOI: 10.1111/j.1096-0031.1990.tb00528.x

Felsenstein, J. 1973. Maximum-likelihood estimation of evolutionary trees from continuous characters. *American journal of human genetics*, **25**, 471–492.

Felsenstein, J. 1978. Cases in which parsimony or compatibility methods will be positively misleading. *Systematic zoology*, **27**, 401–410 DOI: 10.1093/sysbio/27.4.401

Felsenstein, J. 1985. Phylogenies and the comparative method. *The American Naturalist*, **125**, 1–15 DOI: 10.1086/284325

Felsenstein, J. 1988. Phylogenies and quantitative characters. *Annual Review of Ecology and Systematics*, **19**, 445–471 DOI: 10.1146/annurev.es.19.110188.002305

Fischer, J., Voigt, S., Franz, M., Schneider, J. W., Joachimski, M. M., Tichomirowa, M., Götze, J., & Furrer, H. 2012. Palaeoenvironments of the late Triassic Rhaetian Sea: implications from oxygen and strontium isotopes of hybodont shark teeth. *Palaeogeography, Palaeoclimatology, Palaeoecology*, **353**, 60–72.

Foth, C., Ezcurra, M. D., Sookias, R. B., Brusatte, S. L., & Butler, R. J. 2016. Unappreciated diversification of stem archosaurs during the Middle Triassic predated the dominance of dinosaurs. *BMC Evolutionary Biology*, **16**, 188. DOI: 10.1186/s12862-016-0761-6

Fraas, E. 1896. *Die schwäbischen Trias-Saurier nach dem Material der Kgl.* Naturalien-Sammlung in Stuttgart zusammengestellt. Stuttgart (Schweizerbart). 18 pp.

Frazzetta, T. H. 1988. The mechanics of cutting and the form of shark teeth (Chondrichthyes, Elasmobranchii). *Zoomorphology*, **108**, 93–107.

Garcia-Cruz, J., & Sosa, V. 2006. Coding quantitative character data for phylogenetic analysis: a comparison of five methods. *Systematic Botany*, **31**, 302–309 DOI: 10.1600/036364406777585739

Gift, N., & Stevens, P. F. 1997. Vagaries in the delimitation of character states in quantitative variation—an experimental study. *Systematic Biology*, **46**, 112–125 DOI: 10.1093/sysbio/46.1.112

Gill, P. G., Purnell, M. A., Crumpton, N., Brown, K. R., Gostling, N. J., Stampanoni, M., & Rayfield, E. J. 2014. Dietary specializations and diversity in feeding ecology of the earliest stem mammals. *Nature*, **512**, 303.

Gingerich, P. D. 1993. Quantification and comparison of evolutionary rates. *American Journal of Science*, **293**, 453–478.

Godoy, P. L., Ferreira, G. S., Montefeltro, F. C., Vila Nova, B. C., Butler, R. J., & Langer, M. C. 2018. Evidence for heterochrony in the cranial evolution of fossil crocodyliforms. *Palaeontology*, **61**, 543–558.

Goillot, C., Blondel, C., & Peigné, S. 2009. Relationships between dental microwear and diet in Carnivora (Mammalia)—Implications for the reconstruction of the diet of extinct taxa. *Palaeogeography, Palaeoclimatology, Palaeoecology*, **271**, 13–23.

Goloboff, P. A. 1993. Estimating character weights during tree search. *Cladistics*, **9**, 83–91 DOI: 10.1111/j.1096-0031.1993.tb00209.x

Goloboff, P. A., & Pol, D. 2005. Parsimony and Bayesian phylogenetics. Pp. 148–159 in V. A. Albert (ed) *Parsimony, Phylogeny, and Genomics*. Oxford University Press, Oxford, UK.

Goloboff, P. A., Mattoni, C. I., & Quinteros, A. S. 2006. Continuous characters analyzed as such. *Cladistics*, **22**, 589–601 DOI: 10.1111/j.1096-0031.2006.00122.x

Goloboff, P. A., Carpenter, J. M., Arias, J. S., & Esquivel, D. R. M. 2008a. Weighting against homoplasy improves phylogenetic analysis of morphological data sets. *Cladistics*, **24**, 758–773 DOI: 10.1111/j.1096-0031.2008.00209.x

Goloboff, P. A., Farris, J. S., & Nixon, K. C. 2008b. TNT, a free program for phylogenetic analysis. *Cladistics*, **24**, 774–786 DOI: 10.1111/j.1096-0031.2008.00217.x

Goloboff, P. A., & Catalano, S. A. 2011. Phylogenetic morphometrics (II): algorithms for landmark optimization. *Cladistics*, **27**, 42–51 DOI: 10.1111/j.1096-0031.2010.00318.x

Goloboff, P. A., & Catalano, S. A. 2016. TNT version 1.5, including a full implementation of phylogenetic morphometrics. *Cladistics*, **32**, 221–238 DOI: 10.1111/cla.12160

Goloboff, P. A., Torres, A., & Arias, J. S. 2017. Weighted parsimony outperforms other methods of phylogenetic inference under models appropriate for morphology. *Cladistics*, **34**, 407–437 DOI: 10.1111/cla.12205

Goloboff, P. A., Torres Galvis, A., & Arias, J. S. 2018. Parsimony and model-based phylogenetic methods for morphological data: comments on O'Reilly et al. *Palaeontology*, **61**, 625–630 DOI: 10.1111/pala.12353

Goodall, R. H., Darras, L. P., & Purnell, M. A. 2015. Accuracy and precision of silicon based impression media for quantitative areal texture analysis. *Scientific Reports*, **5**, 10800.

Gower D.J. 2003. Osteology of the early archosaurian reptile *Erythrosuchus africanus* Broom. *Ann South African Museum*, **110**, 1–84.

Greaves, W. S. 1995. Functional predictions from theoretical models of the skull and jaws in reptiles and mammals; Pp. 99–115 in Thomason, J. (ed) *Functional morphology in vertebrate paleontology*. Cambridge University Press, Cambridge, U.K.

Greene, H. W. 1986. Diet and arboreality in the emerald monitor, *Varanus prasinus*, with comments on the study of adaptation. *Fieldiana Zool*, **31**, 1–12.

Gregory, J. T. 1962a. The genera of phytosaurs. *American Journal of Science*, **260**, 652–690 DOI: 10.2475/ajs.260.9.652

Gregory, J. T. 1962b. The relationships of the American phytosaur Rutiodon. *American Museum Novitates*, **2095**, 22 pp.

Gregory, J. T. 1969. Evolution und interkontinentale Beziehungen der Phytosauria (Reptilia). *Paläontologische Zeitschrift*, **43**, 37–51 DOI: 10.1007/BF02987926

Gregory, J. T. 1972. Vertebrate faunas of the Dockum Group, Triassic, eastern New Mexico and West Texas. *New Mexico Geological Society 23rd Fall Field Conference, Guidebook*, 120-123.

Griffin, C. T., Stefanic, C. M., Parker, W. G., Hungerbühler, A., & Stocker, M. R. 2017. Sacral anatomy of the phytosaur Smilosuchus adamanensis, with implications for pelvic girdle evolution among Archosauriformes. *Journal of Anatomy*, **231**, 886–905 DOI: 10.1111/joa.12681

Hammer, Ø., Harper, D. A. T., & Ryan, P. D. 2001. PAST: Paleontological Statistics software package for education and data analysis. *Palaeontologia Electronica*, **4**, 9pp.

Hansen, T. F. 1997. Stabilizing selection and the comparative analysis of adaptation. *Evolution*, **51**, 1341–1351 DOI: 10.1111/j.1558-5646.1997.tb01457.x

Hastings, A. K., Bloch, J. I., & Jaramillo, C. A. 2015. A new blunt-snouted dyrosaurid, *Anthracosuchus balrogus* gen. et sp. nov. (Crocodylomorpha, Mesoeucrocodylia), from the Palaeocene of Colombia. *Historical Biology*, **27**, 998–1020.

Heckert, A. B., Lucas, S. G., Hunt, A. P., & Harris, J. D. 2001. A giant phytosaur (Reptilia: Archosauria) skull from the Redonda Formation (Upper Triassic: Apachean) of east-central New Mexico. *New Mexico Geological Society Guidebook*, **52**, 171–178.

Heckert, A. B., & Lucas, S. G. 2003. Stratigraphy and paleontology of the lower Chinle Group (Adamanian; latest Carnian) in the vicinity of St. Johns, Arizona. *New Mexico Geological Society Guidebook*, **54**, 281-288.

Heckert, A. B., & Camp, J. 2007. Tooth enamel microstructure of selected archosaurs Reptilia: Archosauria from the upper Triassic Chinle Group, western USA: taxonomic and evolutionary significance. *Geological Society of America Abstracts with Programs*, **39**, p. 77.

Heckert, A. B., Jenkins, H. S., Lucas, S. G., & Hunt, P. 2013. Mandibles of juvenile phytosaurs (Archosauria: Crurotarsi) from the Upper Triassic Chinle Group of Texas and New Mexico, USA. *New Mexico Museum of Natural History and Science Bulletin*, **61**, 228–236.

Heller, F. 1954. Ein Parasuchier-Schädelrest aus dem Oberen Burgsandstein von Coburg. *Geologische Blätter für Nordost-Bayern und angrenzende Gebiete*, 4, 1-14.

Herrera, Y., Gasparini, Z., & Fernández, M. S. 2015. *Purranisaurus potens* Rusconi, an enigmatic metriorhynchid from the Late Jurassic–Early Cretaceous of the Neuquén Basin. *Journal of Vertebrate Paleontology*, **35**, e904790.

Holloway, W. L., Claeson, K. M., & O'keefe, F. R. 2013. A virtual phytosaur endocast and its implications for sensory system evolution in archosaurs. *Journal of Vertebrate Paleontology*, **33**, 848–857 DOI: 10.1080/02724634.2013.747532

Huelsenbeck, J. P. 1994. Comparing the stratigraphic record to estimates of phylogeny. *Paleobiology*, **20**, 470–483 DOI: 10.1017/S009483730001294X

Huelsenbeck, J. P. 1995. Performance of phylogenetic methods in simulation. *Systematic biology*, **44**, 17–48 DOI: 10.1093/sysbio/44.1.17

Huene, F. von. 1909. Vorläufige Mitteilung über einen neuen *Phytosaurus*-Schädel aus dem schwäbischen Keuper. *Centralblatt für Mineralogie, Geologie und Paläontologie*, **1909** 583-592.

Huene, F. von. 1911. Beiträge zur Kenntnis und Beurteilung der Parasuchier. *Geologische und Paläontologische Abhandlungen, Neue Folge*, **10**, 67-121.

Huene, F. von. 1913: A new phytosaur from the Palisades near New York. *Bulletin of the American Museum of Natural History*, **32**, 275–283,

Huene, F. von. 1915. On reptiles of the New Mexican Trias in the Cope Collection. *Bulletin of the American Museum of Natural History*, **34**, 485–507.

Huene, F. von. 1922. Neue Beiträge zur Kenntnis der Parasuchier. *Jahrbuch der Preussischen Geologischen Landesanstalt*, **42**, 146-148.

Hungerbühler, A. 1998a. *Cranial anatomy and diversity of the Norian phytosaurs of Southwestern Germany*. Unpublished PhD thesis, University of Bristol, 464 pp.

Hungerbühler, A. 1998b. Taphonomy of the prosauropod dinosaur *Sellosaurus*, and its implications for carnivore faunas and feeding habits in the late Triassic. *Palaeogeography, Palaeoclimatology, Palaeoecology*, **143**, 1–29.

Hungerbühler, A. 2000. Heterodonty in the European phytosaur *Nicrosaurus kapffi* and its implications for the taxonomic utility and functional morphology of phytosaur dentitions. *Journal of Vertebrate Paleontology*, **20**, 31–48.

Hungerbühler, A. 2002. The late Triassic phytosaur *Mystriosuchus westphali*, with a revision of the genus. *Palaeontology*, **45**, 377–418 DOI: 10.1111/1475-4983.00242

Hungerbühler, A., & Hunt, A. P. 2000. Two new phytosaur species (Archosauria, Crurotarsi) from the Upper Triassic of southwest Germany. *Neues Jahrbuch fur Geologie und Palaontologie-Monatshefte*, **8**, 467–484.

Hungerbühler, A., & Sues, H. D. 2001. Status and phylogenetic relationships of the late Triassic phytosaur *Rutiodon carolinensis*. *Journal of Vertebrate Paleontology*, **21**, 64A.

Hungerbühler, A., Chatterjee, S., & Cunningham, D. P. 2003. A new phytosaur species from the Triassic of west Texas: new information on cranial anatomy, taxonomy, and sexual dimorphism in Pseudopalatinae. *Journal of Vertebrate Paleontology*, **23**, 63A-64A.

Hungerbühler, A., Mueller, B., Chatterjee, S., & Cunningham, D. P. 2013. Cranial anatomy of the late Triassic phytosaur *Machaeroprosopus*, with the description of a new species from West Texas. *Earth and Environmental Science Transactions of the Royal Society of Edinburgh*, **103**, 269–312 DOI: 10.1017/S1755691013000364

Hunt, A. P. 1989. Cranial morphology and ecology among phytosaurs; Pp. 349–354 in Lucas, S.G., & Hunt, A.P. (eds) *Dawn of the Age of Dinosaurs in the American Southwest*. New Mexico Museum of Natural History and Science, Albuquerque.

Hunt, A. P. 1991. Two phytosaur (Reptilia: Archosauria) skeletons from the Bull Canyon Formation (late Triassic) of east-central New Mexico with preserved stomach contents. *New Mexico Geology*, **13**, 93.

Hunt, A. P. 1994a. *Vertebrate paleontology and biostratigraphy of the Bull Canyon Formation (Chinle Group, Upper Triassic), east-central New Mexico with revisions of the families Metoposauridae (Amphibia: Temnospondyli) and Parasuchidae (Reptilia: Archosauria).* Unpublished PhD thesis, University of New Mexico, 404 pp.

Hunt, A. P. 1994b. The phylogeny and biochronology of the Parasuchidae (Reptilia: Archosauria). *Journal of Vertebrate Paleontology*, **14**(3), 30A DOI: 10.1080/02724634.1994.10011592

Hunt, A. P., & Lucas, S. G. 1989. New genotype designations for the phytosaurs *Mystriosuchus* and *Rutiodon* with a discussion of the taxonomic status of *Mystriosuchus*, *Clepsysaurus* and *Rutiodon*. Pp. 340–348 in S. G. Lucas & A. P. Hunt (eds) *Dawn of the Age of Dinosaurs in the American Southwest*. New Mexico Museum of Natural History and Science, Albuquerque.

Hunt, A. P., & Lucas, S. G. 1991. The *Paleorhinus* biochron and the correlation of the non-marine Upper Triassic of Pangaea. *Palaeontology*, **34**, 487–501.

Hunt, A. P., & Lucas, S. G. 1993. A new phytosaur (Reptilia: Archosauria) genus. *New Mexico Museum of Natural History and Science Bulletin*, **3**, 193–196.

Hunt, A. P., Lucas, S. G., & Bircheff, P. 1993. Biochronological significance of the co-occurrence of the phytosaurs (Reptilia: Archosauria) *Angistorhinus* and *Rutiodon* in the Los Esteros Member of the Santa Rosa Formation, Santa Fe County, New Mexico, USA. *New Mexico Museum of Natural History and Science Bulletin*, **3**, 203–204.

Hunt, A. P., Lucas, S. G., & Spielmann, J. A. 2006. Sexual dimorphism in a large brachyrostral phytosaur (Archosauria: Crurotarsi) from the late Triassic of western North America. *New Mexico Museum of Natural History and Science Bulletin*, **37**, 563–567.

Hurlburt, G. R., Heckert, A. B., & Farlow, J. O. 2003. Body mass estimates of phytosaurs (Archosauria: Parasuchidae) from the Petrified Forest Formation (Chinle Group: Revueltian) based on skull and limb bone measurements. *New Mexico Museum of Natural History and Science Bulletin*, **24**, 105–113.

Huxley, T. H. 1875. On *Stagonolepis Robertsoni*, and on the evolution of the Crocodylia. *Quarterly Journal of the Geological Society of London*, **31**, 423–438, 1 pl.

ICZN 2003. *Parasuchus hislopi* Lydekker, 1885 (Reptilia, Archosauria): lectotype replaced by a neotype. *Bulletin of Zoological Nomenclature*, **60**, Opinion 2045.

International Organization for Standardization. 2012. Geometrical product specifications (GPS) – Surface texture: Areal – Part 2: Terms, definitions and surface texture parameters *(ISO 25178-2)*. 1–42.

Iori, F. V., & Carvalho, I. S. 2011. *Caipirasuchus paulistanus*, a new sphagesaurid (Crocodylomorpha, Mesoeucrocodylia) from the Adamantina Formation (Upper Cretaceous, Turonian-Santonian), Bauru Basin, Brazil. *Journal of Vertebrate Paleontology*, **31**, 1255–1264.

Irmis, R. B. 2005. The vertebrate fauna of the Upper Triassic Chinle Formation in northern Arizona. *Mesa Southwest Museum Bulletin,* **9**, 63-88.

Irmis, R. B. 2007. Axial skeleton ontogeny in the Parasuchia (Archosauria: Pseudosuchia) and its implications for ontogenetic determination in archosaurs. *Journal of Vertebrate Paleontology*, **27**, 350–361 DOI: 10.1671/0272-4634(2007)27[350:ASOITP]2.0.CO;2

Jaeger, G. F. 1828. *Über die fossilen Reptilien, welche in Würtemberg aufgefunden worden sind.* Metzler, Stuttgart, 48 pp.

Jaekel O. 1910. Über einen neuen Belodonten aus dem Buntsandstein von Bernberg. *Sitzungsberichte Gesellschaft naturforschender Freunde zu Berlin*, **5**, 197–229.

Juarez, B. H. 2015. *Ecomorphological change in lobe-finned fishes (Sarcopterygii): disparity and rates*. Unpublished MSc thesis, University of Michigan, Ann Arbor: 74 pp.

Kaliontzopoulou, A., Adams, D. C., Van Der Meijden, A., Perera, A., & Carretero, M. A. 2012. Relationships between head morphology, bite force perfromance and ecology in two species of *Podarcis* wall lizards. *Ecology and Evolution*, **26**, 825–845.

Kammerer, C. F., Butler, R. J., Bandyopadhyay, S., & Stocker, M. R. 2015. Relationships of the Indian phytosaur *Parasuchus hislopi* Lydekker, 1885. *Papers in Palaeontology*, **2**, 1–23 DOI: 10.1002/spp2.1022

Kimmig, J. 2009. *Functional morphology and systematic palaeontology of the Phytosauria (Archosauria; Crurotarsi) and the development of their late Triassic habitats*. Unpublished MSc Thesis, Imperial College, London, UK. 118 pp.

Kimmig, J., & Arp, G. 2010. Phytosaur remains from the Norian Arnstadt Formation (Leine Valley, Germany), with reference to European phytosaur habitats. *Palaeodiversity*, **3**, 215–224.

Kimmig, J., & Spielmann, J. A. 2011. Biologic factors influencing phytosaur (Archosauria: Phytosauridae) taxonomy: a prospectus. *New Mexico Museum of Natural History and Science Bulletin*, **53**, 289–294.

Kischlat, E. E., & Lucas, S. G. 2003. A phytosaur from the Upper Triassic of Brazil. *Journal of Vertebrate Paleontology*, **23**, 464–467.

Klassen, G. J., Mooi, R. D., & Locke, A. 1991. Consistency indices and random data. *Systematic Biology*, **40**, 446–457 DOI: 10.1093/sysbio/40.4.446

Koch, N. M., Soto, I. M., & Ramírez, M. J. 2015. First phylogenetic analysis of the family Neriidae (Diptera), with a study on the issue of scaling continuous characters. *Cladistics*, **31**, 142–165 DOI: 10.1111/cla.12084

Kolaczkowski, B., & Thornton, J. W. 2004. Performance of maximum parsimony and likelihood phylogenetics when evolution is heterogeneous. *Nature*, **431**, 980–984 DOI: 10.1038/nature02917

Kuhn, O. 1936. Weitere Parasuchier und Labyrinthodonten aus dem Blasensandstein des mittleren Keuper von Ebrach. *Palaeontographica Abteilung* A, **83**, 61–98.

Kuhner, M. K., & Felsenstein, J. 1994. A simulation comparison of phylogeny algorithms under equal and unequal evolutionary rates. *Molecular biology and evolution*, **11**, 459–468 DOI: 10.1093/oxfordjournals.molbev.a040126

Langston, W. 1949. A new species of *Paleorhinus* from the Triassic of Texas. *American Journal of Science*, **247**, 324–341 DOI: 10.2475/ajs.247.5.324

Laurin, M. 2004. The Evolution of Body Size, Cope's Rule and the Origin of Amniotes. *Systematic Biology*, **53**, 594–622.

Lautenschlager, S., & Butler, R. J. 2016. Neural and endocranial anatomy of Triassic phytosaurian reptiles and convergence with fossil and modern crocodylians. *PeerJ*, **4**, e2251 DOI: 10.7717/peerj.2251

Laverty, T. M., & Dobson, A. P. 2013. Dietary overlap between black caimans and spectacled caimans in the Peruvian Amazon. *Herpetologica*, **69**, 91–101.

Lee, M. S., & Worthy, T. H. 2012. Likelihood reinstates Archaeopteryx as a primitive bird. *Biology letters*, **8**, 299–303 DOI: 10.1098/rsbl.2011.0884

Lee, M. S., & Yates, A. M. 2018. Tip-dating and homoplasy: reconciling the shallow molecular divergences of modern gharials with their long fossil record. *Proceedings of the Royal Society B: Biological Sciences*, **285**, 20181071.

Lees, J. H. 1907. The skull of *Paleorhinus*: a Wyoming phytosaur. *The Journal of Geology*, **15**, 121-151 DOI: 10.1086/621382

Lemanis, R. 2012. *Feeding behaviour of phytosaurs*. Unpublished PhD thesis, University of Bristol, Bristol: 57 pp.

Lemanis, R., Jones, A. S., Butler, R. J., Anderson, P. S. L., & Rayfield, E. J. In Prep. Comparative biomechanical analysis demonstrates functional convergence between slender-snouted crocodilians and phytosaurs.

Lewis, P. O. 2001. A likelihood approach to estimating phylogeny from discrete morphological character data. *Systematic biology*, **50**, 913–925 DOI: 10.1080/106351501753462876

Li, C., Wu, X. C., Zhao, L. J., Sato, T., & Wang, L. T. 2012. A new archosaur (Diapsida, Archosauriformes) from the marine Triassic of China. *Journal of Vertebrate Paleontology*, **32**, 1064–1081 DOI: 10.1080/02724634.2012.694383

Livesey, B. C., & Zusi, R. L. 2007. Higher-order phylogeny of modern birds (Theropoda, Aves: Neornithes) based on comparative anatomy. *Zool J Linn Soc*, **149**, 1–95.

Lloyd, G. T., Wang, S. C., & Brusatte, S. L. 2011. Identifying heterogeneity in rates of morphological evolution: discrete character change in the evolution of lungfish (Sarcopterygii; Dipnoi). *Evolution*, **66**, 330–348. DOI: 10.1111/j.1558-5646.2011.01460.x

Long, R. A., & Ballew, K. L. 1985. Aetosaur dermal armor from the late Triassic of southwestern North America, with special reference to material from the Chinle Formation of Petrified Forest National Park. *Museum of Northern Arizona Bulletin*, **47**, 45–68.

Long, R. A., & Murry, P. A. 1995. late Triassic (Carnian and Norian) tetrapods from the southwestern United States. *New Mexico Museum of Natural History and Science Bulletin*, **4**, 1–254.

Losos, J. B., & Greene, H. W. 1988. Ecological and evolutionary implications of diet in monitor lizards. *Biological Journal of the Linnean Society*, **35**, 379–407.

Lucas, F. A. 1898. Contributions to palaeontology. 1. A new crocodile from the Trias of southern Utah. 2. A new species of *Dinictis* (*D. major*). *American Journal of Science (1880-1910)*, **6**, 399–400.

Lucas, P., Constantino, P., Wood, B., & Lawn, B. 2008. Dental enamel as a dietary indicator in mammals. *BioEssays*, **30**, 374–385.

Lucas, S. G. 2010. The Triassic timescale based on nonmarine tetrapod biostratigraphy and biochronology. *Geological Society, London, Special Publications*, **334**, 447–500 DOI: 10.1144/SP334.15

Lucas, S. G., & Hunt, A. P. 1993. Tetrapod biochronology of the Chinle Group. *New Mexico Museum of Natural History and Science Bulletin*, **3**, 327–329.

Lucas, S. G., Heckert, A. B., Zeigler, K. E., & Hunt, A. P. 2002. The type locality of *Belodon buceros* Cope, 1881, a phytosaur (Archosauria: Parasuchidae) from the Upper Triassic of north-central New Mexico. *New Mexico Museum of Natural History and Science Bulletin*, **21**, 189-192.

Lydekker, R. 1885. The Reptilia and Amphibia of the Maleri and Denwa groups. *Palaeontologia Indica, Series 1*, **1**, 1–38.

Maddison, W. P., & Maddison, D. R. 2016. Mesquite: a modular system for evolutionary analysis. Version 3.04. 2015.

Marsh, O. C. 1896. A new belodont reptile (*Stegomus*) from the Connecticut River sandstone. *American Journal of Science*, **7**, 59-62.

Martz, J. W., & Parker, W. G. 2017. Revised Formulation of the late Triassic Land Vertebrate "Faunachrons" of Western North America: Recommendations for Codifying Nascent Systems of Vertebrate Biochronology. Pp. 39–125 in K. E. Zeigler & W. G. Parker (eds) *Deciphering complexities through multiple stratigraphic methods*. Terrestrial Depositional Systems, 1st Edition, Elsevier.

Mateus, O., Butler, R. J., Brusatte, S. L., Whiteside, J. H., & Steyer, J. S. 2014. The first phytosaur (Diapsida, Archosauriformes) from the late Triassic of the Iberian Peninsula. *Journal of Vertebrate Paleontology*, **34**, 970-975 DOI: 10.1080/02724634.2014.840310

McCormack L, Parker WG. 2017. A new occurrence of the phytosaur (Archosauriformes, Phytosauria) *Pravusuchus hortus* from the Monitor Butte Memeber (Upper Triassic; Chinle Formation) of Utah. *Journal of Vertebrate Paleontology Program and Abstracts, 2017*, 161 pp

McCurry, M. R., Evans, A. R., Fitzgerald, E. M., Adams, J. W., Clausen, P. D., & McHenry, C. R. 2017a. The remarkable convergence of skull shape in crocodilians and toothed whales. *Proceedings of the Royal Society of London B: Biological Sciences*, **284**, 20162348.

McCurry, M. R., Fitzgerald, E. M., Evans, A. R., Adams, J. W., & McHenry, C. R. 2017b. Skull shape reflects prey size niche in toothed whales. *Biological Journal of the Linnean Society*, **121**, 936–946.

McDonald, J. H. 2014. *Handbook of Biological Sciences (3rd ed.)*, Baltimore, Maryland, USA, Sparky House Publishing.

McGregor, J. H. 1906. The Phytosauria, with especial reference to *Mystriosuchus* and *Rhytidodon*. *Memoirs of the American Museum of Natural History*, **9**, 27–101, 5 pls

McHenry, C. R., Clausen, P. D., Daniel, W. J., Meers, M. B., & Pendharkar, A. 2006. Biomechanics of the rostrum in crocodilians: a comparative analysis using finite-element modeling. *The Anatomical Record Part A*, **288**, 827–849. DOI: 10.1002/ar.a.20360

Mehl, M. G. 1913. *Angistorhinus*, a new genus of Phytosauria from the Trias of Wyoming. *The Journal of Geology*, **21**, 186–191 DOI: 10.1086/622049

Mehl, M. G. 1915. The Phytosauria of the Trias. *The Journal of Geology*, **23**, 129–165 DOI: 10.1086/622217

Mehl, M. G. 1916. New or little known phytosaurs from Arizona. Pp. 5–28 in M. G. Mehl, W. C. Toepelmann and G. M. Schwartz (eds) *New or Little Known Reptiles from the Trias of Arizona and New Mexico with Notes on the Fossil Bearing Horizons near Wingate, New Mexico*. Quarterly Bulletin of the University of Oklahoma, New Series, **103**, 5–44.

Mehl, M. G. 1922. A new phytosaur from the Trias of Arizona. *The Journal of Geology*, **30**, 144-157 DOI: 10.1086/622860

Mehl, M. G. 1928. The Phytosauria of the Wyoming Triassic. *Journal of the Denison University Laboratories, Denison University*, **23**, 141–172.

Merceron, G., Escarguel, G., Angibault, J. M., & Verheyden-Tixier, H. 2010. Can dental microwear textures record inter-individual dietary variations? *PLoS One*, **5**, e9542.

Metzger, K. A., & Herrel, A. 2005. Correlations between lizard cranial shape and diet: a quantitative, phylogenetically informed analysis. *Biological Journal of the Linnean Society*, **86**, 433–466.

Meunier, L. M. V., & Larsson, H. C. E. 2017. Revision and phylogenetic affinities of *Elosuchus* (Crocodyliformes). *Zoological Journal of the Linnean Society*, **179**, 169–200.

Meyer, H. von. 1860. Briefliche Mittheilung an Prof. Bronn. *Neues Jahrbuch fur Mineralogie, Geognosie, Geologie und Petrefakten-Kunde*, 556–560.

Meyer, H. von. 1861. Reptilien aus dem Stubensandstein des oberen Keupers. *Palaeontographica*, **7**, 253–300.

Meyer, H. von. 1863. Der Schädel des *Belodon* aus dem Stubensandstein des oberen Keupers. *Palaeontographica*, **10**, 227–246.

Meyer, H. von. 1865. Reptilien aus dem Stubensandstein des oberen Keupers (Dritte Folge). *Palaeontographica*, **14**, 99–124.

Mickevich, M. F., & Johnson, M. S. 1976. Congruence between morphological and allozyme data in evolutionary inference and character evolution. *Systematic Zoology*, **25**, 260–270 DOI: 10.2307/2412494

Mook, C. C. 1932. A study of the osteology of *Alligator prenasalis* (Loomis). *Bulletin of the Museum of Comparative Zoology*, **74**, 17–41.

Narváez, I., Brochu, C. A., Escaso, F., Pérez-García, A., & Ortega, F. 2015. New crocodyliforms from southwestern Europe and definition of a diverse clade of European Late Cretaceous basal eusuchians. *PLoS ONE*, **10**, e0140679.

Nesbitt, S. J. 2011. The early evolution of archosaurs: relationships and the origin of major clades. *Bulletin of the American Museum of Natural History*, **352**, 1–292 DOI: 10.1206/352.1

O'Reilly, J. E., Puttick, M. N., Parry, L., Tanner, A. R., Tarver, J. E., Fleming, J., Pisani, D., & Donoghue, P. C. 2016. Bayesian methods outperform parsimony but at the

expense of precision in the estimation of phylogeny from discrete morphological data. *Biology Letters*, **12**, 20160081 DOI: 10.1098/rsbl.2016.0081

O'Reilly, J. E., Puttick, M. N., Pisani, D., & Donoghue, P. C. 2017. Probabilistic methods surpass parsimony when assessing clade support in phylogenetic analyses of discrete morphological data. *Palaeontology*, **61**, 105–118 DOI: 10.1111/pala.12330

Parins-Fukuchi, C. 2017. Use of Continuous Traits Can Improve Morphological Phylogenetics. *Systematic biology*, **67**, 328–339 DOI: 10.1093/sysbio/syx072

Parins-Fukuchi, C. 2018. Bayesian placement of fossils on phylogenies using quantitative morphometric data. *Evolution*, (accepted article) DOI: 10.1111/evo.13516

Parker, W. G. 2002. Correlation of locality numbers for vertebrate fossil sites in Petrified Forest National Park, Arizona. *New Mexico Museum of Natural History and Science Bulletin*, **21**, 37-42.

Parker, W. G., & Irmis, R. B. 2006. A new species of the late Triassic phytosaur *Pseudopalatus* (Archosauria: Pseudosuchia) from Petrified Forest National Park, Arizona. *Museum of Northern Arizona Bulletin*, **62**, 126–143.

Parker, W. G., & Martz, J. W. 2011. The late Triassic (Norian) Adamanian–Revueltian tetrapod faunal transition in the Chinle Formation of Petrified Forest National Park,

Arizona. *Earth and Environmental Science Transactions of the Royal Society of Edinburgh*, **101**, 231-260.

Parker, W. G., Hungerbühler, A., & Martz, J. W. 2012. The taxonomic status of the phytosaurs (Archosauriformes) *Machaeroprosopus* and *Pseudopalatus* from the late Triassic of the western United States. *Earth and Environmental Science Transactions of the Royal Society of Edinburgh*, **103**, 265–268 DOI: 10.1017/S1755691013000339

Parrish, J. M. 1989. Vertebrate paleoecology of the Chinle Formation (late Triassic) of the southwestern United States. *Palaeogeography, Palaeoclimatology, Palaeoecology*, **72**, 227–247.

Parrish, J. M., & Carpenter, K. 1986. A new vertebrate fauna from the Dockum Formation (late Triassic) of eastern New Mexico. Pp. 151–160 in K. Padian (ed) *The Beginning of the Age of Dinosaurs: Faunal Change Across the Triassic-Jurassic Boundary*. Cambridge University Press, Cambridge.

Pastore, M. 2017. overlapping: Estimation of Overlapping in Empirical Distributions. R package version 1.5.0. https://CRAN.R-project.org/package=overlapping

Perrard, A., Lopez-Osorio, F., & Carpenter, J. M. 2016. Phylogeny, landmark analysis and the use of wing venation to study the evolution of social wasps (Hymenoptera: Vespidae: Vespinae). *Cladistics*, **32**, 406–425 DOI: 10.1111/cla.12138

Pierce, S. E., Angielczyk, K. D., & Rayfield, E. J. 2008. Patterns of morphospace occupation and mechanical performance in extant crocodilian skulls: a combined geometric morphometric and finite element modeling approach. *Journal of morphology*, **269**, 840–864. DOI: 10.1002/jmor.10627

Pimentel, R. A., & Riggins, R. 1987. The nature of cladistic data. *Cladistics*, **3**, 201–209 DOI: 10.1111/j.1096-0031.1987.tb00508.x

Pinna, G. 1987. I nuovi Lagerstaetten fossili del Triassico Italiano. *Le Scienze*, **224**, 62–70.

Piras, P., Buscalioni, A. D., Teresi, L., Raia, P., Sansalone, G., Kotsakis, T., & Cubo, J. 2013. Morphological integration and functional modularity in the crocodilian skull. *Integrative Zoology*, **9**, 498–516. DOI: 10.1111/1749-4877.12062

Piras, P., Teresi, L., Buscalioni, A. D., & Cubo, J. 2009. The shadow of forgotten ancestors differently constrains the fate of Alligatoroidea and Crocodyloidea. *Global Ecology and Biogeography*, **18**, 30–40. DOI: 10.1111/j.1466-8238.2008.00426.x

Poe, S., & Wiens, J. J. 2000. Character selection and the methodology of morphological phylogenetics. Pp. 20–36 in J. J. Wiens (ed) *Phylogenetic Analysis of Morphological Data*. Smithsonian Institution Press, Washington, D.C.

Pol, D., & Norell, M. A. 2001. Comments on the Manhattan stratigraphic measure. *Cladistics*, **17**, 285–289 DOI: 10.1111/j.1096-0031.2001.tb00125.x

Pol, D., & Norell, M. A. 2006. Uncertainty in the age of fossils and the stratigraphic fit to phylogenies. *Systematic Biology*, **55**, 512–521 DOI: 10.1080/10635150600755446

Pol, D., Nascimento, P. M., Carvalho, A. B., Riccomini, C., Pires-Domingues, R. A., & Zaher, H. 2014. A new notosuchian from the Late Cretaceous of Brazil and the phylogeny of advanced notosuchians. *PLoS ONE*, **9**, e93105.

Pol, D., & Leardi, J. M. 2015. Diversity patterns of Notosuchia (Crocodyliformes, Mesoeucrocodylia) during the Cretaceous of Gondwana. *Publicación Electrónica de la Asociación Paleontológica Argentina*, **15**, 172–186.

Purnell, M. A., Hart, P. J., Baines, D. C., & Bell, M. A. 2006. Quantitative analysis of dental microwear in threespine stickleback: a new approach to analysis of trophic ecology in aquatic vertebrates. *Journal of Animal Ecology*, **75**, 967–977.

Purnell, M. A., Bell, M. A., Baines, D. C., Hart, P. J., & Travis, M. P. 2007. Correlated evolution and dietary change in fossil stickleback. *Science*, **317**, 1887–1887.

Purnell, M., Seehausen, O., & Galis, F. 2012. Quantitative three-dimensional microtextural analyses of tooth wear as a tool for dietary discrimination in fishes. *Journal of the Royal Society Interface*, **9**, 2225–2233. DOI: 10.1098/rsif.2012.0140

Purnell, M. A., Crumpton, N., Gill, P. G., Jones, G., & Rayfield, E. J. 2013. Within-guild dietary discrimination from 3-D textural analysis of tooth microwear in insectivorous mammals. *Journal of Zoology*, **291**, 249–257.

Purslow, P. P. 1991. Measuring meat texture and understanding its structural basis; Pp. 35–56 in Vincent, J. F. V., & Lillford, P. J. (eds) *Feeding and the Texture of Food*. Cambridge University Press, Cambridge, U.K.

R Core Team. 2016. *R: A language and environment for statistical computing.* R Foundation for Statistical Computing, Vienna, Austria. Updated at: https://www.R-project.org/, accessed 11 January 2018.

Rae, T. C. 1998. The logical basis for the use of continuous characters in phylogenetic systematics. *Cladistics*, **14**, 221–228 DOI: 10.1111/j.1096-0031.1998.tb00335.x

Rahman, K. M. M., Khan, M. M. H., & Rakhimov, I. I. 2015. Scavenging behavior of the Bengal Monitor (*Varanus bengalensis*) in Jahangirnagar University Camus. *Bangladesh Journal of Scientific Research & Report*, **7**, 539–550.

Rahman, K. M., Rakhimov, I. I., & Khan, M. M. H. 2017. Activity budgets and dietary investigations of *Varanus salvator* (Reptilia: Varanidae) in Karamjal ecotourism spot of Bangladesh Sundarbans mangrove forest. *Basic and Applied Herpetology*, **31**, 45–56.

Ranjitkar, S., Kaidonis, J. A., Townsend, G. C., Vu, A. M., & Richards, L. C. 2008. An in vitro assessment of the effect of load and pH on wear between opposing enamel and dentine surfaces. *Archives of oral biology*, **53**, 1011–1016.

Rashid, S. M. A. 2004. *Population ecology and management of water monitors, Varanus salvator (Laurenti 1768) at Sungei Buloh Wetland Reserve, Singapore*. PhD Thesis, National Institute of Education, Nanyang Technological University, 508 pp.

Renesto, S., & Paganoni, A. 1998. A phytosaur skull from the Norian (late Triassic) of Lombardy (northern Italy). *Rivista Italiana di Paleontologia e Stratigrafia*, **104**, 115–121.

Rice, A. N., Ross, J. P., Finger, A. G., & Owen, R. 2005. Application and evaluation of a stomach flushing technique for alligators. *Herpetological Review*, **36**, 400–401.

Rieppel, O. 1995. The status of the sauropterygian reptile *Nothosaurus juvenilis* from the Middle Triassic of Germany. *Palaeontology*, **37**, 733–746.

Rohlf, F. J. 2015. The tps series of software. *Hystrix, the Italian Journal of Mammalogy*, **26**, 9–12.

Rohlf, F. J., & Bookstein, F. L. 1990. *Proceedings of the Michigan Morphometrics Workshop*. University of Michigan Museums, Ann Arbor, MI.

Ronquist, F., & Huelsenbeck, J. P. 2003. MrBayes 3: Bayesian phylogenetic inference under mixed models. *Bioinformatics*, **19**, 1572–1574 DOI: 10.1093/bioinformatics/btg180

Rozhdestvensky, A. K. 1965. Growth changes in Asian dinosaurs and some problems of their taxonomy. *Palaeontologicheskii Zhurnal*, **3**, 95–109.

Runemark, A., Sagonas, K., & Svensson, E. I. 2015. Ecological explanations to island gigantism: dietary niche divergence, predation, and size in an endemic lizard. *Ecology*, **96**, 2077–2092.

Ruta, M., Pisani, D., Lloyd, G. T., & Benton, M. J. 2007. A supertree of Temnospondyli: cladogenetic patterns in the most species-rich group of early tetrapods. *Proceedings of the Royal Society of London B: Biological Sciences*, **274**, 3087–3095.

Sadleir, R. W., & Makovicky, P. J. 2008. Cranial shape and correlated characters in crocodilian evolution. *Journal of Evolutionary Biology*, **21**, 1578–1596. DOI: 10.1111/j.1420-9101.2008.01602.x

Sah, S. A. M., & Stuebing, R. B. 1996. Diet, growth and movements of juvenile crocodiles *Crocodylus porosus* Schneider in the Klias River, Sabah, Malaysia. *Journal of Tropical Ecology*, **12**, 651–662.

Sampson, S. D., Ryan, M. J., & Tanke, D. H. 1997. Craniofacial ontogeny in centrosaurine dinosaurs (Ornithischia: Ceratopsidae): taxonomic and behavioral implications. *Zoological Journal of the Linnean Society*, **121**, 293–337 DOI: 10.1111/j.1096-3642.1997.tb00340.x

Sansom, R. S., Choate, P. G., Keating, J. N., & Randle, E. 2018. Parsimony, not Bayesian analysis, recovers more stratigraphically congruent phylogenetic trees. *Biology letters*, **14**, 20180263 DOI: 10.1098/rsbl.2018.0263

Scannella, J. B., & Horner, J. R. 2010. *Torosaurus* Marsh, 1891, is *Triceratops* Marsh, 1889 (Ceratopsidae: Chasmosaurinae): synonymy through ontogeny. *Journal of Vertebrate Paleontology*, **30**, 1157–1168 DOI: 10.1080/02724634.2010.483632

Scheyer, T. M., Aguilera, O. A., Delfino, M., Fortier, D. C., Carlini, A. A., Sánchez, R., Carrillo-Briceño, J.D., Quiroz, L., Sánchez-Villagra, M. R. 2013. Crocodylian diversity peak and extinction in the late Cenozoic of the northern Neotropics. *Nature communications*, **4**, 1907.

Schulz, E., Calandra, I., & Kaiser, T. M. 2013. Feeding ecology and chewing mechanics in hoofed mammals: 3D tribology of enamel wear. *Wear*, **300**, 169–179.

Scott, R.S., Ungar, P.S., Bergstrom, T.S., Brown, C.A., Grine, F.E., Teaford, M.F., & Walker, A. 2005. Dental microwear texture analysis shows within-species diet variability in fossil hominins. *Nature*, **436**, 693–695.

Sellwood, B. W., & Valdes, P. J. 2006. Mesozoic climates: General circulation models and the rock record. *Sedimentary Geology*, **190**, 269–287. DOI: 10.1016/j.sedgeo.2006.05.013

Sepkoski, J. J. 1982. *A compendium of fossil marine families*. Contributions in biology and geology, 51, Milwaukee Public Museum, Milwaukee, Wisconsin, USA. 125 pp.

Sereno, P. C. 1991. Basal archosaurs: phylogenetic relationships and functional implications. *Journal of Vertebrate Paleontology*, **11**(S4), 1–53 DOI: 10.1080/02724634.1991.10011426

Sereno, P. C., & Novas, F. E. 1994. The skull and neck of the basal theropod *Herrerasaurus ischigualastensis*. *Journal of Vertebrate Paleontology*, **13**, 451–476.

Sherratt, E., Serb, J. M., & Adams, D. C. 2017. Rates of morphological evolution, asymmetry and morphological integration of shell shape in scallops. *BMC evolutionary biology*, **17**, 248. DOI: 10.1186/s12862-017-1098-5

Siddall, M. E. 1996. Stratigraphic consistency and the shape of things. *Systematic Biology*, **45**, 111–115 DOI: 10.2307/2413516

Siddall, M. E. 1998. Stratigraphic fit to phylogenies: a proposed solution. *Cladistics*, **14**, 201–208 DOI: 10.1111/j.1096-0031.1998.tb00333.x

Sidlauskas, B. 2008. Continuous and arrested morphological diversification in sister clades of characiform fishes: a phylomorphospace approach. *Evolution: International Journal of Organic Evolution*, **62**, 3135–3156.

Small, B. J. 2002. Cranial anatomy of *Desmatosuchus haplocerus* (Reptilia: Archosauria: Stagonolepididae). *Zoological Journal of the Linnean Society*, **136**, 97–111.

Smith, U. E., & Hendricks, J. R. 2013. Geometric morphometric character suites as phylogenetic data: extracting phylogenetic signal from gastropod shells. *Systematic Biology*, **62**, 366–385.

Sookias, R. B. 2016. The relationships of the Euparkeriidae and the rise of Archosauria. *Royal Society open science*, **3**, 150674 DOI: 10.1098/rsos.150674

Spielmann, J. A., & Lucas, S. G. 2012. Tetrapod fauna of the Upper Triassic Redonda Formation, east-central New Mexico: the characteristic assemblage of the Apachean land-vertebrate faunachron. *New Mexico Museum of Natural History and Science Bulletin*, **55**, 1–119.

Stevens, P. F. 1991. Character states, morphological variation, and phylogenetic analysis: a review. *Systematic Botany*, **16**, 553–583 DOI: 10.2307/2419343

Stocker, M. R. 2010. A new taxon of phytosaur (Archosauria: Pseudosuchia) from the late Triassic (Norian) Sonsela Member (Chinle Formation) in Arizona, and a critical reevaluation of *Leptosuchus* Case, 1922. *Palaeontology*, **53**, 997–1022 DOI: 10.1111/j.1475-4983.2010.00983.x

Stocker, M. R. 2012. A new phytosaur (Archosauriformes, Phytosauria) from the Lot's Wife beds (Sonsela Member) within the Chinle Formation (Upper Triassic) of Petrified Forest National Park, Arizona. *Journal of Vertebrate Paleontology*, **32**, 573–586 DOI: 10.1080/02724634.2012.649815

Stocker, M. R. 2013. A new taxonomic arrangement for *Paleorhinus scurriensis*. *Earth and Environmental Science Transactions of the Royal Society of Edinburgh*, **103**, 1–13 DOI: 10.1017/S1755691013000340

Stocker, M. R., & Butler, R. J. 2013. Phytosauria. *Geological Society, London, Special Publications*, **379**, 91–117 DOI: 10.1144/SP379.5

Stocker, M. R., Zhao, L. J., Nesbitt, S. J., Wu, X. C., & Li, C. 2017. A short-snouted, Middle Triassic phytosaur and its implications for the morphological evolution and biogeography of Phytosauria. *Scientific Reports*, **7**, 46028 DOI: 10.1038/srep46028

Stovall, J. W., & Wharton Jr, J. B. 1936. A new species of phytosaur from Big Spring, Texas. *The Journal of Geology*, **44**, 183–192 DOI: 10.1086/624416

Stubbs, T. L., Pierce, S. E., Rayfield, E. J., & Anderson, P. S. 2013. Morphological and biomechanical disparity of crocodile-line archosaurs following the end-Triassic extinction. *Proceedings of the Royal Society B*, **280**, 20131940.

Sues, H. D. 1989. The place of crocodilians in the living world; Pp. 67–91 in Ross, C. A. (ed) *Crocodiles and Alligators*. New York, Facts on File.

Sulej, T. 2010. The skull of an early late Triassic aetosaur and the evolution of the stagonolepidid archosaurian reptiles. *Zoological Journal of the Linnean Society*, **158**, 860–881.

Swofford, D., Olsen, G., Paddell, P., & Hills, D. 1996. Phylogenetic inference; Pp. 407–514 in D. Hillis, C. Moritz, & B. Mable (eds) *Molecular Systematics*. Sinauer, Sunderland, Massachusetts.

Taylor, J. A. 1979. The foods and feeding habits of subadult *Crocodylus Porosus* Schneider in Northern Australia. *Australian Wildlife Research*, **6**, 347–359.

Teaford, M. F., & Oyen, O. J. 1989. Differences in the rate of molar wear between monkeys raised on different diets. *Journal of Dental Research*, **68**, 1513–1518.

Thiele, K. 1993. The holy grail of the perfect character: the cladistic treatment of morphometric data. *Cladistics*, **9**, 275–304 DOI: 10.1111/j.1096-0031.1993.tb00226.x

Thorbjarnarson, J. B. 1988. The status and ecology of the American crocodile in Haiti. *Bulletin of the Florida State Museum. Biological Sciences*, **33**, 1–86.

Thorbjarnarson, J. B. 1990. Notes on the feeding behavior of the gharial (*Gavialis gangeticus*) under semi-natural conditions. *Journal of Herpetology*, **24**, 99–100.

Thorpe, R. S. 1984. Coding morphometric characters for constructing distance Wagner networks. *Evolution*, **38**, 244–255 DOI: 10.1111/j.1558-5646.1984.tb00282.x

Throckmorton, G. Y. S. 1976. Oral food processing in two herbivorous lizards, *Iguana iguana* (Iguanidae) and *Uromastix aegyptius* (Agarnidae). *Journal of Morphology*, **148**, 363–390.

Tschopp, E., Mateus, O., & Benson, R. B. J. 2015. A specimen-level phylogenetic analysis and taxonomic revision of Diplodocidae (Dinosauria, Sauropoda). *PeerJ*, **3**, e857 DOI: 10.7717/peerj.857

Tsuihiji T, Watabe M, Tsogtbaatar K, Tsubamoto T, Barsbold R, Suzuki S, Lee AH, Ridgely RC, Kawahara Y, Witmer LM. 2011. Cranial osteology of a juvenile specimen of *Tarbosaurus bataar* (Theropoda, Tyrannosauridae) from the Nemegt Formation (Upper Cretaceous) of Bugin Tsav, Mongolia. *Journal of Vertebrate Paleontology*, **31**, 497–517 DOI: 10.1080/02724634.2011.557116

Turner, A. H., & Sertich, J. J. 2010. Phylogenetic history of *Simosuchus clarki* (Crocodyliformes: Notosuchia) from the Late Cretaceous of Madagascar. *Journal of Vertebrate Paleontology*, **30(sup1)**, 177–236.

Ungar, P. S., Grine, F. E., & Teaford, M. F. 2008. Dental microwear and diet of the Plio-Pleistocene hominin *Paranthropus boisei*. *PLoS one*, **3**, e2044.

Ungar, P. S., Merceron, G., & Scott, R. S. 2007. Dental microwear texture analysis of Varswater bovids and early Pliocene paleoenvironments of Langebaanweg, Western Cape Province, South Africa. *Journal of Mammalian Evolution*, **14**, 163–181.

Upchurch, P., Tomida, Y., & Barrett, P. M. 2004. A new specimen of *Apatosaurus ajax* (Sauropoda: Diplodocidae) from the Morrison Formation (Upper Jurassic) of Wyoming, USA. *National Science Museum Monographs*, **26**, 1–118.

Vitt, L. J., & Pianka, E. R. 2005. Deep history impacts present-day ecology and biodiversity. *Proceedings of the National Academy of Sciences*, **102**, 7877–7881.

Wagner, P. J. 2012. Modelling rate distributions using character compatibility: implications for morphological evolution among fossil invertebrates. *Biology Letters*, **8**, 143–146 DOI: 10.1098/rsbl.2011.0523

Wainwright, P. C., Alfaro, M. E., Bolnick, D. I., & Hulsey, C. D. 2005. Many-to-one mapping of form to function: a general principle in organismal design? *Integrative and comparative biology*, **45**, 256–262.

Walker, A. D. 1964. Triassic reptiles from the Elgin area: *Ornithosuchus* and the origin of carnosaurs. *Philosophical Transactions of the Royal Society of London B*, **248**, 53–134.

Wallace, K. M., & Leslie, A. J. 2008. Diet of the Nile crocodile (*Crocodylus niloticus*) in the Okavango Delta, Botswana. *Journal of Herpetology*, **42**, 361–368.

Walmsley, C. W., Smits, P. D., Quayle, M. R., McCurry, M. R., Richards, H. S., Oldfield, C. C., Wroe, S., Clausen, P. D., & McHenry, C. R. 2013. Why the long face? The mechanics of mandibular symphysis proportions in crocodiles. *PLoS One*, **8**, e53873. DOI: 10.1371/journal.pone.0053873

Westphal, K. W. 1979. Missing holotype of *Machaeroprosopus validus* (Mehl, 1916). *Journal of Paleontology*, **53**, 741.

Whitlock, J. A. 2011. Inferences of diplodocoid (Sauropoda: Dinosauria) feeding behavior from snout shape and microwear analyses. *PLoS One*, **6**, e18304.

Wiens, J. J. 1998. Testing phylogenetic methods with tree congruence: phylogenetic analysis of polymorphic morphological characters in phrynosomatid lizards. *Systematic Biology*, **47**, 427–444 DOI: 10.1080/106351598260806

Wiens, J. J. 2001. Character analysis in morphological phylogenetics: problems and solutions. *Systematic Biology*, **50**, 689–699 DOI: 10.1080/106351501753328811

Wilberg, E. W. 2015. What's in an outgroup? The impact of outgroup choice on the phylogenetic position of Thalattosuchia (Crocodylomorpha) and the origin of Crocodyliformes. *Systematic Biology*, **64**, 621–637.

Williams, V. S., Barrett, P. M., & Purnell, M. A. 2009. Quantitative analysis of dental microwear in hadrosaurid dinosaurs, and the implications for hypotheses of jaw mechanics and feeding. *Proceedings of the National Academy of Sciences*, **106**, 11194–11199.

Williams, V. S., & Doyle, A. M. 2010. Cleaning fossil tooth surfaces for microwear analysis: Use of solvent gels to remove resistant consolidant. *Palaeontologia Electronica*, **13**, 2T.

Williston, S. W. 1904. Notice of some new reptiles from the Upper Trias of Wyoming. *The Journal of Geology*, **12**, 688-697 DOI: 10.1086/621190

Wills, M. A. 1999. Congruence between phylogeny and stratigraphy: randomization tests and the gap excess ratio. *Systematic Biology*, **48**, 559–580 DOI: 10.1080/106351599260148

Wills, M. A., Barrett, P. M., & Heathcote, J. F. 2008. The modified gap excess ratio (GER*) and the stratigraphic congruence of dinosaur phylogenies. *Systematic Biology*, **57**, 891–904 DOI: 10.1080/10635150802570809

Witmer, L. M. 1997. The evolution of the antorbital cavity of archosaurs: a study in soft-tissue reconstruction in the fossil record with an analysis of the function of pneumaticity. *Journal of Vertebrate Paleontology*, **17**(S1), 1-76 DOI: 10.1080/02724634.1997.10011027

Wright, A. M., & Hillis, D. M. 2014. Bayesian analysis using a simple likelihood model outperforms parsimony for estimation of phylogeny from discrete morphological data. *PLoS One*, **9**, e109210 DOI: 10.1371/journal.pone.0109210

Wright, A. M., Lloyd, G. T., & Hillis, D. M. 2015. Modeling character change heterogeneity in phylogenetic analyses of morphology through the use of priors. *Systematic biology*, **65**, 602–611 DOI: 10.1093/sysbio/syv122

Wroblewski, A. 2003. Application of cladistic analysis towards resolving biostratigraphic uncertainty; an example from the Upper Triassic. *Geological Society of America Abstracts with Programs*, **35 (5)**, p. 15

Wu, X. C., Brinkman, D. B., & Russell, A. P. 1996. A new alligator from the Upper Cretaceaous of Canada and the relationship of early eusuchians. *Palaeontology*, **39**, 351–376.

Xia, J., Zheng, J., Huang, D., Tian, Z. R., Chen, L., Zhou, Z., Ungar, P. S., & Qian, L. 2015. New model to explain tooth wear with implications for microwear formation and diet reconstruction. *Pro ceedings of the National Academy of Sciences*, **112**, 10669–10672.

Young, M. T. 2014. Filling the 'Corallian Gap': re-description of a metriorhynchid crocodylomorph from the Oxfordian (Late Jurassic) of Headington, England. *Historical Biology*, **26**, 80–90.

Young, M. T., Brusatte, S. L., Ruta, M., & de Andrade, M. B. 2010. The evolution of Metriorhynchoidea (Mesoeucrocodylia, Thalattosuchia): an integrated approach using geometric morphometrics, analysis of disparity, and biomechanics. *Zoological Journal of the Linnean Society*, **158**, 801–859.

Zeigler, K. E., Lucas, S. G., & Heckert, A. B. 2002a. The late Triassic Canjilon quarry (Upper Chinle Group, New Mexico) phytosaur skulls: evidence of sexual dimorphism in phytosaurs. *New Mexico Museum of Natural History and Science Bulletin*, **21**, 179–188.

Zeigler, K. E., Lucas, S. G., & Heckert, A. B. 2002b. A phytosaur skull from the upper Triassic Snyder Quarry (Petrified Forest Formation, Chinle Group). *Upper Triassic Stratigraphy and Paleontology: Bulletin*, **21**, 171-178.

Zeigler, K. E., Heckert, A. B., & Lucas, S. G. 2003a. Phytosaur (Archosauria: Parasuchidae) cranial and mandibular material from the Upper Triassic Snyder quarry (Petrified Forest Formation, Chinle Group). *New Mexico Museum of Natural History and Science Bulletin*, **24**, 81–88.

Zeigler, K. E., Lucas, S. G., & Heckert, A. B. 2003b. Variation in the late Triassic Canjilon quarry (Upper Chinle Group, New Mexico) phytosaur skulls: a case for sexual dimorphism. *Paläontologische Zeitschrift*, **77**, 341 DOI: 10.1007/BF03006946

Zelditch, M., Swiderski, D. L., & Sheets, H. D. 2012. *Geometric Morphometrics for Biologists: A Primer*. Academic Press